

DISSERTATION

PHOTO-INDUCED ELECTRON TRANSFER IN CU(I) BIS-PHENANTHROLINE BASED
ASSEMBLIES

PART I: CHROMOPHORE-ACCEPTOR DIADS

PART II: DONOR-CHROMOPHORE-ACCEPTOR TRIADS

Submitted by

Megan Lazorski

Department of Chemistry

In partial fulfillment of the requirements

For the Degree of Doctor of Philosophy

Colorado State University

Fort Collins, Colorado

Spring 2013

Doctoral Committee:

Advisor: C. Michael Elliott

Matthew P. Shores

Eugene Chen

Travis S. Bailey

James R. Sites

ABSTRACT

PHOTO-INDUCED ELECTRON TRANSFER IN CU(I) BIS-PHENANTHROLINE BASED ASSEMBLIES:

PART I: CHROMOPHORE-ACCEPTOR DIADS

PART II: DONOR-CHROMOPHORE-ACCEPTOR TRIADS

The photophysical behavior of [Cu(I)P₂] (P=2,9-disubstituted-1,10-phenanthroline ligands) in donor-chromophore-acceptor (D-C-A) triads and chromophore-acceptor (C-A) diads is a complex and fascinating area of under developed, yet fundamental, electron transfer chemistry. In metal polypyridyl D-C-A and C-A triads/diads, metal polypyridyl chromophores (C) in which the polypyridyl ligands are covalently linked to acceptor (A) and/or donor (D) moieties, photoexcitation of the chromophore initiates a series of electron transfer events that result in the formation of a charge separated (CS)/charge transfer (CT) state, respectively. The majority of high-performing metal polypyridyl D-C-A/C-A complexes, on which [Cu(I)P₂] D-C-A/C-A research is based, incorporate ruthenium (as [Ru(II)L₃] where L=polypyridyl ligand) or other rare, expensive, and sometimes toxic metals such as osmium, rhenium and platinum. Although [Ru(II)L₃] D-C-A/C-A's have historically set the benchmark for metal polypyridyl D-C-A/C-A performance, it is clear that these complexes are not a practical choice if D-C-A's or C-A's were incorporated into a device for large scale production. However, bisphenanthroline complexes of copper, a much more earth abundant, cheaper and less toxic metal, exhibit very similar photophysical properties to [Ru(II)L₃] and have thus gained recognition as promising new materials for D-C-A/C-A triad/diad construction.

In order to understand the electron transfer (ET) events occurring in [Cu(I)P₂] D-C-A/C-A triads/diads, a complex must be synthesized that is capable of forming a CS with high quantum efficiency ($\Phi_{cs/ct}$) and a long CS/CT lifetime ($\tau_{cs/ct}$). Therefore, the intent of the research reported herein is to synthesize novel, yet functional heteroleptic [Cu(I)P₂] D-C-A/C-A triads/diads and study their fundamental, photo-initiated electron transfer chemistry, specifically the formation of a CS/CT state.

Many challenges, which are not present for [Ru(II)L₃], make the design and synthesis of [Cu(I)P₂] D-C-A/C-A assemblies an art in itself. Therefore, a significant amount of effort was spent on fabricating ligand architectures that (1) are appended with acceptor and/or donor moieties capable of being reduced/oxidized resulting in the formation of a CS/CT, (2) are able to be easily modified so the amount of energy stored in the CS/CT can be tuned, (3) favor the self-assembly of [Cu(I)P₂] complexes, (4) are able to facilitate processes that maximize the $\Phi_{cs/ct}$. Once the ligands were obtained, the complexation equilibria behavior of these [Cu(I)P₂] triads and diads were studied. Despite efforts to design ligand architectures that favor heteroleptic formation, the thermodynamic driving force for heteroleptic D-C-A triad formation is less favorable than expected. Thus, mixing stoichiometric quantities of D, C and A results in a statistical mixture of C-A, C-D and D-C-A products. Furthermore, since the ligands are labile and will rearrange to the most thermodynamically stable configuration of products when these complexes are dissolved, isolation of the D-C-A product is impossible. However, recent advances in ligand design have shown promise for resolving this on-going issue.

Despite having a mixture of products with the D-C-A, the electron transfer processes of the [Cu(I)P₂] D-C-A triads and C-A diads were investigated. Using Transient Absorption (TA) laser spectroscopy, the CT state in the constructed C-A diads and the CS state in the D-C-A tri-

ads were detected and the lifetimes were determined. However, it was found that those lifetimes could be modulated to a small degree by solvent in the C-A diads (c.a. 6x longer in polar solvents), and drastically via the application of a magnetic field in D-C-A triads (c.a. 60x longer). The ability to modulate the lifetimes enabled the deconvolution of the effects due to the C-A diad vs D-C-A triad in the statistical product mixtures. Although the response in a magnetic field was a somewhat expected result, as similar effects occur in the [Ru(II)L₃] D-C-A/C-A's, the magnitude of change in the lifetime and the quantum efficiency offers new insight into the electron transfer events that occur in the CS/CT formation process for [Cu(I)P₂] D-C-A/C-A complexes.

ACKNOWLEDGEMENTS

This thesis is dedicated to my parents, David and Debbie Lazorski, for always believing in me, always pushing me to be my best while giving me the freedom to be myself, and always supporting the person I have become. Your hard work, dedication, wisdom, unconditional love and support continue to show me the type of person that I strive to be. Thank you. I couldn't have done this without you.

Throughout my life, I have been blessed with many excellent teachers. The knowledge, insight, and advice you all have given me over the years helps to guide me in so many different situations. Not only have you fostered my desire to learn, understand, and synthesize information, but have also provided me with the tools to do so on my own. For that, I am truly thankful.

Of all of the amazing educators I have had the good fortune to encounter, there are a few that deserve special recognition:

Dr. Virginia Pett and Dr. Richard Bromund, I can't ever seem to find the right words to express how much I appreciate you both. You challenged me to follow my passions, no matter how disparate, and continue to support and inspire me as I move through each step in my life. You are phenomenal educators, mentors and friends. Thank you for everything.

Dr. C. Michael Elliott, you have taught me so much more than electrochemistry, crazy lab techniques, and "Mexican." Really, you have showed me what it means to be a creative scientist. I highly admire and respect your fervor for understanding and dedication to your work, even when it meant I was going to spend another late night in lab. I can only hope to be as enthusiastic about my own research in the future and as successful at finding inventive, resourceful solutions to even the most difficult problems. Thank you for letting me join your research group, and

be a part of this awesome project. Maybe even more importantly, thank you for all of the other things you have done to help me throughout my time here. You have been an excellent academic mentor, but you have also treated me like family. I didn't know that I needed a "Colorado Dad," but it turns out that I did, and I am glad that it was you.

I would also like to thank the Elliott groupers. When I joined this group, I knew I was interested in the research, but the decision was really based on a gut feeling. I knew immediately upon joining that it was the right choice, and I have been proven right every day that I worked with all of you. We are the island of misfit toys, but we all fit in here, together. You guys are the best, and I look forward to seeing you on the slopes in Steamboat for many years to come.

Finally, I want to thank my wonderful, supportive husband Chris Burgess. An honorary degree should be given to the spouse of every married student, for no one knows how truly arduous this whole process can be better than them. You had to stand witness to countless days when I "just didn't have enough time", "just couldn't make it through", "just had to finish one more thing," and "just couldn't take it anymore." I know I can be a handful when I am stressed and tired (ok, all of the time), but you still stood by me. Thanks for being there with me through the struggles, tears, joys and laughter.

TABLE OF CONTENTS

ABSTRACT.....	ii
ACKNOWLEDGEMENTS.....	v
TABLE OF CONTENTS.....	vii
Chapter 1. Introduction	
1.1. Background on Donor-Chromophore-Acceptor Triads and Chromophore-Acceptor Diads.....	1
1.2. Characteristics of [Ru(II)L ₃] Complexes.....	6
1.3. Characteristics of [Cu(I)P ₂] Complexes.....	11
References.....	25
Chapter 2. Experimental Methods	
2.1. Synthetic Methods.....	28
2.2. Sample Preparation.....	35
2.3. Instrumentation and Measurements.....	45
References.....	50
PART I. CHROMOPHORE-ACCEPTOR DIADS	
Chapter 3. Photo-Induced, Intramolecular Charge Transfer Reactions in Cu(I) bis-Phenanthroline Chromophore-Acceptor Diads	
3.1 Introduction.....	52
3.2 Results.....	58
3.3 Discussion.....	81
3.4 Conclusion.....	101
References.....	103
PART II. DONOR-CHROMOPHORE-ACCEPTOR TRIADS	
Chapter 4. Photo-Induced, Multi-Step, Charge Separation in Heteroleptic Cu(I) bis-Phenanthroline Based Donor-Chromophore-Acceptor Triads	
4.1 Introduction.....	106
4.2 Results.....	109
4.3 Discussion.....	132

4.4 Conclusion	140
References	142
Chapter 5. The Spin-Chemical Control of the Kinetics of the Multi-Step, Photo-Induced Charge Separation in Cu(I) bis-Phenanthroline Based Donor-Chromophore-Acceptor Triads	
5.1 Introduction.....	145
5.2 Results.....	151
5.3 Discussion.....	179
5.4 Conclusion	193
References.....	195
Chapter 6. Global Conclusions and Outlook	
References.....	204
LIST OF ABBREVIATIONS.....	205

Chapter 1.

Introduction

1.1. Background on Donor-Chromophore-Acceptor Triads and Chromophore-Acceptor Diads

Donor-Chromophore-Acceptor (D-C-A) and Chromophore-Acceptor (C-A) assemblies are important and interesting systems because they can harvest, and subsequently convert light into a chemical potential, which is stored in a charge separated (CS) or charge transfer (CT) state, as demonstrated in Figure 1.1. The mechanism by which light is harvested and stored in these D-C-A's and C-A's is very similar to that which occurs in plants during photosynthesis. This type of photophysical behavior makes D-C-A and C-A complexes very promising for solar energy harvesting applications in a world on the brink of a major energy crisis.

One of the fundamental photosynthetic processes that enables plants to harvest and use light from the sun is the formation of a photo-induced CS state in photosystems I and II.¹⁻⁴ Several general types of D-C-A/C-A systems exist that are capable of forming a CS/CT based on organic, organometallic, and metal polypyridyl complexes. This project focuses on the electron transfer processes in metal polypyridyl based D-C-A triads and C-A diads: specifically, novel [Cu(I)P₂] complex architectures. Metal polypyridyl D-C-A/C-A triads/diads incorporate a metal polypyridyl chromophore that has a large molar absorptivity ($\epsilon \approx 10^3$ - 10^5 L·mol⁻¹·cm⁻¹) in the visible spectrum and covalently bound D and A moieties capable of donating or accepting electrons as necessary during the CS/CT formation process.^{1,2}

The formation of a CS/CT in previously studied metal (predominantly Ru(II)) polypyridyl D-C-A/C-A triads and diads occurs through a series of electron transfer (ET) steps as shown in Figure 1.1: (1) a photon of light excites an electron from a metal-centered d-orbital to a

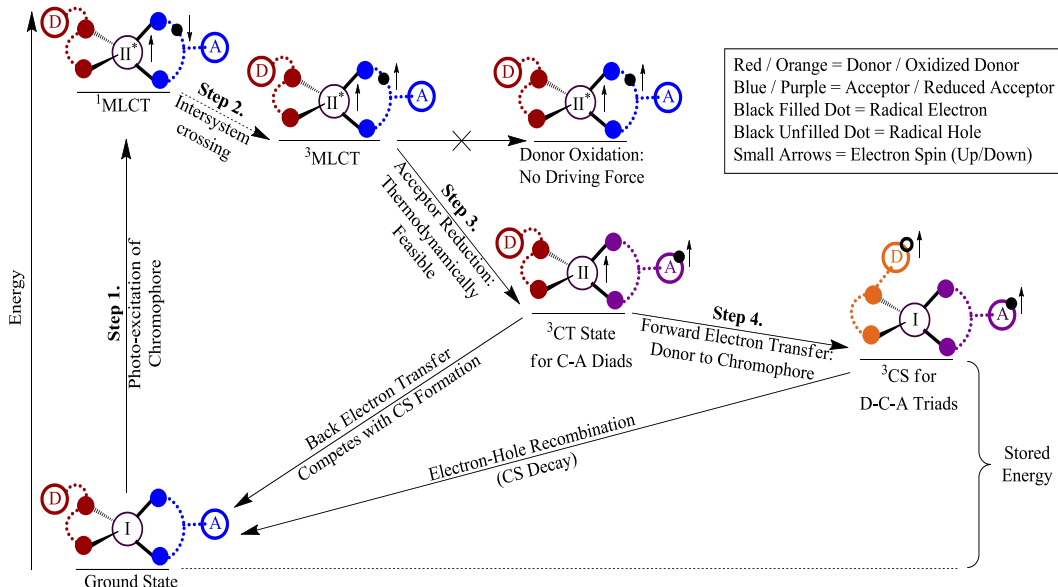


Figure 1.1. A schematic representation of CS/CT formation in $[\text{Cu}(\text{I})\text{P}_2]$ D-C-A complexes. The proposed mechanism is based on the mechanism of CS/CT formation in $[\text{Ru}(\text{II})\text{L}_3]$ C-A and D-C-A assemblies. Thus far, all studies on the CS/CT formation in $[\text{Cu}(\text{I})\text{P}_2]$ D-C-A/C-A's corroborate this mechanism.

ligand based π^* orbital resulting in a singlet metal-to-ligand charge transfer state ($^1\text{MLCT}$, often called the Franck-Condon MLCT, or $\text{FC-}^1\text{MLCT}$), (2) intersystem crossing (ISC) to the triplet MLCT state ($^3\text{MLCT}$) occurs, (3) the electron in the ligand-based π^* orbital of the excited chromophore is transferred to the acceptor (chromophore is oxidized, acceptor is reduced). For a C-A diad, the ET processes stop at step 3 (because no donor is present) resulting in a ^3CT state wherein a radical hole resides in a metal based d-orbital of the chromophore and a radical electron resides in an orbital of the acceptor moiety. However in D-C-A triads, a subsequent ET step occurs: (4) the oxidized chromophore now transfers the hole from the ligand-based, π^* orbital to the donor (chromophore is reduced back to the ground state, donor is oxidized), resulting in a spin-correlated, triplet di-radical CS.⁵⁻⁷ Due to the spin chemistry of the ^3CT and ^3CS , it is possible that a magnetic field could have a dramatic effect on further ET events. This will be discussed in more detail later.

The last ET step (step 4 above) is the bottleneck in the CS formation process because it is constantly competing with back ET to the ground state. This is why the development of new D-

C-A complexes has proved to be a much more challenging task than the development of new C-A diads.⁵ The lifetime of the CS in a D-C-A triad is generally longer than the CT of a C-A diad for two reasons: (1) multi-step electron transfer resulting in a CS spatially separates the radical hole and radical electron by a greater distance, and (2) the hole is located on an organic donor orbital rather than the metal based d-orbital, which generally recombines at a slower rate.^{1,2,8,9} Long lifetimes are desired for CS and CT states because it increases the probability that the stored energy will be able to be used to drive further processes, such as water splitting or charge injection into TiO₂. Therefore, although this research is focused on the development and fundamental study of both novel [Cu(I)P₂] D-C-A triads and C-A diads, the information gained from studying the ET processes in C-A diad complexes is generally intended to inform and help interpret the ET processes and CS formation in the heteroleptic [Cu(I)P₂] D-C-A triads (heteroleptic = non-identical P ligands, P_D-Cu-P_A, where P_D=phenanthroline based donor ligand and P_A= phenanthroline based acceptor ligand).

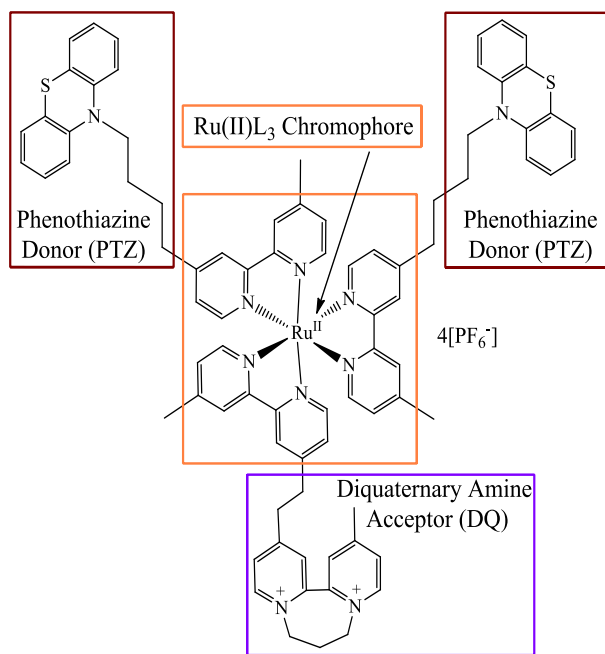


Figure 1.2. A [Ru(II)L₃] D-C-A Complex. Modified from ref 5.

As previously mentioned, [Ru(II)L₃] type C-A and D-C-A complexes, like the one shown in Figure 1.2, have been the archetypal systems used to form a CS/CT in metal polypyridyl complexes.^{4,5,7,10-14} Other metal polypyridyl chromophores based on osmium, rhenium, and platinum have also been used in D-C-A/C-A systems, but are far less common. The rare (not earth-abundant),

expensive, and sometimes toxic, nature of these metals is an obvious drawback.^{15,16} Therefore, a chromophore based on copper (e.g. [Cu(I)P₂]) a much more earth-abundant, cheap, and less-toxic metal is highly desirable.^{17,18}

The similarity in the photophysical behavior of [Ru(II)L₃] and [Cu(I)P₂] complexes has been the primary impetus for studying [Cu(I)P₂] complexes as possible candidates for C-A and D-C-A assemblies based on earth-abundant, cheap materials.¹⁸⁻²³ Typical [Cu(I)P₂] complexes absorb strongly in the visible spectrum ($\epsilon \approx 10^3$ - 10^5 L·mol⁻¹·cm⁻¹) and the MLCT state is the first excited state which can be long lived with proper ligand design (there are no low-lying d-d states, such as exist in [Fe(II)L₃] complexes).^{15,17,19,24-29}

The CT formation in [Cu(I)P₂] C-A complexes is relatively easy to achieve and thus several examples of [Cu(I)P₂] C-A diads exist; however, to my knowledge, there is only one other example^a of a [Cu(I)P₂] D-C-A complex capable of CS formation without the use of additional chromophoric units.^{15,22,30-40} For example, all other [Cu(I)P₂] containing D-C-A's have been made with Zn(II) porphyrins and C₆₀/fullerene or Au(III) porphyrin acceptors which incorporate [Cu(I)P₂] catenane or rotaxane units.³¹⁻⁴⁰ Although these D-C-A's have been shown to achieve efficient, photoinduced, multi-step charge separation, the primary chromophore in these systems is the Zn(II) porphyrin, not the [Cu(I)P₂] catenane unit.³¹⁻³⁴ There are several specific reasons why a CS has been difficult to achieve in [Cu(I)P₂] D-C-A complexes, but in general the process of CS formation in all D-C-A complexes is more difficult to achieve because the last ET step must be highly favored over back ET (so-called "geminate recombination.")

^a A personal communication with Fabrice Odobel, Université de Nantes, CNRS indicated that a similar Cu(I)-based D-C-A triad with different donors and acceptor moieties is being studied in his laboratory. These studies have yet to be published, which is why no details about this complex are included herein.

According to Marcus theory, there are three main factors that influence the rates of forward and back ET in D-C-A/C-A complexes: the free energy/driving force of the reaction (ΔG°), reorganizational energy^b (λ), and the electronic coupling (V_{if}) as shown in Figure 1.3.⁴² For example, in most porphyrin-chromophore-based D-C-A/C-A complexes V_{if} is essentially constant

for the forward and back electron transfer processes at each step leading to and from the CS/CT state.⁵

For instance, if the initial oxidative quenching of the excited chromophore involves a through-bond pathway from an orbital localized on the porphyrin to an orbital localized on the acceptor, the reverse process

would follow a similar pathway with similar coupling. Thus differences in the rates of forward (k_{ct}) and

backward ET (k_{bet}) will largely be governed by the driving forces for the respective processes. In the case of a C-A diad, often the quantum efficiency for quenching is high, but the lifetime of the CT state will depend on the relative values of k_{ct} and k_{bet} . If the latter is larger, little or no CT state will be observable. In the case of a D-C-A triad the situation is more complex. To observe CS, not only does the quenching rate have to be faster than geminate recombination, but the rate of the second electron transfer leading to CS formation, k_{cs} , must be comparable to or greater

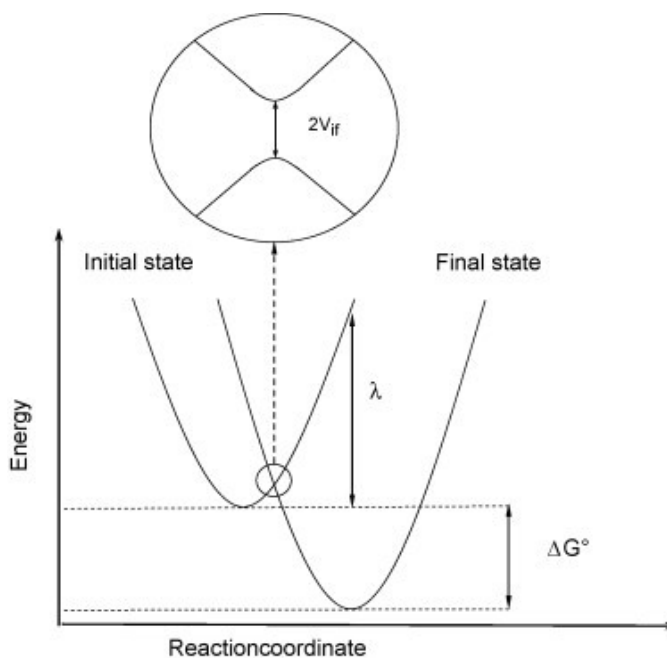


Figure 1.3. Potential energy diagram depicting the variables that have the greatest influence on the rate of electron transfer based on Marcus theory. Reproduced from ref 42.

^b The reorganizational energy is the energy required to perform all structural and solvent sphere changes accompanying CSS formation in a D-C-A.^{2,41}

than the rate of recombination. Thus, the quantum efficiency for CS formation, $\Phi_{cs} = (1 - k_{bet}/k_{cs})$.^{1,2,8} In order to minimize the k_{bet} and maximize Φ_{cs} a common strategy is to design the D-C-A systems such that the back electron transfer is in the Marcus inverted region, and the steps leading to CS is in the Marcus normal region. This type of ET behavior is usually induced by increasing the driving force for CS formation through structural modification.^{1,2,8,43} Often, when the driving force is changed in this way, the energy stored in the CS is lowered and the quantum efficiency of CS formation is low (typically $\Phi_{cs} \leq 0.3$).⁵ Alternately, if the coupling, V_{if} , can be controlled such that it is large for desirable reactions (those leading to CS formation) and substantially diminished for reactions leading away from CS formation, in principle, Φ_{cs} can be made large without a significant loss in stored energy.⁵ In [Ru(II)L₃] D-C-A complexes similar to those illustrated in Figure 1.2, the k_{bet} is hindered by electronic coupling fluctuations that spontaneously occur during CS formation rather than driving force alterations. This is why metal-polypyridyl D-C-A complexes of this sort can generally achieve much higher quantum efficiencies ($\Phi_{cs} \rightarrow 1$) with little loss in energy storage capacity. The research presented herein is intended to mimic the CS formation in [Ru(II)L₃] D-C-A systems using [Cu(I)P₂] complexes as the chromophore. Therefore, presented below are the aspects of the [Ru(II)L₃] D-C-A antecedents that have the greatest influence on the coordination chemistry, ET chemistry, and CS formation.

1.2. Characteristics of [Ru(II)L₃] Complexes

Coordination Chemistry of [Ru(II)L₃] in the Ground and Excited States

In both the ground and excited states, Ru(II/III)L₃ complexes adopt a thermodynamically stable, pseudo-octahedral coordination geometry (D_3); and, being a second row transition metal,

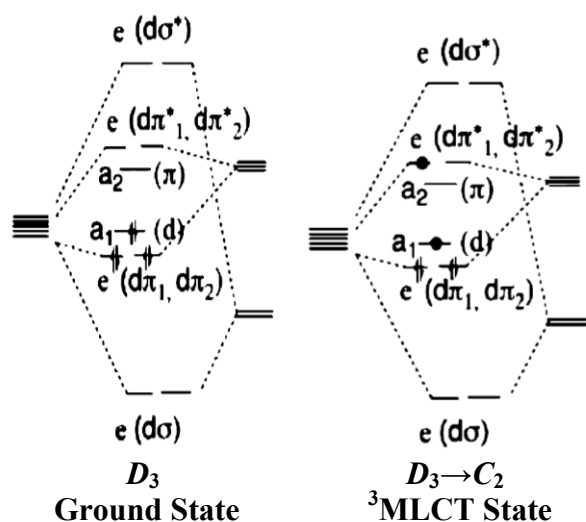


Figure 1.4. Molecular orbital diagrams of the pseudo-octahedral, low spin d^6 $[\text{Ru(II)L}_3]$ ground and low spin d^5 $[\text{Ru(III)L}_3^*]$ excited states. Although the geometry changes due to the localization of the excited electron, the actual coordination geometry does not change dramatically. Adapted from ref 46.

symmetry changes due to the localization of the excited electron onto one of the three L ligands on the vibrational timescale; however, there is little change in the molecular orbital configuration and, therefore, the coordination geometry remains essentially constant as seen in Figure 1.4.^{24,45,46} Therefore, the reorganizational energy (λ) upon photoexcitation is modest, and does not have a large influence on the ET dynamics in $[\text{Ru(II)L}_3]$ complexes.

CS Formation in $[\text{Ru(II)L}_3]$ D-C-A Complexes

As discussed previously, the photophysical properties of $[\text{Ru(II)L}_3]$ complexes make them excellent as chromophores in D-C-A/C-A assemblies: (1) they have large molar absorptivities in the visible spectrum ($\epsilon \approx 10^3\text{-}10^5 \text{ L}\cdot\text{mol}^{-1}\text{cm}^{-1}$), (2) the first excited state is the MLCT and is long-lived enough that the forward electron transfer to the CT state is favored over emission/non-radiative decay, (3) up to 70% of the $^3\text{MLCT}$ energy can be retained in the CS at λ_{max}

the complexes are kinetically inert to ligand substitution.^{44,45} Therefore, once an acceptable method is determined for forming the desired D-C-A structure, purification and isolation of $[\text{Ru(II)L}_3]$ D-C-A complexes is possible.

Upon photoexcitation, an electron from the low-spin, d^6 $[\text{Ru(II)L}_3]$ ground state is first promoted to $^1\text{MLCT}$ state and quickly intersystem crosses to the low-spin, d^5 $^3\text{MLCT}$ excited state with C_2 symmetry. The

and (4) once formed, the CS lifetimes are relatively long (100-300 ns) and, because of spin-chemical considerations, can be lengthened dramatically in the presence of a moderate magnetic field (2 μ s, 500 mT).⁵ Furthermore, the quantum efficiency for the CS is very high for almost all of the [Ru(II)L₃] D-C-A complexes similar to the one shown in Figure 1.2.⁴⁻⁶

Several decades of research has been performed on [Ru(II)L₃] C-A and C-D diads (where D=azine (PXZ) type donor unit and A= methyl viologen (MV), mono-quaternary (MQ), or di-quaternary amine (DQ) type acceptor unit) to understand the CS mechanism in the D-C-A triad complexes. These diad studies, as well as the studies on the D-C-A triads themselves, identified the key factors that enable [Ru(II)L₃] D-C-A complexes to separate charge so efficiently, with only modest energetic loss. As demonstrated in Figure 1.5, a number of competing ET processes are involved in the formation of a CS/CT in [Ru(II)L₃] D-C-A, C-A, and C-D complexes, and the relative rates of these ET processes determine if the CS/CT state is formed, the efficiency of formation, and its lifetime.⁵

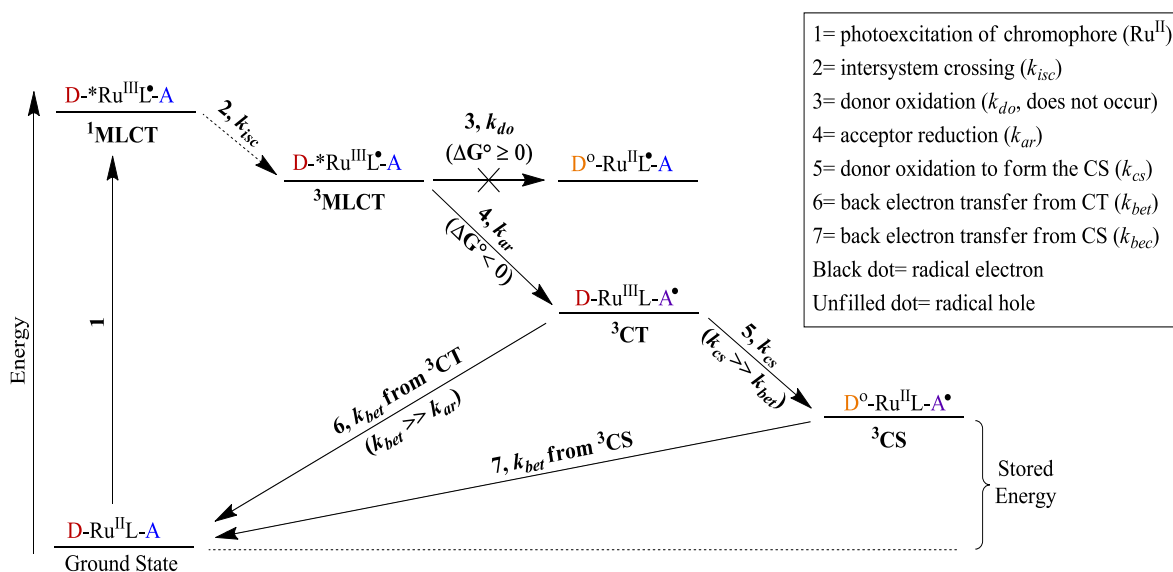


Figure 1.5. A simple representation of the competing electron transfer processes in [Ru(II)L₃] D-C-A triads. Adapted from refs 1 and 11. Considerations of spin-chemical issues have been ignored (see below).

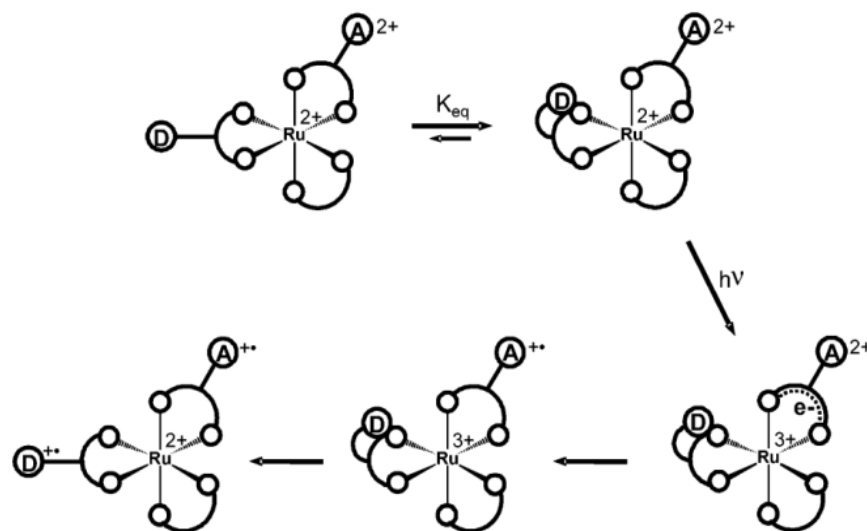
The electron transfer processes in D-C-A triads as well as C-A and C-D diads can be described as a sequence of ET reactions as shown in equations 1.1-1.3 below:



After initial photoexcitation and ISC to the $^3\text{MLCT}$, the rate of reductive quenching, i.e. donor oxidation, is slow ($k_{do} \approx 10^6 \text{ s}^{-1}$) relative to the rate of oxidative quenching, i.e. acceptor reduction ($k_{ar} = 10^7\text{-}10^{10} \text{ s}^{-1}$) with diads of similar linkage lengths.^{4,5} This is due to the ΔG for donor oxidation being small (0-0.1 V) relative to the ΔG for acceptor reduction (0.2-0.4 V) and both are in the Marcus normal region¹¹ However, despite the difference in the rates of forward ET for oxidative and reductive quenching, $k_{bet} \gg k_{do}$ and k_{ar} , which is evidenced by the fact that the $\text{C}^-\text{-D}^{+\circ}$ and $\text{C}^-\text{-A}^\bullet$ products are not detected in nanosecond transient absorption (TA) spectroscopy experiments.^{4,5} These data indicate that in the D-C-A triad systems, the first step in the ET mechanism (after photo-excitation and ISC) is always oxidative quenching of the $^3\text{MLCT}$ state and $k_{cs} \gg k_{bet}$ from the $\text{C}^-\text{-A}^\bullet$ intermediate.^{4,5,11,14}

Studies on the relationship between the rates of ET and the linkage between the C-A and C-D units (i.e., the number of methylene units in the bridge) revealed that the k_{do} decreased slightly with increasing linkage length between C and D units ($k_{do} = 5 \times 10^6$ to $1 \times 10^6 \text{ s}^{-1}$), but k_{ar} decreased by several orders of magnitude ($k_{ar} = 10^{10}$ to 10^7).^{4,5} Furthermore, the k_{ar} for the C-A diads is essentially the same as in the corresponding D-C-A triads incorporating the same acceptor and linkage length. However, as stated above, the k_{bet} in C-A diads (and thus presumably their corresponding D-C-A triads) is always much greater than k_{ct} , independent of linkage length.^{4,5} Since CS formation in $[\text{Ru}(\text{II})\text{L}_3]$ D-C-A triads occurs with ca. $\Phi_{cs} = 1$, these results imply that

Scheme 1.1. A pictorial representation of the donor pre-association (DPA) mechanism. Reproduced from ref 5.



k_{cs} must be significantly larger than k_{bet} despite the fact that the driving force for CS formation is considerably smaller than BET.

Additional studies on the association complexes between free D in solution and C-A

diads indicate that a ground state van der Waals association exists between the D and C (donor/chromophore pre-association = DPA) moieties. Since the π -systems of D and C are in “direct contact,” the electronic coupling between D and C is enhanced, causing the rate of forward ET to the CS state to be much faster than recombination ($k_{cs} \gg k_{bet}$). The DPA mechanism, shown in Scheme 1.1, enables the Φ_{cs} to approach unity regardless of driving force; therefore a system can be designed to have a large Φ_{cs} without forfeiting the amount of energy stored in the CS. Furthermore, the last ET step in CS formation causes the DPA to be broken due to electrostatic repulsion between the positively charged C and the oxidized D, eliminating a “strong coupling” pathway for CS recombination and leading to longer CS lifetimes.^{4,5,11} Since the last step in the DPA mechanism (k_{cs}) depends only on the association between the donor and the chromophore ligands in [Ru(II)L₃] complexes, it is reasonable to expect that a similar association would occur in related metal-polypyridyl complexes such as [Cu(I)P₂] based D-C-A analogs.

Redox Chemistry of [Ru(II)L₃] Complexes

Another aspect of [Ru(II)L₃] complexes that makes them excellent frameworks for D-C-A construction is their well-defined, solvent independent redox chemistry.⁴⁴ As is typical of excited state species, [Ru(II)L₃]⁺² complexes (where L = 4,4'-bipyridine) are both stronger oxidants and reductants in the excited state, due to the excited state having a greater amount of energy than the ground state, as shown in

Figure 1.6.^{25,47} However, in the ground state [Ru(III)L₃] is a strong oxidant and [Ru(I)L₃] is a strong reductant, which makes these complexes excellent candidates for D-C-A's given their in-

herent potential to successfully undergo photo-induced electron transfer reactions.

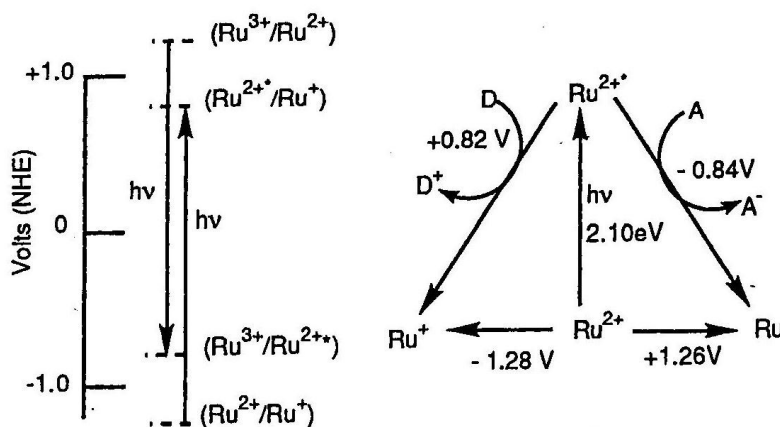


Figure 1.6. The solvent independent ground and excited state redox potentials of [Ru(II)L₃] complexes. As can be seen, ground state [Ru(II)L₃] complexes are potent oxidant and reductants, whose redox potentials are enhanced in the excited state. Reproduced from ref 44.

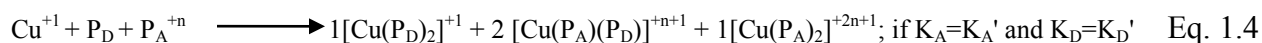
1.3. Characteristics of [Cu(I)P₂] Complexes

The critical parameters affecting the ET processes in [Ru(II)L₃] D-C-A complexes have heavily influenced the design of novel [Cu(I)P₂] D-C-A complexes in the current research. However, when switching to a different metal/ligand architecture with a completely different d-electron configuration, the design challenge is not always as straightforward as it may seem. Mimicking the formation of a CS in an analogous manner to the [Ru(II)L₃] D-C-A's also requires the designer to account for specific characteristics of [Cu(I)P₂] complexes that can seri-

ously influence the rates and probabilities of each ET step. Although [Cu(I)P₂] complexes are promising for novel D-C-A infrastructures, there are many nuances (e.g. relative to the [Ru(II)L₃] analogs) to these systems that could notably influence their performance in a D-C-A.

Coordination Chemistry of [Cu(I)P₂] in the Ground and Excited states

Unlike [Ru(II)L₃] complexes, [Cu(I)P₂] complexes are kinetically labile. In the strategy we have chosen to follow, [Cu(I)P₂] D-C-A complexes are heteroleptic by nature, because the two P ligands aren't identical: one P ligand is appended with a donor (P_D) and the other P ligand with an acceptor moiety (P_A). Therefore, synthesis and isolation of a pure heteroleptic [Cu(I)P₂] D-C-A complex has proven a very difficult task in the literature, and often synthetic procedures result in inseparable mixtures of homoleptic (P ligands are identical) and heteroleptic species as shown in equation 1.4 below.^{48,49}



In order to successfully synthesize a “pure” heteroleptic [Cu(I)P₂] complex in solution the ligands must be designed so that the thermodynamic equilibrium favors the formation of the heteroleptic complex over the homoleptic options. Thermodynamic rather than kinetic control is essential because the ligand substitution is very fast in these complexes. Fortunately, modulation of the product distribution (and therefore the binding constants: K_A, K_A', K_D, K_D', where the prime indicates binding of the second ligand) can, in principle, be achieved by alteration of the electrostatic and steric properties of the ligands, which has been demonstrated by the work on [Cu(I)P(POP)]⁺ complexes (in which POP = bis-[2-(diphenylphosphino)-phenyl]ether) by McMillan and coworkers¹⁹ and the sterically locked [Cu(I)P₂] complexes reported by Schmittel and coworkers.^{19,21,49–55}

Since the primary factors that influence the formation of a heteroleptic $[\text{Cu(I)P}_2]$ complex are electrostatics and the size of the substituents on the 2,9 positions of the 1,10-phenanthrolines, the binding constant of the second P ligand (K_A' and K_D') is significantly influenced by the steric and electronic environment imposed by the first P ligand.⁴⁸ Using this logic, once the P ligand with bulkier substituents on the 2,9-positions is coordinated to Cu(I) the binding constant of a second, less bulky P ligand should be enhanced relative to the binding of a second bulky ligand. Consequently, the P_A and P_D ligands can, in principle, be designed such that the D-C-A will self-assemble in solution into thermodynamically stable and sterically locked complexes.^{21,49,51-53} Alternatively, if the ligands are not sterically locked, then ligands can be designed so their electrostatic properties make the D-C-A the most thermodynamically favorable configuration; thus, even if the ligands scramble in solution they always end up as the D-C-A triad rather than a statistical mixture (50% D-C-A triad, 25% C-A diad and 25% C-D diad).

CT and CS Formation in $[\text{Cu(I)P}_2]$ C-A and D-C-A Complexes

Extensive studies on the photo-physical ET behavior of $[\text{Cu(I)P}_2]$ indicate that coordination and structural characteristics are critical in the design of functional $[\text{Cu(I)P}_2]$ D-C-A and C-A complexes.^{17,23,25,56-61} A key factor that has been identified for $[\text{Cu(I)P}_2]$ complexes (and is essentially not an issue for $[\text{Ru(II)L}_3]$) is the influence of photo-induced structural reorganization on ET behavior and redox properties.^{17,21-23,25,26,54,60} As shown in Figure 1.7, when $[\text{Cu(I)P}_2]$ complexes undergo photo-initiated excitation, an electron in the $3d^{10}$, D_{2d} ground state is promoted to the FC-¹MLCT excited state, resulting in a $3d^9$ complex with local D_{2d} geometry. At this point, unevenly occupied, degenerate e orbitals in the FC-¹MLCT state induce a “flattening” Jahn-Teller distortion which results in D_2 excited state symmetry.^{26,61-63}

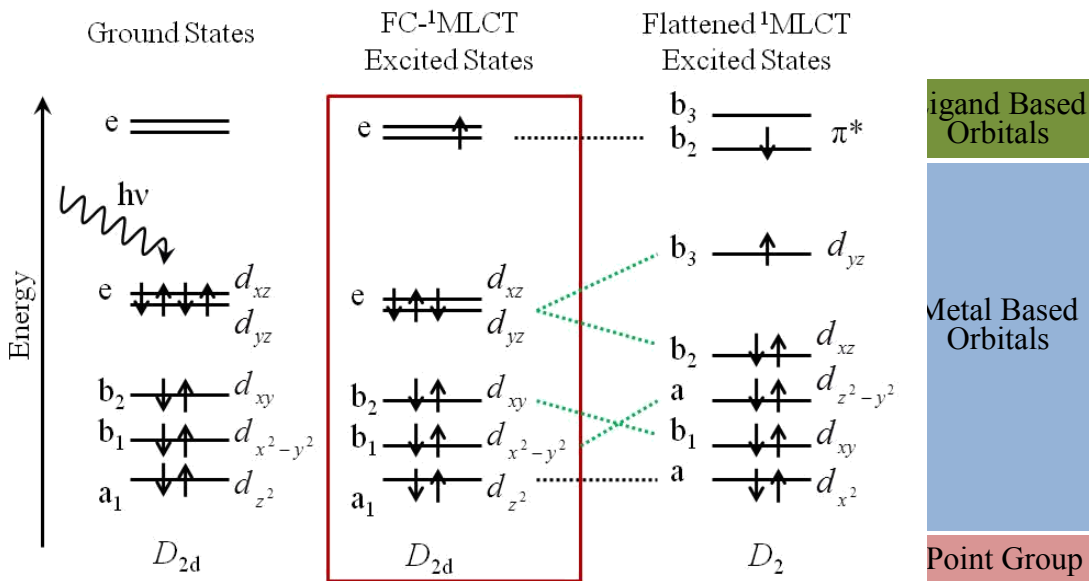


Figure 1.7. Flattening Jahn-Teller distortion in $[\text{Cu}(\text{I})\text{P}_2]$ complexes. In contrast to the $[\text{Ru}(\text{II})\text{L}_3]$ complexes, there is a large degree of structural reorganization that occurs during the process of photo-excitation in $[\text{Cu}(\text{I})\text{P}_2]$ complexes. Adapted from refs 26, 61, and 63.

Previous research has shown that Jahn-Teller (J-T) distortion and subsequent exciplex formation via solvent/counterion adduction in the excited (MLCT) state of these $[\text{Cu}(\text{I})\text{P}_2]$ complexes can reduce the amount of energy in the excited state and increase the rate of non-radiative relaxation (k_{nr}) in accordance with the energy gap law.^{17,18,23,56,58,59,64,65} Figure 1.8 demonstrates how exciplex formation effectively stabilizes the MLCT state, facilitates non-radiative relaxation, and reduces the driving force for forward ET.^{23,57-59} Conversely, if the rate of forward electron transfer to the ^3CT state is faster than the rate of non-radiative relaxation, then the J-T distorted geometry and subsequent solvent adduction can be beneficial.^{22,23,66} In the ^3CT state, the metal has been formally oxidized to Cu(II) so the preferred geometry is penta-coordinate (or even hexa-coordinate). Thus, these coordination changes stabilize the solvent adducted complex and impose a significant reorganizational energy barrier for returning to the Cu(I), tetrahedral ground state. In turn, this decreases k_{bet} and increases the lifetime of the ^3CT state.^{22,23,35,66} Applying this argument to the specific case of a D-C-A assembly, in the ^3CS state,

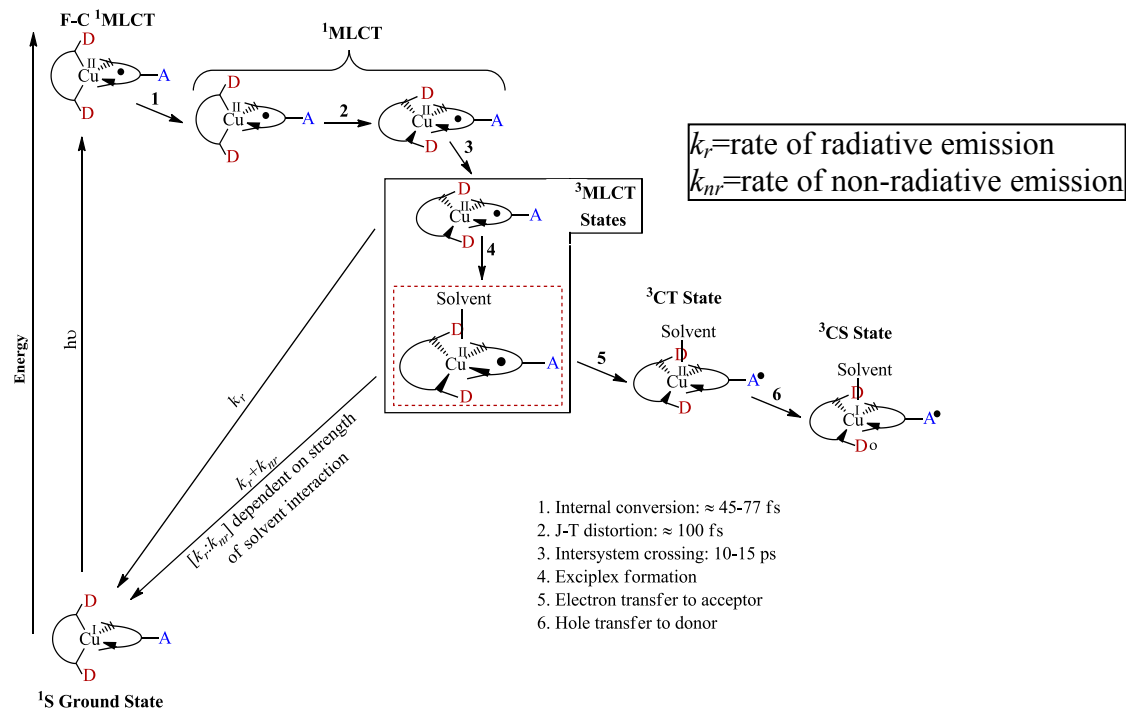


Figure 1.8. Jahn Teller distortion and exciplex formation in $[\text{Cu}(\text{I})\text{P}_2]$ complexes. The J-T distortion in F-C $^1\text{MLCT}$ state causes slow ISC to the $^3\text{MLCT}$ manifold. Solvent coordination to form the exciplex in the $^3\text{MLCT}$ states quenches the excited state of sterically unrestricted $[\text{Cu}(\text{I})\text{P}_2]$ complexes. The black dot represents a radical electron and the circle a radical hole. The listed timescales are for $[\text{Cu}(\text{dmp})_2]^+$. Adapted from ref 23.

after the copper is reduced back to Cu(I) via the oxidation of the donor, the preferred coordination geometry is again tetrahedral and the solvent/counterion adduct must be removed for the complex to re-configure the D_{2d} geometry. Therefore, solvent adduction is not as likely to occur and should not have a significant effect on k_{bet} from the CS state, since the singlet Cu(I) ground state also prefers tetrahedral geometry.

Substituents in the 2,9 position of the phenanthroline influences k_{nr} by limiting the degree of J-T distortion that can occur, and therefore the dihedral angle between the two phenanthroline ligand planes (i.e. flattening). If the substituents are large enough the steric restrictions can become so great that the flattening distortion and exciplex formation/solvent adduction cannot occur because the geometry is forced to remain essentially tetrahedral in the excited and CT states.^{17,62} This situation can have some significant advantages. In a study on $[\text{Cu}(\text{dtbp})_2]^+$ where dtbp = 2,9-di-*tert*-butyl-1,10-phenanthroline), Gothard et al. noticed that the UV-vis spec-

trum lacked a low energy shoulder present in the spectrum at ≈ 525 nm for the less sterically encumbered $[\text{Cu}(\text{dmp})_2]^+$ (dmp=2,9-dimethyl-1,10-phenanthroline), and there was no sub-picosecond rise or blue shift in the transient absorption (TA) spectra.⁶² Both observations were interpreted as an indication of the lack of flattening distortion, the former in the ground state and the latter in the MLCT state. The authors also report that $[\text{Cu}(\text{dtbp})_2]^+$ has a ³MLCT photoluminescence lifetime that is ca. 10x longer for than $[\text{Cu}(\text{dmp})_2]^+$ (1.9 μs and ≈ 100 ns, respectively, in weakly coordinating solvents) and retains more of the initial MLCT state energy due to the lack of MLCT stabilization due to flattening.⁶² Since the flattening is not occurring in these complexes, the energy gap between the ¹MLCT and ³MLCT states was reduced from ≈ 1800 - 2000 cm^{-1} to ≈ 790 cm^{-1} , which increases the rate of ISC and could have important implications in the spin-chemical issues discussed later.

However, when imposing such extreme steric requirements on $[\text{Cu}(\text{I})\text{P}_2]$ complexes there is a price. In the case of $[\text{Cu}(\text{dtbp})_2]^+$ the average Cu-N bond length (2.11 Å) is significantly longer than in less restricted $[\text{Cu}(\text{I})\text{P}_2]$ complexes (2.02-2.08 Å); therefore, the increased steric bulk destabilizes both the ground and excited states. Consequently, the binding constant of the second dtbp ligand is small and specific, air-free techniques must be used to synthesize the complex and coordinating solvents must be avoided. Also, sample degradation was reported during experimentation.^{50,62} Furthermore, evidence of structural changes (other than J-T distortion) were also implied in the study, but cited as a topic for future examination.⁶² Results from this study suggest that ligand architectures incorporating a moderately high degree of steric hindrance, but not quite as extreme as is imposed by t-butyl groups, might be optimal.

Therefore, ligand design is crucial to the functionality of D-C-A/C-A assemblies based on $[\text{Cu}(\text{I})\text{P}_2]$ complexes. The ligands must be able to affect the reorganizational energy enough

such that they hinder the k_{nr} pathways in the $\text{Cu(I)}^* \text{ }^3\text{MLCT}$, but still allow some degree of geometrical flexibility. As mentioned previously, steric hindrance imposed by bulky ligands (typically, with substituents the 2,9-positions on the 1,10-phenanthroline ligand) has been used to successfully decrease J-T distortion in the MLCT and increase the excited state lifetimes in $[\text{Cu(I)P}_2]$ complexes.^{17–19,50,54,56} Following this strategy, it should be possible to optimize the CT and CS lifetimes by incorporating appropriately bulky ligands.

The degree of J-T distortion in $[\text{Cu(I)P}_2]$ complexes permitted by the ligands also has considerable effects on the $\text{Cu}^{+2/+1}$ redox potential.^{27,54,67,68} This is an extremely important point because, for CS formation to occur, the $\text{D-C}^{+*}\text{-A}^{2+}$ excited state first reduces the acceptor to form the $\text{D-Cu}^{2+}\text{-A}^{+}$ CT state, which is followed by oxidation of the donor by Cu^{2+} :



Fortunately, $[\text{Cu(I)P}_2]^*$ is a virulent reductant so acceptor reduction should be facile ($\text{Cu}^{+2/+1*}$: $E_{1/2} \approx -1.4 \text{ V}^c$ for $[\text{Cu(dmp)}_2]^+(\text{PF}_6^-)$).^{45,60,69} However, the ground state $\text{Cu}^{+2/+1}$ oxidation potential is mild ($E_{1/2} \approx 0.64 \text{ V}$ (vs Ag/AgNO_3) in $0.1 \text{ M TBA}^+\text{PF}_6^-/\text{CH}_2\text{Cl}_2$) and solvent dependent.⁶⁹ The strong solvent dependence has been interpreted as a function of structural reorganization (and associated energy) necessary to go from a penta-coordinate, D_2 (Cu^{2+}) to a pseudo-tetrahedral, D_{2d} structure (Cu^+).^{27,67,68,70} Thus, selection of a donor moiety with an appropriate redox potential is crucial for successful CS formation, and finding an organic donor moiety capable of being oxidized by $\text{Cu}^{+2/+1}$ has been a significant challenge in $[\text{Cu(I)P}_2]$ D-C-A research.^{25,45,60,69,71}

^c The excited state potentials are calculated using the following formula: $E_{1/2}^{* \text{ox}} = E_{1/2}^{\text{ox}} - \Delta G_{\text{es}}$.⁶⁹

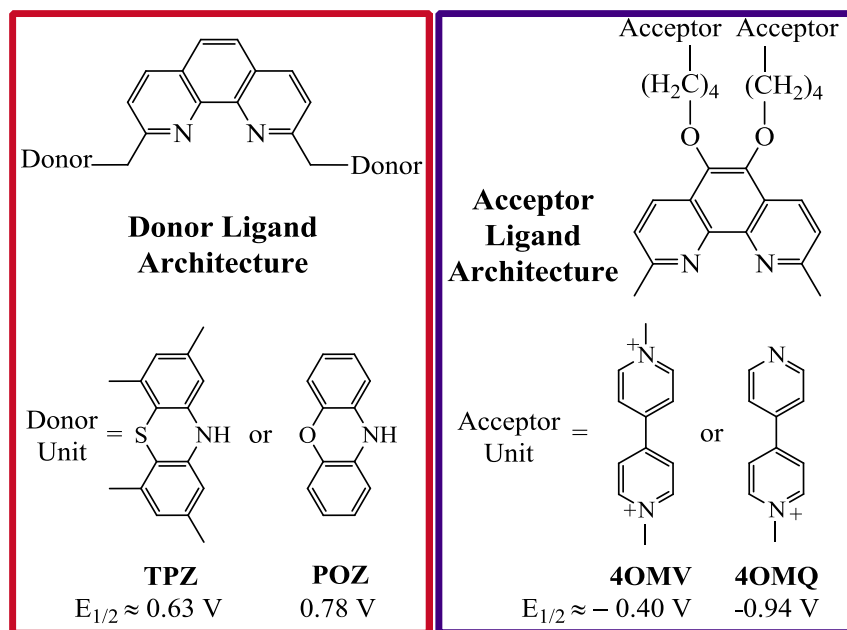


Figure 1.9. The donor and acceptor ligands used for the [Cu(I)P₂] C-A diads and D-C-A triads. The coordination geometry about Cu(I) should be approximately tetrahedral in the ground state. The redox potentials shown are for the 2,9-bis(donor)-1,10-phenanthroline and 2,9-dimethyl-1,10-phenanthroline-5,6-bis(butoxy(acceptor)) and were measured vs a sodium saturated calomel electrode (SSCE).

Other than the unpublished results of Odobel and coworkers mentioned in a footnote above, the only examples of functioning [Cu(I)P₂] containing D-C-A's have circumvented the issue of mild Cu^{2+/1+} oxidation potential by using a

Zn(II) porphyrin complex as the primary chromophore and electron donor.³¹⁻⁴⁰

However, a complex set of energy and electron transfers occur in these systems often resulting in several CT and CS states that are nearly isoenergetic due to nearly identical oxidation potentials of the [Cu(phen)₂]⁺ catenate/rotaxane and Zn(II) porphyrin employed. The authors of these studies suggest that the CT and CS states in their D-C-A system may be in rapid equilibrium and the CS state is in some cases the minor product (based on ratio of products calculated using the A values obtained from fits of the TA data).³¹⁻⁴⁰ Other attempts were made to use ferrocene as the donor moiety, but these complexes only resulted in CT product and no CS could be detected.^{55,71,72}

In this research, azine type donor moieties were chosen due to their inherently favorable redox potentials which can be altered via structural modification as depicted in Figure 1.9. Addition of electron withdrawing/donating groups onto the PXZ ring or changing the X group can

shift the $D/D^+ E_{1/2}$ by several hundred millivolts.⁷³ Furthermore, placing the donors in the 2,9-position of the 1,10-phenanthroline increases the steric bulk of the ligand architecture, which can alter the redox potential of the $Cu^{2+/1+}$ wave as described above. Therefore, using this type of D should enable the redox properties to be tuned so that CS formation can occur.

Clearly, the structure of the ligands in $[Cu(I)P_2]$ complexes has a significant impact on the ET processes that occur during the CS/CT formation. Moreover, controlling the steric restrictions imposed on the Cu(I) coordination sphere can determine the equilibrium distribution of complexes present in solution as has been discussed. Therefore, the ligand design and synthesis comprises a significant portion of this research.

Design of $[Cu(I)P_2]$ D-C-A's for this Project

Having considered the background literature for $[Ru(II)L_3]$ D-C-A systems (DPA mechanism) and the various structural (and other) challenges presented by $[Cu(I)P_2]$ (thermodynamically favoring the D-C-A and/or stability toward ligand substitution, J-T distortion, solvent adduction, and structurally modulated redox potentials), the $[Cu(I)P_2]$ complexes shown in Figure 1.9 were designed for novel D-C-A triad architectures. The azine type donor moieties were chosen due to their steric bulk, favorable redox potentials and synthetic accessibility. Methyl viologen and mono-quaternary amine type acceptors were selected due to the literature precedence for synthetic preparation as well as their favorable redox potentials.^{10-12,14,74}

There are several noteworthy design aspects of the complexes shown in Figure 1.9. First, flexible methylene linkages were incorporated between the donor unit and the P ligand in order to facilitate the same type of D/C orbital coupling responsible for the DPA mechanism in the $[Ru(II)L_3]$ D-C-A triads (i.e., π -stacking between the donor and phenothiazine). Assuming that

the [Cu(I)P₂] complexes follow the same DPA mechanism, incorporating this type of structure should enable [Cu(I)P₂] complexes to form a CS with high quantum efficiency ($\Phi_{CS} \rightarrow 1$). Furthermore, bulky substituents are incorporated into the 2,9-positions of the P ligands (D or phenyl groups). Since the donor units used in this study are composed of conjugated ring systems, in principle, they can π -stack with the second phenanthroline ligand in pseudo-tetrahedral coordination geometry. The π -stacking interactions as well as the imposed steric bulkiness of the donor unit is intended to push the formation equilibrium in favor of self-assembling the heteroleptic D-C-A triad complex in solution, as previously discussed. Theoretically, these substituents will also crowd the [Cu(I)P₂] center, inhibiting the k_{nr} deactivation pathways from the MLCT so there is negligible emission quenching, yet not be too bulky, so the binding constant of the second (acceptor) phenanthroline ligand is favored.

Spin-Considerations and the Magnetic Field Effect (MFE) in [Cu(I)P₂] D-C-A/C-A Complexes

A final point of interest for the ³CS [Cu(I)P₂] D-C-A triads is their spin chemistry. In past studies, a magnetic field dependence of the ³CS lifetime (τ_{cs}) was demonstrated in [Ru(II)L₃] D-C-A/C-A's.^{5,7,13} A longer τ_{cs} provides more time to effectively use the energy stored in the CS. The average ³CS lifetime of [Ru(II)L₃] D-C-A's increased ten-fold in a relatively small applied magnetic field ($\tau_{cs} \approx 2 \mu\text{s}$, 0.5 T).^{6,7,13}

As mentioned previously, charge recombination occurs from the CS state to the ground state as the radical hole and radical electron recombine. The ground state is a singlet and MFE studies demonstrated that the CS state is a triplet (³CS); therefore, CS recombination (k_{bet}) is spin-forbidden.^{6,7,13} However, in the CS the radicals are “normal” organic radicals which are separated by a large distance; thus, the ¹CS and ³CS are nearly degenerate at zero field. Isotropic

hyperfine coupling (IHC) can mix ^1CS and ^3CS increasing the rate of intersystem crossing (k_{isc}) and providing a rapid, spin-allowed recombination pathway.^{6,7,13} Fortunately, the degree of mixing between the ^1CS and ^3CS states can be modulated by the application of a magnetic field which affects k_{isc} as shown in Figure 1.10.^{6,7,13}

In $[\text{Ru(II)L}_3]$ D-C-A's, magnetic field induced Zeeman splitting causes the $^3\text{CS(T}_+)$ and $^3\text{CS(T}_-)$ states to increase/decrease in energy enough that they exceed the influence of the IHC manifold, which makes mixing the ^1CS and ^3CS states much less efficient, thereby slowing the k_{isc} and the rate of overall recombination.^{6,7,13} The Zeeman splitting is manifested in the transient absorption (TA) decay profile as a change from mono-exponential decay at zero field to bi-exponential decay in an applied magnetic field. In this type of relaxation mechanism, the bi-exponential decay has a “fast,” field-independent decay component accounting for $\approx 1/3$ of the overall decay ($A_1 = A_1/(A_1+A_2) \approx 1/3$; $^3\text{CS(T}_0)$) and a “slow,” field-dependent decay component accounting for $\approx 2/3$ of the overall decay ($A_2 = A_2/(A_1+A_2) \approx 2/3$; $^3\text{CS(T}_+ + \text{T}_-)$).^{7,75}

Given that the magnetic fields necessary to enhance ^3CS lifetime in the $[\text{Ru(II)L}_3]$ D-C-A triads can be achieved with a handful of refrigerator magnets^d, this is a promising method for increasing the τ_{cs} .⁷⁸ If the same type of IHC applies to Cu(I) D-C-A complexes then small magnetic fields would be expected to increase the ^3CS lifetime. Furthermore, Cu(I) has less spin orbit coupling than Ru(II) ($\zeta_{\text{Ru(II)}} = 990 \text{ cm}^{-1}$, $\zeta_{\text{Cu(I)}} = 829 \text{ cm}^{-1}$) and structural distortions have been shown to significantly affect the ISC pathways between the $^1\text{MLCT}/^3\text{MLCT}$ states of $[\text{Cu(I)P}_2]$ complexes.^{61,79} Therefore, $[\text{Cu(I)P}_2]$ D-C-A's and C-A's have the potential to be very interesting systems for MFE studies.

^d The magnetic field of a normal refrigerator magnet is typically between 1-10 mT.^{76,77}

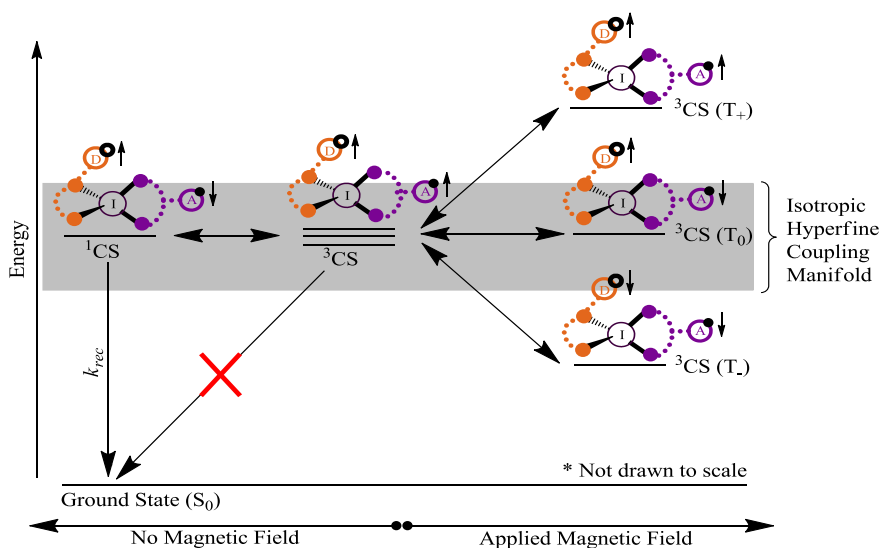


Figure 1.10. Radical pair relaxation mechanism proposed by Hayashi and Nagakura depicting the Zeeman splitting of the degenerate ^3CS energy levels in an applied magnetic field. Note that P_D and P_A are shown with only one donor and acceptor moiety for clarity. Modified from refs 6 and 7.

In the $[\text{Ru}(\text{II})\text{L}_3]$ diads the τ_{ct} is too short to for the CT to be detected by TA spectroscopy so the magnetic field effect on the CT of the $[\text{Ru}(\text{II})\text{L}_3]$ C-A complexes could not be explored.^{5,7,75} However, as mentioned above, the lesser degree of spin-orbit coupling (SOC) in Cu(I) should reduce the amount singlet/triplet mixing in the CT state, causing the τ_{ct} to be increased.⁸⁰ Spin considerations aside, the large reorganization energy involved in back electron transfer in the CT state for $[\text{Cu}(\text{I})\text{P}_2]$ C-A systems apparently results in a much longer lifetime than for $[\text{Ru}(\text{II})\text{L}_3]$ based diads—sufficiently so, that MFE studies are possible.

The Zeeman splitting described above will also occur in the ^3CT of C-A diads. However, when spin states are mixed via IHC interactions, the energy difference between the singlet and triplet states increases as the distance between the radical species decreases.⁸⁰ In the C-A diads presented herein (and in $[\text{Ru}(\text{II})\text{L}_3]$ diads) the separation between the radicals is generally smaller, which can potentially cause the singlet-triplet energy gap to be large enough that the IHC interactions cannot mix the two states. Furthermore, the hole resides in a metal-based orbital which could be subject to significant SOC interactions. Although Cu(I) has smaller SOC than

Ru(II), the SOC of metal based orbitals is usually much larger than ligand based orbitals. Irrespective of the exact mechanism, as will be discussed later τ_{ct} is usually unaffected by small/moderate magnetic fields ($\beta < 1$ T).

One factor that may influence the MFE in [Cu(I)P₂] D-C-A and C-A complexes is the presence of at least two thermally equilibrated, emissive MLCT states. These two MLCT states have been identified as the lowest excited ¹MLCT and ³MLCT states, which are separated by ≈ 1800 - 2000 cm⁻¹.^{45,56,60,81} According to the literature, despite the smaller radiative rate constant (¹MLCT: $k_r \approx 10^7$ s⁻¹ vs ³MLCT: $k_r \approx 10^3$ s⁻¹), the ³MLCT has a greater population suggesting the triplet state is responsible for the relevant ET processes, which is analogous to [Ru(II)L₃] complexes.^{15,25,45,60}

However, the presence of multiple MLCT states may be relevant to the MFE on the τ_{cs}/τ_{ct} and initial TA intensities, especially for the C-A diad complex which is expected to undergo a larger degree of J-T distortion than the D-C-A. Several groups have determined by quantum mechanical calculations and spectroscopic techniques that J-T distortion in [Cu(dmp)₂]⁺ causes the MOs with the smallest degree of SOC to be destabilized (¹MLCT) and the MLCT state with the largest SOC to be stabilized (FC-MLCT and lowest lying ³MLCT).^{23,62-64} The stabilization of the lowest lying ³MLCT state imparted by the flattening distortion may mean that when in the presence of a magnetic field the Zeeman splitting of the ³MLCT state could alter the rate of ISC between the ¹MLCT and ³MLCT. This change in the rate of ISC could influence the relative population of the two MLCT states and therefore the relative population of the ¹CT and ³CT states. If an applied magnetic field causes a portion of the ET to the CS/CT state to derive from the ¹MLCT state then a significant amount of ¹CS/¹CT could be produced in conjunction with the proposed ³CS/³CT. Since the ground state is also a singlet, the presence of ¹CS/¹CT would facili-

tate electron-hole recombination, thereby decreasing the ^1CS lifetime relative to ^3CS . As mentioned above, a shift in the population of the $^1\text{CS}/^1\text{CT}$ and $^3\text{CS}/^3\text{CT}$ states, could affect changes in the initial TA intensities. Since J-T distortion plays a key role in the modulation of the MLCT manifold, ligand design may also be a key factor in controlling the amount of influence multiple MLCT states has on the MFE in the $[\text{Cu}(\text{I})\text{P}_2]$ D-C-A/C-A triads and diads.

References

- (1) Gust, D.; Moore, T. A. *Science* **1989**, *244*, 35–41.
- (2) Wasielewski, M. R. *J. Org. Chem.* **2006**, *71*, 5051–5066.
- (3) Barber, J.; Andersson, B. *Nature* **1994**, *370*, 31–34.
- (4) Larson, S. L.; Elliott, C. M.; Kelley, D. F. *J. Phys. Chem.* **1995**, *99*, 6530–6539.
- (5) Weber, J. M.; Rawls, M. T.; MacKenzie, V. J.; Limoges, B. R.; Elliott, C. M. *J. Am. Chem. Soc.* **2007**, *129*, 313–320.
- (6) Rawls, M. T.; Kollmannsberger, G.; Elliott, C. M.; Steiner, U. E. *J. Phys. Chem. A.* **2007**, *111*, 3485–3496.
- (7) Klumpp, T.; Linsenmann, M.; Larson, S. L.; Limoges, B. R.; Bürssner, D.; Krissinel, E. B.; Elliott, C. M.; Steiner, U. E. *J. Am. Chem. Soc.* **1999**, *121*, 1076–1087.
- (8) Gust, D.; Moore, T. A.; Moore, A. L. *Acc. Chem. Res.* **1993**, *26*, 198–205.
- (9) Meyer, T. J. *Acc. Chem. Res.* **1989**, 163–170.
- (10) Cooley, L. F.; Headford, C. E. L.; Elliott, C. M.; Kelley, D. F. *J. Am. Chem. Soc.* **1988**, *110*, 6673–6682.
- (11) Cooley, L. F.; Larson, S. L.; Elliott, C. M.; Kelley, D. F. *J. Phys. Chem.* **1991**, *95*, 10694–10700.
- (12) Elliott, C. M.; Freitag, R. A.; Blaney, D. D. *J. Am. Chem. Soc.* **1985**, *107*, 4647–4655.
- (13) Klumpp, T.; Linsenmann, M.; Larson, S. L.; Limoges, B. R.; Buerstner, D.; Krissinel, E. B.; Elliott, C. M.; Steiner, U. E. *J. Am. Chem. Soc.* **1999**, *121*, 4092.
- (14) Larson, S. L.; Cooley, L. F.; Elliott, C. M.; Kelley, D. F. *J. Am. Chem. Soc.* **1992**, *114*, 9504–9509.
- (15) Lavie-Cambot, A.; Cantuel, M.; Leydet, Y.; Jonusauskas, G.; Bassani, D. M.; McClenaghan, N. D. *Coord. Chem. Rev.* **2008**, *252*, 2572–2584.
- (16) Robertson, N. *Chem. Sus. Chem.* **2008**, *1*, 977–979.
- (17) Cunningham, C. T.; Cunningham, K. L. H.; Michalec, J. F.; McMillin, D. R. *Inorg. Chem.* **1999**, *38*, 4388–4392.
- (18) Kovalevsky, A. Y.; Gembicky, M.; Coppens, P. *Inorg. Chem.* **2004**, *43*, 8282–8289.
- (19) Cuttell, D. G.; Kuang, S.-M.; Fanwick, P. E.; McMillin, D. R.; Walton, R. A. *J. Am. Chem. Soc.* **2002**, *124*, 6–7.
- (20) McMillin, D. R.; Buckner, M. T.; Ahn, B. T. *Inorg. Chem.* **1977**, *16*, 943–945.
- (21) Miller, M. T.; Gantzel, P. K.; Karpishin, T. B. *J. Am. Chem. Soc.* **1999**, *121*, 4292–4293.
- (22) Ruthkosky, M.; Kelly, C. A.; Zaros, M. C.; Meyer, G. J. *J. Am. Chem. Soc.* **1997**, *119*, 12004–12005.
- (23) Shaw, G. B.; Grant, C. D.; Shirota, H.; Castner Jr., E. W.; Meyer, G. J.; Chen, L. X. *J. Am. Chem. Soc.* **2007**, *129*, 2147.
- (24) Meyer, T. J. *Pure Appl. Chem.* **1986**, *58*, 1193–1206.
- (25) Armaroli, N. *Chem. Soc. Rev.* **2001**, *30*, 113–124.
- (26) Everly, R. M.; McMillin, D. R. *J. Phys. Chem.* **1991**, *95*, 9071–9075.
- (27) Cunningham, K. L.; Hecker, C. R.; McMillin, D. R. *Inorg. Chim. Acta* **1996**, *242*, 143–7.
- (28) Everly, R. M.; Ziessel, R.; Suffert, J.; McMillin, D. R. *Inorg. Chem.* **1991**, *30*, 559–61.
- (29) Eggleston, M. K.; McMillin, D. R.; Koenig, K. S.; Pallenberg, A. J. *Inorg. Chem.* **1997**, *36*, 172–176.
- (30) Armaroli, N.; Diederich, F.; Dietrich-Buchecker, C. O.; Flamigni, L.; Marconi, G.; Nierengarten, J.-F.; Sauvage, J.-P. *Chem.-Eur. J.* **1998**, *4*, 406–416.

- (31) Megiatto, J. D.; Schuster, D. I.; Abwandner, S.; De Miguel, G.; Guldi, D. M. *J. Am. Chem. Soc.* **2010**, *132*, 3847–3861.
- (32) Jakob, M.; Berg, A.; Levanon, H.; Schuster, D. I.; Megiatto, J. D. *J. Phys. Chem. C* **2011**, *115*, 24555–24563.
- (33) Jakob, M.; Berg, A.; Rubin, R.; Levanon, H.; Li, K.; Schuster, D. I. *J. Phys. Chem. A* **2009**, *113*, 5846–5854.
- (34) Flamigni, L.; Talarico, A. M.; Chambron, J.-C.; Heitz, V.; Linke, M.; Fujita, N.; Sauvage, J.-P. *Chem.-Eur. J.* **2004**, *10*, 2689–2699.
- (35) Megiatto, J. D.; Schuster, D. I.; De Miguel, G.; Wolfrum, S.; Guldi, D. M. *Chem. Mater.* **2012**, *24*, 2472–2485.
- (36) Schuster, D. I.; Li, K.; Guldi, D. M. *C.R. Chim.* **2006**, *9*, 892–908.
- (37) Li, K.; Bracher, P. J.; Guldi, D. M.; Herranz, M. Á.; Echegoyen, L.; Schuster, D. I. *J. Am. Chem. Soc.* **2004**, *126*, 9156–9157.
- (38) Li, K.; Schuster, D. I.; Guldi, D. M.; Herranz, M. Á.; Echegoyen, L. *J. Am. Chem. Soc.* **2004**, *126*, 3388–3389.
- (39) Linke, M.; Chambron, J.-C.; Heitz, V.; Sauvage, J.-P.; Encinas, S.; Barigelletti, F.; Flamigni, L. *J. Am. Chem. Soc.* **2000**, *122*, 11834–11844.
- (40) Chambron, J. C.; Harriman, A.; Heitz, V.; Sauvage, J. P. *J. Am. Chem. Soc.* **1993**, *115*, 7419–7425.
- (41) Bauld, N. L. *Radicals, ion radicals, and triplets : the spin-bearing intermediates of organic chemistry*; Wiley-VCH: New York, 1997.
- (42) Albinsson, B.; Martensson, J. *J. Photochem. Photobiol. C: Photochem. Rev.* **2008**, *9*, 138–155.
- (43) Moser, C. C.; Keske, J. M.; Warncke, K.; Farid, R. S.; Dutton, P. L. *Nature* **1992**, *355*, 796–802.
- (44) Kalyanasundaram, K. *Photochemistry of polypyridine and porphyrin complexes*; Academic Press: London; San Diego, 1992.
- (45) Scaltrito, D. V.; Thompson, D. W.; O’Callaghan, J. A.; Meyer, G. J. *Coord. Chem. Rev.* **2000**, *208*, 243–266.
- (46) Ardo, S.; Meyer, G. J. *Chem. Soc. Rev.* **2009**, *38*, 115.
- (47) Juris, A.; Balzani, V.; Barigelletti, F.; Campagna, S.; Belser, P.; Zelewsky, A. V. *Coord. Chem. Rev.* **1988**, *84*, 85–277.
- (48) Pallenberg, A. J.; Koenig, K. S.; Barnhart, D. M. *Inorg. Chem.* **1995**, *34*, 2833–2840.
- (49) Kalsani, V.; Schmittel, M.; Listorti, A.; Gianluca, A.; Armaroli, N. *Inorg. Chem.* **2006**, *45*, 2061–2067.
- (50) Gandhi, B. A.; Green, O.; Burstyn, J. N. *Inorg. Chem.* **2007**, *46*, 3816–3825.
- (51) Schmittel, M.; Michel, C.; Liu, S.-X.; Schildbach, D.; Fenske, D. *Eur. J. Inorg. Chem.* **2001**, 1155–1166.
- (52) Schmittel, M.; Ganz, A. *Chem. Commun.* **1997**, 999–1000.
- (53) Kalsani, V.; Bodenstedt, H.; Fenske, D.; Schmittel, M. *Eur. J. Inorg. Chem.* **2005**, 1841–1849.
- (54) Miller, M. T.; Gantzel, P. K.; Karpishin, T. B. *Angew. Chemie., Int. Ed.* **1998**, *37*, 1556–1558.
- (55) Armaroli, N.; Accorsi, G.; Bergamini, G.; Ceroni, P.; Holler, M.; Moudam, O.; Duhayon, C.; Delavaux-Nicot, B.; Nierengarten, J.-F. *Inorg. Chim. Acta* **2007**, *360*, 1032–1042.
- (56) Ichinaga, A. K.; Kirchoff, J. R.; McMillin, D. R.; Dietrich-Buchecker, C. O.; Marnot, P.

- A.; Sauvage, J. P. *Inorg. Chem.* **1987**, *26*, 4290–4292.
- (57) McMillin, D. R.; Kirchoff, J. R.; Goodwin, K. V. *Coord. Chem. Rev.* **1985**, *64*, 83–92.
- (58) Palmer, C. E. A.; McMillin, D. R. *Inorg. Chem.* **1987**, *26*, 3837–3840.
- (59) Palmer, C. E. A.; McMillin, D. R.; Kirmaier, C.; Holton, D. *Inorg. Chem.* **1987**, *26*, 3167–3170.
- (60) Ruthkosky, M.; Kelly, C. A.; Castellano, F. N.; Meyer, G. J. *Coord. Chem. Rev.* **1998**, *171*, 309–322.
- (61) Siddique, Z. A.; Yamamoto, Y.; Ohno, T.; Nozaki, K. *Inorg. Chem.* **2003**, *42*, 6366–6378.
- (62) Gothard, N. A.; Mara, M. W.; Huang, J.; Szarko, J. M.; Rolczynski, B.; Lockard, J. V.; Chen, L. X. *J. Phys. Chem. A* **2012**, *116*, 1984–1992.
- (63) Iwamura, M.; Takeuchi, S.; Tahara, T. *J. Am. Chem. Soc.* **2007**, *129*, 5248–5256.
- (64) Blaskie, M. W.; McMillin, D. R. *Inorg. Chem.* **1980**, *19*, 3519–3522.
- (65) Cunningham, C. T.; Moore, J. J.; Cunningham, K. L.; Fanwick, P. E.; McMillin, D. R. *Inorg. Chem.* **2000**, *39*, 3638–44.
- (66) Scaltrito, D. V.; Kelly, C. A.; Ruthkosky, M.; Zaros, M. C.; Meyer, G. J. *Inorg. Chem.* **2000**, *39*, 3765–3770.
- (67) Cunningham, K. L.; McMillin, D. R. *Inorg. Chem.* **1998**, *37*, 4114–4119.
- (68) Gushurst, A. K. I.; McMillin, D. R.; Dietrich-Buchecker, C. O.; Sauvage, J. P. *Inorg. Chem.* **1989**, *28*, 4070–2.
- (69) Ruthkosky, M.; Castellano, F. N.; Meyer, G. J. *Inorg. Chem.* **1996**, *35*, 6406–6412.
- (70) Bard, A. J.; Faulkner, L. R. *Electrochemical Methods*; John Wiley & Sons: New York, 1980; Vol. 1st.
- (71) Listorti, A.; Accorsi, G.; Rio, Y.; Armaroli, N.; Moudam, O.; Gégout, A.; Delavaux-Nicot, B.; Holler, M.; Nierengarten, J.-F. *Inorg. Chem.* **2008**, *47*, 6254–6261.
- (72) Megiatto, J. D.; Li, K.; Schuster, D. I.; Palkar, A.; Herranz, M. A.; Echegoyen, L.; Abwandner, S.; De Miguel, G.; Guldi, D. M. *J. Phys. Chem. B* **2010**, *114*, 14408–14419.
- (73) Montalti, M.; Murov, S. L. *Handbook of Photochemistry*; CRC/Taylor & Francis: Boca Raton, 2006.
- (74) Elliott, C. M.; Freitag, R. A. *J. Chem. Soc., Chem. Commun.* **1985**, 156–157.
- (75) Rawls, M. T.; Kollmannsberger, G.; Elliott, C. M.; Steiner, U. E. *J. Phys. Chem. A* **2007**, *111*, 3485–3496.
- (76) Yeh, D. UMBC, Department of Chemistry and Biochemistry <http://www.umbc.edu/nmr/safety.htm> (accessed Sep 13, 2012).
- (77) Palm, E. MagLab - MagLab Dictionary: Tesla (Transcript) <http://www.magnet.fsu.edu/education/tutorials/magnetminute/tesla-transcript.html> (accessed Sep 13, 2012).
- (78) Information on MRI Technique <http://www.nevusnetwork.org/mritech.htm>.
- (79) Murov, S. L.; Hug, G. L.; Carmichael, I. *Handbook of Photochemistry*; M. Dekker: New York, 1993.
- (80) Leffler, J. E. *An introduction to free radicals*; Wiley: New York, 1993.
- (81) Kirchoff, J. R.; Gamache, R. E.; Blaskie, M. W.; Paggio, A. A. D.; Lengel, R. K.; McMillin, D. R. *Inorg. Chem.* **1983**, *22*, 2380–2384.

Chapter 2

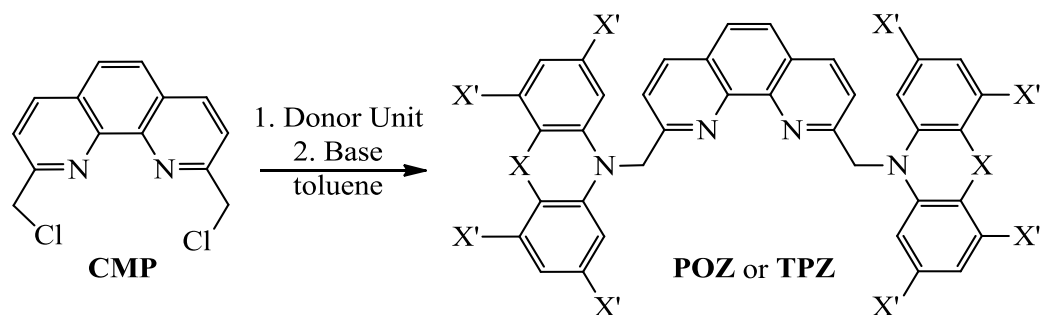
Experimental Methods

2.1. Synthetic Methods

Synthesis of Donor Appended 1,10-Phenanthroline Ligands

Other than the following exceptions, all starting materials and solvents were solvent grade or better, obtained from commercial sources, and used without further purification. The following dry solvents were all obtained from the Williams' group solvent system and used without further purification: toluene, dimethyl formamide (DMF), acetonitrile (ACN), and diisopropyl amine.

In order to make the donor ligand as shown in Figure 2.1, literature methods were used for the preparation of 2,9-bis(trichloromethyl)-1,10-phenanthroline, 2,9-bis(methoxycarbonyl)-1,10-phenanthroline, 2,9-bis(hydroxymethyl)-1,10-phenanthroline, 2,9-bis(chloromethyl)-1,10-phenanthroline (CMP), and 2,4,6,8-tetramethylphenothiazine (TPZ).^{1,2} The model heteroleptic



	<i>Donor Unit</i>	<i>Base</i>	<i>Molar Ratio (diCl:PXZ:Base)</i>	<i>X</i>	<i>X'</i>
POZ Ligand	POZ	K ⁺ <i>tert</i> -butoxide	1:4:4	O	H
TPZ Ligand	TPZ	K ⁺ bis(trimethylsilyl)amide	1:5:5	S	CH ₃

Figure 2.1. General synthesis of donor appended phenanthroline ligand.

Cu(I)P₂ complex with one donor ligand (POZ) and a 2,9-dimethyl-1,10-phenanthroline (DMP) ([Cu(I)(POZ)(DMP)]⁺) and control homoleptic Cu(I)P₂ coordination complexes ([Cu(I)(DMP)₂] and [Cu(I)(POZ)₂]) were synthesized based on literature procedures as discussed below.³⁻⁷

2,9-bis(trichloromethyl)-1,10-phenanthroline: This compound was synthesized based on synthetic methods detailed in the literature¹ yielding cream colored crystalline solids. ¹H NMR (300 MHz, CDCl₃, δ): 8.47 (d, 2H, 4,7-phen), 8.34 (d, 2H, 3,8-phen), 7.98 (s, 2H, 5,6-phen).

2,9-bis(methoxycarbonyl)-1,10-phenanthroline: This compound was synthesized based on synthetic methods detailed in the literature¹ yielding cream colored solids. ¹H NMR (300 MHz, d⁶-dmso, δ): 8.77 (d, 2H, 4,7-phen), 8.44 (d, 2H, 3,8-phen), 8.24 (s, 2H, 5,6-phen), 4.04 (s, 6H, CH₃).

2,9-bis(hydroxymethyl)-1,10-phenanthroline: This compound was synthesized from a literature procedure¹ yielding light yellow solids. ¹H NMR (300 MHz, CDCl₃, δ): 8.23 (d, 2H, 4,7-phen), 7.78 (s, 2H, 5,6-phen), 7.62 (d, 2H, 3,8-phen), 5.29 (broad s, 2H, -OH), 5.13 (broad s, 4H, -CH₂-OH).

CMP: 2,9-bis(chloromethyl)-1,10-phenanthroline: This compound was synthesized from a literature procedure¹ yielding white crystalline solids (needles). ¹H NMR (300 MHz, CDCl₃, δ): 8.34 (d, 2H, 4,7-phen), 7.97 (d, 2H, 3,8-phen), 7.85 (s, 2H, 5,6-phen), 5.12 (s, 4H, -CH₂-Cl).

TPZ Donor Unit: 2,4,6,8-tetramethylphenothiazine: This compound was synthesized from a literature procedure² yielding cream colored solids. ¹H NMR (300 MHz, CD₂Cl₂, δ): 6.56 (s, 2H, 3,7-TPZ), 6.24 (s, 2H, 1,9-TPZ), 5.70 (broad s, 1H, NH), 2.24 (s, 6H, TPZ-CH₃), 2.19 (s, 6H, TPZ-CH₃).

TPZ Donor Ligand: In a typical synthesis, a flask containing TPZ (0.36 g, 1.4 mmol) and K⁺ bis(trimethylsilyl)amide (0.28 g, 1.40 mmol) was charged with 25 mL dry toluene in the glove box and stirred for one hour. To the bright yellow-orange solution of deprotonated TPZ was slowly added CMP (0.076 g, 0.27 mmol). The dark brown reaction mixture was allowed to stir at room temperature for 1.5 h. The reaction flask was stoppered, brought out of the box, and immediately quenched with distilled water (5 mL) before exposing to air. The resulting burnt orange solution was filtered, and the filtrate was collected to which 30 mL distilled water was added. The aqueous solution was extracted with CH₂Cl₂ (30 mL, x2). The organic fraction was rinsed with brine, dried with Na₂SO₄ and dried in vacuo. The dry product mixture was re-dissolved in minimal CH₂Cl₂, filtered, and washed with hexanes to remove un-reacted TMPTZ. The organic filtrate was run through a short silica gel column (packed with hexanes, eluent: toluene). The product fractions were collected, the solvent removed in vacuo, and then recrystallized from isopropanol yielding a light yellow solid. (Yield = 40 %) ¹H NMR (300 MHz, CD₂Cl₂, δ): 8.20 (d, 2H, 4,7-phen), 7.80 (s, 2H, 5,6-phen), 7.71 (d, 2H, 3,8-phen), 6.69 (s, 4H, Ar-TPZ), 6.54 (s, 4H, Ar-TPZ), 5.58 (s, 4H, N-CH₂-N), 2.39 (s, 12H, TPZ-CH₃), 2.11 (s, 12H, TPZ-CH₃). HRMS: ESI/APCI-TOF *m/z* (relative intensity): [M+H]⁺ calcd for C₄₆H₄₃N₄S₂, 714.2924; found 715.2935. [M+Na]⁺ calcd for C₄₆H₄₂N₄NaS₂, 737.2743; found 737.2754.

POZ Donor Ligand: Glassware was dried in the oven at 250 °C for at least 12 h and cooled under Ar. The CMP starting material and K⁺ *tert*-butoxide (tBuOK) were stored in a desiccator overnight. To a cool, dry 3-neck flask CMP (100 mg, 0.36 mmol), phenoxazine (POZ, 205 mg, 1.09 mmol), and dry, de-gassed toluene (24 mL) were added. The solution was purged with Ar. To the reaction solution, tBuOK (85 mg, 0.72 mmol) was added. The reaction mixture was sonicated and heated to 80 °C for 25 h (reaction was followed by TLC). Over the course of

the reaction more tBuOK (85 mg, 0.72 mmol) and POZ (68 mg, 0.36 mmol) were added. The dark, maroon reaction mixture was quenched with glacial acetic acid. Water was added (60 mL) and the product was extracted with CH₂Cl₂ (5x, 50 mL), dried with Na₂SO₄. The product was purified by column chromatography (60% CH₂Cl₂: 40% hexanes). The product was then recrystallized from CHCl₃/MeOH (3:20) resulting in a goldenrod colored solid. (Yield: 39%) ¹H NMR (300 MHz, CDCl₃, δ): 8.22 (d, 2H, 4,7-phen), 7.79 (s, 2H, 5,6-phen), 7.69 (d, 2H, 3,8-phen), 6.75 (m, 12H, Ar-POZ), 6.44 (m, 4H, Ar-POZ), 5.4 (s, 4H, N-CH₂-N). HRMS: ESI/APCI-TOF *m/z* (relative intensity): [M+H]⁺ calcd for C₃₈H₂₇N₄O₂, 571.2129; found 571.2134. [M+Na]⁺ calcd for C₃₈H₂₆N₄NaO₂, 593.1947; found 593.1947.

Synthesis of Acceptor Appended 1,10-Phenanthroline Ligands

Other than the following exceptions, all starting materials and solvents were solvent grade or better, obtained from commercial sources, and used without further purification. The 1,2-difluorobenzene (dfb) was obtained from Oakwood Products, Inc and run through a column of neutral, activated Al₂O₃ before use. The hydrazine sulfate used in the synthesis of M-Diol was recrystallized from water and dried thoroughly in the vacuum oven before use. Tetrakis(acetonitrile)copper(I)tetrafluoroborate ([Cu(ACN)₄]⁺BF₄⁻) was recrystallized from acetonitrile before use and stored in a dessicator. UltimAr acetonitrile (ACN) was obtained from MACRON Chemicals. DriSolv dimethylformamide (DMF), OmniSolv dichloromethane (DCM), and OmniSolv methanol (MeOH) were obtained from EMD Chemicals. Potassium tetrakis(pentafluorophenyl)borate was obtained from Boulder Scientific. Tris(bipyridine)ruthenium(II) hexafluorophosphate ([Ru(bpy)₃]²⁺(PF₆⁻)₂) was synthesized as published previously.⁸ Solutions of MeOH in dfb are reported as v/v percentage. Literature

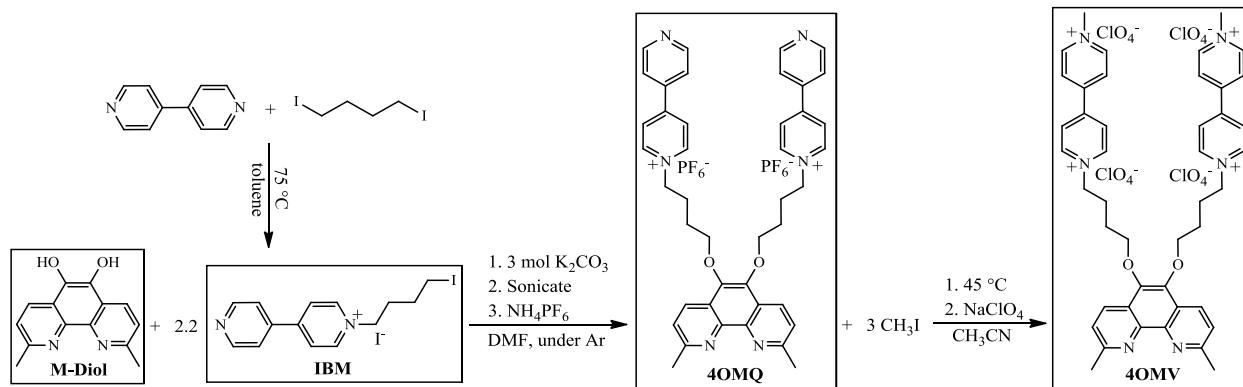


Figure 2.2. Synthesis of 4OMQ and 4OMV acceptor ligands.

methods were used to prepare 2,9-dimethyl-1,10-phenanthroline-5,6-dione (M-Dione) in order to make the acceptor ligand as shown in Figure 2.2.^{9–11}

M-Dione: *2,9-dimethyl-1,10-phenanthroline-5,6-dione*: This compound was synthesized based on synthetic methods detailed in the literature^{9–11} yielding a bright yellow crystalline solid (needles). (Yield: 44.4%). ¹H NMR (300 MHz, CDCl₃, δ): 8.4 (d, 2H, 4,7-phen), 7.44 (d, 2H, 3,8-phen), 2.87 (s, 6H, CH₃).

M-Diol: *2,9-dimethyl-1,10-phenanthroline-5,6-diol*: The synthesis of M-Diol was performed in accordance with literature procedures yielding a dull yellow solid.¹² ¹H NMR (300 MHz, D₂O/2 drops DCl, δ): 8.65 (d, 2H, 4,7-phen), 7.69 (d, 2H, 3,8-phen), 2.70 (s, 6H, CH₃).

IBM: *iodobutyl-monoquat iodide*: To a solution of 4,4'-bipyridine in toluene, was added diiodobutane (1:1 molar ratio). The solution was heated at 75 °C overnight in a stoppered flask. A red precipitate was afforded, which was filtered from the toluene supernatant. The crude solid product was washed with absolute ethanol multiple times. The light yellow ethanol rinses were combined and the solvent was removed in vacuo to give the product as a yellow-orange solid. This product was recrystallized from ethanol to give the purified product. ¹H NMR (400 MHz, CD₃CN, δ): 8.85 (t, 4H, Ar-pyridine), 8.34 (d, 2H, Ar-pyridine), 7.80 (d, 2H, Ar-pyridine), 4.62 (t, 2H, -N-CH₂), 3.29 (t, 2H, I-CH₂), 2.11 (m, 2H, I-CH₂-CH₂), 1.89 (m, 2H, -N-CH₂-CH₂).

4OMQ²⁺(PF₆⁻)₂ Acceptor Ligand: To a 100 mL round bottomed flask was added 0.510 g potassium carbonate, 0.295 g M-Diol, and 1.20 g of IBM (3:1: 2.1 mol), each of which was dried in the vacuum oven for at least 12 hours before use. The flask was purged with Ar and 10 mL of dry, degassed dimethylformamide (DMF) was added via syringe. The flask containing the reaction mixture was placed in an ultrasonic bath filled with ice. The bath was allowed to slowly warm to 45 °C (due to the sonication) as the reaction proceeded. Sonication was continued at 45 °C for 12 hours. The DMF was removed in vacuo and the resulting viscous brown oil was sonicated in excess water until it appeared nothing more was dissolving in the water. The water was then filtered through celite leaving a black tarry film on the surface. The aqueous filtrate was collected, reduced in volume, and ammonium hexafluorophosphate, NH₄PF₆, was added. The resulting precipitate was collected via centrifugation. The crude product was purified by dissolving in hot methanol, and filtering through celite. As the filtrate cooled, the product precipitated out of solution as light beige solids which were collected by filtration. ¹H NMR (400 MHz, CD₃CN, δ): 8.86 (dd, 4H, Ar-pyridine), 8.74 (d, 4H, Ar-pyridine), 8.41 (d, 2H, 4,7-phen), 8.27 (d, 4H, Ar-pyridine), 7.77 (dd, 4H, Ar-pyridine), 7.54 (d, 2H, 3,8-phen), 4.62 (t, 4H, N-CH₂), 4.25 (t, 4H, O-CH₂), 2.76 (s, 6H, CH₃), 2.25 (m, 4H, -O-CH₂-CH₂), 1.89 (m, 4H, -N-CH₂-CH₂). HRMS: ESI/APCI-TOF *m/z* (relative intensity): [(M-PF₆)+H]⁺ calcd for C₄₂H₄₂F₆N₆O₂P, 807.3006; found 807.3009.

4OMV⁴⁺(ClO₄⁻)₄ Acceptor Ligand: To a cold solution of 0.10 g of 4OMQ in 2 mL of acetonitrile was added 20 μL of methyl iodide (1:3 mol). A teflon lined vial cap was placed on the reaction vial and the reaction mixture was heated to 45 °C for 24 hrs. A red precipitate resulted which was filtered, rinsed with acetonitrile, and subsequently with methanol. The methanol rinseate was collected and 1 mL of NaClO₄ (sat'd) in methanol was added. The beige precipi-

tate was collected via filtration and rinsed with 15 mL hot methanol. To the hot methanol rinseate was added 5 mL of isopropanol and quickly cooled to -17 °C. The product was collected as light beige solids. ^1H NMR (400 MHz, CD_3CN , δ): 8.96 (d, 4H, Ar-pyridine), 8.86 (d, 4H, Ar-pyridine), 8.48 (d, 2H, 4,7-phen), 8.40 (d, 8H, Ar-pyridine), 7.60 (d, 2H, 3,8-phen), 4.74 (t, 4H, N- CH_2), 4.41 (s, 6H, CH_3 -pyridine), 4.28 (t, 4H, O- CH_2), 2.80 (s, 6H, 2,9-phen- CH_3), 2.32 (m, 4H, -O- CH_2 - CH_2), 1.97 (m, 4H, -N- CH_2 - CH_2). HRMS: ESI/APCI m/z (relative intensity): $[\text{M}-\text{ClO}_4]^{+}$ calcd for $\text{C}_{44}\text{H}_{48}\text{Cl}_3\text{N}_6\text{O}_{14}$, 991.2271; found 991.2267.

Synthesis of the Dtbp ligand

Dtbp: *2,9-di-tertbutyl-1,10-phenanthroline*: The synthesis of dtbp was performed in accordance with literature procedures¹³ yielding white crystalline needles. ^1H NMR (300 MHz, CDCl_3 , δ): 8.10 (d, 2H, 4,7-phen), 7.66 (s, 2H, 5,6-phen), 7.67 (d, 2H, 3,8-phen), 1.56 (s, 18H, CH_3). HRMS: ESI/APCI-TOF m/z (relative intensity): $[\text{M}+\text{H}]^{+}$ calcd for $\text{C}_{20}\text{H}_{25}\text{N}_2$, 293.2012; found 293.2020.

Ligand and Copper Complex Characterization

UV-visible Characterization: Static UV-visible (UV-vis) spectra were obtained using air-tight cells (vide infra) and an Agilent 8453 diode array spectrometer. For all samples where air-tight cells were not necessary, regular open air procedures were used in quartz or glass UV-vis cells with a wide spectral range.

Ligand and Copper Complexes: Typically, in addition to structural verification by ^1H NMR, the purity of intermediates and final ligands was verified by silica gel TLC. In the case of compounds which are charged, the elution solvent was 5:4:1 acetonitrile: water: KNO_3 (*sat. aq.*).

2.2. Sample Preparation

¹H NMR Titration Samples

¹H NMR titrations were performed to determine if the D-C-A self-assembles in solution. These experiments were also used to determine the approximate equilibrium concentrations of the different self-assembly products in solution. Unless otherwise specified, the samples for these experiments were typically prepared in one of two ways, both of which yield essentially the same results.

i. ¹H NMR Titration Method 1:

Stock solutions of the donor, $[\text{Cu}(\text{I})(\text{ACN})_4]^+(\text{BF}_4^-)$, and acceptor were made in the deuterated solvent of interest. An NMR sample of ligand was made by adding the stock solution (10^{-6} - 10^{-5} mol ligand) to an NMR tube via syringe, adding solvent if necessary, and purging the sample with Ar.

For homoleptic complexes (Method 1): an NMR solution of the donor ligand (P_D) or acceptor ligand (P_A) was prepared and an ¹H NMR was obtained as a reference. Then the stock $[\text{Cu}(\text{I})(\text{ACN})_4]^+(\text{BF}_4^-)$ solution in the appropriate deuterated solvent was titrated into the ligand NMR solution in 0.5 molar equivalents. An ¹H NMR was run after each addition affording spectra of the following species: (i) ligand, (ii) 2 mol ligand:0.5 mol Cu(I), (iii) 2 mol ligand :1 mol Cu(I) (iv) 2 mol ligand: 1.5 mol Cu(I) and (v) 2 mol ligand: 2 mol Cu(I). However, only the 2:1 (ligand:Cu(I)) complexes are detailed below.

For heteroleptic complexes (Method 1): NMR solutions are prepared as described above and ¹H NMR spectra are obtained for both the P_D and P_A ligand separately. An NMR sample was then prepared with 1:1 ratio of $P_D:P_A$ ligand as described above and an ¹H NMR is obtained as a reference. To the sample containing a 1:1 ratio of $P_D:P_A$ ligands was added the stock

$[\text{Cu(I)(ACN)}_4]^+(\text{BF}_4^-)$ solution in the appropriate deuterated solvent in 0.25 molar equivalents. An ^1H NMR was run after each addition affording spectra of the following species: (i) 1 mol P_D :1 mol P_A ligands, (ii) 1 mol P_D : 0.25 mol Cu(I) : 1 mol P_A , (iii) 1 mol P_D : 0.5 mol Cu(I) : 1 mol P_A (iv) 1 mol P_D : 0.75 mol Cu(I) : 1 mol P_A and (v) 1 mol P_D : 1 mol Cu(I) : 1 mol P_A . However, only the 1:1:1 complexes are detailed below.

ii. ^1H NMR Titration Method 2:

Stock solutions of the P_D , $[\text{Cu(I)(ACN)}_4]^+(\text{BF}_4^-)$, and P_A were made separately in high-quality spectral grade solvents or better. To a clean, dry vial was added ligand stock solution (10^{-6} - 10^{-5} mol ligand), and excess tetrakis(pentafluorophenyl)borate (as necessary). The solvent was removed in vacuo for at least $\frac{1}{2}$ hr and then the sample was redissolved in the appropriate deuterated ^1H NMR solvent, transferred to a clean, dry NMR tube via syringe, filtered through a 0.2 μm PTFE syringe filter upon transfer (as necessary), purged with Ar, and the ^1H NMR spectrum was acquired as a reference.

For homoleptic complexes (Method 2): The ligand solution was made as described above in Method 2, but the $[\text{Cu(I)(ACN)}_4]^+(\text{BF}_4^-)$ solution was also added in varied molar quantities to afford the following spectra out of separately prepared, individual solutions: (i) ligand, (ii) 2 mol ligand:0.5 mol Cu(I) , (iii) 2 mol ligand :1 mol Cu(I) (iv) 2 mol ligand: 1.5 mol Cu(I) and (v) 2 mol ligand: 2 mol Cu(I) . However, only the 2:1 (ligand: Cu(I)) complexes are detailed below.

For heteroleptic complexes (Method 2): The acceptor ligand (P_A) solution was made as described above in Method 2, but the donor ligand (P_D) (in a 1:1 molar ratio to the first ligand) and the $[\text{Cu(ACN)}_4]^+(\text{BF}_4^-)$ (in varied molar quantities) solutions were also added to afford the following spectra out of separately prepared, individual solutions: (i) 1 mol P_D :1 mol P_A ligands, (ii) 1 mol P_D : 0.25 mol Cu(I) : 1 mol P_A , (iii) 1 mol P_D : 0.5 mol Cu(I) : 1 mol P_A (iv) 1 mol P_D :

0.75 mol Cu(I): 1 mol P_A and (v) 1 mol P_D: 1 mol Cu(I): 1 mol P_A. However, only the 1:1:1 complexes are detailed below.

iii. Synthesis of deuterated 1,2-difluorobenzene (dfb):

Deuteration of 1,2-difluorobenzene was accomplished via a modification of the approach reported by Lunelli et al.^{14,15} A two-neck 14/20 pear flask (50 mL) equipped with a condenser and magnetic stir bar was charged with 10 mL of 1,2-difluorobenzene. A mixture of 10 mL of 98% D₂SO₄, 1 mL of D₂O and 1 g of Li⁺ triflate was added to the flask which was then heated to reflux with vigorous stirring for > 96 h under static N₂. The reaction was cooled to room temperature and the aqueous layer pipetted from the flask. The process was repeated twice more with new solutions of 10 mL of 98% D₂SO₄, 1 mL of D₂O and 1 g of lithium triflate, each being refluxed for > 72 h. At the end of the third reflux, after removing most of the aqueous layer, the reaction flask was connected to a collection flask (50 mL) by a ca. 1 cm diameter “L” tube having 14/20 ground-glass ends and a small piece of glass wool located in the center of the tube (to obviate against bumping). The contents of the reaction flask were then frozen by immersing the bottom of the pear flask in liquid N₂. Once the entire contents were solidly frozen, the set up was evacuated and left under static vacuum. The liquid N₂ was moved from the reaction flask to the collection flask and product was allowed slowly warm to room temperature, during which time the product distilled into the collection flask. The level of liquid N₂ contacting the collection flask was adjusted as the reaction flask warmed in order to minimize bumping. After about 15 minutes all of the deuterio-1,2-difluorobenzene had been transferred and the distillation was stopped to minimize any transfer of D₂O. Yield: ca. 2-3 mL, 20-30%.

^1H NMR titration of $[\text{Cu}(\text{I})(\text{TPZ})_2]^+(\text{TPFB}^-)$, $[\text{Cu}(\text{I})(4\text{OMV})_2]^{9+}(\text{TPFB}^-)_9$, and $[\text{Cu}(\text{I})(\text{TPZ})(4\text{OMV})]^{5+}(\text{TPFB}^-)_5$ in $\text{CD}_3\text{OD}/\text{CD}_2\text{Cl}_2$

TPZ Donor Ligand in $\text{CD}_3\text{OD}/\text{CD}_2\text{Cl}_2$ (1:20 by volume) : ^1H NMR (400 MHz, δ): 8.15 (d, 2H, 4,7-phen), 7.74 (s, 2H, 5,6-phen), 7.72 (d, 2H, 3,8-phen), 6.65 (s, 4H, Ar-TPZ), 6.56 (s, 4H, Ar-TPZ), 5.56 (s, 4H, N- CH_2 -N), 2.35 (s, 12H, TPZ- CH_3), 2.08 (s, 12H, TPZ- CH_3).

4OMV $^{4+}(\text{TPFB}^-)_4$ Acceptor Ligand in $\text{CD}_3\text{OD}/\text{CD}_2\text{Cl}_2$ (1:20 by volume): ^1H NMR (400 MHz, δ): 8.96 (d, 4H, Ar-pyridine), 8.85 (d, 4H, Ar-pyridine), 8.36 (d, 2H, 4,7-phen), 8.28 (t, 8H, Ar-pyridine), 7.45 (d, 2H, 3,8-phen), 4.69 (t, 4H, N- CH_2), 4.54 (s, 6H, CH_3 -pyridine), 4.25 (t, 4H, O- CH_2), 2.75 (s, 6H, 2,9-phen- CH_3), 2.30 (m, 4H, -O- CH_2 - CH_2), 1.94 (m, 4H, -N- CH_2 - CH_2).

Homoleptic $[\text{Cu}(\text{I})(\text{TPZ})_2]^+(\text{TPFB}^-)$ in $\text{CD}_3\text{OD}/\text{CD}_2\text{Cl}_2$ (6:11 by volume): ^1H NMR (300 MHz, δ): 8.58 (d, 4H, 4,7-phen), 8.18 (s, 4H, 5,6-phen), 7.94 (d, 4H, 3,8-phen), 6.52 (s, 8H, Ar-TPZ), 5.65 (s, 8H, Ar-TPZ), 5.16 (s, 8H, N- CH_2 -N), 2.24 (s, 24H, TPZ- CH_3), 1.57 (s, 24H, TPZ- CH_3).

Homoleptic $[\text{Cu}(\text{I})(4\text{OMV})_2]^{9+}(\text{TPFB}^-)_9$ in $\text{CD}_3\text{OD}/\text{CD}_2\text{Cl}_2$ (3:2 by volume): ^1H NMR (400 MHz, δ): 9.20 (d, 8H, Ar-pyridine), 9.07 (d, 8H, Ar-pyridine), 8.52 (m, 20H, 4,7-phen, Ar-pyridine), 7.60 (d, 4H, 3,8-phen), 4.82 (t, 8H, N- CH_2), 4.45 (s, 12H, CH_3 -pyridine), 4.31 (t, 8H, O- CH_2), 2.40 (m, 8H, -O- CH_2 - CH_2), 2.25 (s, 12H, 2,9-phen- CH_3), 2.06 (m, 8H, -N- CH_2 - CH_2).

Heteroleptic $[\text{Cu}(\text{I})(4\text{OMV})(\text{TPZ})]^{5+}(\text{TPFB}^-)_5$ in $\text{CD}_3\text{OD}/\text{CD}_2\text{Cl}_2$ (3:2 by volume): ^1H NMR (400 MHz, δ): *Heteroleptic complex*: 9.22 (d, 4H, Ar-pyridine), 9.08 (d, 4H, Ar-pyridine), 8.64 (d, 2H, 4,7-phen), 8.54 (m, 10H: (8H) Ar-Pyridine, (2H) 4,7-phen), 8.05 (s, 2H, 5,6-phen), 7.89 (d, 2H, 3,8-phen), 7.77 (d, 2H, 3,8-phen), 6.44 (s, 4H, Ar-TPZ), 5.75 (s, 4H, Ar-TPZ), 4.88 (s, 4H, N- CH_2 -N (TPZ)), 4.83 (m, 4H, N- CH_2 (4OMV)), 4.45 (s, 6H, CH_3 -pyridine (4OMV)),

4.32 (t, 4H, O-CH₂), 2.53 (s, 6H, 2,9-CH₃-phen (4OMV)), 2.39 (m, 4H, -O-CH₂-CH₂), 2.10 (m, 8H, -N-CH₂-CH₂), 2.09 (s, 12H, TPZ-CH₃), 1.84 (s, 12H, TPZ-CH₃). *Homoleptic [Cu(I)(4OMV)₂]⁹⁺(TPFB⁻)₉ impurity:* 9.22 (d, 8H, Ar-pyridine), 9.08 (d, 8H, Ar-pyridine), 8.54 (m, 20H: (4H) 4,7-phen, (16H) Ar-pyridine), 7.62 (d, 4H, 3,8-phen), 4.83 (t, 8H, N-CH₂), 4.45 (s, 12H, CH₃-pyridine), 4.32 (t, 8H, O-CH₂), 2.39 (m, 8H, -O-CH₂-CH₂), 2.27 (s, 12H, 2,9-phen-CH₃), 2.10 (m, 8H, -N-CH₂-CH₂). *Homoleptic [Cu(I)(TPZ)₂]⁺(TPFB⁻) impurity:* 8.54 (d, 4H, 4,7-phen), 8.11 (s, 4H, 5,6-phen), 7.94 (d, 4H, 3,8-phen), 6.38 (s, 8H, Ar-TPZ), 5.62 (s, 8H, Ar-TPZ), 5.11 (s, 8H, N-CH₂-N), 2.11 (s, 24H, TPZ-CH₃), 1.51 (s, 24H, TPZ-CH₃). Since one of each 4OMV and TPZ ligands are responsible for the heteroleptic complex signal and two 4OMV/TPZ ligands generate the signals for the homoleptic complexes, the calculated product ratio is c.a. 56% [Cu(I)(4OMV)(TPZ)]⁵⁺(TPFB⁻)₅: 21% [Cu(I)(TPZ)₂]⁺(TPFB⁻): 24% [Cu(I)(4OMV)₂]⁹⁺(TPFB⁻)₉, based on their relative integrations.

¹H NMR titration of [Cu(I)(TPZ)₂]⁺(BF₄⁻), [Cu(I)(4OMV)₂]⁹⁺(BF₄⁻)(ClO₄⁻)₈, and [Cu(I)(TPZ)(4OMV)]⁵⁺(BF₄⁻)(ClO₄⁻)₄ in CD₃CN/CD₂Cl₂

TPZ Donor Ligand in CD₃CN/CD₂Cl₂ (1:1 by volume): ¹H NMR (300 MHz, δ): 8.18 (d, 2H, 4,7-phen), 7.78 (s, 2H, 5,6-phen), 7.66 (d, 2H, 3,8-phen), 6.66 (s, 4H, Ar-TPZ), 6.54 (s, 4H, Ar-TPZ), 5.52 (s, 4H, N-CH₂-N), 2.34 (s, 12H, TPZ-CH₃), 2.07 (s, 12H, TPZ-CH₃).

4OMV⁴⁺(ClO₄⁻)₄ Acceptor Ligand in CD₃CN/CD₂Cl₂ (1:1 by volume): ¹H NMR (300 MHz, δ): 9.03 (d, 4H, Ar-pyridine), 8.88 (d, 4H, Ar-pyridine), 8.45 (m, 10H, 4,7-phen, Ar-pyridine), 7.56 (d, 2H, 3,8-phen), 4.80 (t, 4H, N-CH₂), 4.43 (s, 6H, CH₃-pyridine), 4.25 (t, 4H, O-CH₂), 2.81 (s, 6H, 2,9-phen-CH₃), 2.37 (m, 4H, -O-CH₂-CH₂), 2.00 (m, 4H, -N-CH₂-CH₂).

Homoleptic $[\text{Cu}(\text{I})(\text{TPZ})_2]^+(\text{BF}_4^-)$ in $\text{CD}_3\text{CN}/\text{CD}_2\text{Cl}_2$ (1:1 by volume): ^1H NMR (300 MHz, δ): 8.57 (d, 4H, 4,7-phen), 8.13 (s, 4H, 5,6-phen), 7.91 (d, 4H, 3,8-phen), 6.45 (s, 8H, Ar-TPZ), 5.67 (s, 8H, Ar-TPZ), 5.11 (s, 8H, N- CH_2 -N), 2.16 (s, 24H, TPZ- CH_3), 1.55 (s, 24H, TPZ- CH_3).

Homoleptic $[\text{Cu}(\text{I})(4\text{OMV})_2]^{9+}(\text{BF}_4^-)(\text{ClO}_4^-)_8$ in $\text{CD}_3\text{CN}/\text{CD}_2\text{Cl}_2$ (1:1 by volume): ^1H NMR (300 MHz, δ): 9.10 (d, 8H, Ar-pyridine), 8.80 (s, 4H, Ar-pyridine), 8.71 (d, 4H, 4,7-phen), 8.49 (q, 16H, Ar-pyridine), 7.80 (d, 4H, 3,8-phen), 4.84 (t, 8H, N- CH_2), 4.43 (s, 12H, CH_3 -pyridine), 4.36 (t, 8H, O- CH_2), 2.42 (m, 8H, -O- CH_2 - CH_2), 2.37 (s, 12H, 2,9-phen- CH_3), 2.10 (m, 8H, -N- CH_2 - CH_2).

Heteroleptic $[\text{Cu}(\text{I})(4\text{OMV})(\text{TPZ})]^{5+}(\text{BF}_4^-)(\text{ClO}_4^-)_4$ in $\text{CD}_3\text{CN}/\text{CD}_2\text{Cl}_2$ (1:1 by volume): ^1H NMR (300 MHz, δ): *Heteroleptic complex:* 9.10 (t, 4H, Ar-pyridine), 8.88 (d, 4H, Ar-pyridine), 8.76 (d, 2H, 4,7-phen), 8.56 (d, 2H, 4,7-phen), 8.49 (m, 8H, Ar-Pyridine), 8.11 (s, 2H, 5,6-phen), 7.91 (d, 2H, 3,8-phen), 7.87 (d, 2H, 3,8-phen), 6.54 (s, 4H, Ar-TPZ), 5.81 (s, 4H, Ar-TPZ), 4.92 (s, 4H, N- CH_2 -N (TPZ)), 4.82 (m, 4H, N- CH_2 (4OMV)), 4.43 (s, 6H, CH_3 -pyridine (4OMV)), 4.33 (t, 4H, O- CH_2), 2.56 (s, 6H, 2,9- CH_3 -phen (4OMV)), 2.42 (m, 4H, -O- CH_2 - CH_2), 2.19 (s, 12H, TPZ- CH_3), 2.09 (m, 8H, -N- CH_2 - CH_2), 2.00 (s, 12H, TPZ- CH_3). *Homoleptic $[\text{Cu}(\text{I})(4\text{OMV})_2]^{9+}(\text{BF}_4^-)(\text{ClO}_4^-)_8$ impurity:* 9.10 (d, 8H, Ar-pyridine), 8.88 (d, 8H, Ar-pyridine), 8.71 (d, 4H, 4,7-phen), 8.48 (m, 16H, Ar-pyridine), 7.79 (d, 4H, 3,8-phen), 4.82 (t, 8H, N- CH_2), 4.43 (s, 12H, CH_3 -pyridine), 4.33 (t, 8H, O- CH_2), 2.42 (m, 8H, -O- CH_2 - CH_2), 2.38 (s, 12H, 2,9-phen- CH_3), 2.10 (m, 8H, -N- CH_2 - CH_2). *Homoleptic $[\text{Cu}(\text{I})(\text{TPZ})_2]^+(\text{BF}_4^-)$ impurity:* 8.59 (d, 4H, 4,7-phen), 8.14 (s, 4H, 5,6-phen), 7.92 (d, 4H, 3,8-phen), 6.45 (s, 8H, Ar-TPZ), 5.69 (s, 8H, Ar-TPZ), 5.12 (s, 8H, N- CH_2 -N), 2.16 (s, 24H, TPZ- CH_3), 1.55 (s, 24H, TPZ- CH_3). Since one of each 4OMV and TPZ ligands are responsible for the heteroleptic complex signal and two

4OMV/TPZ ligands generate the signals for the homoleptic complexes, the calculated product ratio is c.a. 70% $[\text{Cu(I)(4OMV)(TPZ)}]^{5+}(\text{BF}_4^-)(\text{ClO}_4^-)_4$: 12% $[\text{Cu(I)(TPZ)}_2]^{+}(\text{BF}_4^-)$: 18% $[\text{Cu(I)(4OMV)}]^{9+}(\text{BF}_4^-)(\text{ClO}_4^-)_8$, based on their relative integrations.

^1H NMR titration of $[\text{Cu(I)(TPZ)}_2]^{+}(\text{TPFB}^-)$, $[\text{Cu(I)(4OMV)}_2]^{9+}(\text{TPFB}^-)_9$, and $[\text{Cu(I)(TPZ)(4OMV)}]^{5+}(\text{TPFB}^-)_5$ in dfb/MeOH (17:3 by volume)

These experiments were performed in a Wilmad 520-1A, 5 mm microprobe NMR sample tube.

1:1 solution of 4OMV⁴⁺(ClO₄⁻) and TPZ Ligands in dfb/MeOH (17:3 by volume): ^1H NMR (400 MHz, δ): 9.36 (d, 8H, Ar-pyridine; 4OMV), 8.77 (d, 8H, Ar-pyridine; 4OMV), 8.66 (d, 2H, 4,7-phen), 8.15 (d, 2H, phen), 8.04 (d, 2H, phen), 7.64 (s, 2H, 5,6-phen; TPZ), 7.61 (d, 2H, 3,8-phen), 6.95 (s, 4H, Ar-TPZ), 6.81 (s, 4H, Ar-TPZ), 5.71 (s, 4H, N-CH₂-N; TPZ), 5.13 (t, 4H, N-CH₂; 4OMV), 4.84 (s, 6H, CH₃-pyridine; 4OMV), 4.69 (t, 4H, O-CH₂; 4OMV), 3.05 (s, 6H, 2,9-phen-CH₃; 4OMV), 2.72 (m, 4H, -O-CH₂-CH₂; 4OMV), 2.56 (s, 12H, TPZ-CH₃), 2.34 (m, 4H, -N-CH₂-CH₂; 4OMV), 2.32 (s, 12H, TPZ-CH₃).

Homoleptic $[\text{Cu(I)(TPZ)}_2]^{+}(\text{TPFB}^-)$ in dfb/MeOH (17:3 by volume): ^1H NMR (400 MHz, δ): 8.56 (d, 4H, 4,7-phen), 8.33 (s, 4H, 5,6-phen), 8.07 (d, 4H, 3,8-phen), 6.59 (s, 8H, Ar-TPZ), 6.05 (s, 8H, Ar-TPZ), 5.55 (s, 8H, N-CH₂-N), 2.34 (s, 24H, TPZ-CH₃), 1.89 (s, 24H, TPZ-CH₃).

Homoleptic $[\text{Cu(I)(4OMV)}_2]^{9+}(\text{TPFB}^-)$ in dfb/MeOH (17:3 by volume): ^1H NMR (400 MHz, δ): 9.46 (d, 8H, Ar-pyridine), 9.32 (d, 8H, Ar-pyridine), 8.89 (d, 8H, Ar-pyridine), 8.85 (d, 4H, 4,7-phen), 8.78 (d, 8H, Ar-pyridine), 7.75 (d, 4H, 3,8-phen), 5.23 (t, 8H, N-CH₂), 4.82 (s, 12H, CH₃-pyridine), 4.75 (t, 8H, O-CH₂), 2.88 (m, 8H, -O-CH₂-CH₂), 2.60 (s, 12H, 2,9-phen-CH₃), 2.54 (m, 8H, -N-CH₂-CH₂).

Heteroleptic $[\text{Cu}(\text{4OMV})(\text{TPZ})]^{5+}(\text{TPFB}^-)$ in dfb/MeOH (17:3 by volume): ^1H NMR (400 MHz, δ): *Heteroleptic complex:* 9.55 (q, 4H, Ar-pyridine), 9.39 (m, 4H, Ar-pyridine), 8.99 (d, 2H, 4,7-phen), 8.92 (m, 4H Ar-Pyridine), 8.82 (m, 4H Ar-Pyridine), 8.42 (d, 2H, 4,7-phen), 8.10 (d, 2H, 3,8-phen), 8.00 (d, 2H, 3,8-phen), 7.85 (s, 2H, 5,6-phen), 6.63 (s, 4H, Ar-TPZ), 6.10 (s, 4H, Ar-TPZ), 5.25 (s, 4H, N- CH_2 -N (TPZ)), 5.25 (t, 4H, N- CH_2 (4OMV)), 4.81 (s, 6H, CH_3 -pyridine (4OMV)), 4.74 (m, 4H, O- CH_2), 2.94 (s, 6H, 2,9- CH_3 -phen (4OMV)), 2.84 (m, 4H, -O- CH_2 - CH_2), 2.53 (m, 8H, -N- CH_2 - CH_2), 2.34 (s, 12H, TPZ- CH_3), 2.16 (s, 12H, TPZ- CH_3). *Homoleptic $[\text{Cu}(\text{I})(\text{4OMV})_2]^{9+}(\text{TPFB}^-)_9$ impurity:* 9.55 (q, 8H, Ar-pyridine), 9.39 (m, 8H, Ar-pyridine), 8.92 (m, 16H, Ar-pyridine), 8.85 (d, 4H, 4,7-phen), 7.77 (d, 4H, 3,8-phen), 5.20 (t, 8H, N- CH_2), 4.81 (s, 12H, CH_3 -pyridine), 4.74 (m, 8H, O- CH_2), 2.84 (m, 8H, -O- CH_2 - CH_2), 2.57 (s, 12H, 2,9-phen- CH_3), 2.53 (m, 8H, -N- CH_2 - CH_2). *Homoleptic $[\text{Cu}(\text{I})(\text{TPZ})_2]^+(\text{TPFB}^-)$ impurity:* 8.56 (d, 4H, 4,7-phen), 8.31 (d, 4H, 3,8-phen), 8.07 (s, 4H, 5,6-phen), 6.57 (s, 8H, Ar-TPZ), 6.03 (s, 8H, Ar-TPZ), 5.53 (s, 8H, N- CH_2 -N), 2.32 (s, 24H, TPZ- CH_3), 1.87 (s, 24H, TPZ- CH_3). *Heteroleptic $[\text{Cu}(\text{I})(\text{TPZ})(\text{MeOH})]^+(\text{TPFB}^-)$ impurity:* 8.26 (d, 4H, 4,7-phen), 8.08 (*not observed*; d, 4H, 3,8-phen), 8.03 (*not observed*; s, 4H, 5,6-phen), 6.96 (*not observed*; s, 8H, Ar-TPZ), 6.73 (s, 8H, Ar-TPZ), 5.93 (s, 8H, N- CH_2 -N), 2.45 (*not observed*; s, 24H, TPZ- CH_3), 2.34 (*not observed*; s, 24H, TPZ- CH_3). Since one of each 4OMV and TPZ ligands are responsible for the heteroleptic complex signal and two 4OMV/TPZ ligands generate the signals for the homoleptic complexes, the calculated product ratio is c.a. 49% $[\text{Cu}(\text{I})(\text{4OMV})(\text{TPZ})]^{5+}(\text{TPFB}^-)_5$: 24% $[\text{Cu}(\text{I})(\text{4OMV})_2]^{9+}(\text{TPFB}^-)_9$: 22% $[\text{Cu}(\text{I})(\text{TPZ})_2]^+(\text{TPFB}^-)$: 5% $[\text{Cu}(\text{I})(\text{TPZ})(\text{MeOH})]^+(\text{TPFB}^-)$, based on their relative integrations. The chemical shifts listed for unobserved peaks from the $[\text{Cu}(\text{I})(\text{TPZ})(\text{MeOH})]^+(\text{TPFB}^-)$ complex were determined from an independently prepared sample of homoleptic $[\text{Cu}(\text{I})(\text{TPZ})_2]^+(\text{TPFB}^-)$ into which additional Cu(I) was added.

Additional ^1H NMR Spectra

Since the following homoleptic acceptor C-AQ ($[\text{Cu}(\text{I})(4\text{OMQ})_2]^{5+}(\text{TPFB}^-)_5$) and homoleptic donor C-DP ($[\text{Cu}(\text{I})(\text{POZ})_2]^+(\text{TPFB}^-)$) diads were discussed in the body of the thesis but were not studied as systematically in the ^1H NMR titration experiments, their ^1H NMR spectra are listed here.

C-AQ Diad: *Homoleptic Acceptor* $[\text{Cu}(\text{I})(4\text{OMQ})_2]^{5+}(\text{TPFB}^-)_5$: ^1H NMR (400 MHz, CD_3CN , δ): 8.83 (q, 16H, Ar-pyridine), 8.66 (d, 4H, 4,7-phen), 8.34 (d, 8H, Ar-pyridine), 7.78 (dd, 8H, Ar-pyridine), 7.74 (d, 4H, 3,8-phen), 4.68 (t, 8H, N- CH_2), 4.33 (t, 8H, O- CH_2), 2.31 (m, 8H, -O- CH_2 - CH_2), 2.31 (s, 12H, 2,9-phen- CH_3), 2.00 (m, 8H, -N- CH_2 - CH_2).

C-DP Diad: *Homoleptic Donor* $[\text{Cu}(\text{I})(\text{POZ})_2]^+(\text{TPFB}^-)$: ^1H NMR (300 MHz, CD_2Cl_2 , δ): 8.62 (d, 4H, 4,7-phen), 8.12 (s, 4H, 5,6-phen), 7.97 (d, 4H, 3,8-phen), 6.67 (m, 16H, 4,6,4',6'-POZ), 6.41 (m, 8H, 5,5'-POZ), 5.91 (d, 8H, 3,3'-POZ), 4.76 (s, 8H, CH_2).

Preparation of samples for transient absorption (TA) laser studies

i. Preparation of P_A , P_D , dtbp, and $[\text{Cu}(\text{I})(\text{ACN})_4]^+(\text{BF}_4^-)$ stock solutions:

Stock solutions of donor ligand (P_D), acceptor ligand (P_A), dtbp ligand and $[\text{Cu}(\text{I})(\text{ACN})_4]^+(\text{BF}_4^-)$ were prepared in separate volumetric flasks (1-10 mL) in mM concentrations and dissolved in an appropriate solvent (usually Spectro grade dichloromethane for P_D ligands, and UltimAr acetonitrile for P_A ligands and $[\text{Cu}(\text{I})(\text{ACN})_4]^+(\text{BF}_4^-)$). The stock solutions were stoppered, sealed with parafilm, and stored at $-24\text{ }^\circ\text{C}$ between use.

ii. Preparation of homoleptic C-AX and C-DX stock solutions:

The stock solutions of P_A , P_D and $[\text{Cu}(\text{I})(\text{ACN})_4]^+(\text{BF}_4^-)$ were used to prepare stock solutions of homoleptic C-AX or C-DX diads as follows: To a vial containing ca. 1 ml of UltimAr

acetonitrile was added potassium tetrakis(pentafluorophenyl)borate (ca. 1.5 molar xs TPFB⁻), 2 molar equivalents of P_A stock solution (or P_D, for C-DX diads), and 1 molar equivalent of the [Cu(I)(ACN)₄]⁺(BF₄⁻) in UltiAr acetonitrile in that order using a microliter syringe, to yield a solution containing ca. 10⁻⁷ mols of diad. The solvent was removed in via rotary evaporation and then the sample was dried further in the vacuum oven at 0-35 °C for > 1 hr. The sample was then dissolved in the appropriate solvent for laser studies (dfb, CH₂Cl₂, MeOH, CH₃CN or combinations thereof) either on the benchtop or in the glove box to yield a ca. 10⁻⁴ M stock solution of C-AX or C-DX diads. This method was also used to make individual samples, but at concentrations of ca. 10⁻⁵ M (see below).

iii. Preparation of heteroleptic C-AVB and “D-C-A Mixture A/D” stock solutions:

The stock solutions of dtbp, P_A, P_D and [Cu(I)(ACN)₄]⁺(BF₄⁻) were used to prepare stock solutions of C-AVB and “D-C-A Mixtures A/D” as follows: To a vial containing ca. 1 ml of UltiAr acetonitrile was added potassium tetrakis(pentafluorophenyl)borate (ca. 1.5 molar xs TPFB⁻), 1 molar equivalent of P_A stock solution, 1 molar equivalent or P_D (or dtbp for the C-AVB diad) stock solution, and 1 molar equivalent of the [Cu(I)(ACN)₄]⁺(BF₄⁻) in UltiAr acetonitrile in that order using a microliter syringe, to yield a solution containing ca. 10⁻⁷ moles of Cu(I) (since the resulting solution is a mixture of heteroleptic and homoleptic complexes, the stoichiometry is defined by [Cu(I)]). The solvent was removed in via rotary evaporation and the sample was dried further in the vacuum oven at 0-35 °C for > 1 hr. The sample was then dissolved in the appropriate solvent for laser studies (dfb, CH₂Cl₂, MeOH, CH₃CN or combinations thereof) either on the benchtop or in the glove box to yield a ca. 10⁻⁴ M stock solution of C-AVB diad or “D-C-A Mixture A/D”. This method was also used to make individual samples, but at concentrations of ca. 10⁻⁵ M (see below).

iv. Preparation of individual laser samples:

The stock solutions of C-AX, C-DX or “D-C-A Mixtures A/D” were then used to make individual laser samples in the glove box in rectangular 1 cm × 1 cm or 3 mm x 1 cm optical glass cells, and sealed with an air-tight teflon screw plug. Typically, individual samples (prepared on the benchtop or in the glove box from stock solutions) were prepared at a given concentration (dfb/X% MeOH) in order to achieve a specific ground state absorption (e.g. typically $A \approx 0.3-0.5$ at λ_{\max} or λ_{ex} depending on the experiment, which usually corresponded to a concentration on the order of 10^{-5} M for these samples). Therefore, it is common to prepare the sample, run a UV-vis, and then adjust the concentration by adding additional solvent ($\text{CH}_2\text{Cl}_2/\text{X}\%$ MeOH or dfb/X% MeOH) as necessary to achieve the desired absorbance value. Additional solvent was then added to the samples on the benchtop and the samples were degassed by freeze-pump-thawing the sample under vacuum multiple times and sealing under vacuum. Alternatively, to minimize oxygen content, the sample was brought back into the glove box, where additional solvent was added and the sample was allowed to equilibrate with the glovebox atmosphere for ≥ 5 min. In the latter case, the Teflon screw cap was degassed in the antechamber for >12 hours before use.

2.3. Instrumentation and Measurements

Spectroelectrochemistry

A home-built optically transparent thin layer working electrode (OTTLE) spectroelectrochemical cell shown in Figure 2.3, was employed to obtain quantitative spectra of the one-electron reduction product of methyl viologen ($\text{MV}^{+\bullet}$) in dfb solvent with 0.1 M $\text{TBA}^+\text{PF}_6^-$ electrolyte.¹⁶⁻¹⁸ The OTTLE cell consisted of a rectangular Au minigrad sandwiched between quartz

plates. The solution was purged with Ar prior to introduction into the cell. The prepared cell was then mounted in the light path of the Agilent 8453 UV-vis spectrometer and potential control was afforded employing a BAS 100B potentiostat.

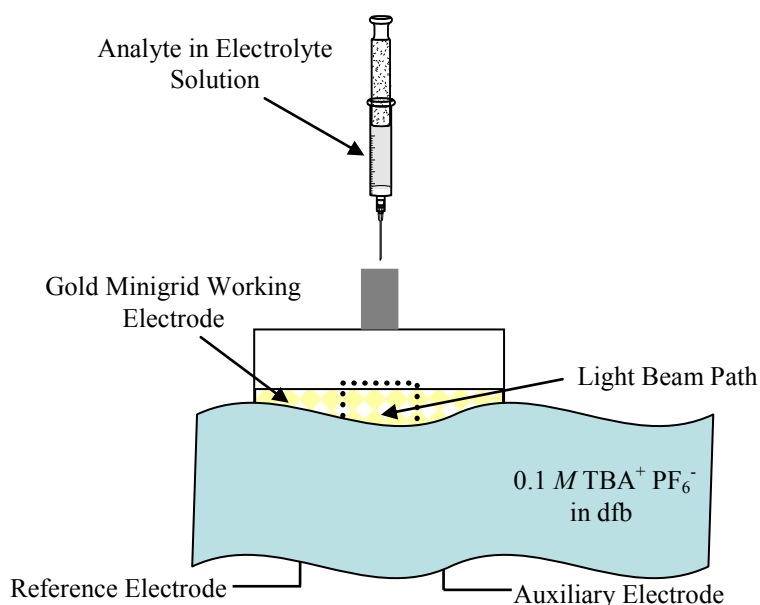


Figure 2.3. Optically transparent thin layer (OTTLE) cell used for the spectroelectrochemical studies. Reproduced from ref 18.

Electrochemistry

Typical cyclic voltammetric experiments were executed using a BAS 100B Potentiostat. A glassy carbon disk was used for the working electrode (ca. 0.7 mm²) versus a saturated sodium chloride calomel (SSCE) reference electrode, and a platinum wire auxiliary electrode for the sample solutions with 0.1 M tetrabutylammonium hexafluorophosphate (TBA⁺PF₆⁻) supporting electrolyte. Generally, the sample solutions were made in either Spectro grade dichloromethane (POZ and TPZ units), UltimAr acetonitrile (4OMV and 4OMQ ligands, and C-AV and C-AQ complexes) or \approx 1:1 solution of UltimAr CH₃CN: Spectro CH₂Cl₂ (POZ and TPZ ligands, C-DP and C-DT diads) and degassed by bubbling vigorously with N₂ in the cell.

Laser Spectroscopy Measurements

i. Transient Absorption (TA) Spectroscopy and Magnetic Field Effect (MFE) Measurements

The recombination kinetics of the C-A diads and D-C-A triads were determined by transient absorption laser spectroscopy on a nanosecond laser system as shown in Figure 2.4A. An Opotek optical parametric oscillator (OPA) pumped by the 355 nm harmonic of a Nd:Yag laser was used to supply the pump beam ($\lambda_{\text{ex}} = 450$ or 475 nm; pulse width ca. 7 ns), with an average power between 45-65 mW, depending on the wavelength. The probe beam was provided by a continuous 100 W xenon arc lamp chopped at 20 Hz with a 2% duty cycle. For measurements in the absence of a magnetic field the pump and probe beams were incident upon the sample at right angles. The probe beam was focused through the slit of a monochromator (Jarrel Ash, model 82-310) and directed through an attached photomultiplier tube (Hamamatsu R2496) and the signal was collected by an oscilloscope (Tektronics) triggered by a photodiode (Thorlabs DET210) that was spatially (i.e. temporally) separated from the detector. Each TA decay curve was an averaged spectrum of 100-800 laser shots, which was recorded on the oscilloscope as a ratio of intensities ($I_t/I_{t=0}$) with respect to time, and consisted of 500 data points. The 500 data points were collected over 10 divisions on the oscilloscope, such that 50 data points were collected per division; thus, the timescale of each experiment was determined by the time interval of each division (each data point represented $1/50^{\text{th}}$ of the specified timescale. e.g. on a 500 ns timescale, the $I_t/I_{t=0}$ value would be recorded every 10 ns). Data collection began at the specified time interval before each detected laser pulse begin (e.g. on a 500 ns timescale, data collection began 500 ns before the laser pulse). Each TA decay curve collected was an adjusted spectrum calculated from four separate data sets in which different beams were blocked: (1) pump + probe, (2) probe only (pump blocked), (3) pump only (probe blocked), and (4) pump blocked + probe

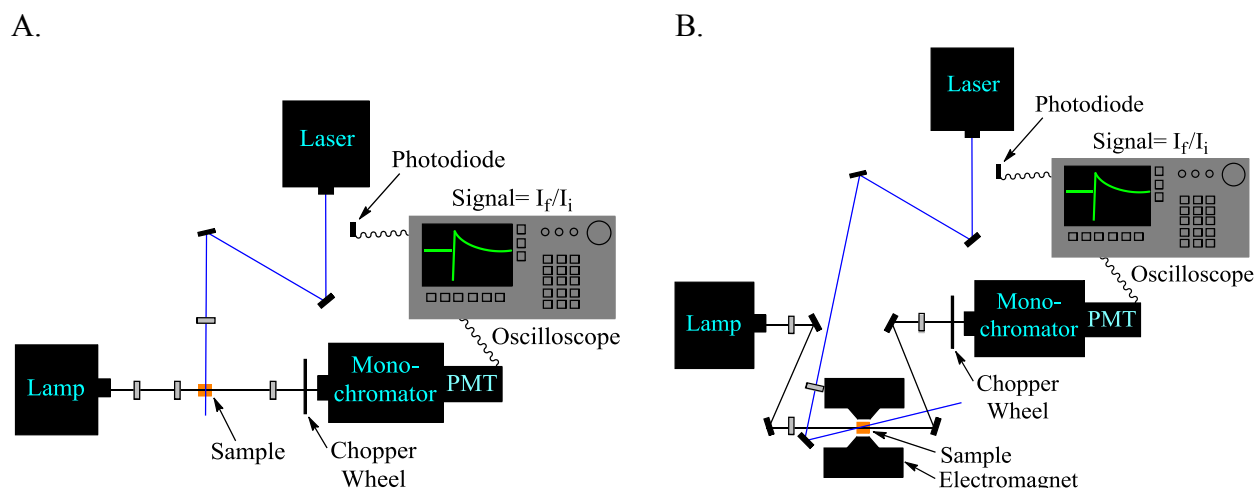


Figure 2.4. Schematic of the transient absorption laser set-up. A) Set-up used to determine CT/CS lifetime, quantum yield and transient absorption spectra in absence of magnetic field. B) Set-up used for determining lifetime of CT/CS and initial intensities in a magnetic field.

blocked. Therefore, the adjusted data was calculated as follows: $(I_t/I_{t=0}) = [(1)-(2)]/[(3)-(4)]$ and then converted to Δ absorbance values by $\Delta A_t = -\log(I_t/I_{t=0})$.

The MFE studies on the recombination kinetics of the CT state and formation quantum yield were also measured by TA spectroscopy using the altered laser set-up shown in Figure 2.4B. For these experiments, the pump and probe beams were directed through the center of a Walker Scientific, Inc. (Model: HV4H) electromagnet in a nearly collinear orientation. All TA data (in presence and absence of a magnetic field) was fit using Origin 7.5 advanced fitting function.

Quantum Yield Measurements

These measurements were performed outside of the magnet using the same laser set-up as described above and in the same manner as described in the literature^{19,20} with the following changes: The reference complex was $[\text{Ru}(\text{bpy})_3]^{2+}(\text{PF}_6^-)_2$ and pump beam was 475 nm. Furthermore, the triplet-triplet and ground state absorption of $[\text{Ru}(\text{bpy})_3]^{2+}(\text{PF}_6^-)_2$ at $\Delta\epsilon_{450}$ and $\Delta\epsilon_{370}$, respectively, were taken into account in the calculations (The reference complex used herein was

determined to have a ³MLCT TA maximum at 368 nm and a bleach maximum at 450.) The molar absorptivity of the bleach at 450 nm is $\Delta\epsilon_{450} = 14,500 \text{ M}^{-1} \text{ cm}^{-1}$ and the triplet-triplet absorption is $\epsilon_{450} = 2,000 \text{ M}^{-1} \text{ cm}^{-1}$.²¹ Therefore, the corrected value used for $\Delta\epsilon_{450, \text{corr}} = 14,500 \text{ M}^{-1} \text{ cm}^{-1} - 2,000 \text{ M}^{-1} \text{ cm}^{-1} = 12,500 \text{ M}^{-1} \text{ cm}^{-1}$. This correction was also applied for $\Delta\epsilon_{368}$. The full formula used to find the $\Delta\epsilon_{368, \text{corr}}$ was: $\Delta\epsilon_{368, \text{corr}} = [(\Delta A_{368} / \Delta A_{450}) \times \Delta\epsilon_{450, \text{corr}}] - \Delta\epsilon_{368}$.

References

- (1) Newkome, G. R.; Kiefer, G. E.; Puckett, W. E.; Vreeland, T. *J. Org. Chem.* **1983**, *48*, 5112–5114.
- (2) Hebký, J.; Kejha, J.; Karasek, M. *Collect. Czech. Chem. Commun.* **1961**, *26*, 1559.
- (3) Gandhi, B. A.; Green, O.; Burstyn, J. N. *Inorg. Chem.* **2007**, *46*, 3816–3825.
- (4) Kalsani, V.; Schmittel, M.; Listorti, A.; Gianluca, A.; Armaroli, N. *Inorg. Chem.* **2006**, *45*, 2061–2067.
- (5) Schmittel, M.; Michel, C.; Liu, S.-X.; Schildbach, D.; Fenske, D. *Eur. J. Inorg. Chem.* **2001**, 1155–1166.
- (6) Schmittel, M.; Ganz, A. *Chem. Commun.* **1997**, 999–1000.
- (7) Kalsani, V.; Bodenstedt, H.; Fenske, D.; Schmittel, M. *Eur. J. Inorg. Chem.* **2005**, 1841–1849.
- (8) Hong, J.; Shores, M. P.; Elliott, C. M. *Inorg. Chem.* **2010**, *49*, 11378–11385.
- (9) Calderazzo, F.; Marchetti, F.; Pampaloni, G.; Passarelli, V. *J. Chem. Soc., Dalton. Trans.* **1999**, 4389–4396.
- (10) Garas, A. M. S.; Vagg, R. S. *J. Heterocycl. Chem.* **2000**, *37*, 151–158.
- (11) Margiotta, N.; Bertolasi, V.; Capitella, F.; Maresca, L.; Moliterni, A. G. G.; Vizza, F.; Natile, G. *Inorg. Chim. Acta* **2004**, *357*, 149–158.
- (12) Wu, J.-Z.; Li, H.; Zhang, J.-G.; Xu, J.-H. *Inorg. Chem. Commun.* **2002**, *5*, 71–75.
- (13) Sugihara, H.; Okada, T.; Hiratani, K. *Anal. Sci.* **1993**, *9*, 593–597.
- (14) Lunelli, B.; Grazia Giorgini, M. *Journal of Molecular Spectroscopy* **1977**, *64*, 1–14.
- (15) Lunelli, B.; Pecile, C. *Canadian Journal of Chemistry* **1968**, *46*, 391–396.
- (16) Finke, R. G.; Smith, B. L.; Droegge, M. W.; Elliott, C. M.; Hershenhart, E. *J. Organomet. Chem.* **1980**, *202*, C25–C30.
- (17) Elliott, C. M.; Hershenhart, E. J. *J. Am. Chem. Soc.* **1982**, *104*, 7519–7526.
- (18) Rawls, M. T. Charge Separation in Covalently Bound and Self-Assembled Donor Chromophore Acceptor Systems, PhD Thesis, Colorado State University, Chemistry: Fort Collins, 2007.
- (19) Klumpp, T.; Linsenmann, M.; Larson, S. L.; Limoges, B. R.; Bürsner, D.; Krissinel, E. B.; Elliott, C. M.; Steiner, U. E. *J. Am. Chem. Soc.* **1999**, *121*, 1076–1087.
- (20) Klumpp, T.; Linsenmann, M.; Larson, S. L.; Limoges, B. R.; Bürsner, D.; Krissinel, E. B.; Elliott, C. M.; Steiner, U. E. *J. Am. Chem. Soc.* **1999**, *121*, 4092.
- (21) Kalyanasundaram, K. *Photochemistry of polypyridine and porphyrin complexes*; Academic Press: London; San Diego, 1992.

PART I. CHROMOPHORE-ACCEPTOR DIADS

PART I
Chapter 3

Photo-Induced, Intramolecular Charge Transfer Reactions in Cu(I) bis-Phenanthroline Chromophore-Acceptor Diads^{e,f,g}

3.1 Introduction

For many decades trisbipyridineruthenium(II), [Ru(II)L₃], has been the prototypical chromophore in many photoinduced charge separation schemes. Its photophysical, electrochemical and coordination properties are nearly unique and, taken together, make it an ideal candidate for intramolecular photoinduced charge separation studies.¹ Most serious competition in this regard has come from other second and third row transition metal complexes (e.g., Os, Pt, Re, Ir) which are just as rare and often have coordination chemistry that is even more of a challenge than that of ruthenium.¹⁻⁴ One notable exception to this general rule is bisphenanthrolinecopper(I), [Cu(I)P₂]. Like [Ru(II)L₃], bisphenanthrolinecopper(I) exhibits a strong MLCT transition in the visible and the resulting excited state is a thermodynamically powerful reductant.^{1,4-6} As such, [Cu(I)P₂]^{*} can undergo oxidative quenching reactions in much the same way as [Ru(II)L₃]^{*}. In many ways, however, the chemistry of [Cu(I)P₂] is much more complex than that of [Ru(II)L₃].^{1,4-6} Two things in particular contribute to this complexity: First, Cu(I) is d¹⁰ and thus its complexes are usually very labile.^{1,7-11} Consequently, unlike for [Ru(II)L₃], it is not often possible to prepare, isolate and purify [Cu(I)P₂]-type complexes via such techniques as chromatography. Second, much like [Ru(II)L₃], to a good first approximation the MLCT state can be

^e Manuscript in preparation. Added to dissertation with permission from all authors involved

^f Megan Lazorski and C. Michael Elliott, Department of Chemistry, Colorado State University, Ft. Collins, CO 80523.

^g Ulrich E. Steiner, Fachbereich Chemie, Universität Konstanz, Konstanz, Germany, D-78457

thought of as $[\text{Cu}(\text{II})(\text{P}^*)(\text{P})]^*$. Consequently, the resulting d^9 Cu(II) undergoes a rapid Jahn-Teller distortion towards a “flattened” square planar geometry.^{7,12-15} In these complexes, the flattening distortion is achieved by a reduction in the dihedral angle between the two phenanthroline ligands (from $\varphi \approx 90^\circ$ in the ground state and Franck Condon MLCT state (FC-MLCT) to $\varphi \geq 68^\circ$ in the flattened $^1\text{MLCT}$ and $^3\text{MLCT}$ state for $[\text{Cu}(\text{dmp})_2]^+$).¹³⁻¹⁵ Moreover, in the presence of coordinating solvents or anions, a fifth ligand can coordinate in the J-T distorted Cu(II) geometry, forming a non-emissive exciplex.^{13,15-20} While non-emissive, this exciplex is still capable of undergoing oxidative quenching.^{6,21-25} However, the driving force of oxidative quenching is dependent upon the strength of the interaction of the fifth ligand which is mitigated by several factors: the steric bulk and K_a of the incoming ligand, steric bulk of the phenanthroline ligands, and degree of flattening due to J-T distortion.^{16-20,26-30} While examples of photoinduced electron transfer chemistry with $[\text{Cu}(\text{I})\text{P}_2]$ -type complexes go back many decades, the complications that arise from lability and excited-state geometry changes have made it much less of a focus than $[\text{Ru}(\text{II})\text{L}_3]$.

While introducing an additional level of complexity, the excited-state distortions and exciplex formations, also can be potentially advantageous in studies of photoinduced intramolecular electron transfer processes. For example, consider the case of simple "diad" molecular assemblies where a chromophore is covalently bound to some electron acceptor (C-A) such that the electronically excited chromophore, C^* , is capable of reducing the acceptor in one single electron transfer step to form an intramolecular charge transfer (CT) product $\text{C}^{+\circ}-\text{A}^{(n-1)+}$ as shown in Figure 3.1. A large number of such diads, assemblies in which the C is a $[\text{Ru}(\text{II})\text{L}_3]$ -type complex and the acceptor, A, is a range of organic species (frequently either viologen, mono-quaternary amine, or di-quaternary amine moieties) have been prepared and studied. Invariably for these

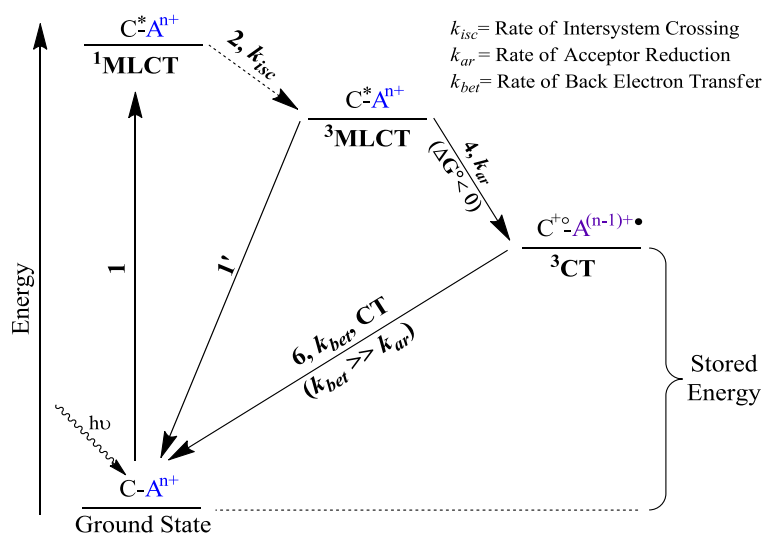


Figure 3.1. Jablonski diagram (not to scale) indicating the electron-transfer pathways for a generic C-Aⁿ⁺ diad after photo-excitation. The C represents the entire chromophore (ML_x, where M=metal such as Ru(II) or Cu(I) and L=polypyridyl ligand), Aⁿ⁺ is a covalently attached acceptor moiety, and the solid dot (•) represents a radical electron.

Additional electron transfer step is required, usually one in which the oxidized chromophore is reduced: for example, D-C^{*}-A → D-C⁺-A⁻ → D⁺-C-A⁻. In contrast to these [Ru(II)L₃] systems, Meyer and coworkers reported the efficient formation of relatively long-lived (up to 2 μs in dimethylsulfoxide, DMSO) charge-transfer products in several Cu(I) bipyridine-viologen-based diad assemblies.^{23,24} In these studies, the lifetime of the C⁺-A^{(n-1)+•} product was demonstrated to be highly solvent dependent, varying by two orders of magnitude between CH₂Cl₂ (shortest) and DMSO (longest).^{23,24} The authors speculated that the long lifetime of the CT products in these copper-based systems might be due (at least in part) to the large reorganization energy afforded by the geometric and coordination number changes required for the recombination reaction.^{7,23,24,31}

Another feature that [Ru(II)L₃] and [Cu(I)P₂] share is similar, but not identical, spin chemistry. Both are singlets in the ground state. Both undergo intersystem crossing from the initially formed ¹MLCT to form ³MLCT photo-excited states.^{1,5,7,13-15,31} However, differences in

systems, efficient oxidative quenching occurs, but the back electron transfer from the C⁺-A^{(n-1)+•} product is faster than the quenching ($k_{bet} > k_{ar}$); thus, no appreciable amount of the charge transfer product persists. In such [Ru(II)L₃]-based systems, in order to form any appreciable amount of persistent charge separated species, at least one addi-

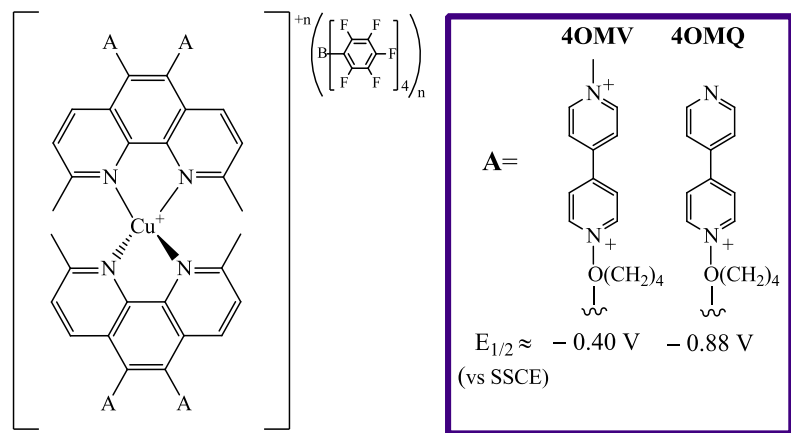
the energy separating the $^1\text{MLCT}$ and $^3\text{MLCT}$ states, spin-orbit coupling (SOC), singlet and triplet character of the fully equilibrated excited states, and relative excited state populations make the situation more complex for $[\text{Cu(I)P}_2]$ than the $[\text{Ru(II)L}_3]$ systems.^{7,13–15,28,32} As is outlined in greater detail in the Discussion section, most of these differences in excited state properties/dynamics in $[\text{Cu(I)P}_2]$ systems are a result of flattening distortions that occur shortly after photoexcitation (ca. 700 fs).^{13–15,28} Understanding these differences in the excited state properties/dynamics may provide insight into the spin chemistry of the CT state and how the CT state kinetics are influenced by a magnetic field.

As discussed in the Introduction to this thesis, the spin-chemistry of $[\text{Ru(II)L}_3]$ complexes has been studied in some depth.^{33–36} As mentioned above, back electron transfer from the CT (k_{bet}) state occurs from the ^3CT state to the singlet ground state as the radical hole and radical electron recombine, making the recombination process spin-forbidden (c.f. Figure 3.1).^{33,34,36} However, in “normal” organic radicals, when the radical hole and electron are separated by a large distance, the singlet and triplet states can be nearly degenerate in zero magnetic field. In this case, intersystem crossing is facile (k_{isc}) between the singlet and triplet states because coherent isotropic hyperfine coupling (IHC) interactions efficiently mix the states and provide a rapid, spin-allowed recombination pathway.^{33,34,36} Therefore, application of a magnetic field can affect the efficacy of singlet/triplet mixing, and thereby modulate k_{isc} .^{33,34,36}

In $[\text{Ru(II)L}_3]$ D-C-A's, the application of relatively small magnetic field was able to increase the average ^3CS lifetime of ten-fold ($\tau_{cs} \approx 2 \mu\text{s}$, 0.5 T).^{33,34,36} This effect on the CS decay kinetics was rationalized based on the so-called *relaxation mechanism* proposed by Hayashi and Nagakura, shown in Figure 3.2.³⁷ The application of a magnetic field to the ^3CS radical pair in $[\text{Ru(II)L}_3]$ D-C-A's induces Zeeman splitting of the $^3\text{CS(T}_+)$ and $^3\text{CS(T}_-)$ states, which causes

orbit coupling can also affect the $^1\text{CT}/^3\text{CT}$ mixing and could provide alternative spin-mixing pathways.

Because of the smaller energy separation between the singlet and triplet for copper (relative to ruthenium), we anticipate interesting spin-chemical consequences on both the photoinduced charge separation and its recombination that could be probed by magnetic field dependent studies. To that end, we have prepared a Cu(I)-based C-AX diad systems for study related to one originally reported by Meyer and coworkers, as shown in Figure 3.3. Our complex differs primarily in that the copper ligands are based on 2,9-dimethyl-1,10-phenanthroline (dmp) rather than bipyridine (bpy). Additional structural rigidity afforded by the phenanthroline ligand can inhibit molecular motions that occur in copper complexes with bpy ligands. Therefore, phenanthroline ligands can help control structural distortions in the coordination sphere, which is particularly important for the Cu(II) excited state and discussed in detail in the Discussion section. As we report below, this system undergoes moderately efficient single-step photoinduced charge



C-AX Diads	A Moiety
C-AV	4OMV
C-AQ	4OMQ

Figure 3.3. The structure of the C-AX diad complexes and the acceptor (A) moieties used for the 4OMV and 4OMQ ligands.

separation to form a charge transfer product (CT) in which the copper is oxidized to Cu(II) and the viologen or mono-quaternary amine electron acceptor is reduced to the cationic or neutral radical species (note that the viologen(mono-quaternary amine) acceptor is a di-cation(cation); therefore,

one-electron reduction yields a cationic(neutral) radical). The life-time of the CT product is solvent dependent, and seemingly dependent on an applied magnetic field (between fields of 0 and 2.25 T), though the changes in lifetime with applied field are very small. The quantum efficiency for CT formation is also field dependent in a significant way. The changes in lifetime and quantum efficiency with magnetic field could be due to the so-called relaxation mechanism proposed by Hayashi and Nagakura, described in the Introduction to this thesis. However, we also propose that the magnetic field dependence could be changing the singlet/triplet distribution in the MLCT state of the $[\text{Cu}(\text{I})\text{P}_2]^+$ from which the charge separation initiates.

3.2 Results

The recombination kinetics and formation quantum yield of the photoinduced ET product of $[\text{Cu}(\text{I})(4\text{OMX})_2]^{n+}(\text{TPFB}^-)_n$, were studied in 1,2-difluorobenzene/methanol (dfb/X% MeOH, where X = 0-10%) solvent using transient absorption (TA) spectroscopy as described in the Experimental section ($[\text{Cu}(\text{I})(4\text{OMX})_2]^{n+}(\text{TPFB}^-)_n = \text{C-AX diad}$, structures of the C-AX diads in this study are shown in Figure 3.3). The intramolecular ET product is formed by oxidative quenching of the $[\text{Cu}(\text{I})\text{P}_2]^{+*}$ MLCT excited state by one of the attached electron acceptor units yielding a $\text{Cu}(\text{II})\text{P}_2\text{--}4\text{OMX}^{n+}$ charge transfer state (CT). The dfb/X% MeOH solvent system was chosen for three reasons: (A) 1,2-difluorobenzene is particularly stable with respect to radical initiated photochemistry, (B) C-AX is soluble in dfb and dfb/X% MeOH, and (C) the lifetime of the CT is longer in a coordinating solvent or with coordinating anions present. As briefly described above, the lengthened lifetime has been attributed to stabilization of the $\text{Cu}(\text{II})\text{P}_2$ moiety in the CT state via association of, in this case, MeOH to the fifth coordination site of the J-T distorted complex.²⁴ The latter point is important because the lifetime of CT in dfb alone is too short

($\tau_{ct} \approx 7$ ns) to adequately deconvolute from the laser pulse with our instrumentation (pulse width ≈ 7 ns). Furthermore, the lifetime of the CT state is highly influenced by the concentration of MeOH in the solution (vide infra). Finally, the sample solutions exhibited negligible changes in their static UV-vis spectra before and after repeated laser excitation, confirming their stability under these conditions.

Studies on $[Cu(4OMV)_2]^{9+}(TPFB^-)_9$ and $[Cu(4OMV)(dtbp)]^{5+}(TPFB^-)$ Diads

The formation of the proposed CT product was verified before embarking on the detailed kinetic study. First, spectroelectrochemistry (SE) was used to obtain a quantitative spectrum for the one-electron reduction product

of methyl viologen (MV, dfb solvent) to serve as a model for the reduced acceptor ligand, $4OMV^{3+}$.

A comparison of the spectrum for MV^{+} and the TA spectrum obtained from the C-AV diad complex is given in Figure 3.4. As is evident

in Figure 3.4, the peak positions in the TA spectrum are in good agreement with those of the MV^{+} spectrum from the SE data. The

relative peak intensities do not agree as well, but the difference could be rationalized on the basis of monochromator slit-width issues for the sharp peak of the $4OMV^{+}$ at short wavelength ($\lambda_{max} =$

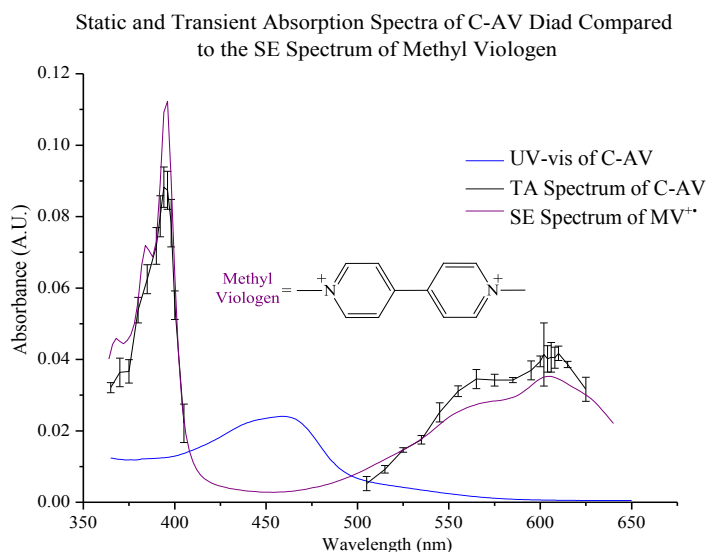


Figure 3.4. Transient absorption spectrum of the C-AV diad in dfb/5% MeOH after excitation at 475 nm (black), the static spectrum of C-AV (blue) and spectroelectrochemical spectrum for MV^{+} (red). The MV^{+} spectrum was scaled by a constant factor such that the summed point-by-point difference between that spectrum and the TA spectrum was minimized. Each point in the TA spectrum was generated from the average ΔA at 13-17 ns after $t=0$. The UV-vis spectrum was scaled down by an arbitrary value to indicate the wavelength region where a bleach is expected.

396 nm). The bleach of the MLCT region of the $[\text{Cu}(\text{I})\text{P}_2]$ chromophore was not investigated in the TA spectrum, but is planned for future study. The presence of a bleach would confirm the loss of $[\text{Cu}(\text{I})\text{P}_2]$ ground state absorption due to fast oxidative quenching to the $[\text{Cu}(\text{II})(4\text{OMV}^{4+})(4\text{OMV}^{3+})]^{+9}$ on the nanosecond time scale.

As mentioned above, the lifetime of the CT state was found to be highly solvent dependent. Figure 3.5A shows typical, single-wavelength TA decay curves monitored at 396 nm after excitation using a 475 nm pump beam for the C-AV complex in dfb solvent containing varying concentrations of MeOH. As is evident from Figure 3.5A, the lifetime of the CT state increases from c.a. 7 ns with dfb/0% MeOH, to c.a. 40-45 ns in dfb/5-10% MeOH. The initial intensity also increases with increasing MeOH concentration. However, there is a concomitant increase in the magnitude of the $[\text{Cu}(\text{I})\text{P}_2]$ MLCT band in the static absorption spectrum as shown in Figure 3.5B with the first several additions of MeOH to the cell. Although no solids were visible in the initial solution, these data together suggest that it is likely the increased absorbance, in this case, is at least partially due to the increased solubility of the complex when MeOH is present. This

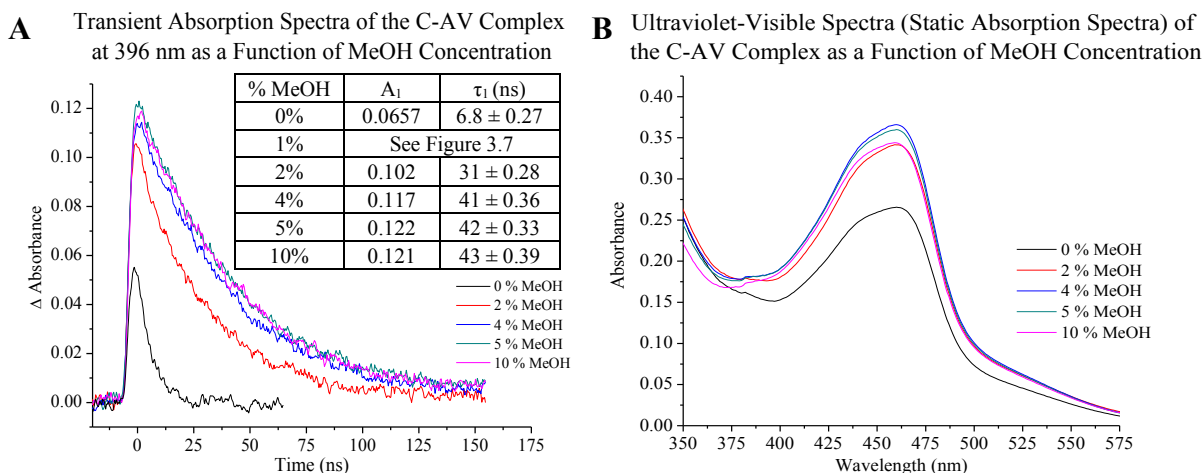


Figure 3.5. The effect on the transient absorption of C-AV in dfb at 396 nm after excitation at 475 nm (**A**) and static spectra ($\lambda_{\text{max}}=460$ nm) (**B**) as a function of added MeOH. The data in (**A**) were obtained with a small (25 mT) applied magnetic field (see text); however, the effect of a magnetic field on the lifetime of the decay is very small so these lifetimes are still accurate within a couple of nanoseconds. See Figure 3.9.

explanation is supported by the fact that there is also essentially no difference in the MLCT band shape in the presence and absence of MeOH in solution. The effect of MeOH on the CT lifetime seems to saturate at ca. 4% MeOH. The slight decrease in the initial intensity of the CT absorbance for the highest MeOH concentration is consistent with the simple dilution of the C-AV concentration with the added volume of MeOH (evident in both the static and TA spectra).

Since both solvents (e.g. MeOH) and anions can be Lewis bases and form adduct complexes that could influence the recombination kinetics in the C-AX diads, an anion dependence is also possible. Although anion dependence wasn't studied explicitly, C-AX diads in solutions containing additional anions other than TPFB (anions remaining in solution from the in-situ metathesis, see Experimental Methods) did not seem to influence the recombination kinetics. However, only a few anions could be used for these studies due to the solubility of the C-AX diads with different anions in dfb/X% MeOH and the redox activity of some anions (e.g. I⁻) which could interfere with CT formation.

Another probable explanation for the increase in initial intensity with MeOH concentration (Figure 3.5A) is the response function of the laser instrument. As the lifetime of a species decreases, the observed initial intensity depends on the response function of the laser because the laser pulse is not a delta function. If the lifetime of the CT state is similar to, or shorter than the pulse width of the laser, a significant population of molecules that are excited on the leading edge of the laser pulse have decayed away within the pulse itself. Therefore, the only signal that is observed is due to the molecules that are excited near the following edge of the laser pulse and the decay shape is convoluted with the laser pulse. This is not an issue when the lifetime is significantly longer than the laser pulse width because the amount of signal that has decayed within the width of the laser pulse is very small with respect to the overall amount of signal, which ex-

plains why the initial intensity is higher when $> 4\%$ MeOH is used ($\tau_{ct} \approx 40\text{-}45$ ns). In depth investigation of the response function for the laser system used in this study has not been performed, but is planned for the near future.

Another interesting solvent effect occurs in the C-AV diad systems, which is the change in decay characteristics with changing MeOH concentration. As shown in Figure 3.6, the decay changes from, presumably, mono-exponential in dfb/0% MeOH to bi-exponential in dfb/1% MeOH. As the concentration of MeOH is increased up to 2%, the decay becomes more mono-exponential again; although, a very small portion of the second decay component seems to remain, but is too small to be fit in Origin. Once the concentration of MeOH has increased to 4%, the decay is mono-exponential when monitored at 396 nm. At 584 nm, the same trend occurs, but the second decay component never completely disappears, it just drastically decreases in intensity (Figure 3.6, bottom left vs right). However, at 584 nm there is significantly lower absorbance when the $\lambda_{ex} = 475$ nm (which is the pump wavelength used for the majority of these data) and a smaller S/N ratio, which could obfuscate the results. Furthermore, at longer wavelengths (550-650 nm), there is always additional “laser only” signal that is not present in the short wavelength regions studied. It is uncertain if this additional signal is due to emission or some other unknown process, but it is possible that it is inadequately subtracted from the data making it seem like a second decay component is present at 584 nm, but not at 396 nm.

Since the timescale of the first decay component of the C-AV diad in dfb/1% MeOH is so fast, the fit could not be performed in a normal fashion. When fit using a mono-exponential decay from 10 ns after $t = 0$, which is a typical fitting procedure for this timescale and a laser pulse width of ca. 7 ns, the fit significantly underestimates the initial absorbance as shown in Figure 3.7A. When fit with a bi-exponential decay from 10 ns after $t = 0$, the fit either

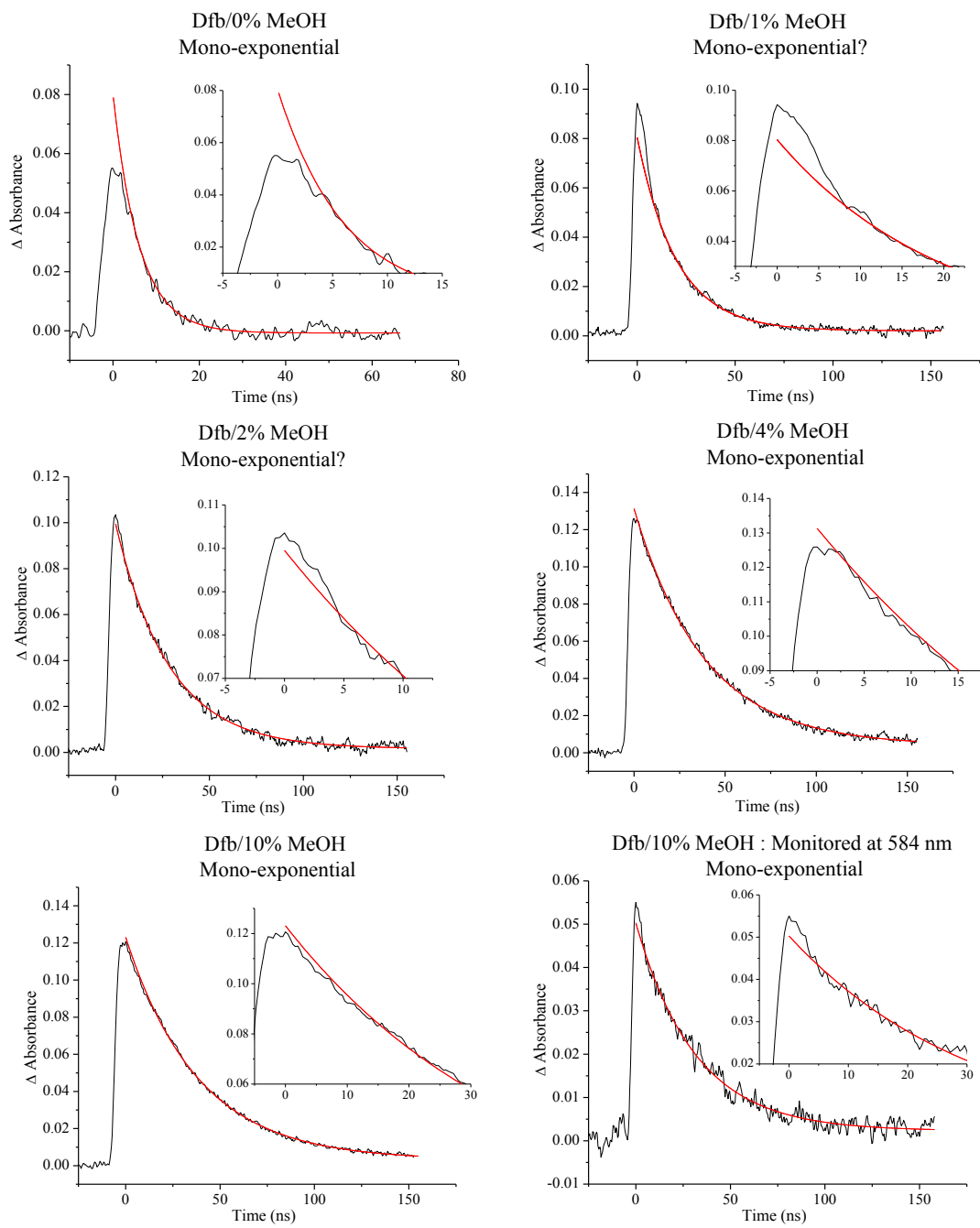


Figure 3.6. TA decay data for the C-AV diad monitored at 396 nm (except where noted, 584 nm) in dfb/X% MeOH at zero applied magnetic field. As the percentage of MeOH increases from 0-1% the decay changes from mono- to bi-exponential and then back to mono-exponential as the MeOH concentration increases above 2% MeOH. It seems that there is still some remnant of bi-exponential character in the 2% MeOH at all fields, but it is so small that it could not be fit with a bi-exponential decay. This change in decay characteristic was also generally observed for the data monitored at 584 nm, but the second decay component just drastically reduces in size, never disappearing. Furthermore, the 584 nm data was less conclusive due to significantly lower absorbance when the $\lambda_{\text{ex}} = 475$ nm (which is the pump wavelength used for the majority of these data) and a smaller S/N ratio. The two spectra taken in dfb/10% MeOH at 396 nm (bottom, left) and 584 nm (bottom, right) are both averaged from 6 individual runs that were averages of 400 individual laser shots. The insets in each panel show a close up view of the data and fits at $t = 0$.

produced absurd values for the A_1 and τ_1 of the first decay component, or treated the fit as if the data were mono-exponential, producing identical lifetimes for both τ_1 and τ_2 . To make absolutely sure that the data was not mono-exponential, the data was then fit with a mono-exponential decay from $t = 0$ because the timescale of this data is so short and such a large fraction of the data could not be fit adequately using either of the two previous fitting procedures. This resulted in a fit like the one shown in Figure 3.7B, with a large degree of mismatch between the mono-exponential fit and the data, which suggests that these data are, in fact, bi-exponential. In order to obtain a satisfactory fit of these data, the following fitting procedure was followed. First the data were fit using a bi-exponential fit from $t = 0$ (Figure 3.7C), then the A_1 and τ_1 values obtained in that fit were plugged in to a new fit of the data performed from 10 ns after $t = 0$ and held constant, allowing the A_2 and τ_2 values to vary (Figure 3.7D). This method allowed the data to be fit in a satisfactory manner and produced lifetimes for the second decay component (τ_2) that were very similar to those obtained by fitting the data from with a mono-exponential decay from 10 ns after $t = 0$ (Figure 3.7A), while also fitting the curvature of the first decay component. This is an un-common fitting procedure, and the lifetimes of the first decay component (τ_1) are not considered to be very reliable due to the convolution of the data with the laser pulse. However, this was the only fitting procedure that could produce satisfactory fits for the data in dfb/1% MeOH. Furthermore, this bi-exponential decay characteristic was observed in multiple data sets for dfb/1% MeOH, adding credence to the change in decay profile with MeOH concentration. Note that the response function of the instrument could be affecting this result, as the decay characteristic in dfb/0% MeOH could also be bi-exponential, but the fastest decay component could be too short to be observed on this laser system.

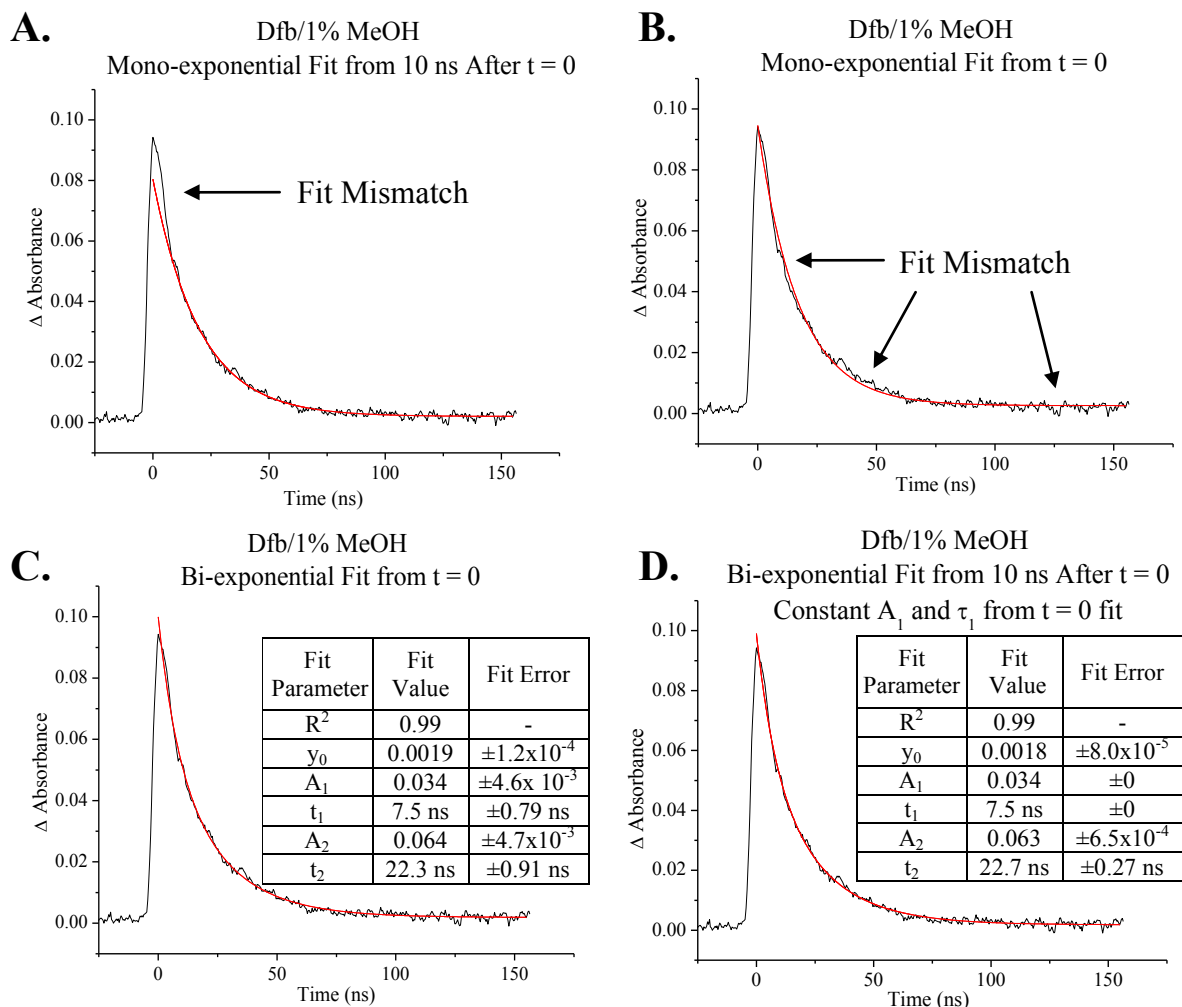


Figure 3.7. The TA decay data from the C-AV diad in dfb/1% MeOH at 396 nm could not be adequately fit with a mono-exponential decay from 10 ns after $t = 0$ (**A**) or when fit from $t = 0$ (**B**), the latter of which is an uncommon fitting practice due to convolution of the signal with the laser pulse. However, these data could also not be fit using a bi-exponential fit from 10 ns after $t = 0$ (not shown). Therefore, the data was fit using a bi-exponential decay from $t = 0$ (**C**), then re-fit using a bi-exponential decay from 10 ns after the laser pulse, by using the values obtained for A_1 and t_1 from the $t = 0$ fit (**D**). Note, that the slight over-estimation of the initial intensity in these fits is not labeled as a fit mismatch because the convolution of the signal with the laser pulse often causes this type of fit error.

The effect of an applied external magnetic field on the CT recombination kinetics was also investigated via TA spectroscopy at 396 and 584 nm. The 396 nm data are shown in Figure 3.8. These data show that the lifetime of the CT state seems to have a very small dependence on an applied magnetic field. At first, sample-to-sample fluctuations in lifetime due to convolution

Transient Absorption Spectra of the C-AV Complex at 396 nm
for a Range of Applied Magnetic Fields (mT)

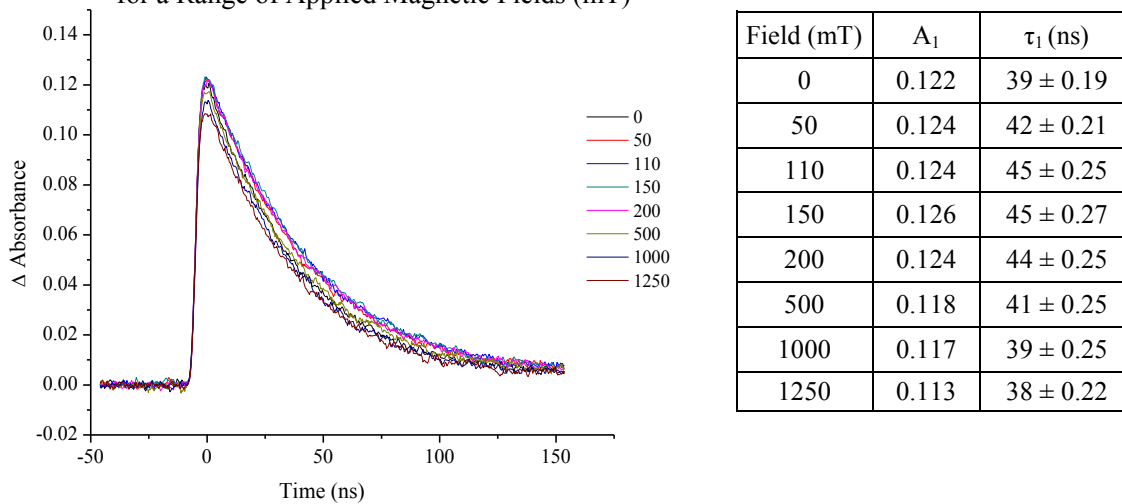


Figure 3.8. Single wavelength decay curves at 396 nm for C-AV in dfb/10% MeOH as a function of applied magnetic field (mT) after excitation at 475 nm (left) and their fit values for initial intensity (A_1) and lifetime (τ_1) (right).

of the signal with the laser

pulse and instability of the

laser system made it seem that

these changes in lifetime were

within experimental error.

However, upon further inspection

of the data a very small

change in lifetime is evident.

As shown in Figure 3.9, the

lifetime of the C-AV diad in-

creases with magnetic field

from its zero field value up to

a maximum between 50-200 mT, then gradually decreases again to nearly the original value by

1000 mT. The overall change in lifetime from the zero field value to the maximum is always

Lifetime of C-AV Diad at 396 nm in Dfb/X% MeOH
vs Applied Magnetic Field

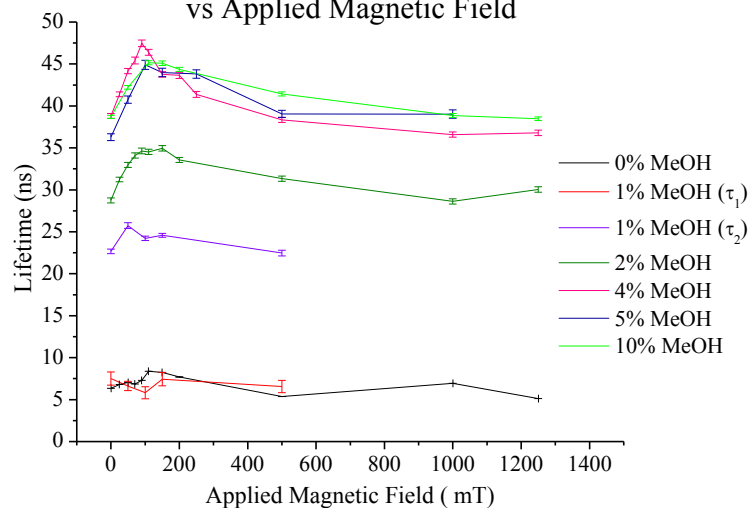


Figure 3.9. The lifetime of the C-AV diads monitored at 396 nm in dfb/X% MeOH in varied applied magnetic fields. The sample in 1% MeOH was bi-exponential at all applied field, as discussed below. The first lifetime component, τ_1 , was very similar to the lifetime of the C-AV diad in 0% MeOH. The lifetime of the C-AV diad in all of the other solvent compositions was essentially mono-exponential. The error bars reflect the error of the fit.

within 10 ns, which is why this effect has been so difficult to differentiate from normal experimental fluctuations. However, the changes observed in lifetime are consistent for several different samples, in different solvent compositions, and at two different wavelengths (584 nm data not shown), indicating that the effect is indeed real. The changes in lifetime are not as consistent in dfb/0% MeOH, which is expected due to convolution of the signal with the laser pulse.

There is also a marked effect on the initial intensity with magnetic field, as shown in Figure 3.10. The initial intensity first increases with applied field, reaching a maximum between 75-150 mT, and then decreases until approximately 500 mT, after which it remains essentially constant. This trend in initial intensity tracks closely with the changes observed in the lifetime. The apparent relative change in initial intensity between 0 mT and the field where the maximum value of initial intensity is obtained (between 75-150 mT), ΔI_0 , depends on the amount of MeOH

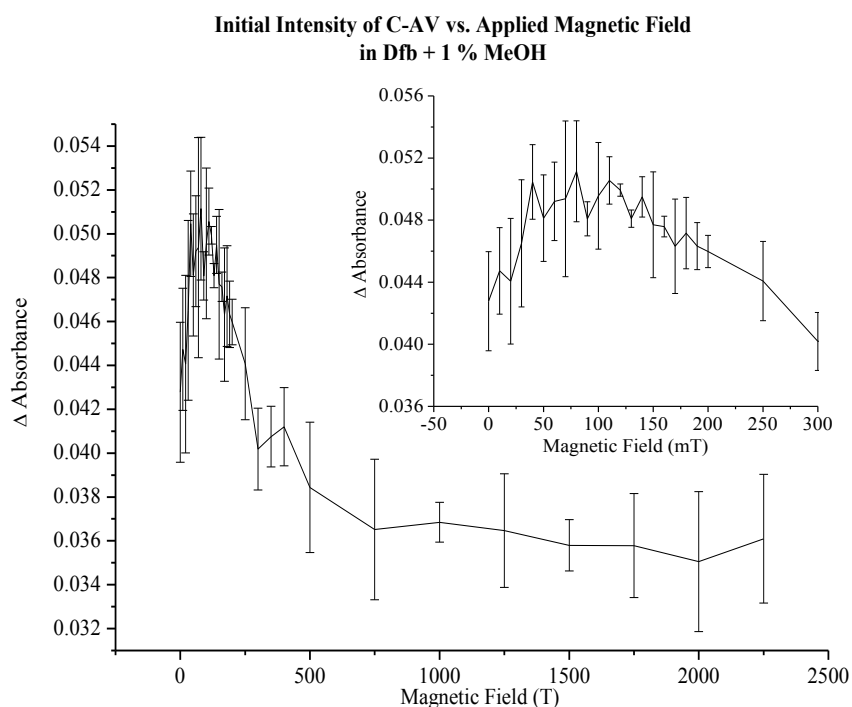


Figure 3.10. The initial intensity, I_0 , of the C-AV complex monitored at 584 nm as a function of applied magnetic field after excitation at 450 nm. Each point was generated from the average ΔA at 10-12 ns after $t = 0$, at which point ca. 77% of the first decay component should have decayed away in this solvent. The data was then averaged for 5 separate runs.

in solution (Figure 3.11).

The biggest ΔI_0 is observed

for pure dfb and decreases as

the percentage of MeOH is

increased up to ca. 4%

MeOH where the effect ap-

pears to plateau. As dis-

cussed above, there is also an

increase in absolute initial

intensity, I_0 , which also plat-

aus around 4% MeOH. The fact that the largest changes,

is for the diad in dfb/0% MeOH,

which has the shortest zero field lifetime, implies that these changes in initial intensity may be just a reflection of the change in lifetime.

At this point it is appropriate to comment on the relative size of the error bars on the data in Figures 3.10 and 3.11. Each data point represents the average of at least 4 measurements which are, in turn, themselves the averages of at least 400 individual laser excitations. The magnitude of the error bars notwithstanding, these experiments were repeated a large number of times on many different solutions and, qualitatively, the shapes of the curves represented in Figures 3.10 and 3.11 were consistently the same. During this series of measurements we experienced a pulse-to-pulse variation in excitation laser power which we estimate to be in the range of 40%. We, therefore, must conclude that the actual uncertainty for the data in these two figures is likely to be considerably smaller than is implied by the mathematically determined error bars.

The ΔI_0 in an Applied Magnetic Field (Black) and I_0 in Zero Field of the C-AV Complex (Red) vs % MeOH in Dfb

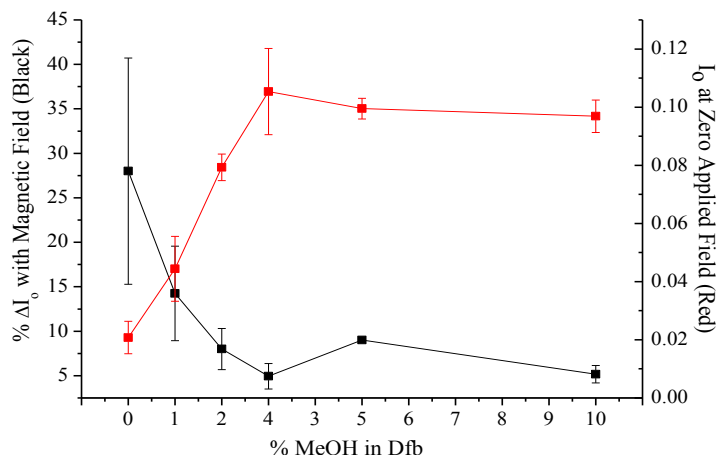
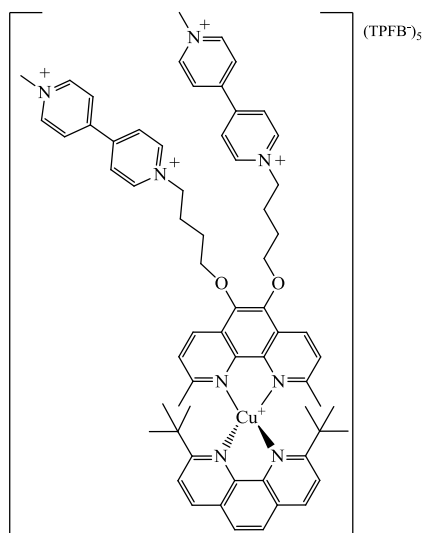


Figure 3.11. The absolute I_0 (red curve, right hand axis) and ΔI_0 (black curve, left-hand axis) for the C-AV diad in dfb with magnetic field as a function of MeOH concentration after excitation at 475 nm). See text for details.

We also attempted to determine a quantum efficiency for the CT formation, Φ_{CT} , as described in the Experimental section. Given the relative experimental uncertainties we estimate that Φ_{CT} in dfb with 1.6% MeOH is $55 \pm 15\%$ in the absence of any applied field. The I_0 data in Figure 3.6 shows an 18% increase in CT concentration with an applied field of 100 mT. This corresponds to a Φ_{CT} of 65% (again with the same relative $\pm 15\%$ error bars).

The effect of a magnetic field on the CT recombination kinetics/ET dynamics was also studied for an alternate, heteroleptic C-AX diad with a 4OMV acceptor moiety and a 2,9-di(*t*-butyl)-1,10-phenanthroline (dtbp) ligand, which will be referred to as C-AVB and is shown in Figure 3.12. This complex was studied to determine if added steric bulk about the $[Cu(I)P_2]$ coordination sphere influences the CT kinetics/ET dynamics in a magnetic field. Imposing greater steric restrictions in $[Cu(I)P_2]$ complexes reduces the energy gap between the $^1MLCT/{}^3MLCT$ states, which influences the SOC (i.e. k_{isc}) between the two states and changes their relative pop-



C-AVB Diad

Figure 3.12. The structure of an alternate C-AX diad using the 4OMV acceptor ligand, C-AVB = $[Cu(4OMV)(dtbp)]^{5+}(TPFB)^5_5$ (dtbp = 2,9-di(*t*-butyl)-1,10-phenanthroline).

ulations.^{13–15,28,32,39,40} Although current literature studies have focused on the effect of changing steric restrictions on the excited state dynamics, the goal of this study was to determine if the ET dynamics of CT formation and decay are also affected by these changes in the presence and absence of a magnetic field. The CT state is directly populated by oxidative quenching of the excited state, thus, it is likely the ET dynamics will change due to the increased steric bulk.

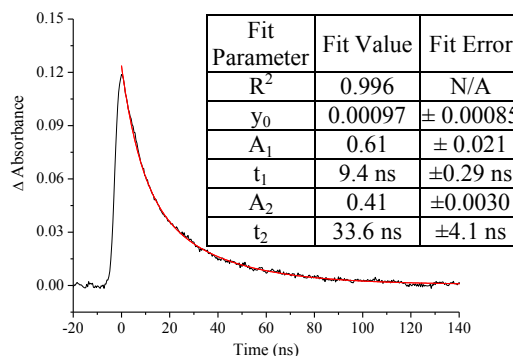
Since the studies on the C-AVB diad solution were performed in different solvent systems than the C-AV diad (vida supra) a direct, conclusive comparison between results

is impossible. Furthermore, the stoichiometry has not been verified by ^1H NMR and an equimolar solution of Cu(I):4OMV:dtbp can result in a solution containing some mixture of $[\text{Cu}(\text{4OMV})_2]^{9+}(\text{TPFB}^-)_9$ and $[\text{Cu}(\text{4OMV})(\text{dtbp})]^{5+}(\text{TPFB}^-)_5$ products. Therefore, for the remainder of this chapter the “C-AVB Solution” will refer to the equimolar solution of Cu(I):4OMV:dtbp which likely results in a mixture of products. Studies on heteroleptic $[\text{Cu}(\text{I})\text{P}_2]$ complexes have been performed that indicate introducing bulky groups in the 2,9-positions of the phenanthroline causes the equilibrium to shift in favor of the heteroleptic complex.^{8–10,29,41} If the steric restrictions are large enough, exclusive formation of the heteroleptic product can be achieved. Based on these studies, it is expected that the “C-AVB Solution” will contain primarily C-AVB diad and a small fraction of C-AV diad.^{8–10,29,41,42} However, despite these limitations, the preliminary data indicates that the increased steric bulk of the C-AVB diad could be influencing the CT kinetics/ET dynamics in the absence and presence of an applied magnetic field.

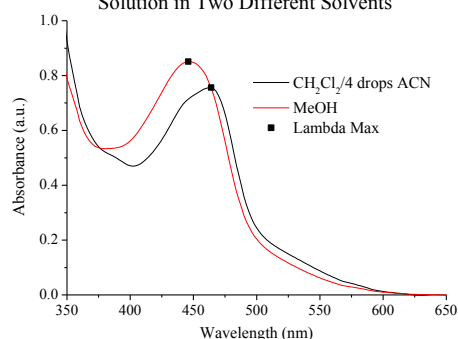
In contrast to the CT decay kinetics of the C-AV diad in dfb/ > 2% MeOH, the data presented in Figure 3.13A indicates that there are two lifetime components in the CT decay kinetics of the “C-AVB Solution” ($\tau \approx 8$ ns, $\tau \approx 30$ ns) when dissolved in MeOH. The bi-exponential nature of the decay could be a result of several factors: the presence of both C-AV and C-AVB complexes in the mixture, ^1CT and ^3CT decay to the ground state, or differing rates of CS decay for the complex with and without the presence of an adducted solvent molecule (4-coordinate vs. 5-coordinate complex).²⁸ If there is a mixture of C-AV and C-AVB products present in the MeOH solution, it is reasonable to think that the longer lifetime ($\tau \approx 30$ ns) is due to the C-AV complex for the following reason; the formation of a solvent adduct complex lengthens the CT state lifetime of the C-AX diad complexes,^{23,24} and the C-AVB diad has additional steric bulk in the Cu(I)PP' coordination sphere that could hinder solvent adduction. However, the longer

lifetime component in this experiment ($\tau \approx 30$ ns) is still significantly shorter than would be expected for the C-AV complex in this solvent as indicated by the data in Figure 3.5 ($\tau_{ct} \approx 35$ -45 ns for C-AV complex in dcb/ > 5% MeOH). Therefore, it is more likely that the 30 ns lifetime is actually the τ_{ct} of the C-AVB complex. The differences in the ground state absorption spectra of the “C-AVB Solution” in MeOH and in DCM/ACN support the C-AVB $\tau_{ct} \approx 34$ ns assignment. As is demonstrated by the static absorption spectra of the “C-AVB Solution” in Figure 3.9B, the intensity of the long wavelength side band (≈ 530 nm) is slightly smaller in MeOH than in DCM/ACN, which could indicate that the species formed in the MeOH solution undergoes less flattening distortion than the one formed in the DCM/ACN.^{5,28,32,43} In the UV-vis spectra, the λ_{max} shifts from 446 nm in MeOH to 464 nm in DCM/ACN, which is very similar to the λ_{max} of the C-AV diad (See Figure 3.4).

A CT Kinetics of the C-AVB Diad Solution in MeOH in Zero Applied Magnetic Field



B Ground State Absorption Spectra of the C-AVB Solution in Two Different Solvents



C CT Kinetics of the C-AVB Diad Solution in CH₂Cl₂/4 drops ACN in Zero Applied Magnetic Field

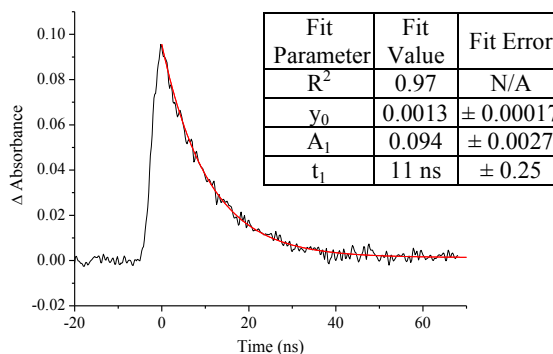


Figure 3.13. Single wavelength TA spectrum at 552 nm (black) and fit (red, from normalized data) of the C-AVB diad solution in MeOH (black) (A), the ground state absorption spectrum (UV-vis) of the C-AVB solution in MeOH (red) and dichloromethane (DCM)/4drops ACN (black)(B). The shift in the lambda max and the reduced absorbance of the 530 nm side band in the MeOH solution indicates that the C-AVB diad is the major product in the MeOH solution and the C-AV diad is the major product in the DCM/ACN solution. The single wavelength TA spectrum at 552 nm (black) and the fit (red) of the C-AVB diad solution in DCM/4 drops ACN (C).

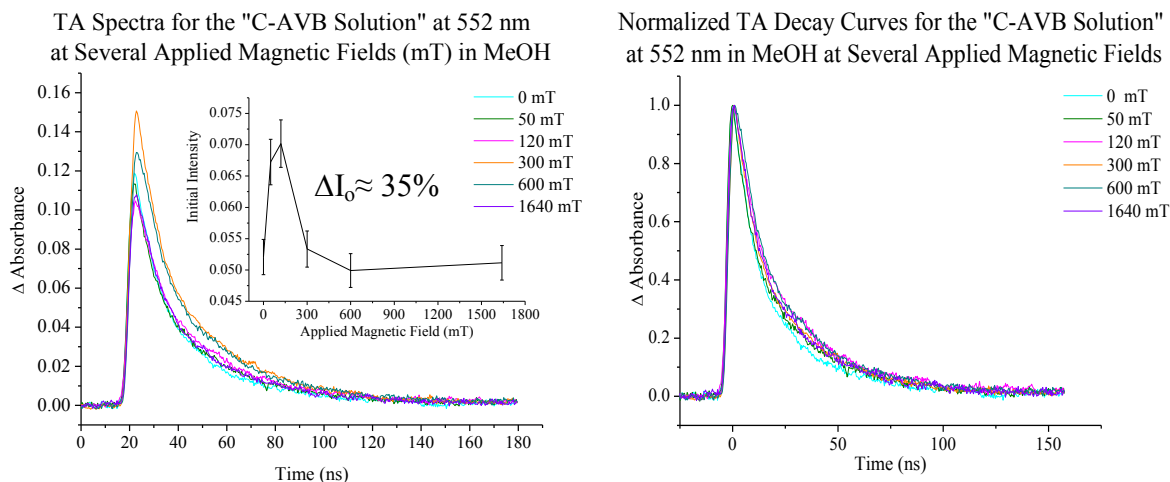
These data imply that C-AVB diad is most likely the major product in MeOH and C-AV may be the major product in DCM/ACN. Furthermore, despite the Lewis basicity of MeOH, Miller et al. report that a similar complex, $[\text{Cu}(\text{dtbp})(\text{dmp})]^+$, is stable towards ligand displacement to the solvento complex in methanolic solutions, but results in a mixture of $[\text{Cu}(\text{dtbp})(\text{dmp})]^+$, $[\text{Cu}(\text{dmp})_2]^+$, and $[\text{Cu}(\text{dtbp})(\text{ACN})_2]^+$ when dissolved in ACN.⁴¹ These results, taken together, indicate that the C-AVB diad is the major product in the MeOH “C-AVB Solution” and the 34 ns lifetime component of the bi-exponential decay is the τ_{ct} of the C-AVB diad.

At this time, the origin of the “short” decay component (ca. 9 ns) for the C-AVB diad in MeOH is not certain. As mentioned previously, the C-AV diad has a ca. 35-45 ns lifetime in dfb/ > 5% MeOH; therefore, it is unlikely that the “short” component in the C-AVB decay profile is due to C-AV diad that could be present in the “C-AVB Solution”. However, there are two possibly scenarios that could give rise to bi-exponential decay behavior for the C-AVB itself: the “short” decay component could be a result of recombination from (A) the ^1CT state or (B) the 4-coordinate ^3CT state. For either of these scenarios, the “short” decay component would have to be due to a portion of the CT population that decays via a different decay mechanism. For example, if the energy gap of the $^1\text{MLCT}/^3\text{MLCT}$ (which should be smaller than the energy gap in less sterically encumbered complexes³²) is retained for the $^1\text{CT}/^3\text{CT}$ states once the acceptor has been reduced, then the population of each CT state could be different for C-AVB relative to complexes with a larger $^1\text{CT}/^3\text{CT}$. Therefore, the “short” decay component could be due to the recombination directly from the ^1CT state and the “long” decay component could be due to recombination from the ^3CT state. However, any recombination from the ^1CT state is likely to be so fast that it is not detectable with a nanosecond laser system. Therefore, a more probable explanation could be that the ^3CT state population is in equilibrium between 5-coordinate and 4-

coordinate species since the C-AVB diad is not as prone to solvent adduction as complexes with less steric bulk. Therefore, the 4-coordinate complexes would require less reorganizational energy to recombine back to the singlet ground state than their 5-coordinate counterparts, i.e. faster k_{bet} in the 4-coordinate geometry. The latter scenario could be supported by the fact that a “short” decay component with a similar lifetime (ca. 7.5 ns) is present in the CT decay of the C-AV diad in dfb/1% MeOH (see Figures 3.6 and 3.7),^h which could be a characteristic lifetime associated with 4-coordinate [Cu(I)P₂] C-AX diad species. Since the C-AVB diad has a greater degree of steric bulk, it is possible that the equilibrium between the 4- and 5-coordinate species is not shifted as far toward the 5-coordinate complex by the presence of a coordinating solvent, so decay from both complexes is observed even in 100% MeOH. However, the assignment of the 9 ns lifetime is much less conclusive.

The effect of an applied external magnetic field on the CT recombination kinetics and ET dynamics of the C-AVB diad was also investigated via TA spectroscopy monitored at 552 nm. Although the normalized TA decay curves presented in Figure 3.14 suggest otherwise, the lifetime changes indicated from fits of these data seem too random to imply that there is an effect on the CT lifetime in the presence of a magnetic field in MeOH. It is possible that in this complex, the changes in lifetime are even smaller than for the C-AV diad complex, making it very hard to ascertain any change from the fits. In order to determine if the magnetic field is actually affecting the CT decay, repeated studies are necessary. However, the preliminary magnetic field effect studies on the initial intensity of the “C-AVB Solution” show that the changes in I_0 follow a similar pattern, but are even more pronounced in this complex than for the C-AV diad, as shown in the inset of Figure 3.14. The absolute initial intensity values, I_0 , were calculated by averaging

^h The lifetime of the C-AV diad in DCM/4 drops of ACN is much shorter than in MeOH, which is understandable since there is very little ACN in this solution, and it is likely being incorporated by the [Cu(dtbp)(ACN)₂]⁺ solvent complex as well, although there is no direct spectroscopic evidence for that complex.



Field Strength (mT)	R ²	A ₁	τ ₁	A ₂	τ ₂
0	0.996	0.61	9.4 ± 0.29 ns	0.41	33.6 ± 0.41 ns
50	0.995	0.46	7.4 ± 0.28 ns	0.56	30.9 ± 0.32 ns
120	0.996	0.44	9.7 ± 0.54 ns	0.57	33.9 ± 0.36 ns
300	0.997	0.49	8.4 ± 0.26 ns	0.53	34.3 ± 0.28 ns
600	0.997	0.56	11 ± 0.54 ns	0.47	37.9 ± 0.41 ns
1640	0.995	0.53	9.8 ± 0.42 ns	0.49	34.4 ± 0.41 ns

Figure 3.14. The effect of a magnetic field on the CT recombination kinetics and initial intensity (inset) for the “C-AVB Solution” in MeOH. The ΔI_0 was calculated from 12-14 ns after $t = 0$, which should eliminate $\approx 77\%$ of the short decay component (ca. 9 ns). These are preliminary studies so the error bars were calculated using the average error from the C-AV experiments as described in the text. The inset table shows the fit data obtained from fitting the normalized data using the non-conventional fitting method described in Figure 3.7.

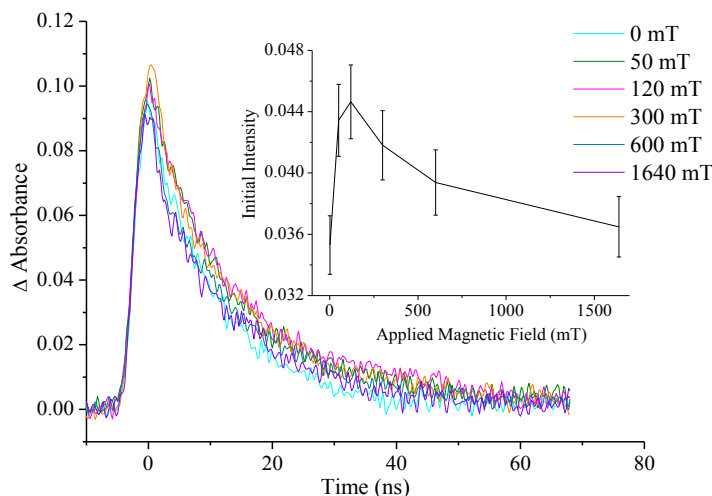
the data from 12-14 ns after the $t = 0$ at every applied field, at which point ca. 77% of the first decay component should have decayed away. In the MeOH solution, the initial intensity first increases with applied field reaching a maximum at 120 mT, then decreases again until it has returned to essentially the zero field value at approximately 300 mT, where it remains until 1640 mT. The absolute ΔI_0 between 0 mT and the maximum value (around 120 mT) is 35% in MeOH. However, these studies were preliminary and error bars were not able to be calculated. The error bars shown were calculated using the average error generated in the independently prepared, pure C-AV diad experiments described above, which was ca. $\pm 5.4\%$ (per each value, not ΔI_0); using these error values, the actual ΔI_0 in MeOH could be between 20-50%. Even on

the lowest end, this ΔI_0 value is ca. 4-10 times larger than the value obtained in the 10% MeOH for the C-AV diad. However, as mentioned previously, the error bars are heavily influenced by the shot-to-shot power fluctuations of the laser system, and are likely to be much larger than the actual error in the measurement.

In the DCM/ACN solution, the lifetime of the CT decay also seems to change as a function of magnetic field, like the C-AV diad. These data had to be fit in the same manner as described previously for the C-AV diad in dcb/1% MeOH. In the table shown in Figure 3.15, the

error in τ_1 is from the fits performed from $t = 0$ and the error in τ_2 is from the fit performed from 10 ns after $t = 0$, using the A_1 and τ_1 values from the $t = 0$ fit. As shown in Figure 3.15, the decay of the C-AVB diad in DCM/ACN goes from mono-exponential at zero field to bi-exponential, exhibiting a “fast” and “slow” field dependent lifetime, in all applied fields studied. The lifetime of the “fast” decay component steadily decreases with applied field from 11 ns at zero field to 0.7 ns at

TA Spectra for the "C-AVB Solution" at 552 nm for Several Applied Magnetic Fields (mT) in $\text{CH}_2\text{Cl}_2/\text{ACN}$



Field Strength (mT)	R ²	A ₁	τ ₁	A ₂	τ ₂
0	0.970	0.094	11 ± 0.25 ns	-	-
50	0.971	0.049	8.2 ± 1.9 ns	0.049	19.0 ± 0.85 ns
120	0.972	0.058	8.6 ± 0.60 ns	0.042	30.0 ± 2.0 ns
300	0.973	0.034	3.3 ± 0.38 ns	0.080	15.4 ± 0.42 ns
600	0.978	0.021	1.8 ± 0.22 ns	0.077	14.7 ± 0.34 ns
1640	0.955	0.019	0.69 ± 0.13 ns	0.073	14.4 ± 0.48 ns

Figure 3.15. The effect of a magnetic field on the CT recombination kinetics monitored at 552 nm and the changes in initial intensity (inset) for the “C-AVB Solution” in and DCM/4 drops ACN. These are preliminary studies so the error bars were calculated using the average error from the C-AV experiments as described in the text.

1640 mT. A second “slow” decay component appears in the presence of a magnetic field and increases with increasing field up to the maximum value of 27 ns at 120 mT, then decreases again to a value of 14 ns at 1640 mT, which was the largest field studied for this complex. As mentioned previously, lifetimes this short (particularly the lifetime of the “fast” component) are not reliable without mathematically deconvoluting the signal from the laser pulse, therefore, there could be a significant amount of error associated with these lifetimes. However, if nothing else, these data corroborate the bi-exponential decay characteristics observed for the C-AV diad in dfb/1% MeOH, which is a similar solvent system to DCM/ 4 drops ACN (though the actual solvent composition was not determined for this sample, and it is likely that there is < 1% ACN, which could significantly affect the observed lifetimes). It is interesting that the decay characteristics change from mono- to bi-exponential when in an applied magnetic field for the “C-AVB Solution” in DCM/ACN. At this point, more studies are necessary to verify this behavior, but if it is real it could indicate several interesting things about this system. Despite the changes in the static absorption spectrum and the similarity in the lifetimes at zero applied field (when C-AV diad is in dfb/0% MeOH), this change in decay profile could imply that the C-AV diad may not be the major product in the equilibrium mixture of the “C-

AVB Solution” in DCM/ACN since the same change was not observed for the C-AV diad system in a similar solvent, as shown in Table 3.1. However, since solvent seems to have a

Table 3.1. A comparison of fit values obtained for the C-AV diad in dfb/1% MeOH at 584 nm and the “C-AVB Solution” in DCM/ACN.

Species	“C-AVB Solution”		C-AV Diad	
Solvent	DCM/ACN		dfb/1% MeOH	
Monitoring λ	552 nm		584 nm	
Field Strength (mT)	τ_1 (ns)	τ_2 (ns)	τ_1 (ns)	τ_2 (ns)
0	11 \pm 0.25	-	5.2 \pm 0.53	24.1 \pm 0.26
50	8.2 \pm 1.9	19.0 \pm 0.85	4.6 \pm 1.5	24.6 \pm 0.37
120	8.6 \pm 0.60	30.0 \pm 2.0	5.5 \pm 0.63	27.0 \pm 0.27
250	-	-	5.4 \pm 0.71	26.6 \pm 0.32
300	3.3 \pm 0.38	15.4 \pm 0.42	-	-
500	-	-	4.9 \pm 0.46	26.2 \pm 0.33
600	1.8 \pm 0.22	14.7 \pm 0.34	-	-
1500	-	-	5.6 \pm 0.78	23.9 \pm 0.33
1640	0.69 \pm 0.13	14.4 \pm 0.48	-	-

huge effect on these complexes, these solvent systems are not close enough to make that determination. Furthermore, these data could indicate that the magnetic field has some influence on the equilibrium mixture present in the solution, whether it be between C-AV and C-AVB species or 4-coordinate and 5-coordinate C-AVB species.

The changes in initial intensity of the “C-AVB Solution” in DCM/ACN are similar to those observed in the independently prepared, pure C-AV diad in dcb/0-2% MeOH and the “C-AVB Solution” in MeOH as described earlier. As presented in Figure 3.15, the initial intensity first increases with applied field until the maximum value around 120 mT, then decreases until 600 mT, and continues to decrease at a slower rate until 1640 mT. The absolute ΔI_0 between 0 mT and the maximum value (around 120 mT) is 26% DCM/ACN. Again, the error bars were not generated in this experiment, but calculated based on the C-AV diad studies as described above, and the actual ΔI_0 could be between 14-40% in DCM/ACN. This ΔI_0 behavior is very similar to the results presented in Figures 3.6 and 3.7 for the independently prepared, pure C-AV diad, which either adds credence to the hypothesis that the major product in the “C-AVB Solution” in DCM/ACN is actually the C-AV diad and $[\text{Cu}(\text{dtbp})(\text{ACN})_2]^+$ or indicates that the I_0 of the primarily 4-coordinate C-AVB diad (since there is very little coordinating solvent present) changes in a similar manner to the C-AV diad when in this solvent. However, as mentioned previously, the changes in solvent and lack of detailed study on this system preclude any direct comparison between the “C-AVB Solution” and the independently prepared, pure C-AV diad.

Studies on the $[\text{Cu}(\text{4OMQ})_2]^{5+}(\text{TPFB}^-)_5$ Diad

The formation of the proposed CT product, CT recombination kinetics, and ET dynamics in the C-AQ diad (C-AQ= $[\text{Cu}(\text{4OMQ})_2]^{5+}(\text{TPFB}^-)_5$) incorporating the 4OMQ instead of the

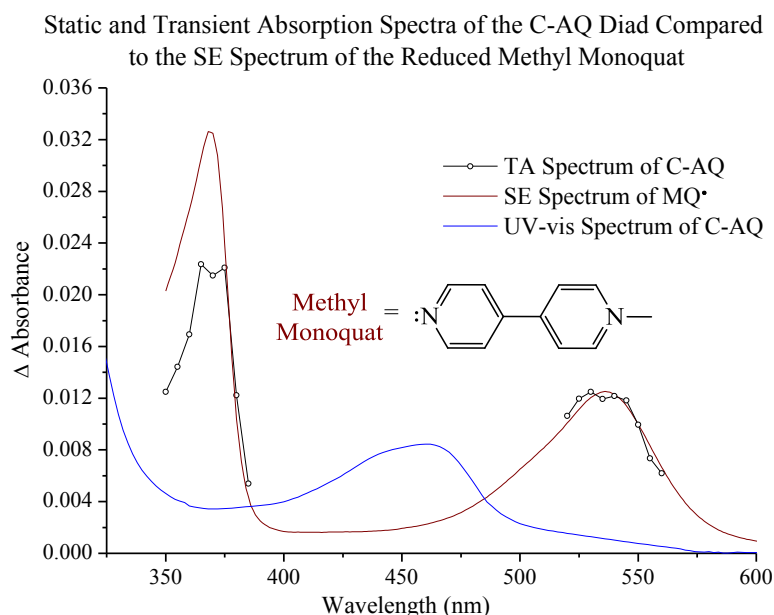


Figure 3.16. Transient absorption spectrum of C-AQ in dfb after excitation at 450 nm (black), the static spectrum of C-AQ (blue) and spectroelectrochemical spectrum for MQ[•] (red). The MQ[•] spectrum was scaled by a constant factor such that the summed point-by-point difference between that spectrum and the TA spectrum was minimized. Each point in the TA spectrum was generated from the average ΔA at 10-12 ns after $t=0$.

4OMV acceptor moiety was also investigated.

Spectroelectrochemistry (SE) was again used to obtain a quantitative spectrum for methyl monoquaternary amine (“methyl monoquat” = MQ, dfb solvent), having been reduced by one-electron, to serve as a model for the reduced acceptor ligand, 4OMQ^{•+}.

Figure 3.16 contains a comparison of the SE spectrum for MQ[•] and the TA spectrum of the C-AQ diad complex which demonstrates that the peak positions in the TA spectrum agree well with those of the MQ[•] spectrum from the SE data. The disparity in the relative peak intensities for the short wavelength ($\lambda_{\text{max}}=368$ nm) peak of the 4OMQ^{•+} is not well understood for this complex. However, it is important to note that the absorbance at short wavelength for the 4OMQ^{•+} occurs between < 350 nm-380 nm, which is far enough into the UV that there could be overlap with the bleach of the MQ⁺. Furthermore, at these wavelengths the response of the monochromator begins to decrease, making it harder to obtain reliable intensity data. The bleach of the MLCT region of the [Cu(I)P₂] chromophore was not investigated in the TA spectrum for this complex, but is planned for future study.

Figure 3.17 presents a TA decay curve at 540 nm after excitation at 450 nm for the C-AQ complex in dfb solvent. The CT lifetime of the C-AQ in dfb/0% MeOH ($\tau_{ct} \approx 8$ ns) is nearly the same as the lifetime of the C-AV complex in this solvent. Since there is no difference in steric bulk in the $[\text{Cu}(\text{I})\text{P}_2]$ coordination sphere, it is reasonable to think that the τ_{ct} of the C-AQ diad would have a similar

TA Spectrum for the C-AQ Diad at 540 nm in Dfb at Zero Applied Magnetic Field

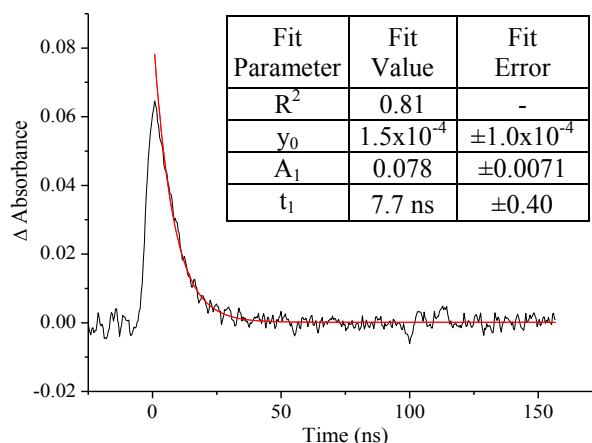
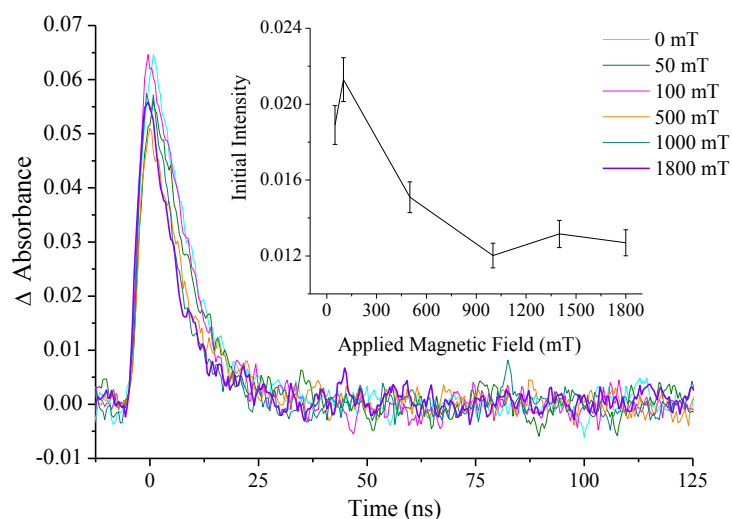


Figure 3.17. The TA spectrum of the C-AQ diad in 1,2-difluorobenzene (black) and the fit (red). The fit does not accurately model the initial intensity due to the convolution of the very short C-AQ lifetime with the laser pulse.

solvent dependence as the C-AV diad. This is important because ≤ 7 ns lifetime is essentially the same as the laser pulse width, which makes the accurate determination of the lifetime very difficult. Furthermore, the convolution of the laser pulse and the C-AQ signal often causes the observed initial intensity value to be smaller than expected because some population of the CT states produced have recombined within the width of the laser pulse (see previous discussion of response function). This often causes the fitting function to have a large degree of error in the initial intensity values as is demonstrated by the red fit line in Figure 3.17. Therefore, it would be beneficial to repeat these studies in a dfb/5% MeOH to verify the legitimacy of the results reported below.

Interestingly, these data seem to demonstrate some “rise time” component, which is also present in the C-AV diad in dfb, but seems to be less noticeable in other solvents (c.f. Figure 3.6). This “rise time” could be associated with the time scale of photo-excitation, flattening distortion, CT formation, or other processes. However, in order to elucidate the origin of this kind

TA Spectra for the C-AQ Diad at 540 nm
in Dfb at Several Magnetic Fields (mT)



Field Strength	R^2	A_1	τ_1
0 mT	0.810	0.078	7.7 ± 0.40 ns
50 mT	0.741	0.076	8.1 ± 0.50 ns
100 mT	0.793	0.098	7.0 ± 0.38 ns
500 mT	0.694	0.051	8.8 ± 0.62 ns
1000 mT	0.546	0.077	5.9 ± 0.57 ns
1400 mT	0.541	0.085	5.6 ± 0.54 ns
1800 mT	0.596	0.059	6.8 ± 0.59 ns

Figure 3.18. The effect of a magnetic field on the CT recombination kinetics and initial intensity (inset) for the C-AQ in dfb. It is evident that the initial intensity is affected by the applied magnetic field and it is possible that the lifetimes may be as well, though it is not conclusively apparent in this data. The zero field data for the initial intensity was not included in the inset because that data had to be re-collected on a different sample and day. However, qualitatively similar changes occur in the initial intensity as for the C-AV and “C-AVB Solutions” in MeOH and DCM/ACN. Again, these studies were preliminary so the error bars were calculated using the average error from the C-AV experiments as described in the text.

ously, the lifetime is so short in dfb, it is very uncertain from these data if the effect is real, especially considering that the lifetimes presented are almost statistically identical. In order to verify that there is a real change in the lifetime of the C-AQ with magnetic field, the sample would have to be studied in a more coordinating solvent (such as dfb/5% MeOH) so the lifetime is long enough to observe without being significantly convoluted with the laser pulse. However, from

of “rise time” component, TA studies on a laser system with a much shorter time resolution are necessary.

Despite the short lifetime, TA spectroscopy was used to study the effect of an applied external magnetic field on the CT recombination kinetics at 375 and 540 nm. The 540 nm data are shown in Figure 3.18. As with the other C-AV diad and the “C-AVB Solution” in DCM/ ACN presented herein, the lifetime of the CT state may be slightly influenced by the applied magnetic field.

However, as mentioned previ-

the data presented in the inset table in Figure 3.18, the lifetime of the C-AQ CT state may be increasing with magnetic field from ca. 8 ns at zero applied field to the maximum value of 9 ns at 500 mT then decreasing with further applied field to around 6 ns at 1000-1400 mT and could possibly increase again to 6.8 ns at 1800 mT. If these data were not similar to the changes presented for the other diads, the lifetimes would have been considered identical. However, based on the precedence of the C-AV diad, it is possible that these data do represent a real, albeit very small, change in CT lifetime.

The initial intensity of the C-AQ diad is also affected by the application of an external magnetic field in a similar fashion to all of the other C-AX diads discussed. As shown in Figure 3.18 (inset graph), the initial intensity first increases with applied field, reaching a maximum at 100 mT, and then decreases until approximately 500 mT, after which it decreases at a slower rate until 1000 mT, where it plateaus and remains essentially constant through 1800 mT. This was a preliminary study, so the error bars had to be calculated based on the average error in the C-AV experiments, as described previously. Moreover, in this study, the initial intensity at zero field was excluded from the data set because the zero field data had to be re-collected on a separate sample. Therefore, the apparent relative change in initial intensity between 0 mT and the field where the maximum value of initial intensity is obtained (100 mT), ΔI_0 , cannot be calculated absolutely. However, the actual ΔI_0 must be $> 11\%$, which is the change in I_0 between 50 and 100 mT. Clearly, further studies on this complex are necessary to verify these preliminary results.

3.3 Discussion

In [Ru(II)L₃] C-A diad complexes, the photo-induced CT state formation via one-electron reduction of a viologen or monoquat type acceptor moiety is efficient, but is unable to be detect-

ed due to the rapid rate of electron-hole recombination (k_{bet}). However, as is readily apparent from the TA decay data presented above, each of the four [Cu(I)P₂] C-AX complexes studied are capable of photo-induced one-electron reduction of the respective acceptor moieties (4OMV or 4OMQ) resulting in a detectable amount of CT state. The CT lifetime of the [Cu(I)P₂] C-AX diads is much longer than their [Ru(II)L₃] analogs because the intrinsic structural rearrangement in the [Cu(II)P₂]^{*} excited state affects the rate of recombination. Since the [Ru(II)L₃] C-AX diads undergo very minimal structural changes during the photo-excitation process, the k_{ct} and k_{bet} are both very fast, but $k_{bet} \gg k_{ct}$ which is why the C-AXⁿ⁺ product is not able to be detected. However, as discussed previously, with the proper ligand geometry, J-T distortion and subsequent exciplex formation in the [Cu(II)P₂]^{*} excited state can attenuate the k_{bet} such that $k_{bet} < k_{ct}$ due to the amount of structural reorganization (and the associated energy barrier) that must occur for the [Cu(II)P₂]^{*} to return to the ground state geometry. Therefore, [Cu(II)(4OMX^{m+})(4OMX^{(m-1)+})]ⁿ⁺ is long lived enough to be detected on the timescale of our laser system. However, this change in geometry and coordination environment introduces concomitant changes in SOC, ¹MLCT/³MLCT energy gap, and ¹MLCT/³MLCT populations, which complicate the interpretation of the data presented herein.

Structural and Solvent Effects on the τ_{ct} of C-AX diads

Recall that J-T distortion results in a reduction of the dihedral angle between the two phenanthroline ligand planes. In the presence of coordinating solvents or anions, a fifth ligand can coordinate in the J-T distorted Cu(II) geometry, forming an exciplex.^{6,13,15-24,31} The driving force for oxidatively quenching the exciplex (and the k_{bet}) is dependent upon the strength of the interaction of the fifth ligand.^{16-20,26-30} For example, in studies by Meyer and coworkers on a

[Cu(I)P₂] C-AV diad similar to those presented in this study, the CT lifetime was attenuated over 2 orders of magnitude by changing from a weakly (CH₂Cl₂, $\tau_{ct} \approx 20$ ns) to a strongly coordinating solvent (DMSO, $\tau_{ct} \approx 1.8$ μ s).^{23,24} As shown in Figure 3.19, J-T distortion and exciplex formation are major contributors to the overall reorganizational energy that occurs in the excited state, which directly affects the rate of forward and back electron transfer to and from the CT states. Therefore, varying the degree of structural rearrangement in the excited state should manifest itself as differences in CT lifetimes. In this study, the degree of structural rearrangement was controlled in 2 ways, varying the composition of the solvent (i.e. incorporation of MeOH (or ACN) in varying concentrations) and increased steric bulk on the 2,9-positions of the phenanthroline in the C-AVB complex.

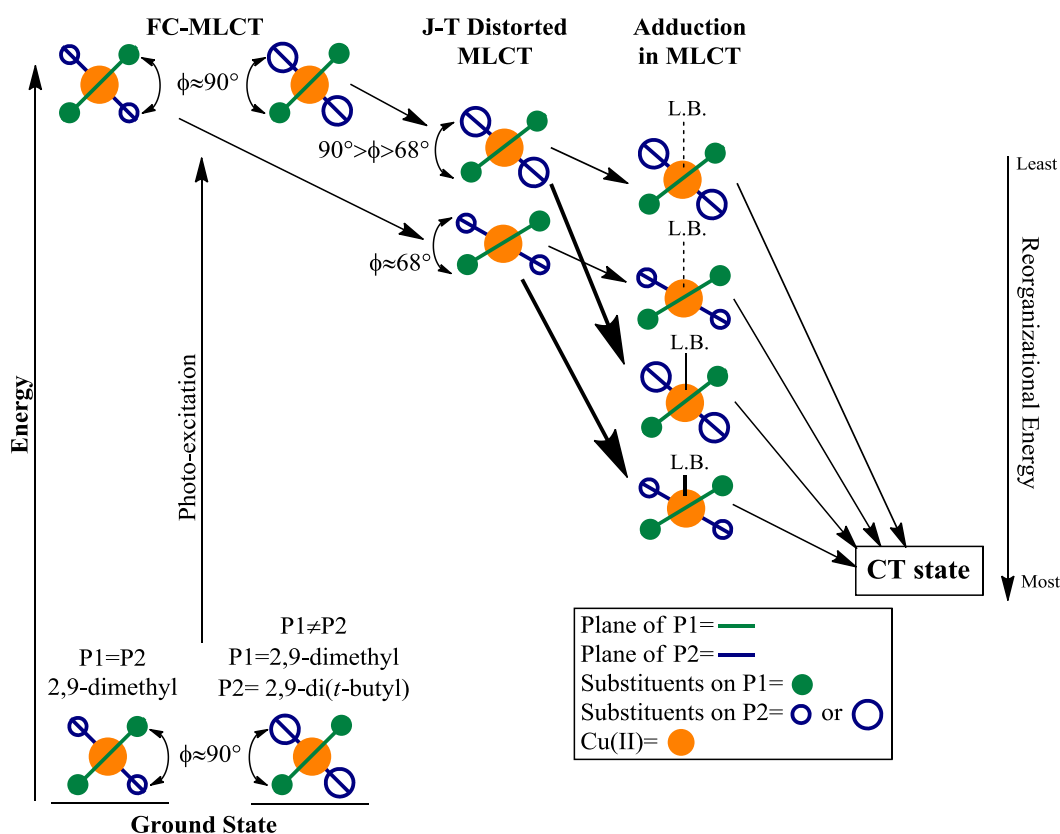


Figure 3.19. A Jablonski-type diagram (not to scale) detailing how the degree of J-T distortion and adduct formation stabilizes the CT state, which affects the τ_{ct} . The bold arrows from the “J-T distorted MLCT” to the “Adduction in MLCT” states represent strong Lewis base interactions, and the non-bold arrows between those states represent weak Lewis base interactions.

Based on the previous argument, the lifetime of the CT state should increase with increased MeOH concentration, which was observed for the C-AV diad ($\tau_{ct} \approx 7$ ns in dfb and $\tau_{ct} \approx 35$ -45 ns in dfb/ > 4% MeOH), the C-AVB diad solutions ($\tau_{ct} \approx 11$ ns in DCM/4 drops ACN and $\tau_{ct1} \approx 9$ ns, $\tau_{ct2} \approx 34$ ns in MeOH (bi-exponential)), and is yet to be investigated in detail for the C-AQ diad. However, the similarity in the lifetimes of the C-AV and C-AQ diads in dfb only, and the fact that there is no difference in steric bulk in the [Cu(I)P₂] coordination sphere suggests that the same solvent dependence observed in the C-AV diads will be manifested in the CT lifetime of the C-AQ diads. In the C-AVB diad the increased steric hindrance imposed by the dtbp ligand on the [Cu(I)P₂] coordination sphere should cause a decrease in the CT lifetime since the interaction of the solvent/counterion adduct is hindered. However, the lifetime of the C-AVB diad in MeOH was only slightly shorter than the C-AV diad in dfb/ > 4% MeOH ($\tau_{ct} \approx 34$ ns for C-AVB and $\tau_{ct} \approx 35$ -45 ns for C-AV). As stated, the C-AVB diad lifetime was measured in MeOH only, which has not been done for the C-AV diad, but the solvent dependence on the long decay component (recall that the decay profile changes from mono- to bi-exponential and back to mono-exponential) of the C-AV diad indicated that in dfb/ > 4 % MeOH the CT lifetime plateaus at $\tau_{ct} \approx 35$ -45 ns. It is unknown if this is a local maximum in CT lifetime or an absolute maximum in this solvent system, which is a subject of further study. However, to a first approximation, the trend in lifetime when comparing diads of lesser and greater steric bulk (C-AV vs C-AVB) is cogent based on the work of Meyer and coworkers.

When considering the changes in the decay characteristics in zero applied field of the C-AV diad with increased MeOH concentration (Figures 3.5 and 3.6), the “C-AVB Solution” in MeOH (Figure 3.14, first decay component), the “C-AVB Solution” in DCM/4 drops ACN (Figure 3.15), and the C-AQ diad in dfb (Figure 3.12), an interesting pattern emerges. In relatively

non-coordinating solvents, all of the C-AX diads studied exhibit a mono-exponential decay, with a lifetime of ca. 6-11 ns (assuming that no additional decay component is present, yet undetectable, due to convolution of the signal with the laser pulse). Furthermore, as the MeOH concentration is increased, the decay characteristics of the C-AV diad changes from mono- to bi-exponential (C-AV diad in dfb/1% MeOH) having a short decay component with a lifetime of ca. 8 ns, and a long decay component with a lifetime of ca. 22 ns. The decay then changes back to mono-exponential in coordinating solvents (C-AVB diad in dfb/ > 2% MeOH) having a lifetime that increases with increasing field until the effect saturates in dfb/ \geq 4% MeOH solutions and a 35-45 ns lifetime. Yet, in MeOH, a very coordinating solvent, the CT decay of the bulky “C-AVB Solution” is bi-exponential, with a short decay component having a lifetime of ca. 9 ns.

Based on these results, one possible interpretation may be that there exists an equilibrium between the 4-coordinate C-AX complex having a short lifetime and a solvent-adducted, 5-coordinate C-AX complex having a longer lifetime due to the associated energy barrier to recombination, as discussed briefly in the Results section. If this interpretation is correct, the 4-coordinate C-AX complex seems to have a characteristic lifetime of ca. 6-11 ns, regardless of the amount of steric bulk in the coordination sphere, and interestingly, the identity (i.e. redox potential) of the acceptor. This latter point may have important implications about the Φ_{ct} as will be discussed in more detail later. However, regarding the effect of steric bulk on the CT decay, if the equilibrium between the 4- and 5-coordinate complex shifts as the concentration of MeOH increases, this shift may be observable as a change in the decay profile (mono- to bi-exponential) and/or the relative contribution of the two decay components, as was observed for the C-AV diad. In this case, the equilibrium may shift so far toward the formation of the 5-coordinate complex that the concentration of the 4-coordinate complex is depleted from solution, and all CT re-

combination must originate from a 5-coordinate complex, yielding a mono-exponential decay profile. For the C-AVB diad having greater steric bulk, which makes it difficult for solvent adduction to occur, it is possible that the equilibrium between the 4- and 5-coordinate species cannot shift as far toward the 5-coordinate complex. Therefore, even in coordinating solvents, both 4- and 5-coordinate species could be present and CT decay could proceed from either species yielding a bi-exponential decay. Although this explanation seems to rationalize the observed results, no direct spectroscopic evidence of these species has been found to support this hypothesis.

Structural and Solvent Effects on the τ_{ct} of the C-AX diads in an Applied Magnetic Field

As discussed in detail above, the CT lifetime of the C-AV diad increased as the concentration of MeOH was increased up to a maximum value of 35-45 ns in dfb/ > 4% MeOH. This increase in lifetime is attributed to the increased probability for solvent adduction in the J-T distorted [Cu(II)P₂] MLCT state, which stabilizes the MLCT state and the subsequent CT state once oxidative quenching has occurred. The stabilization increases the amount of reorganizational energy required for back electron transfer to the ground state causing the CT lifetime to be longer as the interaction between the flattened complex and the fifth ligand is strengthened.

The solvent effects on τ_{ct} at zero field are relatively easily understood based on the literature precedence for solvent induced changes in the lifetime of similar [Cu(I)P₂] C-AX diads.^{23,24} However, the effect of a magnetic field on the ET dynamics in the C-AX diads presented herein are much more novel. For the C-AV diad and the “C-AVB Solution” in DCM/ACN very small changes in the CT lifetime are observed in the presence of a magnetic field. This change in lifetime with applied field is suspected for the C-AQ diad and may occur in the “C-AVB Solution” in MeOH, but the results are less conclusive and further studies are necessary. An applied mag-

netic field was also found to have a marked effect on the initial intensity of all of the C-AX diads. The observed changes in lifetime and initial intensity with applied magnetic field are somewhat unexpected for these complexes as discussed in more detail below. In order to rationalize the observed magnetic field effects (MFE's), a more detailed understanding is needed of the [Cu(I)P₂] excited state dynamics, CT state structure, and in-depth spin-chemical behavior.

In the following interpretations, the changes observed in lifetime and the initial intensity are considered to be separate magnetic field effects. However, in order to be certain that changes in initial intensity are not misinterpreted as changes in lifetime and vice versa, the response function of the laser must be determined experimentally and all of the data must be de-convoluted from the response function. Since the lifetimes are not actually constant, it complicates the interpretation of the ΔI_0 data. Particularly in non-coordinating solvents, the error is expected to be large due to a larger fraction of the CT signal that is convoluted with the laser pulse. In coordinating solvents where the lifetime is long enough that the laser pulse has a diminished effect on the I_0 values, the changes in I_0 still exist, though to a smaller extent. Therefore, it is possible that at least part of observed ΔI_0 is due to changes in the excited state ET dynamics in a magnetic field. With this being said, the explanations presented below are admittedly basic and a more in-depth examination of these results is underway with an expert collaborator, Dr. Ulrich Steiner at the Universität Konstanz in Konstanz, Germany. Until these collaborations are complete, the results are rationalized based on the following preliminary arguments.

As discussed previously, the ³CT state produced is a di-radical species comprised of a radical hole in a metal-based d-orbital and a radical electron in a organic based molecular orbital on the A moiety. Since the ground state is a singlet, electron-hole recombination (k_{bet}) from the ³CT state is spin-forbidden and some mechanism of ¹CT and ³CT mixing must occur to provide a

spin-allowed electron-hole recombination (k_{bet}) pathway.^{33,34,36} If the singlet and triplet energy levels are nearly degenerate at zero field (as is often the case in so-called “normal” organic radicals that are spatially separated over a large distance) singlet/triplet mixing can occur via isotropic hyperfine coupling (IHC).^{33,34,36,38} When a magnetic field is applied to a “normal” organic triplet radical pair species, Zeeman splitting of the triplet (T_+) and (T_-) states occurs. If the degree of Zeeman splitting is large enough that the (T_+) and (T_-) exceed the influence of the IHC manifold, singlet/triplet mixing becomes much less efficient, and retards the k_{isc} , and therefore, the k_{bet} .^{33,34,36} A slowed k_{isc} and k_{bet} of a given species would be evident in the transient absorption (TA) decay profile by a larger value for the magnetic field dependent component of τ and a change in the decay characteristics from mono- to bi-exponential in a magnetic field. However, when spin states are mixed via IHC interactions, the energy difference between the singlet and triplet states increases as the distance between the radical species decreases which alters k_{isc} .³⁸ Although the CT state is predicted to be a triplet di-radical species in the C-AX diads, the distance between the radical hole and radical electron can be relatively small and the hole resides on a metal based orbital, which is likely to be subject to larger spin-orbit coupling (SOC) interactions than typical, organic di-radical species. The smaller spatial separation between radicals can potentially cause the singlet-triplet energy gap to be large enough that the IHC interactions cannot mix the two states: thus τ_{ct} is often expected to be unaffected by small/moderate magnetic fields ($\beta < 1000$ mT). Therefore, isotropic hyperfine coupling (IHC) interactions are not typically responsible for mixing in $^1CT/{}^3CT$ states with relatively close orientation of the radical pair. However, it is possible that the various changes that occur in the [Cu(I)P₂] excited state or the ligand architecture itself may alter the spin-dynamics associated with CT recombination causing mixing to occur via IHC interactions.

Spin-orbit coupling (SOC) interactions can also mix singlet-triplet spin states to enable facile k_{bet} . Since the hole in the C-AX diads resides in a metal based orbital, it is possible that SOC interactions are also actively involved in their spin chemistry. In $[\text{Ru(II)L}_3]$ complexes, the relatively large SOC of the 4d electrons ($\zeta_{\text{Ru(II)}} = 990 \text{ cm}^{-1}$)¹³ efficiently mixes the $^1\text{MLCT}/^3\text{MLCT}$ states enabling facile intersystem crossing (ISC) from the Franck-Condon $^1\text{MLCT}$ (FC- $^1\text{MLCT}$) to the thermalized $^3\text{MLCT}$ stateⁱ (ca. 40 fs)¹³ with a $\Phi \approx 1$.^{1,44} Therefore, essentially all energy and electron transfer events originate from the $^3\text{MLCT}$ in $[\text{Ru(II)L}_3]$ complexes, but the large amount of SOC may also contribute to the fact that the resulting C-A diads have $k_{bet} > k_{ar}$.¹ The 3d electrons of Cu(I) have a slightly smaller degree of SOC ($\zeta_{\text{Cu(I)}} = 829 \text{ cm}^{-1}$)¹³, but also a smaller energy gap between the $^1\text{MLCT}/^3\text{MLCT}$ states (1800-2000 cm^{-1} for $[\text{Cu(dmp)}_2]^+$).^{1,2,13,32,44,45} Based on the 3d SOC and the $^1\text{MLCT}/^3\text{MLCT}$ energy gap, it would be logical to assume that k_{isc} in $[\text{Cu(I)P}_2]$ complexes may be slightly smaller, but similar to their $[\text{Ru(II)L}_3]$ analogs. However, since the coordination geometry upon photo-excitation is relatively constant for $[\text{Ru(II)L}_3]$, but not for $[\text{Cu(I)P}_2]$ complexes, the k_{isc} is much different. Nozaki et al. performed a series of calculations on the $[\text{Cu(II)P}_2]$ excited state indicating that J-T distortion alters $^1\text{MLCT}/^3\text{MLCT}$ energy levels such that ISC has to occur between MOs with weak SOC interactions.¹³ The weak SOC between the $^1\text{MLCT}/^3\text{MLCT}$ states involved in the ISC transition causes ISC to be very slow ($\approx 10 \text{ ps}$) relative to $[\text{Ru(II)L}_3]$, and rationalizes the experimentally observed ISC rates reported by several independent groups.^{13-15,39} In principle, if changes in the $^1\text{MLCT}/^3\text{MLCT}$ energy levels also alters the energetically preferred energy/ET pathways due to SOC interactions, the splitting of the $^3\text{MLCT}$ levels by a magnetic field could have significant implications on the ^3CT state formation. Therefore, it is relevant to consider how the

ⁱ Although there is a large degree of SOC in the Ru(II)L_3 $^1\text{MLCT}/^3\text{MLCT}$ states, calculations indicate the singlet character of the thermally equilibrated MLCT state is only ca. 11%, so it is regarded as a $^3\text{MLCT}$.²

$^1\text{MLCT}/^3\text{MLCT}$ energy levels are influenced by the extent of flattening distortion and other factors that affect the k_{isc} at zero field before considering the magnetic field effects.¹³

As demonstrated in Figure 3.20 A and B there are four competing processes in photo-excited $\text{Cu(II)P}^*\text{P}$ complexes that are attenuated by the steric bulk in the coordination sphere, and therefore, the degree of J-T distortion that can occur: ultra-fast ISC (<45 fs)^{14,28,39} from the FC- $^1\text{MLCT}$ to the $^3\text{MLCT}$, ultra-fast IC (45 fs)^{14,39} from the FC- $^1\text{MLCT}$ to the $^1\text{MLCT}$ state, ultra-fast flattening (J-T) distortion (660 fs)^{14,39}, and slow ISC (7-10 ps)^{13-15,39} from the flattened $^1\text{MLCT}$ state to the flattened $^3\text{MLCT}$ state.^{13-15,28} Furthermore, J-T distortion causes splitting of the FC- $^1\text{MLCT}$, $^1\text{MLCT}$, and $^3\text{MLCT}$ levels (See Figure 3.20-B) destabilizing the metal-centered molecular orbitals (MOs) having strong SOC and stabilizing the ligand-centered MOs having

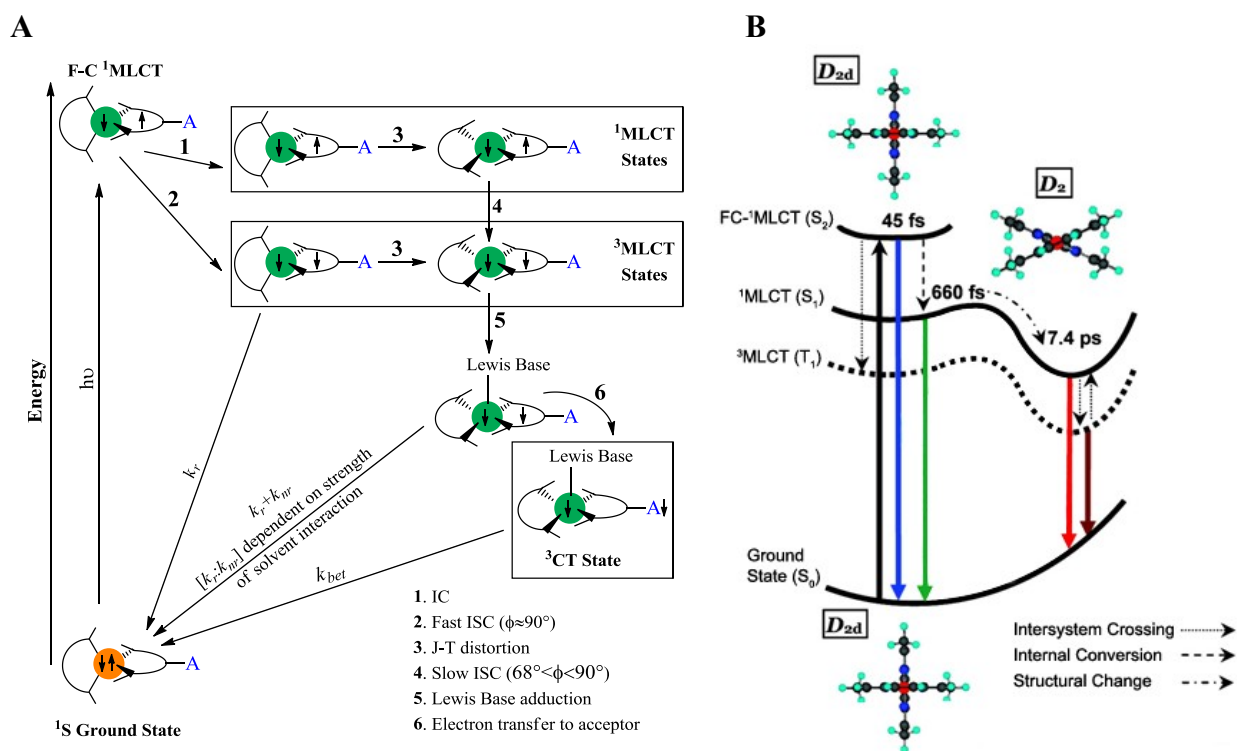


Figure 3.20. Jablonski diagram (not to scale) outlining the J-T distortion and exciplex formation in photo-excited $[\text{Cu(II)P}^*\text{P}]^{n+}$ complexes (**A**). The orange/green circles represent Cu(I/II) respectively. The arched appendages represent the phenanthroline rings. An energy level diagram showing the changes in $^1\text{MLCT}/^3\text{MLCT}$ potential surfaces with structural distortion (**B**). The J-T distortion in F-C $^1\text{MLCT}$ state causes slow ISC to the $^3\text{MLCT}$ manifold. Solvent adduction to form the exciplex in the $^3\text{MLCT}$ states quenches the excited state of sterically unrestricted $[\text{Cu(II)P}^*\text{P}]^{n+}$ complexes. The black dot represents a radical electron and the circle a radical hole. The listed timescales are for $[\text{Cu(dmp)}_2]^+$. Adapted from refs 14 and 22.

weak SOC.¹³ The degree of destabilization/stabilization imposed on these energy levels is directly related to the degree of flattening. Because of the observed energy level splitting, ISC between the metal-centered MOs with the strongest SOC interactions (not shown in Figure 3.20) is highly endothermic ($\approx 5,000 \text{ cm}^{-1}$) and does not occur. Therefore, ISC can only occur via two possible mechanisms: slow ISC from the flattened $^1\text{MLCT}$ to the lowest lying $^3\text{MLCT}$ (energetically feasible ligand-centered MOs, $\text{SOC} \approx 30 \text{ cm}^{-1}$) or ultra-fast ISC from the FC- $^1\text{MLCT}$ to the lowest lying $^3\text{MLCT}$ (energetically feasible metal centered MOs, $\text{SOC} \approx 300 \text{ cm}^{-1}$) before the flattening occurs, as shown in Figure 3.20.¹³ There is debate in the literature about the absolute contribution of the latter ISC pathway with complexes having less steric bulk in the $[\text{Cu}(\text{I})\text{P}_2]$ coordination sphere: however, several independent groups have suggested that this ISC pathway has a non-negligible contribution to the ISC process.^{13,14,39,41}

ISC that occurs via either pathway is not 100% efficient, and results in a mixture of lowest lying $^1\text{MLCT}$ and $^3\text{MLCT}$ excited states.^{13,14,16,28,39,40,45} Despite having a smaller radiative rate constant, the $^3\text{MLCT}$ has the largest population, but the $^1\text{MLCT}/^3\text{MLCT}$ energy gap is small enough for some degree of thermal population of the $^1\text{MLCT}$ at room temperature.^{5,16,32,40,45} Therefore, it is likely that ET primarily proceeds from the $^3\text{MLCT}$ state.

Significantly, the changes in the excited state energy levels due to J-T distortion also changes the $^1\text{MLCT}/^3\text{MLCT}$ energy gap in complexes of differing steric bulk in the $[\text{Cu}(\text{I})\text{P}_2]$ coordination sphere: for example, the $^1\text{MLCT}/^3\text{MLCT}$ energy gap changes from 1800-2000 cm^{-1} for $[\text{Cu}(\text{dmp})_2]^+$ to 700-800 cm^{-1} for $[\text{Cu}(\text{dtbp})_2]^+$.³² This change in the $^1\text{MLCT}/^3\text{MLCT}$ energy gap could also significantly affect the $^1\text{MLCT}/^3\text{MLCT}$ populations and k_{isc} .^{28,32} However, other than the calculations of Nozaki et al., studies on the influence of SOC on k_{isc} pathways in $[\text{Cu}(\text{I})\text{P}_2]$ complexes having systematically varied steric environments is absent in the litera-

ture.¹³ Furthermore, the influence of the $^1\text{MLCT}/^3\text{MLCT}$ energy gap on the k_{isc} , as well as the absolute and relative $^1\text{MLCT}/^3\text{MLCT}$ state populations also seem to be underinvestigated.³²

Considering the recent theoretical and experimental work on the excited state ET dynamics and spin chemistry of $[\text{Cu(I)P}_2]$ complexes, the interpretation of the C-AX diad research presented herein can be examined.^{13-15,28,32,39} First, the magnetic field effect (MFE) on the CT lifetime will be addressed. Recall that for the C-AV diad in all solvents of $\text{dfb}/ > 0\%$ MeOH and the “C-AVB Solution” in DCM/4 drops ACN, a very small change in the CT lifetime was observed with magnetic field. A similar change in lifetime was not conclusively observed for the “C-AVB Solution” in MeOH or the C-AQ diad, but may be occurring based on the changes in the normalized TA decay curves for the former, and the miniscule changes observed in the lifetime in dfb solvent in the latter. For a change in lifetime to occur in these MFE studies, the applied magnetic field must be influencing k_{isc} between the ^1CT and ^3CT states, and therefore, k_{bet} . Furthermore, the modulation of the k_{isc} between the ^1CT and ^3CT states must be affected by some mechanism involving spin-dynamics (possibly IHC or SOC interactions) in both of these complexes. Without further insight into these data from our collaborator, speculation about the spin-dynamics is kept to a minimum. However, these studies provide insight into the structural dynamics in these systems, and in turn, that information could have some relevance in the interpretation of the spin-dynamics in the on-going collaborative efforts.

For all of the C-AV diad samples studied in various solvents ($\text{dfb}/ > 0\%$ MeOH, excluding the dfb only samples), the lifetime increases from the value at zero applied field to a maximum value between 50-200 mT, then decreases with additional applied field until ca. 1000 mT, where it has essentially returned to its zero field value. In all cases, the changes in lifetime are not accompanied by a change from mono- to bi-exponential decay (or bi- to tri-exponential de-

cay for the dfb/1% MeOH samples). This is interesting because, according to the relaxation mechanism outlined in the Introduction section, if the ^1CT and ^3CT states are mixed via IHC interactions then the Zeeman splitting of the ^3CT state in a magnetic field would result in a “fast” field independent decay component responsible for ca. 1/3 of the overall decay (due to ISC between ^1CT and T.) and a “slow” field dependent lifetime component responsible for 2/3 of the overall decay (due to equivalent contributions from ISC between ^1CT and T_+ as well as ^1CT and T.). Since there is no such change in the decay characteristics of the C-AV diad (in dfb/ > 0% MeOH), it is unlikely that the proposed relaxation mechanism is responsible for the spin-dynamics in this system.

For the “C-AVB Solution” in DCM/ACN, the changes in lifetime are seemingly accompanied by a change in decay profile from mono-exponential, at zero applied field, to bi-exponential in all applied fields studied. Interestingly, both the lifetime of the “short” and “long” decay components seem to be dependent on magnetic field. The “short” decay component decreases with applied field from ca. 11 ns in zero applied field to ca. 0.7 ns in 1640 mT, the largest field studied for this complex. The “long” decay component increases with magnetic field up to a maximum value of ca. 30 ns at 120 mT, and then decreases with further applied field to ca. 14 ns at 1640 mT. It is worthwhile to note, again, that the convolution of the signal with the laser pulse makes the accurate determination of the lifetime and the A_1 value for the “short” decay component impossible at this time. Therefore, the relative contributions of the two lifetime components cannot be evaluated. Nevertheless, these data may imply that the MFE in this complex also does not correlate directly with the relaxation mechanism discussed in the Introduction.

Since the studies on the “C-AVB Solution” in both solvent systems were preliminary, it is uncertain if the changes in decay profile are reproducible. If the changes outlined above are

real for the “C-AVB Solution” in DCM/ACN, the different MFE’s observed on the lifetimes of the “C-AVB Solution” in DCM/ACN and the C-AV diads could indicate that the major product in the “C-AVB Solution” in DCM/ACN is actually C-AVB diad and not the C-AV diad as previously proposed based on the changes in the UV-vis presented in Figure 3.13. Assuming that the C-AVB diad is the major product in DCM/ACN and that the interpretation of the solvent dependent equilibrium between the 4- and 5-coordinate complexes presented above is correct, the lifetime of the “C-AVB Solution” in DCM/ACN (ca. 11 ns) would suggest that the species is the 4-coordinate C-AVB diad. If that is the case, then the MFE observed on the lifetime of the “C-AVB Solution” in DCM/ACN should also be observed for the short component of the “C-AVB Solution” in MeOH, since it was proposed that both the 4- and 5- coordinate complexes exist in appreciable quantities in MeOH, the former having the shorter lifetime (ca. 9 ns) and the latter having the longer lifetime (ca. 30 ns). However, this was not observed. Thus, it seems that two other possibilities exist: (A) the C-AV diad is actually the major product in the “C-AVB Solution” in DCM/ACN and the changes in the CT lifetime and decay profile (from mono- to bi-exponential) in a magnetic field would also occur for the C-AV diad in the same solvent system, or may occur already and convolution of the signal with the laser pulse precludes detection, or (B) the effect of a magnetic field on the spin-dynamics of the 4-coordinate C-AVB diad is solvent dependent. Further studies are necessary to elucidate if either of these possibilities are correct.

As stated previously, no conclusive MFE was observed for the CT lifetime of the “C-AVB Solution” in MeOH. However, if the lack of an MFE on the CT lifetime is indeed real, and the solution is primarily composed of an equilibrium mixture between the 4- and 5-coordinate C-AVB diad species as previously discussed, this could suggest that increased steric restrictions in

the coordination sphere can influence the mechanisms of spin-mixing between the $^1\text{CT}/^3\text{CT}$ states in C-AX diads. This is somewhat expected based on the discussion of the $[\text{Cu}(\text{I})\text{P}_2]^*$ $^1\text{MLCT}/^3\text{MLCT}$ dynamics outlined above. More specifically, when steric restriction are minimized, J-T distortion alters the $^1\text{MLCT}/^3\text{MLCT}$ energy gap which changes the thermodynamically favorable ISC pathway from an ISC pathway between strongly spin-orbit coupled $^1\text{MLCT}/^3\text{MLCT}$ states to an ISC pathway between weakly spin-orbit coupled $^1\text{MLCT}/^3\text{MLCT}$ states.¹³ If geometrical changes similarly affect the most energetically favorable ISC pathway between the ^1CT and ^3CT states, it is possible that the ISC pathway for the C-AVB diad is subject to larger SOC interactions than the C-AV or C-AQ diad species, due to the larger steric bulk in the coordination sphere. If the ISC pathway between the $^1\text{CT}/^3\text{CT}$ states has a greater degree of SOC, then the degree of $^1\text{CT}/^3\text{CT}$ mixing could be large enough to be unaffected by Zeeman splitting in a magnetic field. Furthermore, if the structural distortion in the C-AV diad causes ISC to occur through weakly spin-orbit coupled $^1\text{CT}/^3\text{CT}$ states it could possibly explain why there is an observed MFE on the CT lifetime when no such effect was expected due to greater SOC of metal based orbitals, where the radical hole resides.

As discussed in the Results section, a marked MFE on the initial intensity, I_0 , was observed for all of the C-AX diads. It was found that the ΔI_0 studies for the C-AV diad, C-AQ diad, and “C-AVB Solution” in DCM/ACN demonstrate very similar changes in I_0 in the presence of a magnetic field when in similar solvents.^j For the C-AV and C-AQ diads in dfb (Figures 3.10, 3.11 and 3.18), the initial intensity first increases with applied field, reaching a maximum around ca. 100 mT, and then decreases until approximately 500 mT, after which it decreases slightly and eventually plateaus between 750-1000 mT at an I_0 value below that at zero field, and remains

^j The fact that the “C-AVB Solution” in DCM/ACN demonstrates a similar ΔI_0 to the C-AV diad in a similar solvent again suggests that the C-AV diad is the major product in this DCM/ACN solvent.

constant through 1800-2250 mT. In the dfb solvent, the ΔI_0 for the C-AV diad was ca. $27.5 \pm 12.5\%$ and the ΔI_0 for C-AQ was $> 11\%$ (calculated from 50-100 mT instead of 0-100 mT since the 0 field data had to be re-taken on a different sample), which should be considered a lower bound due to the lack of zero field data. In dfb/1% MeOH, the C-AV diad demonstrates the same behavior, with the only difference being a decrease in the absolute ΔI_0 , which decreased to $14 \pm 6\%$. As discussed in the Results section, the absolute ΔI_0 decreases with additional MeOH until the solvent was $> 4\%$ MeOH in dfb, where the effect plateaus at ca. 5%. This solvent composition (dfb/ $> 4\%$ MeOH) seems to be the point at which the MeOH concentration is high enough for all C-AV diad species to be in solution and each excited state has access to MeOH for adduct formation. Similarly to the C-AV and C-AQ diads, the initial intensity of the “C-AVB Solution” in MeOH (Figure 3.14) increases with applied field reaching a maximum around 100-150 mT, then decreases until 300 mT, at which point the I_0 has essentially the same value as at zero field. As the field increases from 300-1640 mT (the largest field studied for this sample) the I_0 remains approximately the same. Although this behavior is qualitatively similar to the behavior of the C-AV and C-AQ diads, the ΔI_0 was calculated to be 34%, and when the error bars from the C-AV diad experiments were applied, the ΔI_0 was calculated to be between 20-50%. This value of ΔI_0 for C-AVB is similar to the value of ΔI_0 for C-AV when in dfb only, but is ca. 7 times larger than the ΔI_0 for C-AV when in dfb/ $> 4\%$ MeOH.

A change in I_0 can only occur if there is a change in the apparent Φ_{ct} , i.e. there is either an absolute change in the number of CT states produced by oxidatively quenching the MLCT excited states, or there is a relative change the number of CT states observed. For example, if the rate of electron-hole recombination from the 1CT state ($^1k_{bet}$) is much greater than the rate of 3CT state formation ($^3k_{ct}$), then the Φ_{ct} observed could be less than the actual Φ_{ct} produced, because

the population of ^1CT could be decaying back to the ground state before it can be detected (c.f. Figure 3.21). Therefore, Zeeman splitting of the $^3\text{MLCT}$ in an applied magnetic field could possibly contribute to the observed ΔI_0 by attenuating the k_{isc} between the $^1\text{MLCT}/^3\text{MLCT}$ states or the relative populations of the $^1\text{MLCT}/^3\text{MLCT}$ states. If the

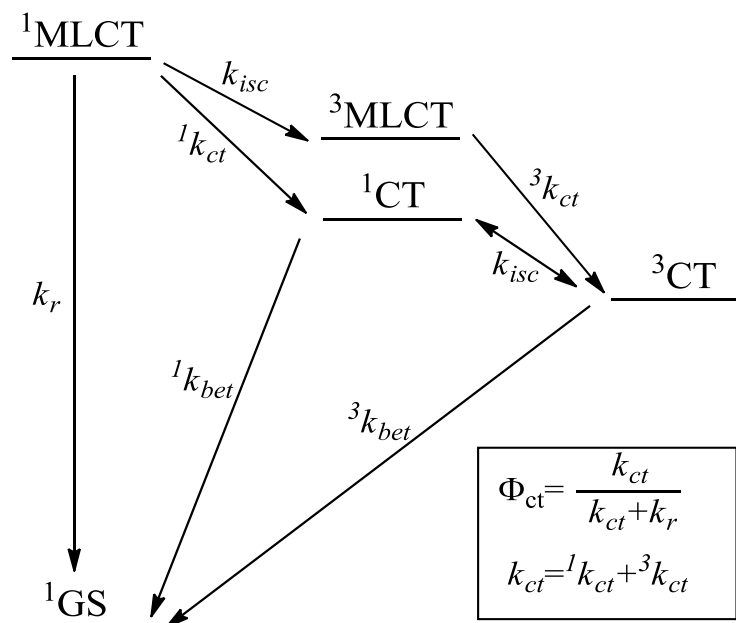


Figure 3.21. The possible pathways of ^1CT and ^3CT formation and recombination that could affect the observed Φ_{ct} .

population of the $^3\text{MLCT}$ state increases relative to the population of the $^1\text{MLCT}$ state, then theoretically, a larger amount of the ^3CT state will be formed which would be observed as an increase in the I_0 , and vice versa. Alternatively, Zeeman splitting of the ^3CT state could also cause a shift in the equilibrium populations of the $^1\text{CT}/^3\text{CT}$ states, which could also cause ^3CT state to increase/decrease with applied field. Furthermore, changes in the energy levels and k_{isc} in the MLCT states only affects the rate of CT formation and Φ_{ct} , but not k_{bet} from the CT state. Therefore, unless the convolution of the signal with the laser pulse is significantly affecting the observed I_0 even when the CT lifetime is > 30 ns, there must be some MFE on the absolute or relative Φ_{ct} observed in these C-AX diads.

Since Zeeman splitting effectively changes the T_+ and T_- energy levels of the $^3\text{MLCT}$ state, the energy gap between the T_+ , T_- and $^1\text{MLCT}$ states would change in a magnetic field. As discussed previously, other factors that change the $^1\text{MLCT}/^3\text{MLCT}$ energy gap are: restricting J-

T distortion by increased steric bulk in the [Cu(I)P₂] coordination sphere (destabilizes MLCT), and solvent adduction (stabilizes MLCT). Therefore, when considering the data on the C-AX diads, the identical steric environments in the [Cu(I)P₂] coordination sphere would imply that the C-AV and C-AQ diads will undergo essentially the same amounts of J-T distortion and solvent adduction. On these grounds alone, it would be logical to expect C-AV and C-AQ diads to have similar changes in I₀ with magnetic field, as was observed. However, there is a large difference in driving force for acceptor reduction in these two C-AX diads (E_{1/2} ≈ -0.40 for 4OMV, E_{1/2} ≈ -0.94 for 4OMQ). Based on Marcus theory, such a large difference in driving force should cause an appreciable change in the rate of forward electron transfer (to the CT state), and therefore affect the Φ_{ct}. The data presented herein does not indicate any gross difference in the Φ_{ct} of the C-AV and C-AQ diads, as would be predicted by Marcus theory. Therefore, for each of these diads the rate of CT state formation (k_{ct}) must be much larger than the rate of relaxation from the excited state (k_r), causing the absolute Φ_{ct} ≈ 1. The fact that the ΔI₀ occurs, suggests that the observed Φ_{ct} must be smaller than the absolute Φ_{ct} and must result from a distribution of population between the ¹CT and ³CT states. Therefore, CT decay must be composed of a very fast component (from the ¹CT state population) which is not observed and a slow decay component that accounts for all of the observed Φ_{ct} (from the ³CT state population). Therefore, the change in the observed Φ_{ct} is most likely due to either a magnetic field induced shift in the equilibrium populations of the ¹MLCT/³MLCT states due to Zeeman splitting of the MLCT state, which then imparts a shift in the populations of the ¹CT and ³CT states, or a magnetic field induced change in the populations of the ¹CT and ³CT states due to the Zeeman splitting in the ³CT state. Or, both of the proposed mechanisms could be contributing to the observed changes in I₀ to varying degrees. It is worthwhile to note that, as stated previously in the Results section, the fast decay

component resulting from the ^1CT state recombination is likely to be much faster than can be observed on the timescale of our instrument, and therefore is not likely to be the cause of the second decay component observed in the C-AV diads in dfb/1% MeOH, “C-AVB Solution” in DCM/ACN or the “C-AVB Solution” in MeOH. Furthermore, the relative distribution of $^1\text{CT}/^3\text{CT}$ states are not likely to change with solvent composition, as was observed in the C-AV diad.

Although two possible mechanisms have been proposed that could impart changes in the observed Φ_{ct} (i.e. the ΔI_0) it doesn't explain why the ΔI_0 would be larger in the C-AVB diad than the C-AV and C-AQ diads. The data presented above indicate that, in the absence of strongly coordinating solvents (dfb only), the C-AV and C-AQ diads could undergo a similar amount of change in initial intensity as the C-AVB diad. However, recall that in dfb/0% MeOH the lifetimes of the C-AV and C-AQ diads are short enough to be significantly convoluted with the laser pulse, and have a much larger associated error. In moderately coordinating solvents like dfb/ > 4% MeOH, the C-AV diad (and likely the C-AQ diad) experiences a significantly smaller change in initial intensity than the C-AVB diad. As stated previously, studies have indicated that the $^1\text{MLCT}/^3\text{MLCT}$ energy gap decreases with increased steric bulk. Furthermore, since the changes in the observed Φ_{ct} may be directly related to a shift in the equilibrium population of the $^1\text{MLCT}/^3\text{MLCT}$ energy levels in an applied magnetic field, these observations could imply that the higher the energy of the $^3\text{MLCT}$ state and the smaller the $^1\text{MLCT}/^3\text{MLCT}$ energy gap the larger the change in initial intensity. However, additional, more extensive, studies are necessary to verify this hypothesis.

One way to rationalize these findings could be based on the differences in SOC between complexes with different degrees of J-T distortion. As stated above, as the $[\text{Cu}(\text{I})\text{P}^*\text{P}]^{n+}$ complex

distorts, the FC-¹MLCT, ¹MLCT, and ³MLCT levels split causing the main ISC pathway to occur between MOs with weak spin-orbit coupling interactions (lowest lying ¹MLCT to the lowest lying ³MLCT). However, a non-negligible, but un-elucidated contribution of ultra-fast ISC from the FC-¹MLCT to the lowest lying ³MLCT may occur through energetically feasible, strongly spin-orbit coupled, metal centered MOs before the flattening distortion occurs.¹³ If the C-AVB diad restricts the J-T distortion enough such that the fast ISC pathway is favored over the slow ISC pathway, this could possibly change the zero field population distribution in the ¹MLCT/³MLCT states. Thus, as a magnetic field instigates Zeeman splitting of the ³MLCT state, the population distribution of the ¹MLCT/³MLCT states could be expected to change in a different way relative to the C-AV and C-AQ diads. Therefore, a different change in the I₀ could also be expected due to the different mechanism of ³CT formation. Furthermore, if similar changes in the ISC pathways occur for the ISC between the ¹CT and ³CT states, causing ISC to occur via a pathway with a larger degree of SOC, this could cause a greater degree of ¹CT/³CT mixing. Thus, increased steric restrictions imparting a change in ISC pathways could also support the fact that no MFE was observed in the lifetime of the “C-AVB Solution” in MeOH as discussed previously.

However, based on the bi-exponential lifetime of the “C-AVB Solution” in MeOH and the proposed equilibrium between 4- and 5- coordinate C-AVB complexes described previously, it is likely that the steric bulk in the coordination sphere of the C-AVB diad is not large enough to hinder all solvent adduct interactions. Therefore, some degree of J-T distortion is probably occurring in this complex, and the ISC pathway through the weakly SOC ¹MLCT and ³MLCT state is also probably still contributing to the ISC in this complex.

An alternate explanation could be that the Zeeman splitting of the $^3\text{MLCT}$ energy levels causes ISC between the lowest lying $^1\text{MLCT}$ state and other $^3\text{MLCT}$ states that have stronger SOC with the $^1\text{MLCT}$, but were not accessible for ISC in the absence of a magnetic field because of the endothermicity of the transition. Recall that the ISC pathways described above were the only energetically favorable pathways in the absence of a magnetic field. If Zeeman splitting of these higher lying $^3\text{MLCT}$ states lowers the energy of the T. state enough such that the transition from the lowest lying $^1\text{MLCT}$ to the T. state of a strongly SOC, higher lying $^3\text{MLCT}$ state is favorable, then the ISC pathway could change in this way as well.

3.4 Conclusion

The spectroscopic data on the series of C-AX diads verifies that one-electron reduction of a methyl viologen or monoquaternary amine type acceptor can oxidatively quench the excited state of a $[\text{Cu}(\text{I})\text{P}_2]^*$ complex forming a di-radical charge transfer state with a quantum yield of $55 \pm 15\%$ in dfb/1.6% MeOH. In contrast to related $[\text{Ru}(\text{II})\text{L}_3]$ diad complexes, the lifetimes of the CT states in the C-AX diads based on $[\text{Cu}(\text{I})\text{P}_2]$ are long enough to be detected on the nano-second timescale due to structural rearrangements that occur in the excited state coordination environment. Furthermore, the lifetime shows a positive dependence on the concentration of coordinating solvents such as MeOH, which supports the findings of Meyer et al. on a similar $[\text{Cu}(\text{I})\text{P}_2]$ C-A diad.^{23,24}

Magnetic field effects on the C-AX diads were observed that are not well understood. A very small, but persistent change in the CT lifetime with magnetic field was observed for the C-AV diads, and is suspected to be present in the C-AQ diads, but could not be verified because convolution of the CT absorbance with the laser pulse obscures the result in dfb solvent. Inter-

estingly, this change in CT lifetime was not observed in the C-AVB diad, which has a greater degree of steric bulk in the coordination sphere. A marked effect on the quantum yield of the CT state was also observed in all of the C-AX diads studied in an applied magnetic field, but due to convolution of the lifetime with the laser pulse, are not able to be verified conclusively. In the absence of a detailed kinetic analysis of the spin-chemical effects, these results are rationalized based on changes in the ISC mechanisms in the excited state, which attenuate the relative populations of the $^1\text{MLCT}/^3\text{MLCT}$ states, and therefore the resulting ^3CT product.

References

- (1) Kalyanasundaram, K. *Photochemistry of polypyridine and porphyrin complexes*; Academic Press: London; San Diego, 1992.
- (2) Meyer, T. J. *Pure Appl. Chem.* **1986**, *58*, 1193–1206.
- (3) Balzani, V.; Juris, A.; Barigelletti, F.; Campagna, S.; Belser, P.; Von Zelewsky, A. *Coord. Chem. Rev.* **1988**, *84*, 84–277.
- (4) Robertson, N. *Chem. Sus. Chem.* **2008**, *1*, 977–979.
- (5) Armaroli, N. *Chem. Soc. Rev.* **2001**, *30*, 113–124.
- (6) Lavie-Cambot, A.; Cantuel, M.; Leydet, Y.; Jonusauskas, G.; Bassani, D. M.; McClenaghan, N. D. *Coord. Chem. Rev.* **2008**, *252*, 2572–2584.
- (7) Scaltrito, D. V.; Thompson, D. W.; O’Callaghan, J. A.; Meyer, G. J. *Coord. Chem. Rev.* **2000**, *208*, 243–266.
- (8) Schmittel, M.; Michel, C.; Liu, S.-X.; Schildbach, D.; Fenske, D. *Eur. J. Inorg. Chem.* **2001**, 1155–1166.
- (9) Schmittel, M.; Ganz, A. *Chem. Commun.* **1997**, 999–1000.
- (10) Kalsani, V.; Schmittel, M.; Listorti, A.; Gianluca, A.; Armaroli, N. *Inorg. Chem.* **2006**, *45*, 2061–2067.
- (11) Pellegrin, Y.; Sandroni, M.; Blart, E.; Planchat, A.; Evain, M.; Bera, N. C.; Kayanuma, M.; Sliwa, M.; Rebarz, M.; Poizat, O.; Daniel, C.; Odobel, F. *Inorg. Chem.* **2011**, *50*, 11309–11322.
- (12) McMillin, D. R.; Kirchoff, J. R.; Goodwin, K. V. *Coord. Chem. Rev.* **1985**, *64*, 83–92.
- (13) Siddique, Z. A.; Yamamoto, Y.; Ohno, T.; Nozaki, K. *Inorg. Chem.* **2003**, *42*, 6366–6378.
- (14) Iwamura, M.; Takeuchi, S.; Tahara, T. *J. Am. Chem. Soc.* **2007**, *129*, 5248–5256.
- (15) Shaw, G. B.; Grant, C. D.; Shirota, H.; Castner, E. W.; Meyer, G. J.; Chen, L. X. *J. Am. Chem. Soc.* **2007**, *129*, 2147–2160.
- (16) Palmer, C. E. A.; McMillin, D. R.; Kirmaier, C.; Holton, D. *Inorg. Chem.* **1987**, *26*, 3167–3170.
- (17) McMillin, D. R.; Kirchoff, J. R.; Goodwin, K. V. *Coord. Chem. Rev.* **1985**, *64*, 83–92.
- (18) Everly, R. M.; McMillin, D. R. *Photochem. Photobiol.* **1989**, *50*, 711–16.
- (19) Palmer, C. E. A.; McMillin, D. R. *Inorg. Chem.* **1987**, *26*, 3837–3840.
- (20) Everly, R. M.; Ziessel, R.; Suffert, J.; McMillin, D. R. *Inorg. Chem.* **1991**, *30*, 559–61.
- (21) Armaroli, N. *Chem. Soc. Rev.* **2001**, *30*, 113–124.
- (22) Scaltrito, D. V.; Thompson, D. W.; O’Callaghan, J. A.; Meyer, G. J. *Coord. Chem. Rev.* **2000**, *208*, 243–266.
- (23) Ruthkosky, M.; Kelly, C. A.; Zaros, M. C.; Meyer, G. J. *J. Am. Chem. Soc.* **1997**, *119*, 12004–12005.
- (24) Scaltrito, D. V.; Kelly, C. A.; Ruthkosky, M.; Zaros, M. C.; Meyer, G. J. *Inorg. Chem.* **2000**, *39*, 3765–3770.
- (25) Ruthkosky, M.; Kelly, C. A.; Castellano, F. N.; Meyer, G. J. *Coord. Chem. Rev.* **1998**, *171*, 309–322.
- (26) Cuttell, D. G.; Kuang, S.-M.; Fanwick, P. E.; McMillin, D. R.; Walton, R. A. *J. Am. Chem. Soc.* **2002**, *124*, 6–7.
- (27) Cunningham, C. T.; Cunningham, K. L. H.; Michalec, J. F.; McMillin, D. R. *Inorg. Chem.* **1999**, *38*, 4388–4392.

- (28) Gothard, N. A.; Mara, M. W.; Huang, J.; Szarko, J. M.; Rolczynski, B.; Lockard, J. V.; Chen, L. X. *J. Phys. Chem. A* **2012**, *116*, 1984–1992.
- (29) Gandhi, B. A.; Green, O.; Burstyn, J. N. *Inorg. Chem.* **2007**, *46*, 3816–3825.
- (30) Eggleston, M. K.; McMillin, D. R.; Koenig, K. S.; Pallenberg, A. J. *Inorg. Chem.* **1997**, *36*, 172–176.
- (31) Ruthkosky, M.; Kelly, C. A.; Castellano, F. N.; Meyer, G. J. *Coord. Chem. Rev.* **1998**, *171*, 309–322.
- (32) Asano, M. S.; Tomiduka, K.; Sekizawa, K.; Yamashita, K.; Sugiura, K. *Chem. Lett.* **2010**, *39*, 376–378.
- (33) Rawls, M. T.; Kollmannsberger, G.; Elliott, C. M.; Steiner, U. E. *J. Phys. Chem. A* **2007**, *111*, 3485–3496.
- (34) Klumpp, T.; Linsenmann, M.; Larson, S. L.; Limoges, B. R.; Buerstner, D.; Krissinel, E. B.; Elliott, C. M.; Steiner, U. E. *J. Am. Chem. Soc.* **1999**, *121*, 4092.
- (35) Steiner, U. E.; Wolff, H. J.; Ulrich, T.; Ohno, T. *J. Phys. Chem.* **1989**, *93*, 5147–54.
- (36) Klumpp, T.; Linsenmann, M.; Larson, S. L.; Limoges, B. R.; Buerstner, D.; Krissinel, E. B.; Elliott, C. M.; Steiner, U. E. *J. Am. Chem. Soc.* **1999**, *121*, 1076–1087.
- (37) Hayashi, H.; Nagakura, S. *Bull. Chem. Soc. Jpn.* **1984**, *57*, 322–328.
- (38) Leffler, J. E. *An introduction to free radicals*; Wiley: New York, 1993.
- (39) Iwamura, M.; Watanabe, H.; Ishii, K.; Takeuchi, S.; Tahara, T. *J. Am. Chem. Soc.* **2011**, *133*, 7728–7736.
- (40) Felder, D.; Nierengarten, J.-F.; Barigelletti, F.; Ventura, B.; Armaroli, N. *J. Am. Chem. Soc.* **2001**, *123*, 6291–6299.
- (41) Miller, M. T.; Gantzel, P. K.; Karpishin, T. B. *J. Am. Chem. Soc.* **1999**, *121*, 4292–4293.
- (42) Green, O.; Gandhi, B. A.; Burstyn, J. N. *Inorg. Chem.* **2009**, *48*, 5704–5714.
- (43) Everly, R. M.; McMillin, D. R. *J. Phys. Chem.* **1991**, *95*, 9071–9075.
- (44) Murov, S. L.; Hug, G. L.; Carmichael, I. *Handbook of Photochemistry*; M. Dekker: New York, 1993.
- (45) Kirchhoff, J. R.; Gamache, R. E.; Blaskie, M. W.; Del Paggio, A. A.; Lengel, R. K.; McMillin, D. R. *Inorg. Chem.* **1983**, *22*, 2380–4.

PART II. DONOR-CHROMOPHORE-ACCEPTOR TRIADS

PART II
Chapter 4

Photo-Induced, Multi-Step, Charge Separation in Heteroleptic Cu(I) bis-Phenanthroline Based
Donor-Chromophore-Acceptor Triads^{k,1}

4.1 Introduction

It is not particularly unusual to observe very efficient single-step redox quenching with many types of chromophores as long as they have reasonably long-lived (ns) photo-excited states. Unfortunately, with such single-step processes, the back electron transfer is usually fast; often faster than the original quenching process, as is the case with [Ru(II)L₃] diads. Consequently, little or no charge separated product is observed, despite efficient redox quenching. For molecular assemblies that provide for multi-step charge separation, it is sometimes possible to observe long-lived charge separation.^{1,2} For example, in molecular assemblies that incorporate an appropriate chromophore (C) covalently linked to an electron acceptor (A) and an electron donor (D), a so-called D-C-A triad, it is possible to obtain long-lived, photoinduced, charge separation. The efficiency of charge separated state (CS) formation depends on the relative rates of the desirable second electron transfer step, and geminate recombination of the initial electron transfer product. Thus, the quantum efficiency for CS formation, Φ_{cs} , can be highly variable from system to system, even within a collection of structurally similar assemblies.³⁻⁷

Complexes of [Ru(II)L₃] (L= polypyridine type ligand) are archetypical examples of metal-based chromophores which have been exploited to effect long-lived, multi-step, photoinduced charge separation.^{3,4} In molecular assemblies which incorporate a phenothiazine-type

^k Added to dissertation with permission from all authors involved

¹ Megan S. Lazorski, Riley Gest, and C. Michael Elliott, Department of Chemistry, Colorado State University, Fort Collins, CO 80523

(PXZ) electron donor and a viologen, mono-quat or diquat-type (MX or DX) electron acceptor, the quantum efficiency for CS formation is approximately unity across a large number of structurally diverse D-C-A [Ru(II)L₃]-based assemblies having different driving forces for oxidative quenching.⁸⁻¹³ We have established that the unusually large quantum yield for CS formation in these [Ru(II)L₃]-based D-C-A triads arises as a result of a ground-state association between the donor moiety and the chromophore as described in the Introduction to this thesis.⁸ The exact nature of the interaction is uncertain, but is most likely π -stacking and not charge-transfer in nature. Furthermore, the CS lifetimes are fairly long (100-300 ns), and for reasons of spin chemical effects, the average CS lifetime can be extended to ca. 2 μ s in a modest, applied magnetic field (ca. 0.5 T).^{9,14}

Unfortunately, ruthenium and most other similarly employed 2nd and 3rd row transition metals (e.g., Os, Re, Pt, Ir) are not earth-abundant. However, 1,10-phenanthroline (P) complexes of earth-abundant Cu(I), [Cu(I)P₂], share many of the desirable photo-physical properties of [Ru(II)L₃].^{3,15-23} The MLCT absorption has a large oscillator strength ($\epsilon > 5,000 \text{ M}^{-1}\text{cm}^{-1}$), and the resulting MLCT excited state is relatively long-lived and is a strong reductant.^{3,15-18,21-24} Also, like [Ru(II)L₃], the thermalized MLCT excited state has considerable triplet-spin character.^{21,25-27} The coordination and redox chemistry of Cu(I), however, differ from that of Ru(II) in several important ways: Cu(I) complexes with phenanthroline are highly labile in solution. They generally form tetrahedral rather than octahedral complexes which tend to undergo Jahn-Teller (J-T) distortion in the MLCT state due to the significant Cu(II) character of the metal center. The J-T distortion reduces the dihedral angle between the ligands and opens up access at the metal to solvent or counterion adduction, thus creating an exciplex.^{25,26,28-30} As mentioned in the Introduction to this thesis, exciplex formation increases the rate of non-radiative relaxation and di-

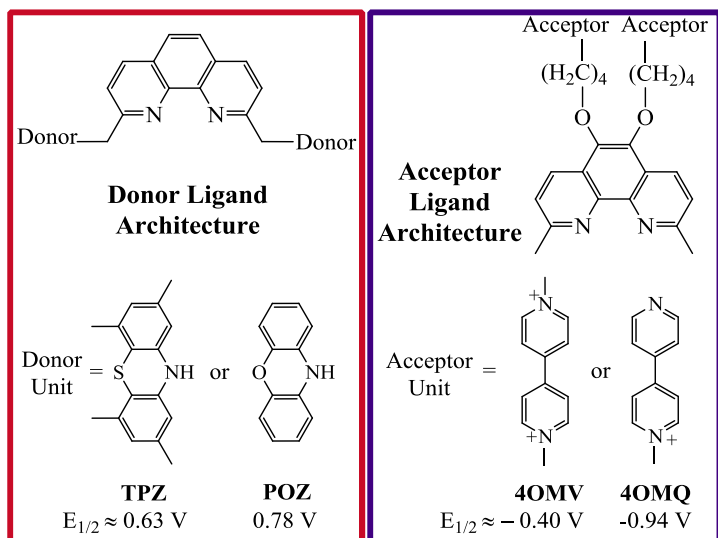


Figure 4.1. Donor and acceptor ligands based on 1,10-phenanthroline and their redox potentials (as free ligand) vs SSCE.

minishes the driving force for reductive quenching.^{15–19,25,26,28–33} Likewise, strong donor solvents shift the ground-state Cu(I/II) potential to more negative values. However, the extent of J-T distortion and accessibility of the metal center to additional ligation can be influenced by steric requirements of substituents located in the 2,9-positions of

the phenanthroline ligand, e.g., as in the donor ligands ($P_D = \text{TPZ}$ or POZ) shown in Figure 4.1.^{20,27,30,32,34} In principle, such bulky substituents can increase the MLCT lifetime and affect the energetics of electron transfer (ET).^{20,27,32,34}

Despite the similarities to $[\text{Ru}(\text{II})\text{L}_3]$, there are very few reported examples where $[\text{Cu}(\text{I})\text{P}_2]$ has been incorporated as the primary chromophore in *multi-step*, light-induced charge separation assemblies. In other words, while there are numerous examples of both inter- and intra-molecular oxidative quenching of $[\text{Cu}(\text{I})\text{P}_2]^+*$ there are only a handful of examples where the product of oxidative quenching, $[\text{Cu}(\text{II})\text{P}_2]^{2+}$, undergoes a subsequent, intramolecular hole transfer to an electron donor.^{19,31,32,35–47} This situation likely arises for two reasons: First, the lability of Cu(I) generally means that there will be an equilibrium mixture of copper complexes in solution if multiple, similar-type ligands are present (thus complicating any data interpretation). Secondly, and probably more importantly, the $[\text{Cu}(\text{II})\text{P}_2]^{2+}$ product of the initial MLCT oxidative quenching is such a weak oxidant that easily oxidizable donors must be employed.^{15,19,31,32} As we demonstrate here, despite the challenges presented by the redox and coordination chemistry

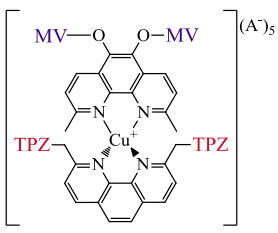
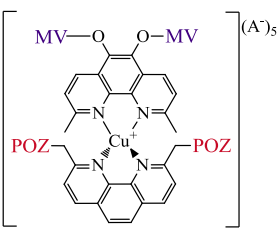
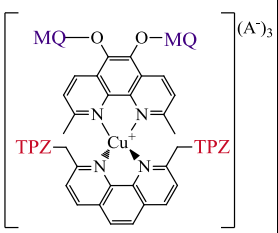
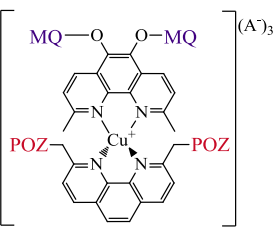
Complex				
Name	[Cu(4OMV)(TPZ)] ⁵⁺ (A ⁻) ₅	[Cu(4OMV)(POZ)] ⁵⁺ (A ⁻) ₅	[Cu(4OMQ)(TPZ)] ³⁺ (A ⁻) ₃	[Cu(4OMQ)(POZ)] ³⁺ (A ⁻) ₃
Energy Stored in CS	1.10 V	1.23 V	1.64 V	1.77 V

Figure 4.2. D-C-A complexes of [Cu(I)P_AP_D]ⁿ⁺ where P_A=acceptor appended 1,10-phenanthroline and P_D= donor appended 1,10-phenanthroline. Also shown is the theoretical amount of energy able to be stored in the CS of each D-C-A based on the redox potentials of the P_A and P_D moieties in the C-AX and C-DX complexes, shown in Figures 4.3 and 4.4 below.

of Cu(I), it is possible to assemble functional [Cu(I)P₂]-based D-C-A assemblies which, like their ruthenium counterparts, undergo efficient, long-lived, multi-step, photoinduced CS formation. In this process we have utilized our extensive experience with [Ru(II)L₃] triad assemblies to design the four [Cu(I)P₂] D-C-A complexes, which are shown in Figure 4.2.

4.2 Results

Studies on the P_A/P_D Ligands and Homoleptic C-AX/C-DX diads

The redox potentials vs SSCE of the P_A ligands, and homoleptic [Cu(I)(P_A)₂]ⁿ⁺(A⁻)_n complexes (C-AX diads, when X = V or Q, P_A = 4OMV or 4OMQ, respectively) were determined by cyclic voltammetry (CV) studies as described in the Experimental section. The data presented in Figure 4.3 clearly show that the redox potentials of the P_A ligands are essentially unaffected when the P_A ligands are complexed by Cu(I) to make the homoleptic C-AX diads. The ΔE_p values for the first wave of the 4OMV ligand and C-AV diad are consistent with one-electron redox processes. The values of ΔE_p for the second wave of the 4OMV ligand, C-AV diad, 4OMQ ligand, and C-AQ diad are somewhat larger than expected for a one-electron process, but this effect is likely due to solvent resistance. Meyer and coworkers calculated the Cu^{2+/+*} redox potential to

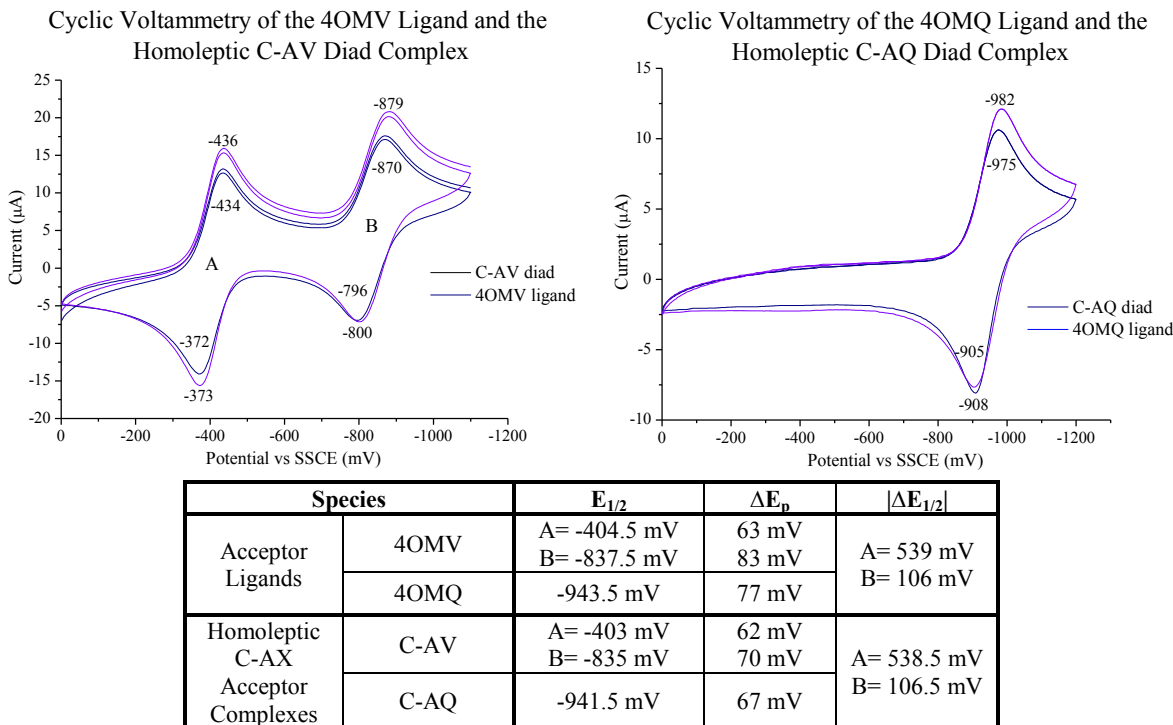
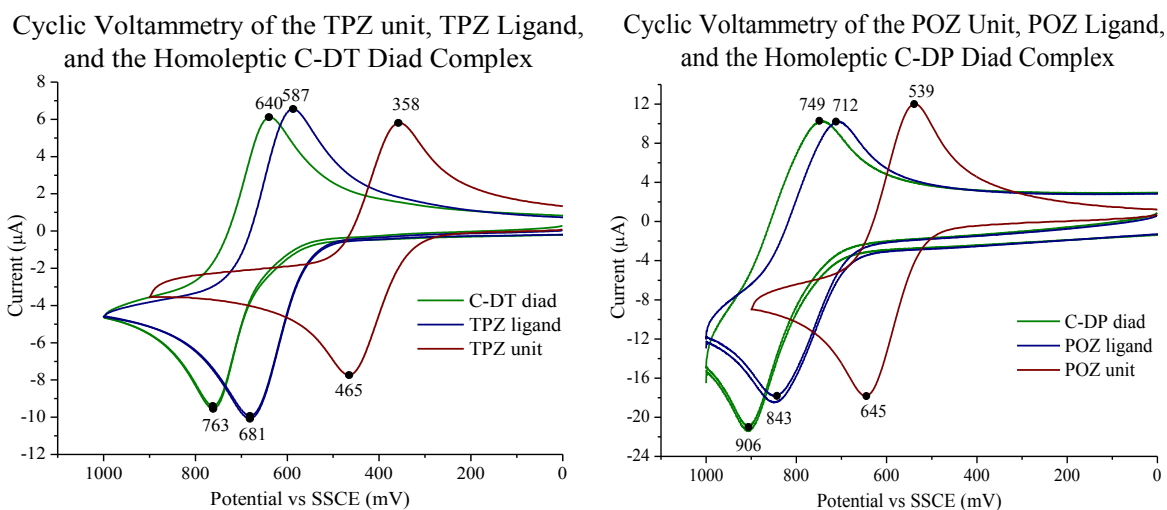


Figure 4.3. CV studies on the P_A ligands and the C-AX diads. These studies were all performed with a glassy carbon working electrode (ca. 7 mm²) vs. SSCE in a 0.1 M solution of TBA⁺PF₆⁻ in CH₃CN. Clearly, forming the heteroleptic complexes of the P_A ligands has little effect on their redox potentials.

be ≈ -1.4 V vs SCE,⁴⁸ which is > 450 mV negative of 4OMQ and 1000 mV negative of the 4OMV species. Thus, there should be a large driving force for acceptor reduction in [Cu(I)P₂] D-C-A species containing either acceptor moiety. Furthermore, D-C-A's containing the 4OMQ acceptor ligand are expected to store ca. 0.54 mV additional energy in the CS state than D-C-A's with the 4OMV acceptor.

The redox potentials vs SSCE of the donor units (when not attached to the phenanthroline ligand), P_D ligands, and homoleptic [Cu(I)(P_D)₂]ⁿ⁺(A⁻)_n complexes (C-DX diads, when X=T or P, P_D = TPZ or POZ, respectively) are shown in Figure 4.4, and were determined by cyclic voltammetry (CV) studies as described in the Experimental section. As is evident in Figure 4.4, the ΔE_p values are larger than expected for one-electron processes, but further studies on the TPZ and POZ units showed that the ΔE_p decreased with decreasing scan rate. Since the solvent



Species		$E_{1/2}$	ΔE_p	$ \Delta E_{1/2} $
Unattached Donor Units	TPZ	411.5 mV	107 mV	180.5 mV
	POZ	592 mV	106 mV	
Donor Ligands	TPZ	634 mV	94 mV	143.5 mV
	POZ	777.5 mV	131 mV	
Homoleptic C-DX Donor Complexes	C-DT	701.5 mV	123 mV	126 mV
	C-DP	827.5 mV	157 mV	

Figure 4.4. Cyclic voltammetry of the donor units (not attached to the P ligands), P_D ligands, and C-DX complexes. These studies were all performed using a glassy carbon working electrode (ca. 7 mm²) vs. SSCE in a 0.1 M solution of TBA⁺PF₆⁻ in either dichloromethane or \approx 1:1 CH₂Cl₂/CH₃CN.

in each of the studies presented in Figure 4.4 was composed of ca. 50% dichloromethane, the resistance of the solvent is likely to be a major contributor to the large values of ΔE_p that were observed.

These CV studies also indicated that the redox potential of the TPZ unit is shifted ca. 180 mV negative of the POZ unit. However, when the TPZ and POZ donor units are attached to phenanthroline to make P_D donor ligands the redox potentials shift back in the positive direction by ca. 180-220 mV. When complexed with Cu(I) to make the C-DX diads, the redox potential of the P_D ligands again shift to a more positive potential. Furthermore, the Cu(I/II) wave is not resolvable from the $P_D^{0/+}$ wave in both C-DX diads, which could imply that there is little to no driving force for oxidation of the donor moieties by the $[Cu(II)(P_D)_2]^{n+}$ complex.

Spectroelectrochemical (SE) oxidation of the C-DX diads was performed in 1,2-difluorobenzene (dfb) in order to determine if the $[\text{Cu}(\text{II})\text{P}_2]^{2+}$ complex (after the initial photoexcitation event and acceptor reduction in D-C-A's) is capable of one-electron oxidation of the donor moiety. The SE data on the C-DT diad is presented in Figure 4.5. As demonstrated by these data, the absorption of the $[\text{Cu}(\text{I})\text{P}_2]^*$ MLCT state (435 nm) is essentially constant for the first 20 min, at which point the absorbance of the oxidized donor (564 nm) has evolved to approximately half of the maximum value achieved during this experiment. The absorbance of the $[\text{Cu}(\text{I})\text{P}_2]^*$ MLCT state then slowly decreases to half of its initial value at 40 min, which is approximately the time at which the absorbance of oxidized donor is maximized. Since there are two TPZ donor units attached to each phenanthroline ligand (four total TPZ units per C-DT complex), these data imply that at least two of the four TPZ moieties are oxidized at a more negative potential than the onset of any metal based oxidation.

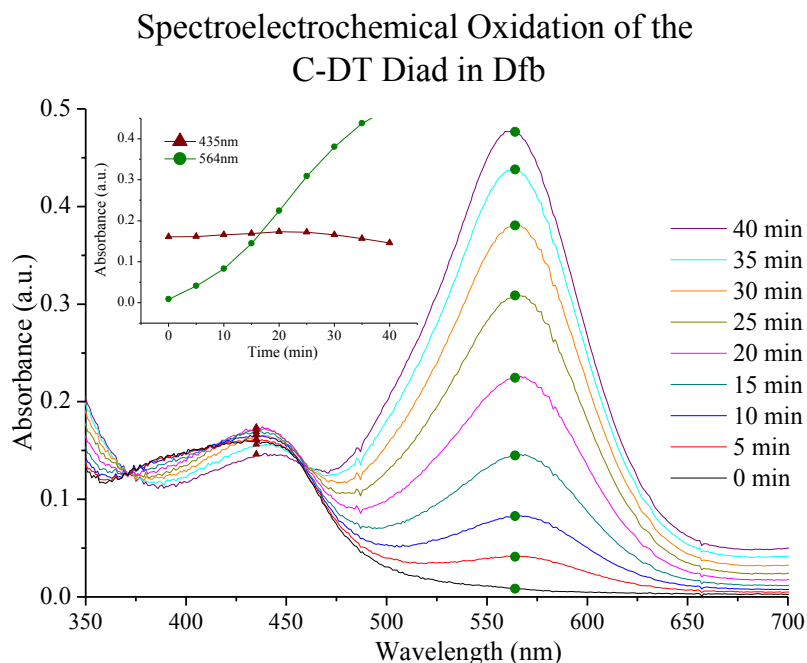


Figure 4.5. Spectroelectrochemical oxidation of the C-DT diad in dfb. The inset graph depicts the change in the absorbance of the $[\text{Cu}(\text{I})\text{P}_2]^*$ MLCT state (435 nm) and the oxidized TPZ donor moiety (564nm).

Spectroelectrochemical Oxidation of the C-DP Diad in Dfb

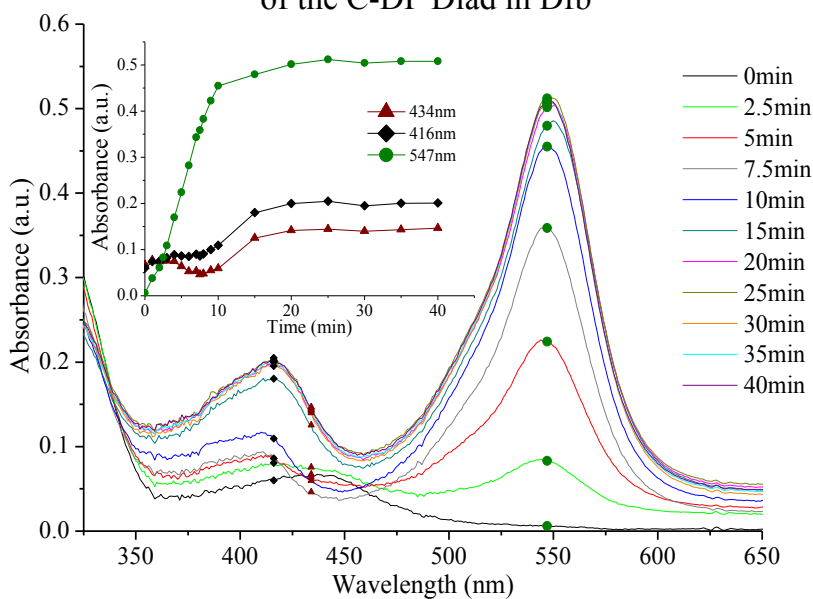


Figure 4.6. The SE oxidation of the C-DP diad complex in dfb. The inset graph depicts the changes in the absorbance of the $[\text{Cu(I)P}_2]^*$ MLCT state (434 nm), the oxidized POZ donor moiety (547 nm), and presumably, the $[\text{Cu(II)P}_2]^{m+}$ MLCT state (416 nm). Some of the data from 0-10 min in the inset was omitted from the spectral data for clarity.

416 nm and 547 nm. In the first 5 min of the experiment, the $[\text{Cu(I)P}_2]^*$ MLCT peak at 434 nm is essentially indistinguishable from the peak at 416 nm. At this point, the absorption due to the $\text{POZ}^{+\circ}$ radical cation at 547 nm and 416 nm had evolved to nearly half of their respective maximum values achieved during this experiment. These data indicate that approximately half of the Cu(I) and at least two of the POZ moieties have been oxidized to $[\text{Cu(II)P}_2]$ and $\text{POZ}^{+\circ}$, respectively. This result is not surprising since the waves for the $\text{POZ}^{0/+}$ ligand and Cu(I/II) are not resolvable in the CV, and therefore, it is likely that the oxidized $\text{POZ}^{+\circ}$ the oxidized $[\text{Cu(II)P}_2]$ complex are evolving simultaneously. Thus, these data imply that there is some driving force for POZ oxidation, but it is smaller than for TPZ, which is consistent with the CV results. Therefore the oxidation products, $[\text{Cu(II)P}_2]$ and $\text{POZ}^{+\circ}$ are likely in a dynamic equilibrium.

Although the SE data presented above implies that there is some driving force for donor oxidation by the oxidized $[\text{Cu(II)P}_2]$ chromophore after acceptor reduction, the $[\text{Cu(I)P}_2]^*$ MLCT

Figure 4.6 shows SE data for the C-DP complex, which is slightly more complicated than C-DT. In the C-DP complex, the $[\text{Cu(I)P}_2]^*$ MLCT state absorption (434 nm) decreases as two new peaks associated with the oxidized $\text{POZ}^{+\circ}$ radical cation grow in at

excited state, itself, is not a strong enough oxidant to oxidize the donor. Therefore, photo-excitation of the C-DX diads is not expected to produce any appreciable amount of CT state. Nevertheless, transient absorption (TA) laser experiments were performed on the homoleptic C-DT complex as described in the Experimental section. As expected, no signal was observed for this C-DX diad. We reasoned that the C-DP diad would yield the same result.

As discussed in Chapter 3, observable, photo-initiated CT state formation does occur in the homoleptic C-AX diads. Since the D-C-A solutions inevitably result in a mixture of C-AX, D-C-A, and C-DT products, as discussed in detail below, the information obtained about the C-AX diads was used to aid in the interpretation of the TA laser studies on the [Cu(I)P₂] D-C-A's presented herein.

Studies on [Cu(4OMV)(TPZ)]⁵⁺(TPFB⁻)₅: "D-C-A Mixture V/T"

Cyclic voltammetry (CV) was performed on the "D-C-A Mixture V/T" (N.B. "D-C-A mixture" denotes a solution containing equimolar amounts of P_A, P_D, and [Cu(I)(ACN)₄]⁺(BF₄⁻), in which P_A = 4OMV, and P_D = TPZ) to verify the purity of the complex as well as estimate the amount of energy stored in the CS. The CV of this study is shown in Figure 4.7, which verifies that the redox potentials of the donor and acceptor moieties do not shift with respect to their C-AV/C-DT values when incorporated into a D-C-A. Therefore, the estimated amount of energy stored in the CS state for this D-C-A complex is the same as reported in Figure 4.2 which was calculated based on the redox potentials of the donor and acceptor moieties in the C-AV and C-DT diads. Thus, to a first approximation, the values of estimated energy stored in the CS of the other three D-C-A complexes quoted in Figure 4.2 are also assumed to be accurate

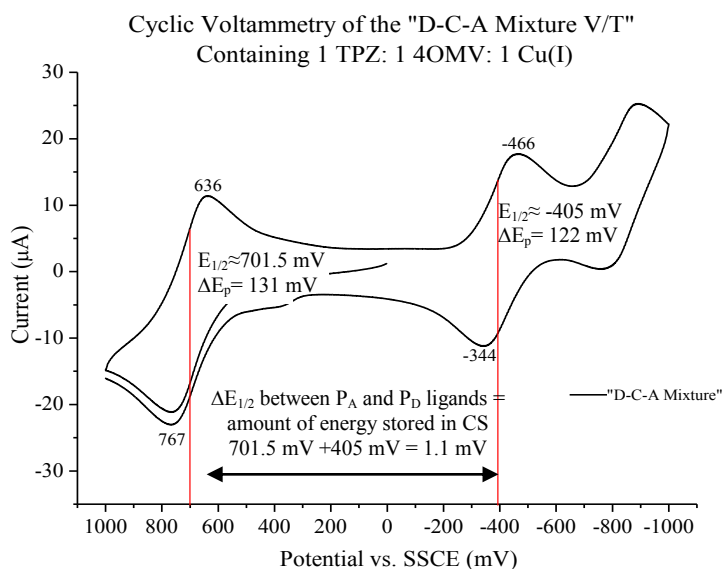


Figure 4.7. Cyclic Voltammetry of the “D-C-A Mixture V/T” as the TPFB salt where the $P_A = 4OMV$ and $P_D = TPZ$ ligands in $0.1 M$ tetrabutylammonium hexafluorophosphate (TBAPF₆) in ACN:CH₂Cl₂ (1:1) on a glassy carbon working electrode (7 mm^2) vs SSCE. The small oxidation peak around 400 mV is due to the presence of I^- left over from the metathesis of the $4OMV$ ligand. The red lines indicate the calculated $E_{1/2}$ values for the P_A and P_D ligands in the D-C-A complex.

As discussed in detail in the Introduction to this thesis, when equimolar amounts of P_A , P_D , and $Cu(I)$ are combined in solution, equilibrium compositions ranging all the way from pure, heteroleptic $[Cu(I)(P_A)(P_D)]^{n+}$ (D-C-A) to a statistical mixture of $[Cu(I)(P_A)_2]^{n+}$: $[Cu(I)(P_A)(P_D)]^{n+}$: $[Cu(I)(P_D)_2]^{n+}$ (i.e. 1:2:1) are, in principle, possible (recall that

$[Cu(I)(P_A)_2]^{n+} = C-AX$ diad and $[Cu(I)(P_D)_2]^{n+} = C-DX$ diad). Therefore, 1H NMR spectra of the “D-C-A Mixture V/T” were used to study the formation behavior of the heteroleptic D-C-A complex and calculate the resulting ratio of D-C-A triad, C-AV diad, and C-DT diad products. The 1H NMR spectrum of the $[Cu(I)(4OMV)(TPZ)]^{5+}(TPFB^-)_5$ D-C-A triad could be extrapolated by comparison to spectra of independently prepared samples of C-DT diad, C-AV diad, 4OMV free ligand, TPZ free ligand, and an equimolar mixture of 4OMV and TPZ free ligands. The chemical shifts, multiplicity, and integration of the phenanthroline peaks were all taken into account during the analysis. This has been done in several different NMR solvents and solvent mixtures as shown in Figure 4.8 (acetonitrile, dichloromethane, dichloromethane/MeOH (of varying concentration)) and the product ratio changes with solvent (the amount of D-C-A product increases to ca. 70% in acetonitrile). However, in order to probe the equilibrium mixture of

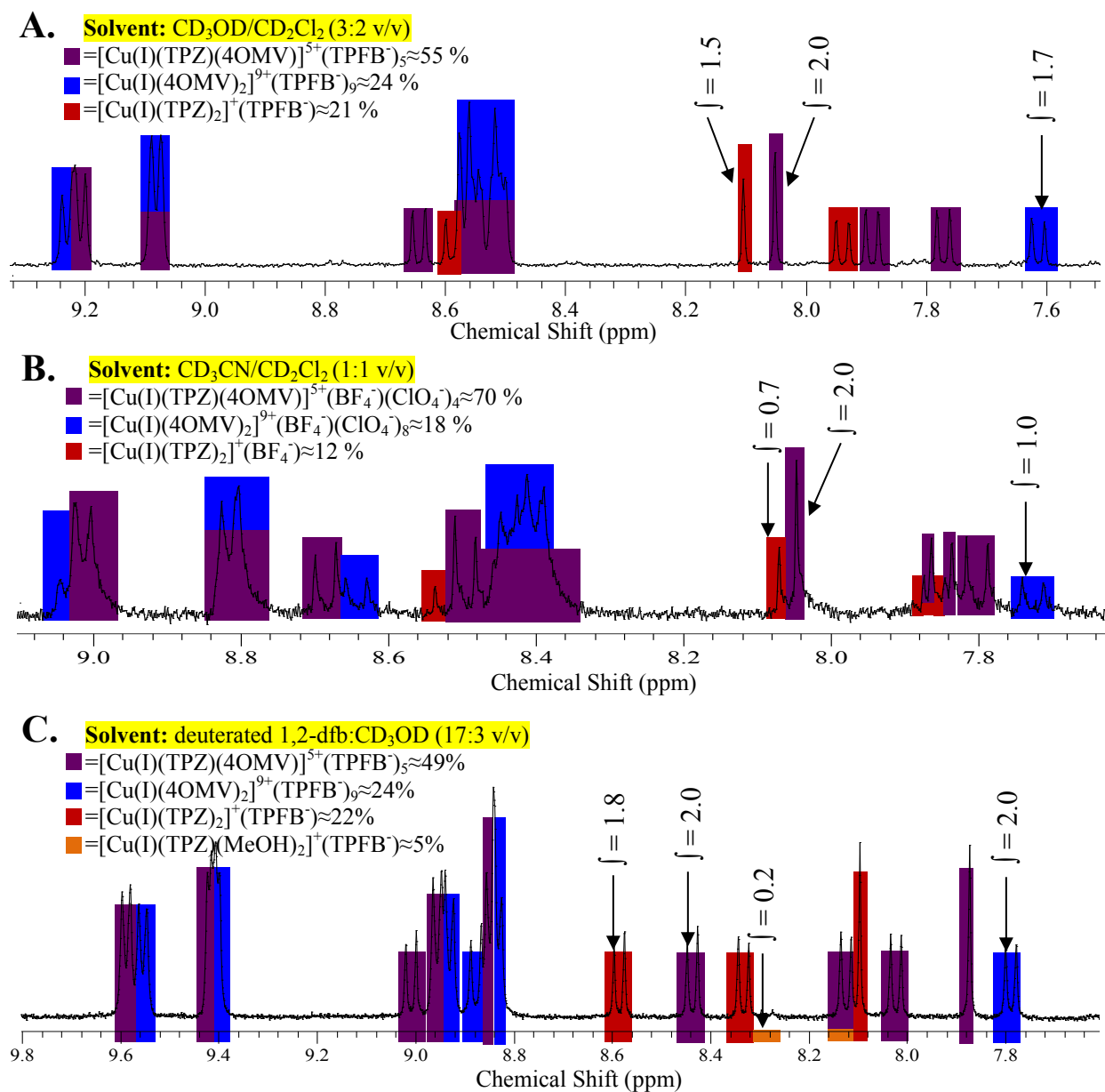


Figure 4.8. ¹H NMR of the “D-C-A Mixture V/T” where P_A = 4OMV, P_D = TPZ in CD₃OD:CD₂Cl₂ (3:2 v/v %) (A) CD₃CN:CD₂Cl₂ (1:1 v/v %) (B), and deuterated dfb:CD₃OD (17:3 v/v %) (C) (phenanthroline and methyl viologen regions shown). The integrations of the peaks used to determine the ratio of products are indicated and the calculated ratios are given in the legend. As can be seen in spectra A-C, the peaks of each species are generally well defined and the integrations of each different component were found to be self-consistent (not shown). This was true for the other peaks in this spectrum, but is most evident in the phenanthroline regions. In spectrum C, some [Cu(I)(TPZ)(MeOH)₂]⁺(TPFB⁻) is present, which likely indicates that the stoichiometry is slightly off from 1:1:1 of 4OMV, TPZ, and Cu(I).

products in the laser studies, which are performed in dfb/X% MeOH (where X = 0-10% v/v), the NMR experiments were also performed in deuterated dfb/15% MeOH. Unfortunately, more MeOH had to be added in these solutions than was used in the actual laser studies due to the sol-

ubility of each component at higher concentration (concentration of species in ^1H NMR experiments $\approx 10^{-3} M$ and in transient absorption laser experiments $\approx 10^{-4}$ - $10^{-5} M$). Since the structural characteristics of the ligands (steric bulk at the 2,9-position of the phenanthroline ligand) used for the other D-C-A complexes presented in Figure 4.2 are very similar to the ligands in the $[\text{Cu}(\text{I})(4\text{OMV})(\text{TPZ})]^{5+}(\text{TPFB}^-)_5$ complex studied by ^1H NMR above, it is assumed that the same or very similar product ratios result for those “D-C-A Mixtures” as well.

The ground state absorption (Ultraviolet-visible, i.e. UV-vis) spectra of “D-C-A Mixture V/T” solutions were generally obtained before and after each laser experiment to gauge sample degradation/changes during the laser experiment. The UV-vis spectra shown in Figures 4.9 and 4.10 were obtained for samples prepared in $\text{CH}_2\text{Cl}_2/\text{MeOH}$, which are not significantly different from those in dfb/MeOH . These spectra were chosen because these solutions were prepared to be the same concentration ($7.0 \times 10^{-4} M$ in total $\text{Cu}(\text{I})$).

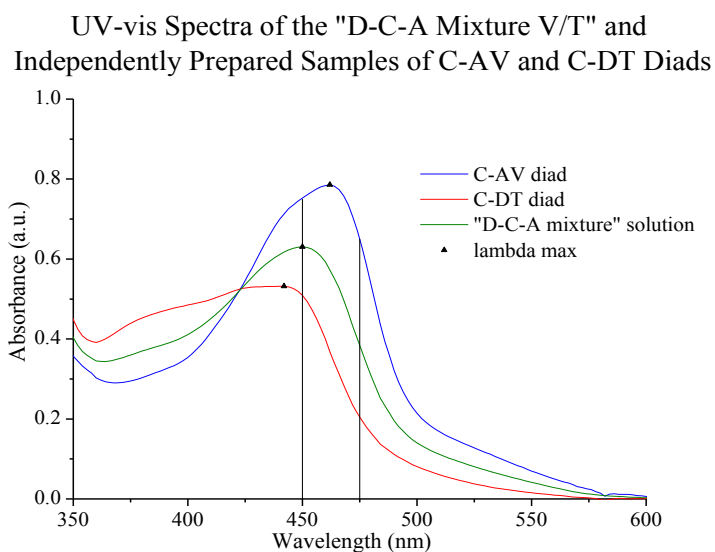


Figure 4.9. UV-vis of the "D-C-A Mixture V/T" compared to the C-AV and C-DT diads in 1:1 $\text{CH}_2\text{Cl}_2/\text{MeOH}$ (v/v) in a 1 cm cell. Each sample was prepared to be the same concentration using $[\text{Cu}(\text{I})] = 7.0 \times 10^{-4} M$. The vertical black lines at 450 and 475 nm indicated the excitation wavelengths for the transient absorption (TA) laser experiments.

Since the UV-vis of the “D-C-A Mixture V/T” is actually a convoluted spectrum of the C-AV diad, C-DT diad, and the $[\text{Cu}(\text{I})(4\text{OMV})(\text{TPZ})]^{5+}(\text{TPFB}^-)_5$ D-C-A triad species it is impossible to measure the ground state extinction coefficient of the pure D-C-A species. Therefore, it is necessary to calculate a predicted ground-state absorption spectrum

of the pure D-C-A complex in order to estimate values for the extinction coefficient. Since all of the spectra shown in Figure 4.9 were made at the same concentration, then the ratio of absorbance values should roughly estimate the ratio of ex-

inction coefficients for each of the species present in the "D-C-A Mixture V/T" spectrum ($A = \epsilon bc$, where b and c are

constant for all spectra). Assuming that the ratio of products in the "D-C-A Mixture V/T" is the same as in the ^1H NMR studies ($1\text{C-AV} : 2[\text{Cu(I)(4OMV)(TPZ)}]^{5+}(\text{TPFB})_5 : 1\text{C-DT}$), then 25% of the overall absorbance of the "D-C-A Mixture V/T" should be due to C-AV diad, 25% should be due to C-DT diad, and 50% should be due to the D-C-A triad. Therefore, if both the C-AV and C-DT diad spectra from Figure 4.9 are separately multiplied by 25%, the resulting spectra should represent the relative contributions of the C-AV and C-DT diads to the overall absorbance of the "D-C-A Mixture V/T." If those resulting spectra ($\text{C-AV} \times 0.25$ and $\text{C-DT} \times 0.25$, shown in Figure 4.10) are then subtracted from the overall absorbance of the "D-C-A Mixture V/T," the

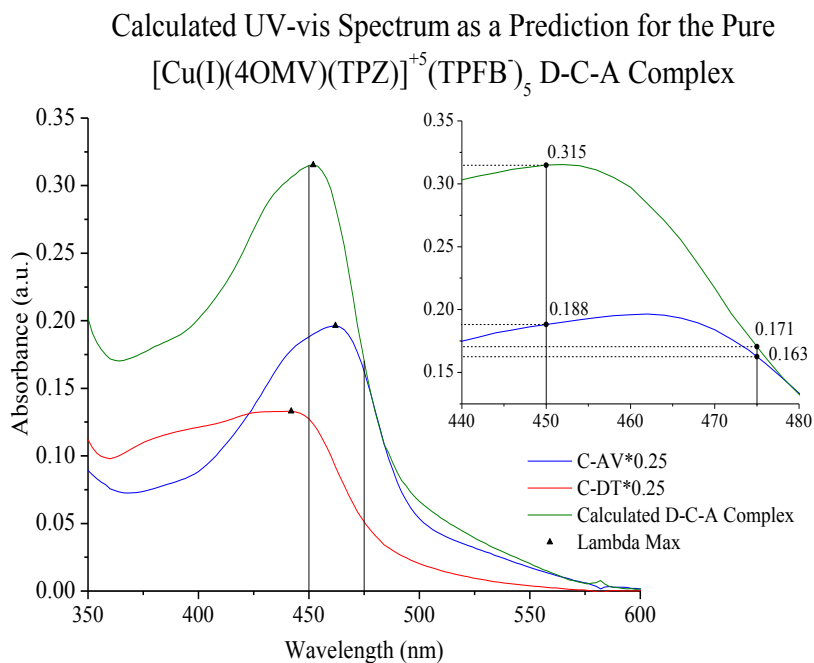


Figure 4.10. Calculated ground state absorption spectrum which serves as a prediction of the pure $[\text{Cu(I)(4OMV)(TPZ)}]^{5+}(\text{TPFB})_5$ D-C-A triad (green). This spectrum was calculated by multiplying the spectra of the C-DT and C-AV diads by 0.25 and subtracting the resulting spectra (red and blue) from the spectrum of the "D-C-A Mixture V/T" from Figure 4.9. The vertical black lines at 450 and 475 nm indicate the excitation wavelengths used for Transient Absorption (TA) laser experiments. The inset graph shows the predicted D-C-A spectrum (green) and the C-AV diad spectrum that has been multiplied by 0.25 (blue) to estimate the ground state extinction coefficient of the pure D-C-A triad relative to the C-AV diad at the excitation wavelengths used in the TA experiments. See text.

final resulting spectrum should, in principle, reflect only the contribution of the pure D-C-A triad to the overall absorbance of the “D-C-A Mixture V/T.” The resulting calculated spectrum is shown in Figure 4.10, and can be considered a rough prediction of the ground state absorption spectrum of the pure D-C-A triad. The vertical black lines at 450 and 475 nm also included in Figure 4.10, represent the two wavelengths used as the pump beam in the TA laser experiments (λ_{ex}). Therefore, the three spectra shown in Figure 4.10 should estimate the relative ground state absorbance of each species in the “D-C-A Mixture V/T,” to a first approximation. The inset in Figure 4.10 is a close-up of the spectra of the two photo-active species in the “D-C-A Mixture V/T,” the C-AV diad and the predicted D-C-A triad, at the pump-wavelengths. This data should enable a coarse estimation of the ground-state extinction coefficient of the D-C-A relative to C-AV. At 450 nm, the absorbance of the D-C-A is ca. 0.315 and the absorbance of the C-AV is ca. 0.188, since the predicted D-C-A spectrum represents twice as many molecules of D-C-A as C-AV then the extinction coefficient of the D-C-A is calculated to be ca. 84% of the C-AV at 450 nm ($[0.315/(0.188 \times 2)] \times 100 = 83.8\%$). Using the same calculation, the extinction coefficient of the D-C-A at 475 nm is calculated to be ca. 52% of the C-AV. Although this is only a rough estimation, it correlates well with the observed changes in the TA decay profile of “D-C-A Mixture V/T” solutions when exciting the sample at different pump wavelengths (c.f. Figure 4.14).

The ground state absorption spectrum shown in Figure 4.11 exemplifies the changes that occur over the course of a typical laser experiment when samples are prepared in the glove box (O_2 content is generally < 1 ppm). Inevitably, some small changes occur, but the sample is relatively stable especially given the large number of laser shots to which the samples are subjected. In some experiments the “before” and “after” spectra are identical, within experimental error. The amount of difference seems to qualitatively correlate with the precision of the ligand and

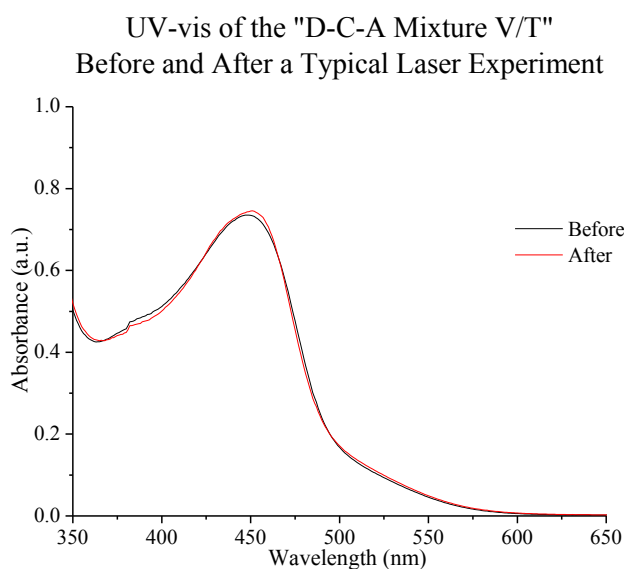


Figure 4.11. Ground State Absorption Spectra of a typical "D-C-A Mixture V/T" solution before and after a full series of Transient Absorption (TA) laser experiments in dfb/5% MeOH (ca. $20\text{--}50 \times 10^3$ laser shots).

Cu(I) stoichiometry. For example, if there is excess Cu(I) present, a spectral signature for 4OMV^{3+} will often develop in the "after" spectrum.

Transient absorption (TA) laser studies were performed in order to study the CS recombination kinetics for the CS of the $[\text{Cu(I)(4OMV}^{3+})(\text{TPZ}^{+o})]^{5+}(\text{TPFB}^-)_5$ D-C-A complex.

The CS decay was observed over a collection of wavelengths at which the CS absorbs in different solvent compositions (1,2-dfb/X% MeOH ($X = 0\text{--}10\%$) and $\text{CH}_2\text{Cl}_2/\text{X}\%$ MeOH) and with different excitation wavelengths (pump = $\lambda_{\text{ex}} = 450$ nm and 475 nm). Figure 4.12A shows a typical single-wavelength TA decay at 396 nm after excitation from a ca. 7 ns, 475 nm laser pulse obtained from the "D-C-A Mixture V/T" in dfb/5% MeOH (v/v): the resulting equilibrium solution having a composition of ca. 1C-AV: $2[\text{Cu(I)(4OMV)(TPZ)}]^{5+}$: 1C-DT. To enhance solubility, the complexes were converted to the tetrakis(pentafluorophenyl)borate (TPFB) salts by metathesis with potassium tetrakis(pentafluorophenyl)borate (K^+TPFB^-) prior to dissolving in dfb/5% MeOH. This metathesis was performed for all other "D-C-A Mixtures" presented in subsequent sections as well.

All photo-products appear entirely within the pulse-width of the laser (ca. 7 ns); thus, the rate constants for formation of the CT state and CS state for, respectively, C-AV diad and $[\text{Cu(I)(4OMV)(TPZ)}_2]^{+5}(\text{TPFB}^-)_5$ D-C-A triad are each $> 1.4 \times 10^8 \text{ s}^{-1}$. The solid red line in Fig-

ure 4.12 is the calculated decay from a bi-exponential fit of the data (in Origin 7.5). The lifetime of the fast component was fixed at 45 ns prior to fitting the data. This 45 ns lifetime is the value obtained from single exponential fits of analogous TA data for independently prepared samples of C-AV diads as described in Chapter 3. Regarding the data in Figure 4.12A, the biexponential fit is quite good. While the fast component lifetime was held constant in the fit, its initial intensity (i.e., at $t = 0$) was allowed to vary. When TA data at various wavelengths (e.g., as in Figure 4.12B) are subjected to the same fit, within experimental error, the same two lifetimes are obtained. Both lifetimes vary with solvent composition, but the longer lifetime of the D-C-A triad, τ_2 in Figure 4.12, varies less dramatically than that of the C-AV diad ($\tau_2 \approx 95$ ns in dfb (or CH_2Cl_2) and $\tau_2 \approx 140$ ns in dfb/ > 4% MeOH (or CH_2Cl_2 / > 4% MeOH). Clearly, the lifetimes are consistent at all wavelengths, indicating that the CT and CS states from the C-AV diad and D-C-A triad, respectively, are the only species responsible for the observed transient absorption.

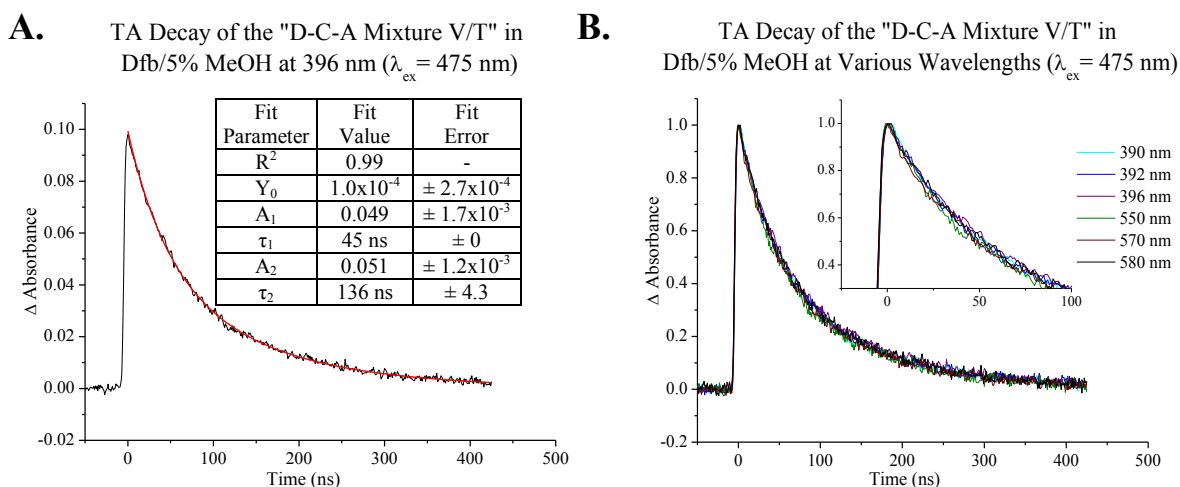


Figure 4.12. TA decay of the "D-C-A Mixture V/T" containing $[\text{Cu}(\text{I})(4\text{OMV}^{3+})(\text{TPZ}^{+0})]^{5+}(\text{TPFB}^-)_5$ and $[\text{Cu}(\text{II})(4\text{OMV}^{4+})(4\text{OMV}^{3+})]^{9+}(\text{TPFB}^-)_9$ at 396 nm (**A**) and at multiple wavelengths (**B**) in dfb/5% MeOH. The inset table in **A** describes the fitting parameters used to fit the data in Origin 7.5 (red). The decay is bi-exponential: the short component ($\tau_1 = 45$ ns, determined independently) is the lifetime of the heteroleptic acceptor C-AV diad and the long component ($\tau_2 = 136$ ns) is the lifetime of the D-C-A. A_1 and A_2 (inset) are the $\Delta A_{t=0}$ of the fast and slow components, respectively. Y_0 is the $\Delta A_{t=\infty}$.

Spectroelectrochemical measurements on the C-DT diad described previously were also performed on a model acceptor, methyl viologen ($MV^{+•}$, in dfb) and used to generate a simulated TA spectrum for the $[Cu(I)(4OMV^{3+•})(TPZ^{+•})]^{5+}$ D-C-A triad. The simulated spectrum was obtained by summing equal-concentration spectra of $MV^{+•}$ and $[Cu(I)(TPZ)(TPZ^{+•})]^{2+}(BF_4^-)_2$ (C-DT diad)

TA Spectrum of $[Cu(I)(4OMV^{3+•})(TPZ^{+•})]^{5+}(TPFB^-)_5$ Compared to the Spectroelectrochemical Predicted Spectrum

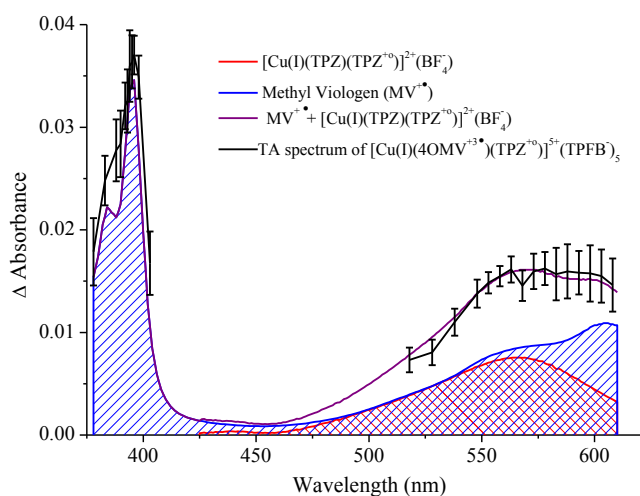


Figure 4.13. The TA spectrum of the $[Cu(I)(4OMV^{3+•})(TPZ^{+•})]^{5+}(TPFB^-)_5$ DCA from 378-608 nm in dfb/5% MeOH (black) after a 100-105 ns delay as compared to the predicted TA spectrum. The spectra of the model reduced acceptor ($MV^{+•}$, blue) and the oxidized homoleptic donor complex, $[Cu(I)(TPZ)(TPZ^{+•})]^{2+}(BF_4^-)_2$, were generated spectroelectrochemically, scaled, and summed to produce the predicted TA spectrum for the DCA (purple dots). See text for details.

and scaling that sum to the average TA absorbance between 518 and 608 nm. Due to the shorter CT lifetime, at 100-105 ns after excitation, the absorbance at each wavelength should be > 90% the result of CS formed from $[Cu(I)(4OMV^{3+•})(TPZ^{+•})]^{5+}$ (i.e., not CT of $[Cu(II)(4OMV^{4+})(4OMV^{3+•})]^{9+}$). Figure 4.13 shows the actual and simulated TA spectra obtained for the $[Cu(I)(4OMV^{3+•})(TPZ^{+•})]^{5+}(TPFB^-)_5$ D-C-A triad in dfb/5% MeOH from 100-105 ns after 475 nm laser excitation as well as the $MV^{+•}$ and $[Cu(I)(TPZ)(TPZ^{+•})]^{2+}(BF_4^-)_2$ spectra used for the simulation.

Changing the laser excitation wavelength from 475 nm to 450 nm, causes a definitive increase in the absorption of the D-C-A triad with respect to the C-AV diad as shown in Figure 4.14. This increase in the absorption of the D-C-A triad is evident by the change in $A_1:A_2$ ratios

A. Normalized TA Decay of the "D-C-A Mixture V/T" in Dfb ($\lambda_{\text{ex}} = 450 \text{ nm}$) **B.** Normalized TA Decay of the "D-C-A Mixture V/T" in Dfb ($\lambda_{\text{ex}} = 475 \text{ nm}$)

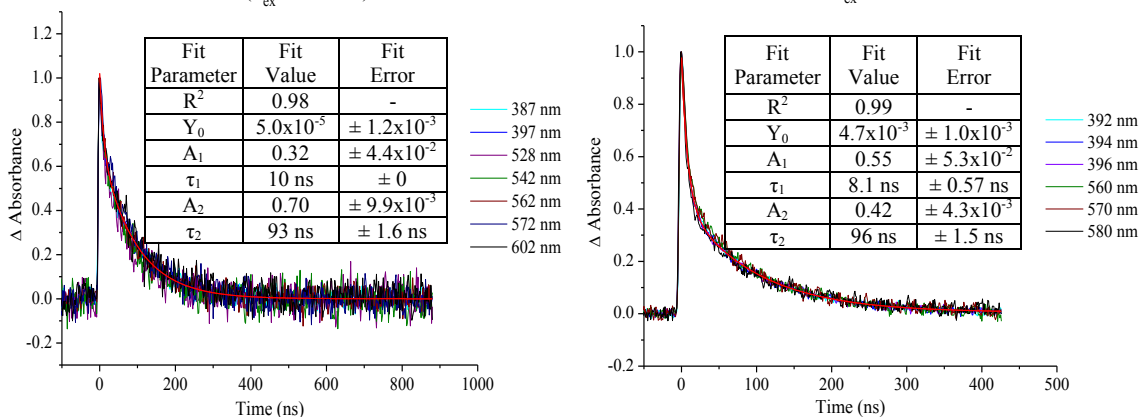


Figure 4.14. The normalized TA decay kinetics of the “D-C-A Mixture V/T” in dfb when the excitation wavelength is 450 nm (A) and 475 nm (B). The fit data in the inset tables was generated by fitting the 397 nm and 396 nm data for A and B, respectively. Recall from Chapter 3 that the lifetime of the C-AV diad in dfb is ca. 7 ns, which is in good agreement with the τ_1 values obtained at both λ_{ex} , within experimental error. These data show two important features: the lifetime of the CS state is shorter in the absence of MeOH, and the $A_1:A_2$ ratios are dependent on λ_{ex} .

from 0.55:0.42 at $\lambda_{\text{ex}} = 475 \text{ nm}$ to 0.3:0.7 at $\lambda_{\text{ex}} = 450 \text{ nm}$. Recall from Figures 4.9 and 4.10 that

the ground state absorption spectrum of the “D-C-A Mixture V/T” is a convolution of the C-AV, D-C-A, and C-DT spectra, and the relative ratio of the absorbing species (D-C-A and C-AV) differs with wavelength. Therefore, a change in the $A_1:A_2$ ratio is expected to occur as the excitation wavelength is changed. Since the actual spectrum of the pure D-C-A complex is unknown, there is no way to accurately predict the $A_1:A_2$ ratios at each wavelength. However, based on the calculated UV-vis spectrum for the pure D-C-A presented in Figure 4.10, it is clear that the absorption coefficient of the D-C-A triad is almost twice as large at 450 nm than at 475 nm. The absorption coefficient of the C-AV diad is slightly larger at 450 nm than at 475 nm. However, it is possible that the error in the A_1 value is too large to observe the change in C-AV diad absorption intensity since these data were taken in dfb (C-AV $\tau_1 \approx 7 \text{ ns}$ in dfb, see Ch. 3) and the lifetime is sufficiently convoluted with the laser pulse.

The data presented for the following “D-C-A Mixtures” incorporating different combinations of the P_A and P_D ligands are very preliminary. Although the data was found to be reproduc-

ible, it was not studied in the same detail as the “D-C-A Mixture V/T.” In general, the samples were prepared on the benchtop, and degassed using the freeze-pump-thaw (FPT) method on the Schlenck line. In each case, the change in ground-state absorption at λ_{max} before and after the laser experiments is ca. $< 10\%$, which was small enough that it does not significantly impact the TA data obtained in these laser experiments. It was later found that the sample integrity was retained for a longer period of time when the samples were prepared in the glove box. Therefore, proper glove box technique will be used if in-depth studies on these complexes are performed in the future. Additionally, fewer laser shots were averaged per experiment to produce each TA data set than in the “D-C-A Mixture V/T,” causing a significant amount of noise in the data.

Finally, these data were obtained using a 249Ω measuring resistor across the photomultiplier tube, causing the response time of the laser instrument to be limited by the increased resistance in the PMT. Therefore, more distortion is expected in the TA data obtained at short times after the laser pulse. Based on the findings for the “D-C-A Mixture V/T” and the C-AX diads in Chapter 3, it is likely that all photo-products appear entirely within the pulse-width of the laser; but studies should be performed without the measuring resistor to verify the rates of formation for the resulting CS states in each respective D-C-A triad. Despite these caveats, these data are presented because they suggest that a CS state forms in each of the D-C-A triads synthesized, and provide a foundation for some nascent hypotheses about the mechanism of CS formation in this new class of $[\text{Cu}(\text{I})\text{P}_2]$ D-C-A’s.

Studies on $[\text{Cu}(\text{I})(4\text{OMQ})(\text{TPZ})]^{3+}(\text{TPFB})_3$: “D-C-A Mixture Q/T”

Ground state absorption spectra of “D-C-A Mixture Q/T” solutions, in which $\text{P}_A = 4\text{OMQ}$ and $\text{P}_D = \text{TPZ}$, were generally obtained before and after each laser experiment to gauge sample

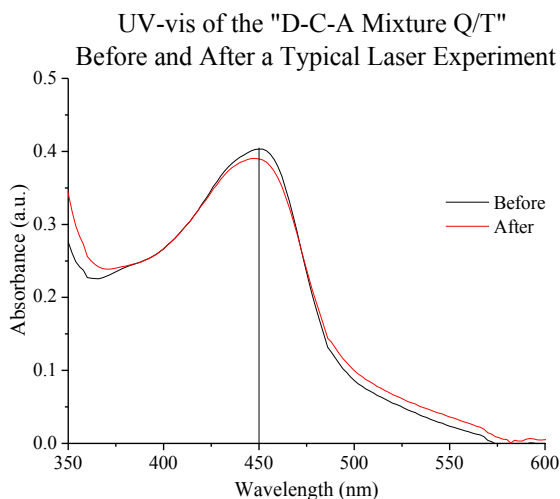


Figure 4.15. The ground state absorption spectrum of the “D-C-A Mixture Q/T” in dfb where $P_A = 40\text{MQ}$ and $P_D = \text{TPZ}$. The vertical black line is positioned at 450 nm, which is the probe wavelength used for the laser studies on this complex.

Transient absorption (TA)

laser studies were performed in order to study the recombination kinetics for the CS of the $[\text{Cu}(\text{I})(4\text{OMQ}^+)(\text{TPZ}^{\circ})]^{3+}(\text{TPFB}^-)_3$ D-C-A complex formed in the “D-C-A Mixture Q/T”. The CS decay for this D-C-A triad was again observed over a range of wavelengths at which the CS absorbs in dfb. Figure 4.16 shows the overlaid, normalized single-wavelength TA decay curves at several different

degradation/changes. The UV-vis spectra shown in Figure 4.15 were obtained for a sample prepared in dfb. It is clear that there is a greater degree of sample degradation for this “D-C-A Mixture Q/T” than for the previous “D-C-A Mixture V/T.” This is probably due to the fact that these data were obtained on a sample that was degassed using the FPT method on a Schlenk line instead of in the glove box.

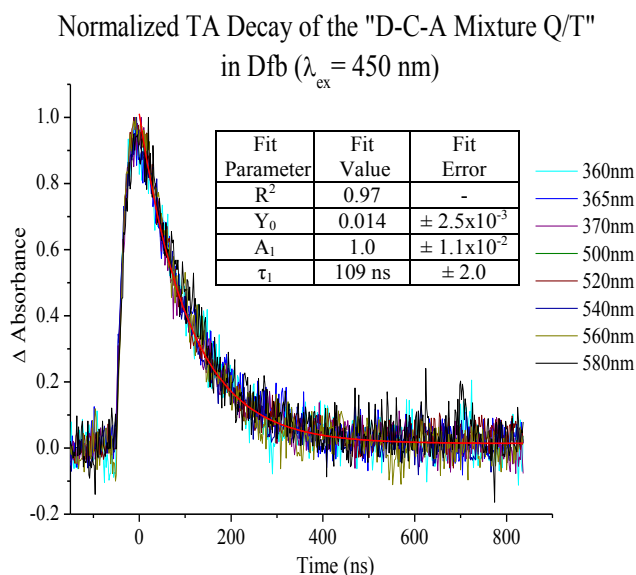


Figure 4.16. TA decay of the “D-C-A Mixture Q/T” containing $[\text{Cu}(\text{I})(4\text{OMQ}^+)(\text{TPZ}^{\circ})]^{3+}(\text{TPFB}^-)_3$ and $[\text{Cu}(\text{II})(4\text{OMQ}^{2+})(4\text{OMQ}^+)]^{5+}(\text{TPFB}^-)_5$ at multiple wavelengths in dfb. The inset table describes the fitting parameters used to fit the data at 370 nm in Origin 7.5 (red). The decay is mono-exponential with a lifetime of $\tau = 109$ ns for the D-C-A. Y_0 is the $\Delta A_{t=\infty}$. These data were obtained with a 249 Ω measuring resistor, which increases the response time of the instrument. Therefore, the lifetime due to the presence of C-AQ diad was likely distorted by the laser pulse signal.

wavelengths after excitation from a 450 nm laser pulse obtained from the “D-C-A Mixture Q/T” in dfb. Based on the ^1H NMR data from the “D-C-A Mixture V/T,” the resulting equilibrium solution is assumed to have a composition of ca. 1C-AQ: 2[Cu(I)(4OMQ)(TPZ)] $^{3+}$: 1C-DT.

As can be seen in Figure 4.16, there is some curvature at the leading edge of the TA decay curve and the decay was found to be mono-exponential. However, this is likely due to the fact that these data were obtained using a 249 Ω measuring resistor (vide infra). The solid red line in Figure 4.16, is the calculated decay from a mono-exponential fit of the data (in Origin 7.5). The longer response time is also probably why the decay is mono-exponential instead of bi-exponential, despite the presence of [Cu(II)(4OMQ $^{2+}$)(4OMQ $^{+}$)] $^{5+}$ (TPFB $^-$) $_5$. Based on the C-AQ diad data presented in Chapter 3, the lifetime of the fast component should have been ca. 7 ns in dfb, which was not apparent in these complexes. Therefore, the lifetime obtained from this

TA Spectrum of [Cu(I)(TPZ $^{+o}$)(4OMQ $^{+}$)] $^{3+}$ (TPFB $^-$) $_3$ Compared to the Spectroelectrochemical Predicted Spectrum

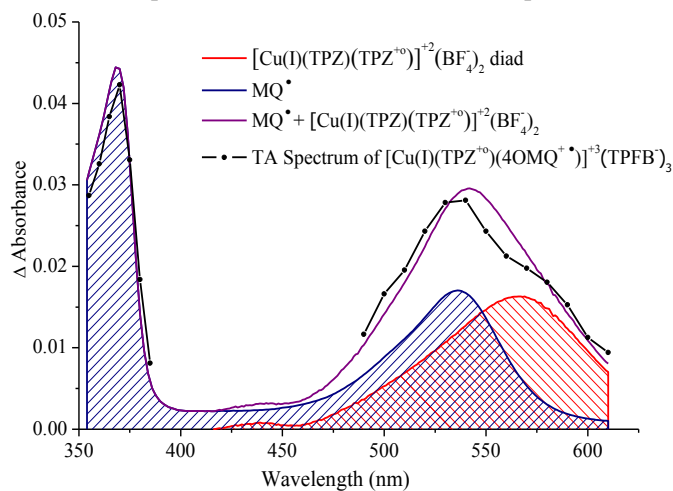


Figure 4.17. The TA spectrum of the [Cu(I)(4OMQ $^{+}$)(TPZ $^{+o}$)] $^{3+}$ (TPFB $^-$) $_3$ D-C-A from 354-610 nm (black) in dfb after a 22-32 ns delay as compared to the predicted TA spectrum. The spectra of the model reduced acceptor (MQ $^{+}$, blue) and the oxidized homoleptic donor complex, ([Cu(I)(TPZ)(TPZ $^{+o}$)] $^{2+}$ (BF $_4^-$) $_2$, red), were generated spectroelectro-chemically, scaled, and summed to produce the predicted TA spectrum for the DCA (purple). See text for details.

fit ($\tau \approx 109$ ns in dfb) is assigned to the electron-hole recombination of the CS state in the D-C-A triad complex. However, it is clear from the overlaid data in Figure 4.16, that the lifetime is consistent at all of the wavelengths studied, indicating that only one CS species is responsible for the observed TA in this D-C-A triad.

The simulated TA spectrum, shown in Figure 4.17, for

the $[\text{Cu(I)(4OMQ}^{\bullet+})(\text{TPZ}^{\circ+})]^{3+}$ CS state was produced using the method described previously. However, due to the shorter CT lifetime in dfb solvent, the TA data presented is from 22-32 ns after 450 nm laser excitation, instead of 100-105 ns. Thus, the absorbance at each wavelength should be > 90% the result of CS formed from $[\text{Cu(I)(4OMQ}^{\bullet+})(\text{TPZ}^{\circ+})]^{3+}$ (i.e., not CT of $[\text{Cu(II)(4OMQ}^{2+})(\text{4OMQ}^{\bullet+})]^{5+}$). Figure 4.17 shows the actual and simulated TA spectra obtained for the $[\text{Cu(I)(4OMQ}^{\bullet+})(\text{TPZ}^{\circ+})]^{3+}(\text{TPFB}^-)_3$ D-C-A in dfb, as well as the MQ^{\bullet} and $[\text{Cu(I)(TPZ)(TPZ}^{\circ+})]^{2+}(\text{BF}_4^-)_2$ spectra used for the simulation.

Studies on $[\text{Cu(I)(4OMV)(POZ)]}^{5+}(\text{TPFB}^-)_5$: "D-C-A Mixture V/P"

Ground state absorption spectra of "D-C-A Mixture V/P" solutions, in which $P_A = 4\text{OMV}$ and $P_D = \text{POZ}$, were also generally obtained before and after each laser experiment to gauge sample degradation/changes. The UV-vis spectra shown in Figure 4.18 were obtained for a sample prepared in dfb. Again, there is a greater degree of sample degradation for this "D-C-A Mixture V/P" than for the previous "D-C-A Mixture V/T," which is likely due to the FPT method used to degas the samples.

Transient absorption (TA) laser studies were again performed in order to study the recombination kinetics for the CS of the $[\text{Cu(I)(4OMV}^{3+})(\text{POZ}^{\circ+})]^{5+}(\text{TPFB}^-)_5$ D-C-A complex formed in the "D-C-A Mixture V/P". These studies were performed in the same manner as for the "D-C-A Mixture Q/T". Fig-

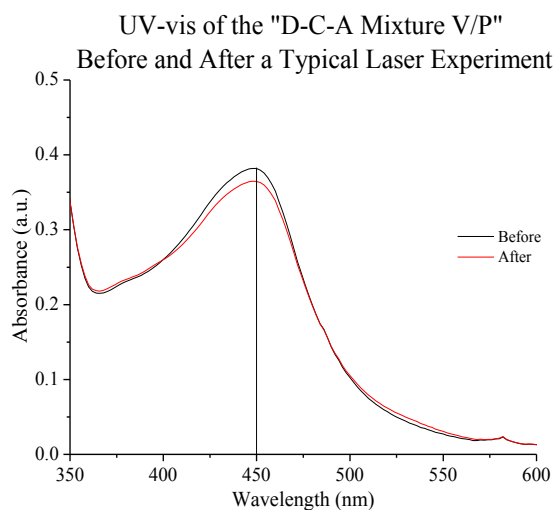


Figure 4.18. The ground state absorption spectrum of the "D-C-A Mixture V/P" in dfb where $P_A = 4\text{OMV}$ and $P_D = \text{POZ}$. The vertical black line is positioned at 450 nm, which is the probe wavelength used for the laser studies on this complex.

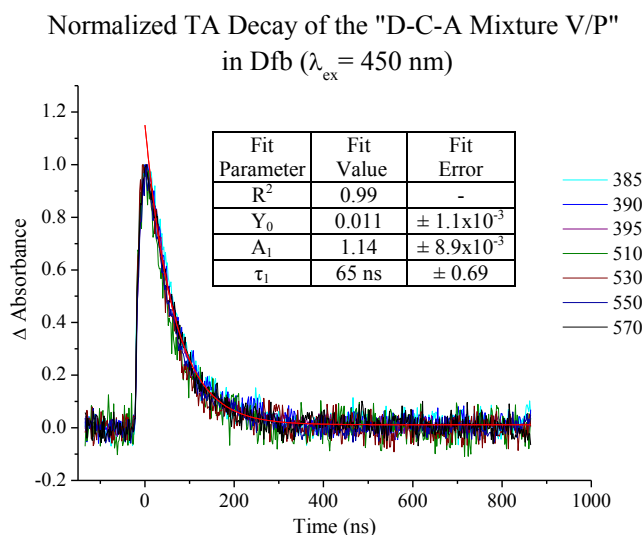


Figure 4.19. TA decay of the “D-C-A Mixture V/P” containing $[\text{Cu}(\text{I})(4\text{OMV}^{3+})(\text{POZ}^{+0})]^{5+}(\text{TPFB}^-)_5$ and $[\text{Cu}(\text{II})(4\text{OMV}^{4+})(4\text{OMV}^{3+})]^{9+}(\text{TPFB}^-)_9$, at multiple wavelengths in dfb. The inset table describes the fitting parameters used to fit the 395 nm data in Origin 7.5 (red). The decay is mono-exponential with a lifetime of $\tau = 65$ ns for the D-C-A. Y_0 is the $\Delta A_{t=\infty}$. These data were obtained with a 249 Ω measuring resistor.

there is a slight curvature at the leading edge of the TA decay curve and the decay was found to be mono-exponential. The solid red line in Figure 4.19, is the calculated decay from a mono-exponential fit of the data (in Origin 7.5). Based on the C-AV diad data presented in Chapter 3, the lifetime of the fast component should have been ca. 7 ns in dfb, which was not detected due to the response time of the instrument. The fact that the mono-exponential fit overshoots the maximum value for the laser data at short time, but fits the curvature very well also implies response time issues as described above. Therefore, the lifetime obtained from this fit ($\tau \approx 65$ ns in dfb) is assigned to the electron-hole recombination of the CS state in the $[\text{Cu}(\text{I})(4\text{OMV}^{3+})(\text{POZ}^{+0})]^{5+}(\text{TPFB}^-)_5$ D-C-A triad. However, it is clear from the overlaid data in Figure 4.19, that the lifetime is consistent at all of the wavelengths, again indicating that only one CS species is responsible for the observed TA in this D-C-A triad.

Figure 4.19 shows the normalized single-wavelength TA decay curves at several different wavelengths after excitation from a 450 nm laser pulse obtained from the “D-C-A Mixture V/P” in dfb. Based on the ^1H NMR data from the “D-C-A Mixture V/T,” the resulting equilibrium solution is assumed to have a composition of ca. 1C-AV: $2[\text{Cu}(\text{I})(4\text{OMV})(\text{POZ})]^{5+}$: 1C-DP.

As can be seen in Figure 4.19,

TA Spectrum of $[\text{Cu}(\text{I})(4\text{OMV}^{3+})(\text{POZ}^{+\circ})]^{5+}(\text{TPFB}^-)_5$ Compared to the Spectroelectrochemical Predicted Spectrum

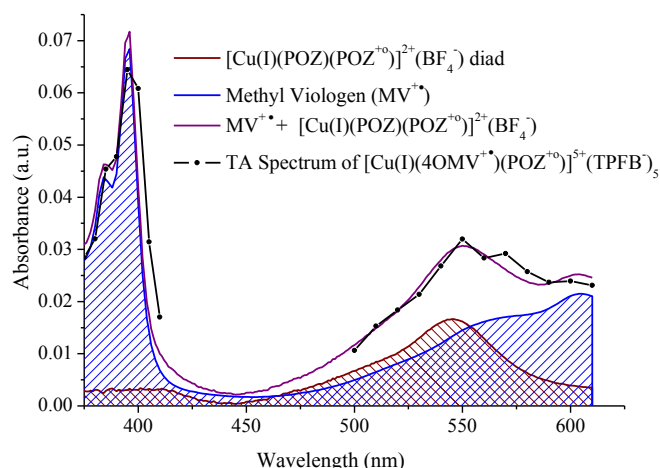


Figure 4.20. The TA spectrum of the $[\text{Cu}(\text{I})(4\text{OMV}^{3+})(\text{POZ}^{+\circ})]^{5+}(\text{TPFB}^-)_5$ D-C-A from 370-610 nm (black) in dfb after a 20-30 ns delay as compared to the predicted TA spectrum. The spectra of the model reduced acceptor ($\text{MV}^{+\bullet}$, blue) and the oxidized homoleptic donor complex, $[\text{Cu}(\text{I})(\text{POZ})(\text{POZ}^{+\circ})]^{2+}(\text{BF}_4^-)_2$, were generated spectroelectro-chemically, scaled, and summed to produce the predicted TA spectrum for the DCA (purple). See text for details.

(4OMV^{3+}) $^{9+}$). Figure 4.20 shows the actual and simulated TA spectra obtained for the $[\text{Cu}(\text{I})(4\text{OMV}^{3+})(\text{POZ}^{+\circ})]^{5+}(\text{TPFB}^-)_5$ D-C-A triad in dfb from 20-30 ns after 450 nm laser excitation as well as the $\text{MV}^{+\bullet}$ and $[\text{Cu}(\text{I})(\text{POZ})(\text{POZ}^{+\circ})]^{2+}(\text{BF}_4^-)_2$ spectra used for the simulation.

Studies on $[\text{Cu}(\text{I})(4\text{OMQ})(\text{POZ})]^{3+}(\text{TPFB}^-)_3$: “D-C-A Mixture Q/P”

Ground state absorption spectra of “D-C-A Mixture Q/P” solutions, in which $\text{P}_\text{A} = 4\text{OMQ}$ and $\text{P}_\text{D} = \text{POZ}$, were again generally obtained before and after each laser experiment to gauge sample degradation/changes. The UV-vis spectra shown in Figure 4.21 were obtained for a sample prepared in dfb. As with the two previous “D-C-A Mixture” solutions degassed using the FPT method, there is a greater degree of sample degradation for this “D-C-A Mixture Q/P” than for the previous “D-C-A Mixture V/T.”

The simulated TA spectrum for the $[\text{Cu}(\text{I})(4\text{OMV}^{3+})(\text{POZ}^{+\circ})]^{5+}$ CS state was produced using the same method as described previously. Again, due to the shorter CT lifetime in dfb solvent, the TA data presented here is from 20-30 ns after excitation instead of 100-105 ns; thus, > 90% of the result of CS formed from $[\text{Cu}(\text{I})(4\text{OMV}^{3+})(\text{POZ}^{+\circ})]^{5+}$ (i.e., not CT of $[\text{Cu}(\text{II})(4\text{OMV}^{4+})$

Transient absorption (TA) laser studies were again used to study the recombination kinetics for the CS of the $[\text{Cu}(\text{I})(4\text{OMQ}^+)(\text{POZ}^{\text{o}})]^{3+}(\text{TPFB}^-)_3$ D-C-A complex formed in the “D-C-A Mixture V/P”. These studies were performed in the same manner as for the “D-C-A Mixture Q/T”. Figure 4.22 shows normalized single-wavelength TA decay curves at several different wavelengths after excitation from

a 450 nm laser pulse obtained from the “D-C-A Mixture Q/P” in dfb. Again, the resulting equilibrium solution is assumed to have a composition of ca. 1C-AQ: 2 $[\text{Cu}(\text{I})(4\text{OMQ})(\text{POZ})]^{3+}$: 1C-

Normalized TA Decay of the "D-C-A Mixture Q/P" in Dfb ($\lambda_{\text{ex}} = 450 \text{ nm}$)

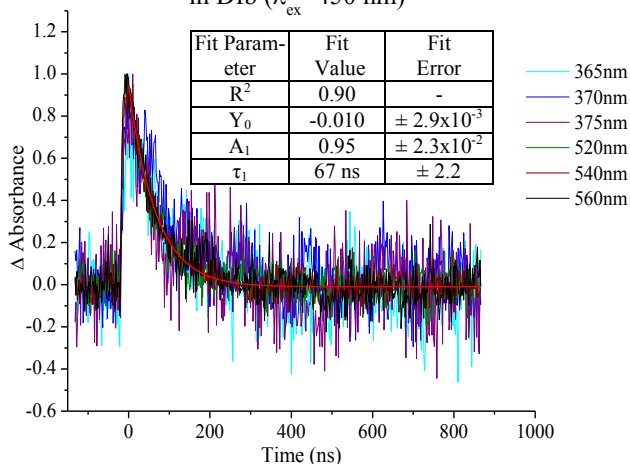


Figure 4.22. TA decay of the “D-C-A Mixture Q/P” containing $[\text{Cu}(\text{I})(4\text{OMQ}^+)(\text{POZ}^{\text{o}})]^{3+}(\text{TPFB}^-)_3$ and $[\text{Cu}(\text{II})(4\text{OMQ}^{2+})(4\text{OMQ}^+)]^{5+}(\text{TPFB}^-)_5$ at multiple wavelengths in dfb. The inset table describes the fitting parameters used to fit the 540 nm data in Origin 7.5 (red). The decay is mono-exponential with a lifetime of $\tau = 67 \text{ ns}$ for the D-C-A. Y_0 is the $\Delta A_{t=\infty}$. These data were obtained using a 249 Ω measuring resistor.

UV-vis of the "D-C-A Mixture Q/P" Before and After a Typical Laser Experiment

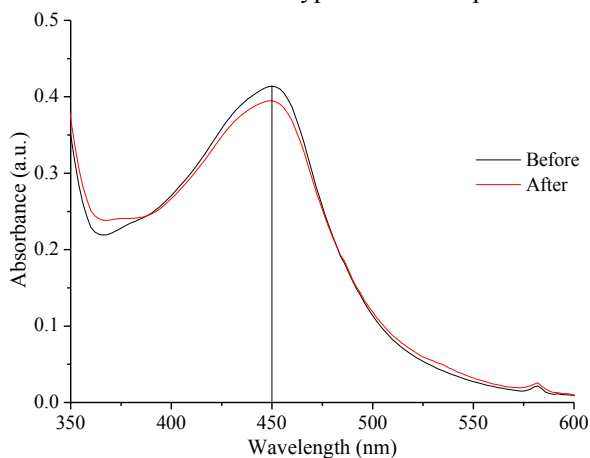


Figure 4.21. The ground state absorption spectrum of the “D-C-A Mixture Q/P” in dfb where $P_A = 4\text{OMQ}$ and $P_D = \text{POZ}$. The vertical black line is positioned at 450 nm, which is the probe wavelength used for the laser studies on this complex.

DP, based on the ^1H NMR data from the “D-C-A Mixture V/T.”

As can be seen in Figure 4.22, the data is extremely noisy, but the decay is seemingly mono-exponential. The solid red line in Figure 4.22, is the calculated decay from a mono-exponential fit of the data (in Origin 7.5). Again, based on the C-AQ diad data presented in Chapter 3, the lifetime of the fast component should be ca. 7 ns in dfb, but is not detected due

to the response time of the instrument or, in this case, possibly the S/N ratio. However, the lifetime obtained from this fit ($\tau \approx 65$ ns in dfb) is tentatively assigned to the electron-hole recombination of the CS state in the $[\text{Cu}(\text{I})(4\text{OMQ}^{+\bullet})(\text{POZ}^{+\circ})]^{3+} (\text{TPFB}^-)_3$ D-C-A triad. The overlaid data in Figure 4.22 are not as convincing as in the previous complexes due to the noise, but the lifetime seems relatively consistent at all of the wavelengths, to a first approximation. Therefore, it is likely that only one CS species is responsible for the observed TA in this D-C-A triad.

The simulated TA spectrum

shown in Figure 4.23 for the

$[\text{Cu}(\text{I})(4\text{OMQ}^{+\bullet})(\text{POZ}^{+\circ})]^{3+}$ CS

state was produced using the same method as described previously.

Again, due to the shorter CT lifetime in dfb solvent, the TA data presented here is from 20-30 ns after excitation instead of 100-105

ns; thus, > 90% the result of CS

formed from $[\text{Cu}(\text{I})(4\text{OMQ}^{+\bullet})$

$(\text{POZ}^{+\circ})]^{3+}$ (i.e., not CT of

$[\text{Cu}(\text{II})(4\text{OMQ}^{2+})(4\text{OMQ}^{+\bullet})]^{5+}$).

Figure 4.23 shows the actual and simulated TA spectra obtained

for the $[\text{Cu}(\text{I})(4\text{OMQ}^{+\bullet})(\text{POZ}^{+\circ})]^{3+} (\text{TPFB}^-)_3$ D-C-A triad in dfb from 20-30 ns after 450 nm laser

excitation as well as the MQ^\bullet and $[\text{Cu}(\text{I})(\text{POZ})(\text{POZ}^{+\circ})]^{2+} (\text{BF}_4^-)_2$ spectra used for the simulation.

TA Spectrum of $[\text{Cu}(\text{I})(4\text{OMQ}^{+\bullet})(\text{POZ}^{+\circ})]^{3+} (\text{TPFB}^-)_3$ Compared to the Spectroelectrochemical Predicted Spectrum

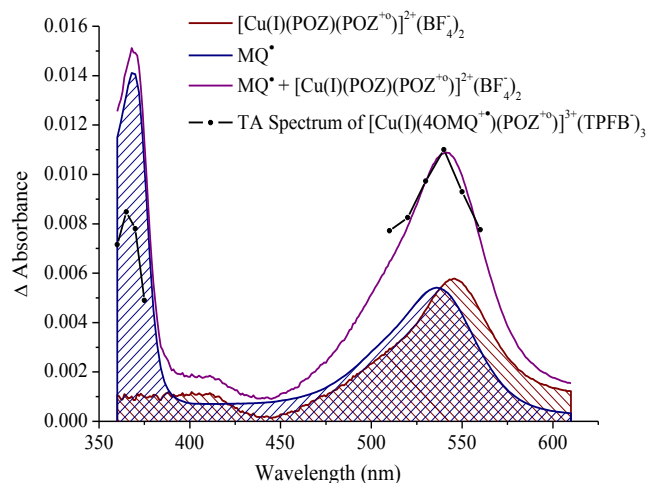


Figure 4.23. The TA spectrum of the $[\text{Cu}(\text{I})(4\text{OMQ}^{+\bullet})(\text{POZ}^{+\circ})]^{3+} (\text{TPFB}^-)_3$ DCA from 360-610 nm (black) in dfb after a 20-30 ns delay as compared to the predicted TA spectrum. The predicted spectrum was generated in the same manner as described previously for the other D-C-A's presented herein. See text for details.

4.3 Discussion

The architecture of the acceptor and donor-containing ligands, P_A and P_D , respectively, is very important for successful construction and CS formation in heteroleptic, $[\text{Cu(I)}(P_A)(P_D)]^{n+}$ D-C-A triads. The P_D ligands, in particular, incorporate a number of design features derived directly from the past work with ruthenium based triads: specifically, using PXZ-type donors and locating them so they can easily π -stack with one of the phenanthroline ligands (a critical feature in efficient CS formation for the $[\text{Ru(II)}L_3]$ triads, *vide supra*). A molecular model of the D-C-A complex where $P_A = 4\text{OMV}$ and $P_D = \text{POZ}$ is shown in Figure 4.24 which indicates that in D_{2d} coordination geometry, attaching the donors on the 2,9-methyl substituents does facilitate the desired, facile π -stacking with the second phenanthroline ligand. It was initially thought that the steric effect of having bulky donors located in the 2,9-position might favor the equilibrium formation of the desired heteroleptic complex (as opposed to the homoleptic bis-donor complex).^{34,50,51} Therefore, based on this logic, the TPZ donor ligand was designed to have increased steric bulk at the 2,9-positions relative to POZ due to the addition of the four methyl groups about the PXZ ring system. Based on the ^1H -NMR studies presented in Figure 4.8, this latter hypothesis has some limited merit in more polar solvents; however, in the relatively non-polar solvent employed in this study (o-difluorobenzene, dfb), the “D-C-A Mixture V/T” (a sample containing 1:1:1 stoichiometry of P_D , P_A and $[\text{Cu(I)}(\text{ACN})_4]^+(\text{BF}_4^-)$ (ACN = acetonitrile, $P_A = 4\text{OMV}$, and $P_D = \text{TPZ}$) results in all of

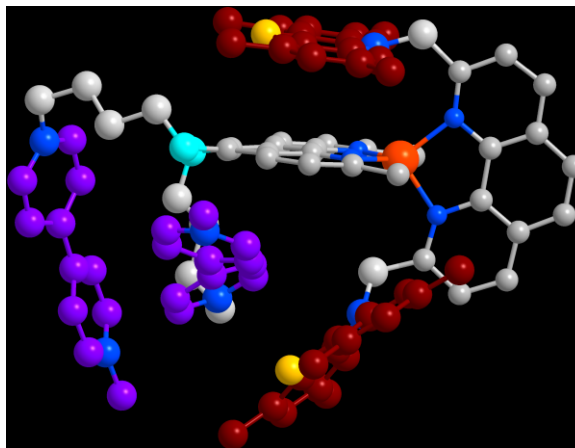


Figure 4.24. A molecular model of the D-C-A complex $[\text{Cu(I)}(4\text{OMV})(\text{POZ})]^{5+}(\text{A}^-)_5$ indicates π -stacking interactions between the donor moiety on the P_D ligand and the phenanthroline ring system of the P_A ligand.

the Cu(I) assembling into one of three complexes: homoleptic acceptor C-AV diad, heteroleptic D-C-A $[\text{Cu(I)(4OMV)(TPZ)}]^{5+}$, and homoleptic donor C-DT diad in essentially statistical amounts (i.e., 1:2:1). Since the NMR study was performed using the P_D with the greatest amount of steric bulk (TPZ), it was assumed that the other D-C-A complexes will have similar formation behavior, since there is no additional impetus for heteroleptic formation in these complexes.

Although, in this case, increasing the steric bulk at the 2,9-positions had little influence on the formation behavior of the heteroleptic complex, there was a formidable effect on the redox potential of the donor ligand. Recall that another reason for synthesizing the TPZ donor ligand (with the four additional methyl groups on each PXZ ring) was to shift the redox potential of the parent PTZ sufficiently negatively so that it could be oxidized by $[\text{Cu(II)P}_2]^{2+}$.⁴⁹ This will be discussed in further detail below.

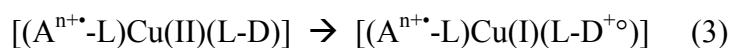
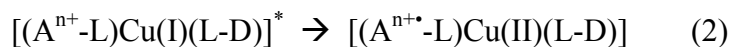
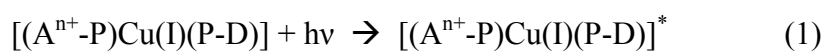
Pure samples of the homoleptic diads, C-AX and C-DX, have been independently prepared and studied. As was indicated by the lack of TA signal for the C-DT complex, the homoleptic donor complexes C-DX, are essentially photo-inactive because the MLCT excited state is too weak an oxidant to oxidize the donor in both diads (Figure 4.25). On the other hand, as discussed in detail in Chapter 3, both C-AX diads undergo single-step, photo-induced charge-transfer state (CT) formation in which one of the four acceptor moieties is reduced and the Cu(I) is oxidized. In stark contrast to related $[\text{Ru}(\text{bpy})_3]^{2+}$ -based C-AX diad assemblies, the solvent-dependent recombination rate of the CT state in $[\text{Cu(I)P}_2]^{n+}$ C-AX diads is relatively slow (ca. $k_{bet} = 2.3 \times 10^7 \text{ s}^{-1}$ in dfb/5% MeOH for C-AV) and is similar to what has been observed by Meyer and coworkers for a closely related $[\text{Cu(I)(bpy)}_2]$ -viologen diad.²⁴ Unfortunately, as demonstrated by the spectroelectrochemical data presented in Figures 4.13, 4.17, 4.20, and 4.23, the UV-visible absorption spectra strongly overlap for the oxidized C-DX^{+o} diads and the reduced model

acceptors, $MV^{+\bullet}$ and MQ^{\bullet} . Thus, in every D-C-A triad studied there is no wavelength where only donor cation absorbs. Consequently, kinetic data for CS recombination must be deconvoluted from the recombination of the CT state of the diad. The detailed transient absorption (TA) studies on the C-AX diads presented in Ch. 3 were used for this purpose.

As stated above, introduction of four methyl substituents onto N-methyl-phenothiazine to make the N-methyl-TPZ unit does shift the one-electron oxidation potential negative by ca. 160 mV relative to unsubstituted analogs. Similarly, changing the heteroatom from sulfur (on N-methyl-phenothiazine) to oxygen to make N-methyl-phenoxazine shifts the redox potential in the negative direction, but to a lesser degree. Thus, donor ligands made with TPZ and POZ should be easier to oxidize than the ligands containing phenothiazine, as are often used with $[Ru(II)L_3]$ D-C-A's. Very similar shifts in redox potentials are reflected in the CV data presented in Figure 4.4, but the phenanthroline ligand appended with phenothiazine donor units in the 2,9-positions has not been synthesized for comparison. Nevertheless, in the solvent systems used, the cyclic voltammetric waves for the redox couples of $Cu^{+/2+}$ and the $TPZ^{0/+}$ ($POZ^{0/+}$) ligand are not resolvable in solutions of C-DT (C-DP) (see Figure 4.4).

Based on the spectroelectrochemical measurements C-DT presented in Figure 4.5, the oxidized $TPZ^{+\circ}$ absorbance at 564 nm increases to approximately half of the maximum value achieved during this experiment before there is any appreciable loss in the MLCT. These data indicate that at least two of the four PTZ moieties are oxidized at a more negative potential than the onset of any metal based oxidation. As shown in Figure 4.6, for the C-DP diad the spectroelectrochemical response was less clear, since absorption at the MLCT state (434 nm) decreases as the absorption due to oxidized $POZ^{+\circ}$ simultaneously increases (416 nm and 547 nm). However, once the MLCT at 434 nm is completely unresolvable due to overlap with absorption from

the oxidized POZ^{+o} moiety at 416 nm peak (≈ 5 min), both of the peaks due to oxidized POZ^{+o} (416 nm and 547 nm) have evolved to nearly half of the respective maximum values achieved during this experiment. Thus, approximately two of the POZ moieties are oxidized concurrently with approximately half of the Cu(I), which implies that there is some driving force for POZ oxidation, but it is smaller than for TPZ. Therefore the oxidation products, [Cu(II)P₂] and POZ^{+o} are likely in a dynamic equilibrium. However, for both species we conclude that the equilibrium for the second electron transfer in CS formation (i.e., donor oxidation) is sufficiently favorable as to be essentially complete; thus, the overall CS formation process is shown in Figure 4.25 and can be schematically represented as:



Figures 4.12, 4.14, 4.16, 4.19, and 4.22, show typical, single-wavelength TA decays after excitation from a 450 or 475 nm laser pulse obtained from the “D-C-A Mixtures” of each

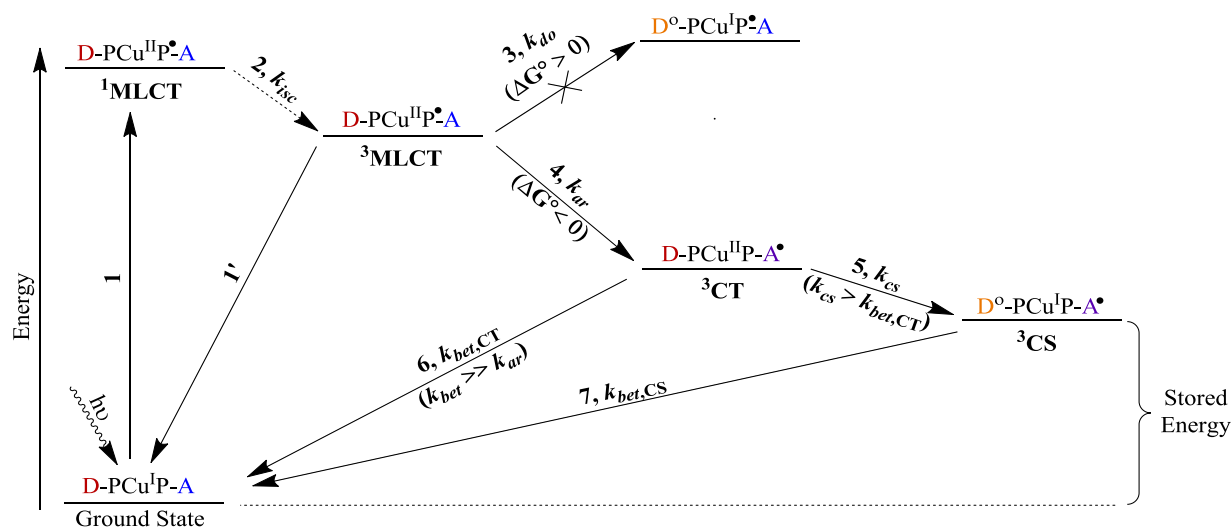


Figure 4.25. Jablonski diagram (not to scale) indicating the different electron-transfer pathways for [Cu(I)(P_D)(P_A)]ⁿ⁺(TPFB)_n after photo-excitation. The acceptor and donor ligands, P_A and P_D, are represented as P-A and D-P, respectively, in the figure to emphasize the mode of bonding. The solid dot (•) and unfilled dot (o) represent the radical electron and hole, respectively.

different complex studied: the resulting equilibrium solution having a composition of ca. 1C-AX: 2D-C-A: 1C-DT. For the “D-C-A Mixture V/T” and the laser experiments on the C-AX diads in Chapter 3, all photo-products seem to appear entirely within the pulse-width of the laser (ca. 7 ns, assuming convolution of the signal with the laser pulse does not obscure a significant initial rise time component); thus, the rate constants for formation of the CT state and CS state for, respectively, C-AX and $[\text{Cu(I)(4OMV)(TPZ)}]^{5+}$ are each $> 1.4 \times 10^8 \text{ s}^{-1}$. Based on these results, it is probable that the photoproducts in each of the “D-C-A Mixtures” are formed on a similar timescale. However, since the spectroelectrochemistry indicates that there is some difference in driving force for oxidation of the TPZ and POZ donors by the $[\text{Cu(II)P}_2]^{2+}$ complex, Marcus theory predicts a change in the rate of CS formation for their respective D-C-A complexes. Although, based on the CV data in Figure 4.4, the change in driving force is probably small enough that the changes in the rate of CS formation will not be significant. Thus, verification of the CS formation kinetics via further TA studies in the absence of a measuring resistor is necessary.

The fit data from each “D-C-A Mixture” is shown in Table 4.1. Recall that the normalized data for the single-wavelength TA decays agree quite well for all of the “D-C-A Mixtures” studied, with the exception of “D-C-A Mixture Q/P” where the magnitude of the noise obscures the results. Therefore, when TA data at various wavelengths (e.g., as in Figure 4.12B) are subjected to the same fit, within experimental error, the same lifetimes are obtained at each wavelength for each respective “D-C-A Mixture” studied. The τ_1 and τ_2 lifetimes obtained from these fits (c.f. Table 4.1) are assigned to the C-AX and D-C-A complexes in each solution, respectively. Based on the ^1H NMR data and studies on the C-AX diads in Chapter 3, it is assumed that τ_1 exists in all of the D-C-A mixtures despite the mono-exponential fits obtained on “D-C-A Mixtures” Q/T, V/P, and Q/P. As mentioned previously, the lack of an initial decay

Table 4.1. The experimental parameters and fit data obtained for the TA decay of each “D-C-A Mixture” solution.

		“D-C-A Mixture”					
		V/T			Q/T	V/P	Q/P
Experimental Parameters	λ_{ex}	450 nm	450 nm	475 nm	450 nm	450 nm	450 nm
	Solvent	Dfb/5% MeOH	Dfb	Dfb	Dfb	Dfb	Dfb
	C-AX, τ	C-AV, 40-45 ns	C-AV, 7 ns	C-AV, 7 ns	C-AQ, 7 ns	C-AQ, 7 ns	C-AQ, 7 ns
	Normalized	No	Yes	Yes	Yes	Yes	Yes
	Measuring Resistor	None	None	None	249 Ω	249 Ω	249 Ω
Fit Parameters	Data from λ used for fit	396 nm	397 nm	396 nm	370 nm	395 nm	540 nm
	R^2	0.99	0.99	0.98	0.97	0.99	0.90
	A_1	0.049	0.55	0.32	-	-	-
	τ_1	45 ns	8.1 ns	10 ns	-	-	-
	A_2	0.051	0.42	0.7	1.0	1.14	0.95
	τ_2	136 ns	96 ns	93 ns	109 ns	65 ns	67 ns
Energy Stored in CS		1.10 V			1.64 V	1.23 V	1.77 V

component due to the C-AX diad in these complexes is likely a result of the increased response time of the instrument when a 249 Ω measuring resistor is used on the PMT.

Considering the data presented in Table 4.1, it seems that the lifetime of the D-C-A complex (τ_2) is dependent on the P_D ligand, which is not unexpected. Since the τ_2 in “D-C-A Mixture Q/T” is similar to the “D-C-A mixture V/T” in dfb, it is likely that the change in the response time of the instrument is not large enough to significantly impact the lifetimes obtained for the D-C-A complexes in the fits. However, the τ_2 lifetimes obtained for the D-C-A complexes incorporating POZ as the donor ligand are significantly shorter than those with the TPZ donor ligand ($P_D = \text{POZ}$, $\tau_2 \approx 65\text{-}70$ ns and $P_D = \text{TPZ}$, $\tau_2 \approx 95\text{-}100$ ns). Based on the spectroelectrochemical data, it is likely that the changes in lifetime are due to the differences in driving force for donor oxidation. As stated above, Marcus theory predicts that the rates of forward electron transfer (k_{et}) and back electron transfer (k_{bet}) are affected when ΔG is changed. When the kinetics of electron transfer (ET) are in the Marcus normal region, the rate of k_{et} is predicted to increase with in-

creased ΔG , and the trend in k_{et} is reversed with increased ΔG in the “Marcus inverted” region. Therefore, it is possible that the smaller ΔG for donor oxidation in complexes with the $P_D = POZ$ changes the rates of k_{et} and k_{bet} relative to the complexes with $P_D = TPZ$. Since information about the CS formation kinetics cannot be inferred from the TA data for the D-C-A complexes with $P_D = POZ$, due to the influence of the measuring resistor, only the kinetics of CS recombination can be evaluated. Therefore, since the ΔG for CS recombination would be larger in the D-C-A's with the POZ donor relative to D-C-A's with the TPZ donor, the observed shorter lifetimes could possibly indicate that back ET from the CS state lies in the Marcus normal region. However a more detailed kinetic analysis is necessary to verify that hypothesis.

As stated above, the difference in driving force between the two donors is small enough that it could have only a minor influence on the rates of forward and back electron transfer, if at all. However, the reduced driving force for POZ oxidation could affect the ET dynamics in a different way. Again, based on the spectroelectrochemistry, it is likely that the $POZ^{+\circ}$ and the $[Cu(II)P_2]$ are in a dynamic equilibrium. Therefore, it is possible that the radical hole in the CS state is distributed between the POZ donor and the copper, e.g. $[POZ^{+\circ}-Cu(I)-4OMV^{3+}]^{5+}$ and $[POZ-Cu(II)-4OMV^{3+}]^{5+}$. If this type of equilibrium occurs in the CS state, it could cause the copper to have some degree of Cu(II) character. Therefore, the hole would be partially distributed onto a metal based orbital (which would likely be subject to larger spin-orbit coupling (SOC) interactions), and the average distance between the radical hole and radical electron would be smaller. Both of these effects could change the degree of mixing between the $^1CS/{}^3CS$ states and facilitate recombination. Furthermore, the geometry of the CS state could be influenced, which, in the MLCT excited states, has been shown to influence the ISC pathway between 1MLCT and 3MLCT states having differing degrees of SOC. All of these changes could, together or separate-

ly, result in a different CS state lifetime. However, it is interesting that the mechanism of CS recombination could be dominated by spin-chemical effects rather than just thermodynamics in D-C-A's with $P_D = POZ$.

Figures 4.13, 4.17, 4.20, and 4.23 show the TA spectra a set time period after 475 nm laser excitation so that $> 90\%$ of the resulting signal is due to the respective D-C-A complexes. These TA spectra are compared with spectra for MX^{n+} and PXZ^{+o} obtained spectroelectrochemically in dfb. Also given in these figures is the simulated spectra obtained by summing equal-concentration spectra of model acceptors MX^{n+} and PXZ^{+o} and scaling that sum to the average TA absorbance between 500 and 610 nm. Despite the differences in lifetime, the agreement between the actual and simulated TA spectra indicates that CS formation is indeed occurring in each of the complexes studied.

Based on preliminary measurements employing $[Ru(bpy)_3]^{2+}$ as an actinometer, the quantum efficiency for CT formation in C-AV is $55 \pm 15\%$ in o-difluorobenzene/1.6% MeOH. These data were used to estimate a Φ_{cs} for the $[Cu(I)(4OMV)(TPZ)]^{5+}(TPFB^-)_5$ D-C-A complex, which was studied in the greatest depth. Comparing the initial intensity values at $t = 0$ from the fits of data in the range between 378 and 403 nm (where only MV^{+} absorbs), correcting for differences in absorbance at the excitation wavelength (discussed in the Results section), and assuming the relative concentrations of C-AV and $[Cu(I)(4OMV)(TPZ)]^{5+}$ are the same as determined by NMR (i.e., 1:2), we estimate the quantum efficiency for CS formation in $[Cu(4OMV)(TPZ)]^{5+}$ also to be $55 \pm 15\%$.

4.4 Conclusion

To our knowledge, these data represent the first demonstration of multi-step, intramolecular, photoinduced CS formation in Cu(I)-based D-C-A triad assemblies where heteroleptic $[\text{Cu(I)P}_A\text{P}_D]^{n+}$ is the sole chromophore present.⁵² In many ways these results mirror the behavior of related $[\text{Ru}(\text{bpy})_3]^{2+}$ triads, but with some important differences. First, while the quantum efficiency for CS formation is relatively large, it is not unity. We speculate that this may have something to do with spin chemistry. The intersystem crossing rate, $^1\text{MLCT} \rightarrow ^3\text{MLCT}$, is about a factor of 10 slower for $[\text{Cu(I)P}_2]^{n+}$ than for $[\text{Ru}(\text{bpy})_3]^{2+}$ and the singlet-triplet energy difference is smaller.^{18,25,53} Because J-T distortion stabilizes the MLCT state with the strongest spin-orbit coupling, which happens to be the lowest energy $^3\text{MLCT}$ state,²⁵⁻²⁷ it is possible that the only CS observable is CS formed with triplet spin multiplicity, at least on the time scale of our current experiments. Preliminary magnetic field studies indicate that there are dramatic magnetic field effects on the CS recombination kinetics, indicating considerable triplet character in the CS radical pair, which will be discussed in more detail in Chapter 5.^{9,54} A complete understanding will require ps time-scale studies of the CS formation kinetics and a detailed magnetic field effect studies, each of which are in progress within our group. Finally, it is highly desirable to study a Cu(I) based system without the complication of having multiple photoactive species simultaneously present in solution. Very recent preliminary studies indicate that, by replacing the 2,9-methyl substituents on the P_A ligand with bulkier substituents in combination with our current P_D ligand, it may be possible to shift the complexation equilibrium such that $[\text{Cu(I)(P}_A)(\text{P}_D)]^{5+}$ is the almost exclusive equilibrium product.^{50,51} This is also under active investigation.

Note: The majority of this chapter was published as a communication in the Journal of the American Chemical Society (DOI: 10.1021/ja3085093). However, significant additions and changes have been made for the preparation of this thesis.

References

- (1) Wasielewski, M. R. *J. Org. Chem.* **2006**, *71*, 5051–5066.
- (2) Gust, D.; Moore, T. A. *Science* **1989**, *244*, 35–41.
- (3) Kalyanasundaram, K. *Photochemistry of polypyridine and porphyrin complexes*; Academic Press: London; San Diego, 1992.
- (4) Schanze, K. S.; Walters, K. A. In *Organic and Inorganic Photochemistry*; Ramamurthy, V.; Schanze, K. S., Eds.; Molecular and Supramolecular Photochemistry; Marcel Dekker: New York, 1998; pp. 75–127.
- (5) Armaroli, N. *Photochem. Photobiol. Sci.* **2003**, *2*, 73–87.
- (6) Scandola, F.; Chiorboli, C.; Indelli, M. T.; Rampi, M. T. In *Biological and Artificial Supramolecular Systems*; Electron Transfer in Chemistry; Wiley: Weinheim, 2003; pp. 337–403.
- (7) Gust, D.; Moore, T. A.; Moore, A. L. *Acc. Chem. Res.* **2001**, *34*, 40–48.
- (8) Weber, J. M.; Rawls, M. T.; MacKenzie, V. J.; Limoges, B. R.; Elliott, C. M. *J. Am. Chem. Soc.* **2007**, *129*, 313–320.
- (9) Klumpp, T.; Linsenmann, M.; Larson, S. L.; Limoges, B. R.; Bürssner, D.; Krissinel, E. B.; Elliott, C. M.; Steiner, U. E. *J. Am. Chem. Soc.* **1999**, *121*, 1076–1087.
- (10) Larson, S. L.; Elliott, C. M.; Kelley, D. F. *J. Phys. Chem.* **1995**, *99*, 6530–6539.
- (11) Larson, S. L.; Cooley, L. F.; Elliott, C. M.; Kelley, D. F. *J. Am. Chem. Soc.* **1992**, *114*, 9504–9509.
- (12) Cooley, L. F.; Larson, S. L.; Elliott, C. M.; Kelley, D. F. *J. Phys. Chem.* **1991**, *95*, 10694–10700.
- (13) Danielson, E.; Elliott, C. M.; Merkert, J. W.; Meyer, T. J. *J. Am. Chem. Soc.* **1987**, *109*, 2519–20.
- (14) Rawls, M. T.; Kollmannsberger, G.; Elliott, C. M.; Steiner, U. E. *J. Phys. Chem. A* **2007**, *111*, 3485–3496.
- (15) Scaltrito, D. V.; Thompson, D. W.; O’Callaghan, J. A.; Meyer, G. J. *Coord. Chem. Rev.* **2000**, *208*, 243–266.
- (16) Ruthkosky, M.; Kelly, C. A.; Castellano, F. N.; Meyer, G. J. *Coord. Chem. Rev.* **1998**, *171*, 309–322.
- (17) Lavie-Cambot, A.; Cantuel, M.; Leydet, Y.; Jonusauskas, G.; Bassani, D. M.; McClenaghan, N. D. *Coord. Chem. Rev.* **2008**, *252*, 2572–2584.
- (18) Armaroli, N. *Chem. Soc. Rev.* **2001**, *30*, 113–124.
- (19) Cunningham, K. L.; Hecker, C. R.; McMillin, D. R. *Inorg. Chim. Acta* **1996**, *242*, 143–7.
- (20) Cuttell, D. G.; Kuang, S.-M.; Fanwick, P. E.; McMillin, D. R.; Walton, R. A. *J. Am. Chem. Soc.* **2002**, *124*, 6–7.
- (21) Everly, R. M.; McMillin, D. R. *J. Phys. Chem.* **1991**, *95*, 9071–9075.
- (22) Blaskie, M. W.; McMillin, D. R. *Inorg. Chem.* **1980**, *19*, 3519–3522.
- (23) Ichinaga, A. K.; Kirchoff, J. R.; McMillin, D. R.; Dietrich-Buchecker, C. O.; Marnot, P. A.; Sauvage, J. P. *Inorg. Chem.* **1987**, *26*, 4290–4292.
- (24) Ruthkosky, M.; Kelly, C. A.; Zaros, M. C.; Meyer, G. J. *J. Am. Chem. Soc.* **1997**, *119*, 12004–12005.
- (25) Shaw, G. B.; Grant, C. D.; Shirota, H.; Castner Jr., E. W.; Meyer, G. J.; Chen, L. X. *J. Am. Chem. Soc.* **2007**, *129*, 2147.
- (26) Siddique, Z. A.; Yamamoto, Y.; Ohno, T.; Nozaki, K. *Inorg. Chem.* **2003**, *42*, 6366–6378.

- (27) Gothard, N. A.; Mara, M. W.; Huang, J.; Szarko, J. M.; Rolczynski, B.; Lockard, J. V.; Chen, L. X. *J. Phys. Chem. A* **2012**, *116*, 1984–1992.
- (28) Palmer, C. E. A.; McMillin, D. R. *Inorg. Chem.* **1987**, *26*, 3837–3840.
- (29) Palmer, C. E. A.; McMillin, D. R.; Kirmaier, C.; Holton, D. *Inorg. Chem.* **1987**, *26*, 3167–3170.
- (30) Everly, R. M.; Ziessel, R.; Suffert, J.; McMillin, D. R. *Inorg. Chem.* **1991**, *30*, 559–61.
- (31) Cunningham, K. L.; McMillin, D. R. *Inorg. Chem.* **1998**, *37*, 4114–4119.
- (32) Eggleston, M. K.; McMillin, D. R.; Koenig, K. S.; Pallenberg, A. J. *Inorg. Chem.* **1997**, *36*, 172–176.
- (33) Gushurst, A. K. I.; McMillin, D. R.; Dietrich-Buchecker, C. O.; Sauvage, J. P. *Inorg. Chem.* **1989**, *28*, 4070–2.
- (34) Cunningham, C. T.; Cunningham, K. L. H.; Michalec, J. F.; McMillin, D. R. *Inorg. Chem.* **1999**, *38*, 4388–4392.
- (35) Megiatto, J. D.; Schuster, D. I.; Abwandner, S.; de Miguel, G.; Guldi, D. M. *J. Am. Chem. Soc.* **2010**, *132*, 3847–3861.
- (36) Jakob, M.; Berg, A.; Levanon, H.; Schuster, D. I.; Megiatto, J. D. *J. Phys. Chem. C* **2011**, *115*, 24555–24563.
- (37) Jakob, M.; Berg, A.; Rubin, R.; Levanon, H.; Li, K.; Schuster, D. I. *J. Phys. Chem. A* **2009**, *113*, 5846–5854.
- (38) Flamigni, L.; Talarico, A. M.; Chambron, J.-C.; Heitz, V.; Linke, M.; Fujita, N.; Sauvage, J.-P. *Chem.-Eur. J.* **2004**, *10*, 2689–2699.
- (27) Several reports of systems have appeared (Ref 35-38, 40-46) in which a $[\text{Cu}(\text{I})\text{P}_2]^+$ catenane, a Zn^{2+} porphyrin and an electron acceptor, such as a fullerene, have all been incorporated and which undergo a complex set of multi-step, photo-induced, energy and/or electron transfers, some of which involve $[\text{Cu}(\text{I})\text{P}_2]^{+*}$. However, in their system the Zn^{2+} porphyrin is the primary light absorbing chromophore.
- (40) Megiatto, J. D.; Schuster, D. I.; de Miguel, G.; Wolfrum, S.; Guldi, D. M. *Chem. Mater.* **2012**, *24*, 2472–2485.
- (41) Megiatto, J. D.; Li, K.; Schuster, D. I.; Palkar, A.; Herranz, M. A.; Echegoyen, L.; Abwandner, S.; de Miguel, G.; Guldi, D. M. *J. Phys. Chem. B* **2010**, *114*, 14408–14419.
- (42) Schuster, D. I.; Li, K.; Guldi, D. M. *C.R. Chim.* **2006**, *9*, 892–908.
- (43) Li, K.; Bracher, P. J.; Guldi, D. M.; Herranz, M. Á.; Echegoyen, L.; Schuster, D. I. *J. Am. Chem. Soc.* **2004**, *126*, 9156–9157.
- (44) Li, K.; Schuster, D. I.; Guldi, D. M.; Herranz, M. Á.; Echegoyen, L. *J. Am. Chem. Soc.* **2004**, *126*, 3388–3389.
- (45) Linke, M.; Chambron, J.-C.; Heitz, V.; Sauvage, J.-P.; Encinas, S.; Barigelletti, F.; Flamigni, L. *J. Am. Chem. Soc.* **2000**, *122*, 11834–11844.
- (46) Chambron, J. C.; Harriman, A.; Heitz, V.; Sauvage, J. P. *J. Am. Chem. Soc.* **1993**, *115*, 7419–7425.
- (47) Armaroli, N.; Accorsi, G.; Bergamini, G.; Ceroni, P.; Holler, M.; Moudam, O.; Duhayon, C.; Delavaux-Nicot, B.; Nierengarten, J.-F. *Inorg. Chim. Acta* **2007**, *360*, 1032–1042.
- (48) Ruthkosky, M.; Castellano, F. N.; Meyer, G. J. *Inorg. Chem.* **1996**, *35*, 6406–6412.
- (49) Hebký, J.; Kejha, J.; Karasek, M. *Collect. Czech. Chem. Commun.* **1961**, *26*, 1559.
- (50) Kalsani, V.; Schmittel, M.; Listorti, A.; Gianluca, A.; Armaroli, N. *Inorg. Chem.* **2006**, *45*, 2061–2067.
- (51) Schmittel, M.; Michel, C.; Liu, S.-X.; Schildbach, D.; Fenske, D. *Eur. J. Inorg. Chem.*

- 2001**, 1155–1166.
- (52) We are aware, through personal communication, that a related Cu(I)-based D-C-A triad having different donors and acceptor moieties is under study in the laboratory of Fabrice Odobel, Université de Nantes, CNRS. Results from these systems will be the subject of a future publication.
- (53) Chen, L. X.; Shaw, G. B.; Novozhilova, I.; Liu, T.; Jennings, G.; Attenkofer, K.; Meyer, G. J.; Coppens, P. *J. Am. Chem. Soc.* **2003**, *125*, 7022–7034.
- (54) Rawls, M. T.; Kollmannsberger, G.; Elliott, C. M.; Steiner, U. E. *J. Phys. Chem. A.* **2007**, *111*, 3485–3496.

Chapter 5

The Spin-Chemical Control of the Kinetics of the Multi-Step, Photo-Induced Charge Separation in Cu(I) bis-Phenanthroline Based Donor-Chromophore-Acceptor Triads

5.1 Introduction

As previously discussed in some detail, trisbipyridineruthenium(II), [Ru(II)L₃], has been regularly investigated as a chromophore for photoinduced charge separation projects mainly due to its favorable photophysical, electrochemical and coordination properties.¹ However, advances in the design and preparation of bisphenanthrolinecopper(I), [Cu(I)P₂], complexes have introduced a viable, new player in the photoinduced charge separation game. Like the [Ru(II)L₃] analogs, bisphenanthrolinecopper(I) complexes exhibit strong MLCT transitions in the visible and the resulting excited state is a thermodynamically powerful reductant. Therefore, the [Cu(I)P₂]^{*} has demonstrated similar oxidative quenching behavior as [Ru(II)L₃]^{*}.¹⁻⁴ Moreover, copper is cheap and abundant, making it more advantageous for real world applications than ruthenium and the other second and third row transition metal complexes (e.g., Os, Pt, Re, Ir) that have been used for photoinduced charge separation schemes.

The chemistry of [Cu(I)P₂] can be much more complicated than that of [Ru(II)L₃].¹⁻⁴ The multifarious behavior of [Cu(I)P₂] complexes is mainly due to the multitude of consequences that result from the fact that Cu(I) is a first-row, d¹⁰ transition metal. Therefore, ligand lability makes isolation and purification using commonly practiced techniques unreasonable for [Cu(I)P₂] complexes.^{1,5-9} Furthermore, upon photo-excitation to the d⁹, [Cu(II)(P^{*})(P)]^{*} MLCT state, rapid Jahn-Teller (J-T) distortion occurs that plays an important role in many of its photo-

physical properties.^{1,5-9} The effect of J-T distortion on the excited state chemistry has been repeatedly reviewed throughout this thesis, so only the issues most relevant to this chapter will be discussed.

At this point, the $[\text{Cu(II)(P}^{\bullet}\text{)}(\text{P})]^*$ MLCT excited state is relatively well understood with regards to the timescale of J-T distortion and the effect of the geometric change on the rates of electron and energy transfer within the MLCT manifold.¹⁰⁻²⁴ The mechanism of forward electron transfer from the MLCT to the charge transfer (CT) and/or charge separated (CS) states have received less attention, but has been well described by several groups.^{4,25-42} In the $[\text{Cu(I)P}_2]$ D-C-A complexes described in Chapter 4, the photo-induced charge separation process occurs via a very similar mechanism to the $[\text{Ru(II)L}_3]$ analogs studied by our group in the past.⁴³⁻⁴⁶ However, there were some important differences such as the smaller quantum efficiency calculated for $[\text{Cu(4OMV)(TPZ)}]^{+5}(\text{TPFB}^-)_5$ ($\Phi_{\text{cs}} \approx 55 \pm 15\%$) compared to the $[\text{Ru(II)L}_3]$ D-C-A's, which typically have $\Phi_{\text{cs}} \approx 1$. Furthermore, the differences in lifetime between $[\text{Cu(I)P}_2]$ D-C-A's incorporating TPZ and POZ donor ligands could be a result of changes in the charge separation mechanism due to the equilibrium between the oxidized $\text{POZ}^{+\circ}$ and Cu(II) . It is possible that the differences in quantum efficiency and lifetimes presented above are due to differences in spin chemistry between the $[\text{Cu(I)P}_2]$ and $[\text{Ru(II)L}_3]$ D-C-A's. However, the spin chemistry of $[\text{Cu(I)P}_2]$ D-C-A's has been relatively unexplored in the literature.^{30,31} Therefore, the focus of this chapter is on the elucidation of the spin-chemical effects in $[\text{Cu(I)P}_2]$ D-C-A complexes discussed in Chapter 4, and shown again in Figure 5.1.

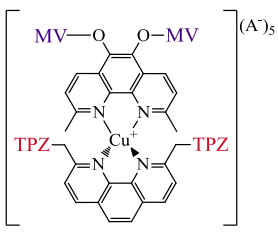
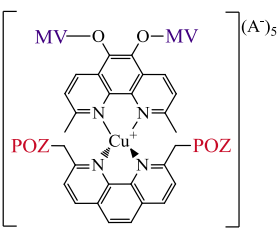
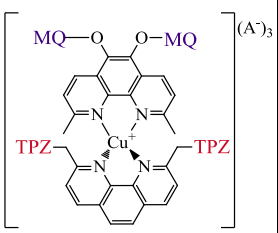
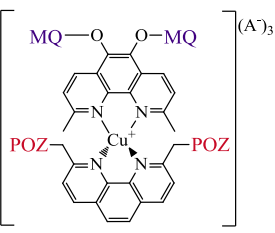
Complex				
Name	[Cu(4OMV)(TPZ)] ⁵⁺ (A ⁻) ₅	[Cu(4OMV)(POZ)] ⁵⁺ (A ⁻) ₅	[Cu(4OMQ)(TPZ)] ³⁺ (A ⁻) ₃	[Cu(4OMQ)(POZ)] ³⁺ (A ⁻) ₃
Energy Stored in CS	1.10 V	1.23 V	1.64 V	1.77 V

Figure 5.1. D-C-A complexes of [Cu(I)P_AP_D]ⁿ⁺ where P_A=acceptor appended 1,10-phenanthroline and P_D= donor appended 1,10-phenanthroline. Also shown is the theoretical amount of energy able to be stored in the CS of each D-C-A based on the ground state redox potentials of the donor and acceptor moieties in the homoleptic C-AX and C-DX complexes.

As stated previously, the spin chemistry of [Ru(II)L₃] is relatively well understood.⁴⁷⁻⁵⁰ Since the magnetic field effects (MFE's) in [Ru(II)L₃] D-C-A's has already been discussed several times in some depth, only a brief description will be given here. For further detail, refer to the Introduction (Chapter 1) and Chapter 3. As mentioned previously, the di-radical CS state is dominated by triplet character, making radical electron-hole recombination to the singlet ground state a spin-forbidden process.^{47,48,50} However, since the di-radical ³CS state of [Ru(II)L₃] D-C-A's is composed of “normal” organic radicals, the ¹CS and ³CS states are mixed via isotropic hyperfine coupling (IHC) interactions enabling facile intersystem crossing and a rapid, spin-allowed recombination pathway from the ³CS.^{47,48,50}

Application of a relatively small magnetic field was found to decrease the ¹CS and ³CS mixing in [Ru(II)L₃] D-C-A's and modulate k_{isc} , which increased the average ³CS lifetime ten-fold ($\tau_{cs} \approx 2 \mu s$, 0.5 T).^{47,48,50} The so-called *relaxation mechanism* proposed by Hayashi and Nagakura shown again in Figure 5.2, was used to explain the effect on the magnetic field of the CS decay in [Ru(II)L₃] D-C-A's.⁵¹ In this relaxation mechanism it is assumed that the spins are mixed via coherent isotropic hyperfine coupling interactions as discussed above. In this mechanism, Zeeman splitting of the ³CS states is induced by the applied magnetic field which causes

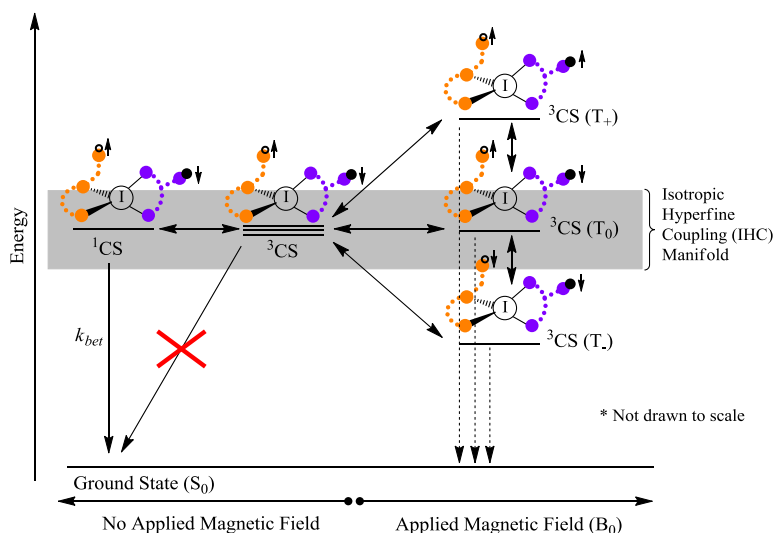


Figure 5.2. Radical pair relaxation mechanism proposed by Hayashi and Nagakura depicting the Zeeman splitting of the degenerate ^3CS energy levels in an applied magnetic field. Note that P_D and P_A are shown with only one donor and acceptor moiety for clarity. The actual P_D and P_A structures are shown in Figure 5.1. The dotted vertical arrows from the T_+ , T_- , and T_0 states represent the contributions of non-coherent spin-relaxation processes to the general mechanism. Adapted from Refs 47, 50, and 51.

the $^3\text{CS}(\text{T}_+)$ and $^3\text{CS}(\text{T}_-)$ states to increase/decrease in energy. At some magnetic field, $B_0 \approx 2\text{-}3$ mT for $[\text{Ru}(\text{II})\text{L}_3]$ D-C-A's,⁴⁷ the $^3\text{CS}(\text{T}_+)$ and $^3\text{CS}(\text{T}_-)$ states exceed the influence of the IHC manifold. Therefore, the changes in the T_+ and T_- energy significantly affect the IHC between the ^1CS and ^3CS states, and therefore, k_{isc} and k_{bet} change with increasing magnetic field.^{47,48,50} A characteristic feature of this mechanism is the saturation of magnetic field effects (MFE's) on the k_{isc} and k_{bet} , which often occurs below 50 mT.⁵² The Zeeman splitting is manifested in the transient absorption (TA) decay profile for the pure $[\text{Ru}(\text{II})\text{L}_3]$ D-C-A solution as a change from mono-exponential decay at zero field to bi-exponential decay in an applied magnetic field, having a “fast” field-independent decay component and a “slow” field-dependent decay component. The “fast,” field-independent decay component would account for $\approx 1/3$ of the overall decay, which is determined by the ratio of the $A_{\text{slow}}:A_{\text{fast}}$ ($A_s:A_f$) values obtained from the fit of CS decay ($A_{\text{slow}} = A_s/(A_s+A_f) \approx 1/3$; $^3\text{CS}(\text{T}_0)$). The “slow,” field-dependent decay component would then account for $\approx 2/3$ of the overall decay ($A_f = A_f/(A_s+A_f) \approx 2/3$; $^3\text{CS}(\text{T}_-$ and $\text{T}_+)$).^{50,53} However, as the applied magnetic field continues to increase in magnitude, incoherent, magnetic-field-

independent processes start to affect the rate of CS recombination such as assisted spin-forbidden recombination via direct spin-orbit coupling (SOC), anisotropic hyperfine interactions (AHFI), electron spin-spin dipolar interaction (ESDI), g-tensor anisotropy (GTA), and spin-rotational interaction (SRI).^{47,48,50} The relative contributions of each of these incoherent processes requires detailed kinetic evaluation based on the spin-chemical behavior in the presence of an applied magnetic field of varying field strengths.

To a first approximation, [Ru(II)L₃] and [Cu(I)P₂] should have similar spin chemistry. If [Cu(I)P₂] D-C-A complexes are similarly affected by a magnetic field, then the ³CS lifetime is also expected to increase in an applied magnetic field. However, as was suggested by the behavior of the C-AV diads presented in Chapter 3, the MFE's for [Cu(I)P₂] D-C-A's may be more complicated than for the [Ru(II)L₃] analogs due to the effects of J-T distortion on the ³MLCT state, which is also susceptible to Zeeman splitting. As previously discussed, J-T distortion in [Cu(dmp)₂]⁺ de-stabilizes the ¹MLCT (MO with the smallest amount of SOC) and stabilizes the ³MLCT (MO with the largest SOC): thus, the thermally equilibrated lowest excited ¹MLCT and ³MLCT states in [Cu(I)P₂] complexes are separated by $\approx 1800\text{-}2000\text{ cm}^{-1}$.^{5,10,11,14,54-57} At zero applied field, the ³MLCT has a greater population and is generally regarded as the state from which the majority of relevant ET processes proceed, which is analogous to [Ru(II)L₃] complexes.^{4,41,57,58} When in the presence of a magnetic field, Zeeman splitting of the ³MLCT state could alter k_{isc} between the ¹MLCT/³MLCT states, influencing their relative populations, and therefore, the relative populations of the ¹CS/³CS states. Increased ¹CS state population would facilitate electron-hole recombination to the ground state, thereby decreasing the observed Φ_{cs} relative to the absolute Φ_{cs} . Finally, in [Cu(I)P₂] complexes, there is a manifold of ¹MLCT/³MLCT states having differing degrees of SOC, which also enables singlet/triplet state mixing. SOC interac-

tions are not predicted to influence the spin-dynamics in the CS state since the radical electron and radical hole are predicted to reside on ligand-based orbitals. However, Zeeman splitting of higher lying $^3\text{MLCT}$ states may enable mixing between states in the presence of a magnetic field that could not occur at zero applied field which could complicate the interpretation of the spin-dynamics. Therefore, the mechanism of charge separation could change when photo-excitation occurs in the presence of a magnetic field. To my knowledge, these possibilities have not yet been addressed in the literature for $[\text{Cu(I)P}_2]$ D-C-A complexes, but are clearly relevant to understanding the CS and recombination processes.

To that end, we have prepared the four Cu(I)-based D-C-A triads depicted in Figure 5.1 for study. Recall from the data presented in Chapter 4, that CS state formation of a has been verified for each of the $[\text{Cu(I)P}_2]$ D-C-A complexes using spectroelectrochemical (SE) and nanosecond transient absorption (TA) spectroscopic techniques. ^1H NMR spectroscopy indicated that a solution containing an equimolar mixture of D, Cu(I), and A in deuterated 1,2-difluorobenzene (dfb)/15% MeOH spontaneously forms a nearly statistical mixture of products, 1 C-AX: 2 mol D-C-A: 1 mol C-DX. Therefore, all spectroscopic measurements are performed on a mixture of all three products, warranting the title “D-C-A Mixture.” However, the C-DX products were found to be photo-inactive due to the inability of the $[\text{Cu(II)(P}^*)(\text{P})]^*$ MLCT excited state to oxidize the donor moiety. As discussed in Chapters 3 and 4, the C-AX acceptors are photo-active and have measurable, solvent-dependent CT lifetimes. The CS decay of the “D-C-A Mixture V/T” was found to be bi-exponential and the short lifetime component was found to be the same as the C-AV, CT state in each different solvent system studied. Therefore, the short lifetime ($\tau \approx 7$ ns in dfb) of the CS decay is attributed to the C-AV diad present in the “D-C-A Mixture V/T.” The long lifetime ($\tau \approx 95$ ns in dfb) is then assigned to the lifetime of the CS state for the D-C-A,

which was also found to be solvent dependent, but to a lesser degree. Although the other “D-C-A Mixtures” were found to be best described by mono-exponential fits, it is assumed that they were also bi-exponential for two reasons: (1) evidence suggesting the presence of C-AX diad in the “D-C-A Mixture,” and (2) the fact that, due to a weaker TA signal, it was necessary to use a measuring resistor across the photomultiplier to acquire those data (thus increasing the instrument response time), which likely caused the short lifetime component, due to the C-AX diad, to be unresolvable.

Based on the data presented in Chapter 4, the formation of a CS state in the $[\text{Cu(I)P}_2]$ D-C-A’s likely occurs in a similar manner as the $[\text{Ru(II)L}_3]$ analogs. The charge separation mechanism is better understood for the D-C-A’s with the TPZ rather than POZ donors due to the possible equilibrium that occurs between the oxidized donor, $\text{POZ}^{+\circ}$ and Cu(II) , indicated by spectroelectrochemical studies. The similarities between all of the $[\text{Cu(I)P}_2]$ D-C-A’s to the $[\text{Ru(II)L}_3]$ systems suggest it is likely that the Cu(I) systems may exhibit similar spin-chemical effects as the $[\text{Ru(II)L}_3]$ analogs as well; however, with a significantly greater degree of complexity.

5.2 Results

Studies on $[\text{Cu(I)(4OMV)(TPZ)]^{5+}(\text{TPFB}^-)_5$: “D-C-A Mixture V/T”

The transient absorption (TA) laser experiments shown in Figure 5.3 were performed to study the effect of an applied magnetic field (or Magnetic Field Effect = MFE) on the CS recombination kinetics of the $[\text{Cu(I)(4OMV}^{3+})(\text{TPZ}^{+\circ})]^{5+}(\text{TPFB}^-)_5$ D-C-A complex using the altered TA laser set-up detailed in the Experimental section. Recall, that a solution containing equimolar amounts of P_A , P_D , and $[\text{Cu(I)(ACN)}_4]^+(\text{BF}_4^-)$ is called a “D-C-A Mixture,” and in this case “D-

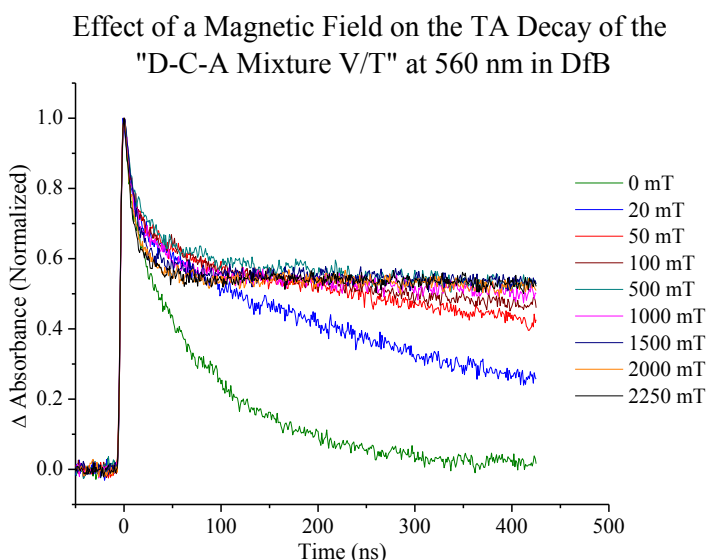


Figure 5.3. Normalized TA decay of the “D-C-A Mixture V/T” at several applied magnetic fields (mT) at 560 nm in dfb ($\lambda_{\text{ex}} = 450 \text{ nm}$). For clarity, not all of the data in Table 5.1 is shown in this figure.

ture” reported. Refer to Chapter 4, Figure 4.11 for a representation of the typical amount of change that occurs in the spectrum over the course of a normal experiment.

The CS decay with respect to applied magnetic field was studied in several different solvent compositions (dfb/X% MeOH, where X = 0-5 %) at different wavelengths, and with different excitation wavelengths. Figure 5.3 depicts a typical set of normalized single wavelength decay curves obtained at 560 nm in 1,2-difluorobenzene (dfb) on a 50 ns timescales. The concentration of the “D-C-A Mixture V/T” solution was $5.3 \times 10^{-5} \text{ M}$, which results in a ground-state absorbance of 0.66 at $\lambda_{\text{max}} = 450 \text{ nm}$ in dfb (which is the pump wavelength for this experiment). These data were normalized so the changes in lifetime were not obscured by the changes in initial intensity that occur with applied magnetic field. These data were also collected on long timescales (e.g. 100 ns-2 μs /division in the oscilloscope, depending on field strength) and fit in Origin in order to determine the lifetime of the slowest decay component and the value for the

C-A Mixture V/T” because $P_A = 4\text{OMV}$ and $P_D = \text{TPZ}$.^m As was done for the TA studies at zero field, the ground state absorption spectrum (UV-vis) for each prepared sample was generally obtained before and after each set of experiments to determine the extent of sample degradation. This was done for each “D-C-A Mix-

^m For all of the “D-C-A Mixtures X_A/X_D ,” the two letter designation indicates the P_A and P_D ligand (in that order) used for that specific mixture: $P_A = 4\text{OMV}$ or 4OMQ , so the first letter will be V or Q, $P_D = \text{TPZ}$ or POZ so the second letter will be either T or P.

baseline (y_0). In these experiments, the long timescale data was obtained on a timescale over which the absorbance had decayed to $\leq 15\%$ of its initial value. The values obtained from the fit for the lifetime of the slow component and the baseline were then plugged into the fit for the short timescale data and held constant, while the other fitting parameters were allowed to vary with the exception of the fastest lifetime component. As previously determined, the fastest lifetime component is the lifetime of the C-AV diad present in the “D-C-A Mixture V/T”. Therefore the fastest lifetime component was held constant at a value which adequately fit the curvature of the decay. Within experimental error, the lifetime of the fastest decay component was near the previously determined values for the C-AV diad lifetimes for every magnetic field strength studied. This fitting procedure was used to obtain the lifetime (τ values) and intensity values (A values) given in Table 5.1. The lifetime of the slowest decay component often varies on a sample-to-sample basis because of extreme oxygen sensitivity: paramagnetic oxygen catalyzes spin relaxation, which facilitates CS decay. Very small amounts of oxygen (ppm) can impart significant changes in lifetime. However, the fitting values presented in Table 5.1 are representative of the values obtained for the “D-C-A Mixture V/T” in dfb solvent when prepared in a glovebox with an oxygen content of ≤ 1 ppm.

Regarding the data presented in Figure 5.3 and Table 5.1, the rate of ^3CS decay is clearly retarded in the presence of an applied magnetic field. More specifically, a slow decay component is present and its lifetime increases to a maximum value of ca. $6\ \mu\text{s}$ at 1000 mT then decreases to ca. $5\ \mu\text{s}$ and stays essentially constant. Based on the general Zeeman splitting scheme for normal organic radical species discussed in the Introduction section, it is expected that the decay will change from mono-exponential to bi-exponential character in an applied magnetic field. However, since the observed absorption is already bi-exponential at zero field

Table 5.1. The values obtained by fitting several CS decay curves at 560 nm for the “D-C-A Mixture V/T” in dfb ($\lambda_{\text{ex}} = 450 \text{ nm}$), which are shown in Figure 5.3. The error shown for the lifetime data is the error in the fit as calculated by the “Advanced Fitting Tool” in Origin. All of the errors are quoted from the fit of the data taken on a short timescale (50 ns) with the exception of τ_3 , which was held constant during that fit. Therefore, the error quoted for τ_3 is from fits of the data taken on the longer timescales (timescale dependent on field strength/lifetime).

Field Strength (mT)	Fit Values						
	R^2	A_1	τ_1	A_2	τ_2	A_3	τ_3
0	0.994	0.0378	9.5 ns	0.0933	94 ± 0 ns	-	-
20	0.988	0.0272	6.0 ns	0.0149	33 ± 4.2 ns	0.0720	435 ± 11 ns
50	0.975	0.0340	7.5 ns	0.0165	50 ± 3.7 ns	0.0707	1190 ± 26 ns
100	0.963	0.0445	8.5 ns	0.0202	77 ± 4.4 ns	0.0735	2297 ± 47 ns
250	0.950	0.0434	10 ns	0.0174	95 ± 6.1 ns	0.0659	4049 ± 48 ns
500	0.937	0.0388	11 ns	0.0179	79 ± 5.4 ns	0.0630	5052 ± 73 ns
750	0.916	0.0399	7.5 ns	0.0235	48 ± 3 ns	0.0603	4879 ± 67 ns
1000	0.910	0.0373	4.0 ns	0.0304	36 ± 1.8 ns	0.0707	5814 ± 86 ns
1250	0.887	0.0382	5.5 ns	0.0298	23 ± 1.9 ns	0.0630	5213 ± 68 ns
1500	0.849	0.0354	9.0 ns	0.0222	18 ± 4.7 ns	0.0629	5127 ± 79 ns
2000	0.812	0.0530	10.5 ns	0.00381	18 ± 9.0 ns	0.0601	4815 ± 58 ns
2250	0.704	0.0584	9.0 ns	-	-	0.0649	4916 ± 57 ns

due to the presence of two absorbing species, the CT state of the C-AV⁹⁺ diad and the CS state of the [Cu(I)(4OMV³⁺)(TPZ⁺)⁵⁺(TPFB⁻)₅ D-C-A triad, it is expected that the decay will go from bi-exponential at zero applied field to tri-exponential in an applied magnetic field, which is generally observed once the field has reached ca. 20 mT. As the field increases from 0-20 mT, the fits of the data are essentially bi-exponential. The existence of the second decay component (τ_2) is questionable until after 20 mT, when it is able to be fit and then the lifetime increases with increasing field strength from ca. 33 ns to 95 ns at its maximum value in a field of 250 mT. The lifetime at its maximum value (ca. 95 ns) is almost identical to the lifetime of the D-C-A at zero applied field. This may have important implications about the way the ³CS states are splitting in the magnetic field and the rates of intersystem crossing between each ³CS state (T_0 , T_+ , T_-) and the ¹CT state. As the field increases further from 250 mT, the lifetime of the second decay component decreases again until around 1500-2250 mT where the data becomes increasingly harder

to fit with a tri-exponential (as indicated by the R^2 values) and eventually must be fit with a bi-exponential decay by 2250 mT. In any given field, the lifetime of the fastest decay component (τ_1) reflects a value that would be expected for the C-AV diad based on the data presented in Chapter 3, within experimental error.

The ratio of A values are often used to determine the percentage of each decay component which constitute the overall decay. However, since the observed absorption results from a mixture of the CT state of the C-AV⁹⁺ diad and the CS state of the [Cu(I)(4OMV³⁺)(TPZ^{+o})]⁵⁺(TPFB⁻)₅ D-C-A triad, both species having different ground state absorptions at the pump wavelength ($\lambda_{\text{ex}} = 450$ nm) the interpretation of these data can be difficult. If the ground-state absorption of both species (C-AV diad and [Cu(I)(4OMV)(TPZ)]⁵⁺(TPFB⁻)₅ triad) and the quantum yields of the CT and CS states were identical at 450 nm, then the A₁:A₂ ratio at 560 nm in the absence of an applied field should be ca. 1:4, which is not the A₁:A₂ ratio obtained from the zero field data presented in Table 5.1. Interpretation of the ratios of A values is further complicated by the Zeeman splitting of the ³CS states induced by a magnetic field and the response function of the laser. Therefore, the ratios of A values are not considered to be exceedingly informative at this time. A more in-depth interpretation of the changes in the ratios of A values may be afforded after a more thorough investigation of the spin chemical dynamics by our collaborator, Dr. Ulrich Steiner at the Universität Konstanz in Konstanz, Germany.

The MFE on the CS decay kinetics of the [Cu(I)(4OMV³⁺)(TPZ^{+o})]⁵⁺(TPFB⁻)₅ D-C-A triad in the “D-C-A Mixture V/T” was also studied in dfb/2.3% MeOH (Figure 5.4) and dfb/5% MeOH (Figure 5.5). These data were taken using at different excitation wavelengths ($\lambda_{\text{ex}} = 450$ and 475 nm, respectively) and monitored at different wavelengths (560 and 396 nm, respectively). This was done because the experiments on the sample in dfb/5% MeOH were performed

after the laser was repaired at which time the laser pulse was more stable at 475 nm than at 450 nm at that time. Also, as discussed in Chapter 4, the absorption due to the D-C-A is less intense when the pump beam is set at 475 nm than at 450 nm; therefore, the D-C-A was monitored at 396 nm because that is the region at which there is the greatest amount of absorption for the CS of the D-C-A (See Chapter 4, Figures 4.13 and 4.14). At first glance, changing the pump beam from 450 nm to 475 nm appears to have a dramatic effect on the lifetime of the D-C-A due to the decreased absorbance of the D-C-A relative to C-AV at 475 nm, as shown in Figure 5.6. However,

as shown in Table 5.2, when fitting the TA curves obtained from samples in similar solvent compositions, the same two lifetimes are afforded from the fits, within

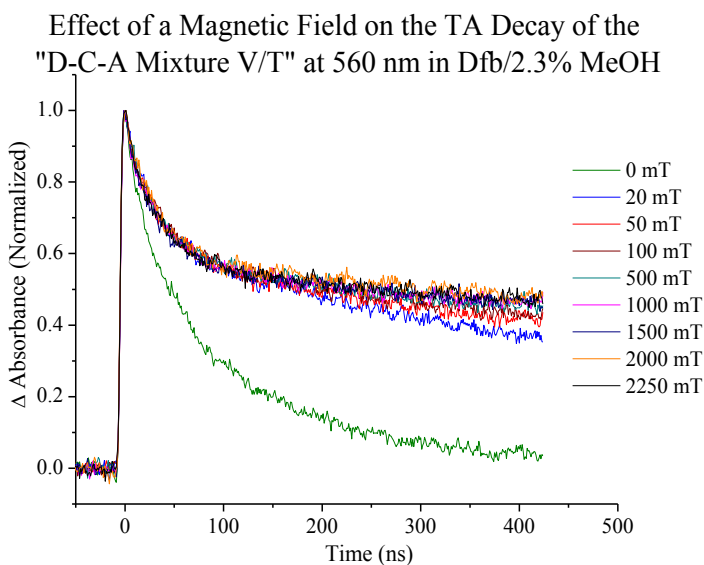


Figure 5.4. Normalized TA decay of a $4.1 \times 10^{-5} M$ "D-C-A Mixture V/T" solution in several applied magnetic fields (mT) at 560 nm in dfb/2.3% MeOH ($\lambda_{\text{ex}} = 450 \text{ nm}$). For clarity, not all of the data that was fit (Table 5.3) is shown.

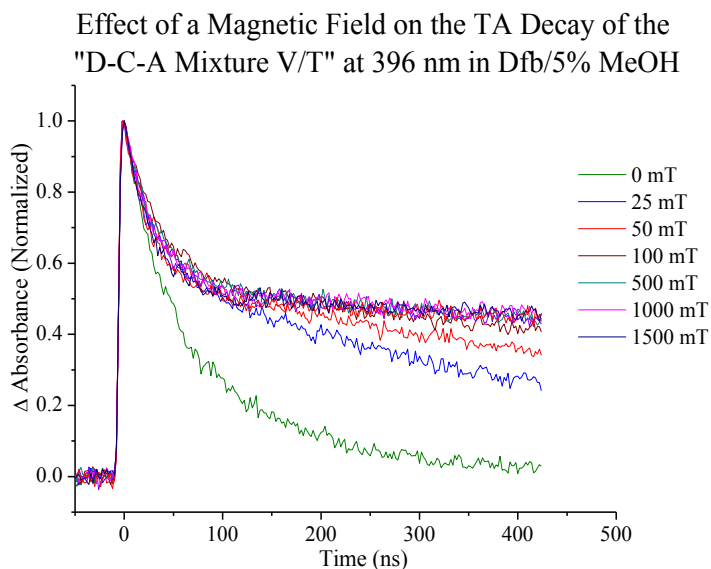


Figure 5.5. Normalized TA decay of a $3.5 \times 10^{-5} M$ "D-C-A Mixture V/T" solution in several applied magnetic fields (mT) at 396 nm in dfb/5% MeOH ($\lambda_{\text{ex}} = 475 \text{ nm}$).

Table 5.2. Origin fits of normalized CS decay data for the “D-C-A Mixture V/T” obtained at different wavelengths, concentrations, pump wavelengths, and in different solvents at zero applied magnetic field. The standard deviations were shown for the lifetimes that had a standard deviation larger than ± 3 ns. The underlined information denotes the samples that are shown in Figure 5.6 to demonstrate the visual differences that results from changes in experimental parameters.

Experimental Parameters	Solvent	Dfb				Dfb/2.3% MeOH	Dfb/5% MeOH	Dfb/5% MeOH	
	Pump (λ_{ex})	450 nm		475 nm		450 nm	475 nm	475 nm	
	λ monitored	394 nm	560 nm	396 nm	560 nm	560 nm	396 nm	396 nm	396 nm
	Concentration (M)	<u>6.4×10^{-5}</u>	5.3×10^{-5}	<u>9.6×10^{-5}</u>	<u>9.6×10^{-5}</u>	<u>4.1×10^{-5}</u>	1.75×10^{-5}	3.5×10^{-5}	<u>9.0×10^{-5}</u>
Data Presented in...	<u>Fig. 5.6</u>	Fig. 5.3	<u>Fig. 5.6</u>	<u>Fig. 5.6</u>	<u>Fig. 5.6</u> and 5.8	Fig. 5.7 and 5.8	Fig. 5.7 and 5.8	<u>Fig. 5.6</u> and 5.7	
Fitting Parameters	R^2	0.990	0.995	0.995	0.987	0.997	0.995	0.998	0.990
	Y_0	0.0011	0.012	0.0050	0.0038	-0.0017	-0.0045	0.01775	0.019
	A_1	0.26	0.28	0.70	0.62	0.29	0.49	0.54566	0.48
	τ_1	8.5 ns	8.5 ns	7.5 ns	7.5 ns	25 ns	30 ns	44 ns	45 ± 4.8 ns
	A_2	0.79	0.71	0.43	0.47	0.71	0.52	0.42	0.47
	τ_2	99 ns	90 ns	95 ns	91 ns	102 ns	128 ± 3.7 ns	148 ± 14 ns	130 ± 9 ns

experimental error, regardless of the wavelength at which the TA was monitored ($\lambda = 394$ nm, 396 nm, or 560 nm) or the pump wavelength ($\lambda_{ex} = 450$ nm vs 475 nm). Therefore, the changes made in the experimental parameters do not have an appreciable effect on the zero field lifetimes when studied in the same solvent, and therefore, should not change the lifetimes when in the presence of an applied magnetic field.

The normalized transient absorption data obtained on the “D-C-A Mixture V/T” in dfb/2.3% MeOH and dfb/5% MeOH, shown in Figures 5.4 and 5.5, clearly demonstrate that a

TA Decay of the "D-C-A Mixture V/T" in Various Concentrations and Solvent Compositions

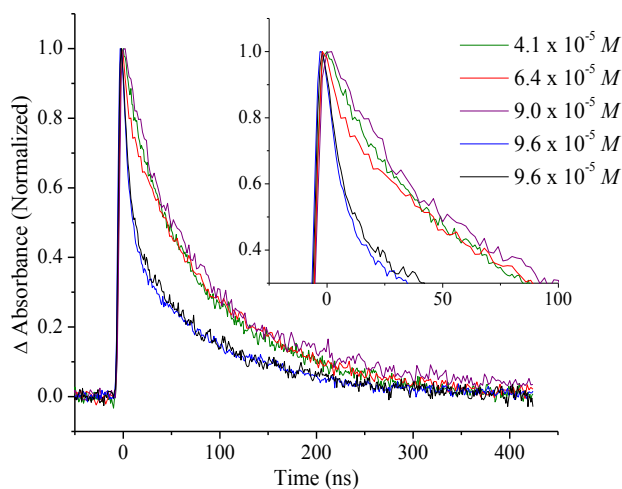
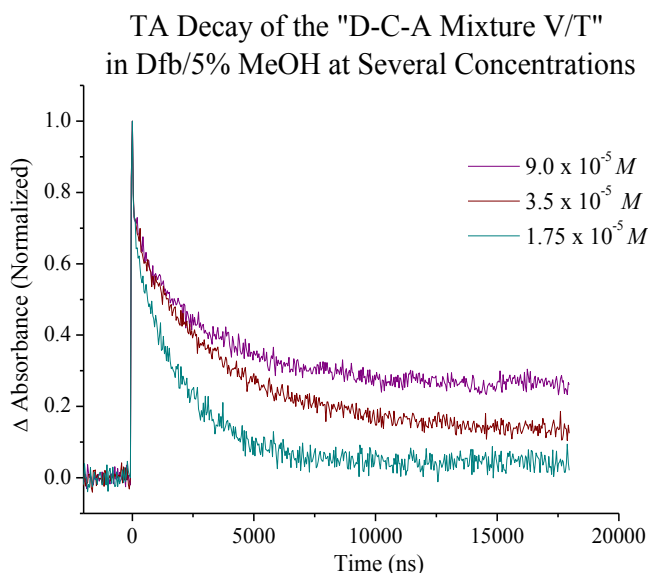


Figure 5.6. Normalized TA decay curves of the “D-C-A Mixture V/T” samples prepared at different concentrations, solvent compositions, and pump wavelengths in zero applied magnetic field. The different experimental parameters are detailed in Table 5.2. The inset graph shows the effect of different excitation wavelengths on the intensity of the absorbance.

very slow decay component evolves in an applied magnetic field in these solvents similarly to the sample in dfb (Figure 5.3). However, in the dfb/5% MeOH sample, another, much slower decay component evolves ($\tau \gg 20 \mu\text{s}$, appreciable contribution in $< 50 \text{ mT}$ applied field) that is evident when the data is displayed on a longer timescale



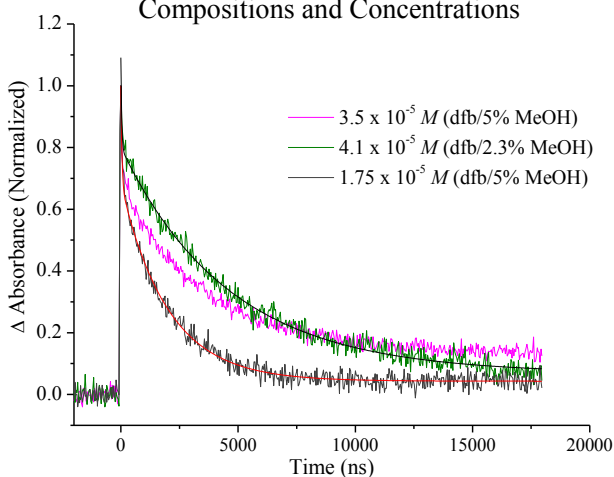
as shown in Figure 5.7. The concentration of the dfb/5% MeOH sample (Figure 5.7) is $3.5 \times 10^{-5} \text{ M}$, which re-

Figure 5.7. Normalized TA decay of the “D-C-A Mixture V/T” in dfb/5% MeOH at 396 nm in a 1000 mT applied field ($\lambda_{\text{ex}} = 475 \text{ nm}$) at three different concentrations. The contribution of the extremely long decay component is drastically reduced in less concentrated solutions. These data indicate that the long decay component is likely due to bi-molecular interactions

sulted in a ground-state absorbance of 0.338 at $\lambda_{\text{max}} = 449 \text{ nm}$, and 0.219 at $\lambda_{\text{ex}} = 475 \text{ nm}$ ($\lambda_{\text{ex}} =$ pump wavelength). The solution was prepared at this concentration to ensure adequate TA signal, but the presence of this unexpected, and extremely long decay component made fitting of the CS decay data nearly impossible. Fortunately, as shown in Figure 5.7, the contribution from this long decay component is drastically reduced in less concentrated solutions indicating that it is likely due to bi-molecular reaction between species in solution. For example, a possible bi-molecular reaction that could be occurring in these complexes is as follows: $\text{D}^{+\circ}\text{-C-A}^{3+\bullet} + \text{D-C-A}^{4+} \rightarrow \text{D-C-A}^{3+\bullet} + \text{D}^{+\circ}\text{-C-A}^{4+}$.

The bi-molecular reactions seem to be much less prominent in the dfb/2.3% MeOH solution, as shown in Figure 5.8, even though the concentration of the solution was similar: $4.1 \times 10^{-5} \text{ M}$ in dfb/2.3% MeOH (Figure 5.8, green trace) vs $3.5 \times 10^{-5} \text{ M}$ in dfb/5% MeOH (Figure 5.8,

TA Decays for the "D-C-A Mixture V/T" Mixture at an Applied Field of 1000 mT in Different Solvent Compositions and Concentrations



Applied Field	1000 mT	
Solvent Composition	Dfb/5% MeOH	Dfb/2.3% MeOH
Pump (λ_{ex})	475 nm	450 nm
λ monitored	396 nm	560 nm
Concentration (M)	1.75×10^{-5}	4.1×10^{-5}
R^2	0.976	0.942
Y_0	0.0434	0.00449
A_1	0.202	0.0133
τ_1	30 ns	10 ns
A_2	0.107	0.0308
τ_2	141 ± 57 ns	39 ± 2 ns
A_3	0.630	0.0500
τ_3	1996 ± 33 ns	4585 ± 71 ns

Figure 5.8. Comparison of normalized TA decay curves obtained on the “D-C-A Mixture V/T” in solutions of varying solvent composition and concentration at an applied field of 1000 mT. It is evident that the lifetime of the slowest CS decay component in the $4.1 \times 10^{-5} M$ sample is much longer than in the less concentrated sample. This effect seems exaggerated due to the change in D-C-A absorbance at different pump wavelengths, but the fit of the data confirms the difference in lifetime. Even though there is evidence of bi-molecular reactions in $4.1 \times 10^{-5} M$ sample, they are much less prominent than in the $3.5 \times 10^{-5} M$ sample in dfb/5% MeOH. Although it is likely that there is some change in the lifetime between the $1.75 \times 10^{-5} M$ sample in dfb/5% MeOH and the $3.5 \times 10^{-5} M$ sample in dfb/2.3% MeOH, the difference is probably not this large because of significant oxidation of the $1.75 \times 10^{-5} M$ sample during the experiment.

pink trace). As can be seen in Figure 5.8, the data from the dfb/2.3% MeOH sample was not obtained on a timescale over which the signal decayed all the way back to the baseline, which could make the contribution of the bi-molecular reactions seem less prominent. Although the CS decay in the dfb/2.3% MeOH sample does not return to the baseline within the timescale of the experiment, it does decay almost to the baseline of the data obtained for the $1.75 \times 10^{-5} M$ sample in dfb/5% MeOH, which had the least amount of contribution from bi-molecular reactions of all the samples in dfb/5% MeOH (Figure 5.8, grey trace). Consequently, the data from the dfb/2.3% MeOH data was able to be fit in the same manner as described for the data in dfb only. As seen in Table 5.3, the fit quality of the data from the dfb/2.3% MeOH sample is quite good, and the y_0 obtained in each fit is very near zero. Furthermore, it is clear that the lifetime of the slowest CS decay component (τ_3 , not the bi-molecular component) is nearly twice as long for the dfb/2.3%

MeOH (red trace) than the $1.75 \times 10^{-5} M$ dfb/5% MeOH sample. The slowest decay component was ca. 2x faster at all the other applied fields as well for the latter sample. However, a significant amount of oxidized donor was apparent in the UV-vis of the $1.75 \times 10^{-5} M$ dfb/5% MeOH sample after the laser experiments were performed (absorbance = 0.175 at $\lambda_{\max} = 452$ nm, absorbance = 0.116 at $\lambda_{\text{ex}} = 475$ nm, and absorbance = 0.0406 at 546 nm, oxidized donor peak present). Thus, it is likely that the lifetimes obtained for that sample are not accurate due to changes in the sample composition. This is important because the data from the $1.75 \times 10^{-5} M$ dfb/5% MeOH sample is the only data able to be fit in the dfb/5% MeOH solvent system due to the reduced contribution from the bi-molecular interactions. Since the lifetimes of the $1.75 \times 10^{-5} M$ sample in dfb/5% MeOH are probably not representative of real changes that occur with changing solvent composition due to sample degradation, the fits obtained from the dfb/2.3% MeOH sample will be used to discuss the effect of a magnetic field on the CS decay in a coordinating solvent.

As shown in Table 5.3, in dfb/2.3% MeOH solvent, a slow decay component grows in and its lifetime increases to a maximum value of ca. 4.8 μs at 1250 mT, then decreases again to ca. 4.2 μs as the field increases to 2250 mT. As in the sample in dfb solvent, it is expected that the decay will change from bi-exponential character at zero applied field to tri-exponential in an applied magnetic field, which is generally observed once the field has reached ca. 40 mT. As the field increases from 0-40 mT, the fits of the data are essentially bi-exponential. The existence of the second decay component (τ_2 , from the D-C-A) is questionable until 40 mT, where the fit clearly indicates its presence. Again, the second decay component increases with increasing field strength from ca. 50 ns to 137 ns at its maximum value in a field of 250 mT. The lifetime at its maximum value (ca. 137 ns) is somewhat larger than the lifetime of the D-C-A at zero applied

Table 5.3. The fit values obtained for several CS decay curves at 560 nm for the “D-C-A Mixture V/T” in 4.1×10^{-5} M dfb/2.3% MeOH ($\lambda_{\text{ex}} = 450$ nm), which are shown in Figure 5.4. The error shown for the lifetime data is the error in the fit as calculated by the “Advanced Fitting Tool” in Origin. All of the errors are quoted from the fit of the data taken on a short timescale (50 ns) with the exception of τ_3 , which was held constant during that fit. Therefore, the error quoted for τ_3 was generated for the fit of the longer timescale data (timescale dependent on field strength/lifetime).

Field Strength (mT)	Fit Values						
	R ²	A ₁	τ_1	A ₂	τ_2	A ₃	τ_3
0	0.996	0.0359	24 ns	0.0910	101 ± 1.6 ns	-	-
20	0.989	0.0393	21 ns	-	-	0.0919	463 ± 5 ns
40	0.985	0.0203	14 ns	0.0282	51 ± 3 ns	0.07363	965 ± 18 ns
50	0.983	0.0383	22 ns	0.0153	111 ± 12 ns	0.0718	1145 ± 19 ns
100	0.977	0.0289	16 ns	0.0236	78 ± 4.5 ns	0.0714	2182 ± 51 ns
250	0.959	0.0336	24 ns	0.0150	137 ± 17 ns	0.0529	3794 ± 75 ns
500	0.944	0.0333	22 ns	0.0145	118 ± 14 ns	0.0535	4637 ± 71 ns
750	0.955	0.0380	24 ns	0.0107	123 ± 19 ns	0.0516	4666 ± 117 ns
1000	0.942	0.0133	10 ns	0.0308	39 ± 2 ns	0.0500	4585 ± 71 ns
1250	0.935	0.0340	22 ns	0.00865	55 ± 13 ns	0.0495	4825 ± 77 ns
1500	0.918	0.0333	16 ns	0.0105	54 ± 8 ns	0.0442	4170 ± 62 ns
2000	0.886	0.0445	18 ns	-	-	0.0498	4413 ± 71 ns
2250	0.866	0.0388	18 ns	-	-	0.0454	4335 ± 71 ns

field, but considering the error bars on the fit and the variance in lifetimes between samples, they are probably statistically identical. However, absolute verification of the previous claim requires further, repeated studies. Assuming that the lifetime of the τ_2 in a 250 mT field is identical to the lifetime of the CS decay for the D-C-A at zero field, this could have important implications about the way the ³CS state(s) is(are) splitting in the magnetic field and the rates of intersystem crossing between each ³CS state (T_0 , T_+ , T_-) and the ¹CT state. As the field increases further from 250 mT, the lifetime of the second decay component decreases again until around 1500-2250 mT where the data becomes increasingly harder to fit with a tri-exponential (as indicated by the R² values) and eventually must be fit with a bi-exponential decay by 2000 mT. Again, the lifetime of the fastest decay component (τ_1) stays essentially constant at values near ca. 20 ns, within experimental error, at all fields.

All of the CS decay data presented so far has been normalized so changes in lifetime were not complicated by changes in initial intensity (ΔI_0) that occur in an applied magnetic field. However, the effect of an applied magnetic field on the initial intensity was explored for the “D-C-A Mixture V/T” in both dfb, dfb/2.3% MeOH, and dfb/5% MeOH as shown in Figure 5.9. For each sample, TA laser data was obtained at one wavelength (560 nm for dfb and dfb/2.3% MeOH and 396 nm for dfb/5% MeOH) on a short timescale (20-50 ns) for all applied magnetic fields from 0-2250 mT (0-1500 mT for dfb/5% MeOH). Each TA decay curve obtained was an averaged spectrum of ≥ 100 laser shots, and at least five TA decay curves were obtained at each applied magnetic field strength for each sample (total of ≥ 500 shots per data point). The absolute initial intensity, I_0 , values were obtained by averaging the data from 12-22 ns after $t = 0$ for every TA decay curve and then averaging the I_0 values obtained for each TA decay curve at all applied magnetic field strengths studied. As shown in Figure 5.9A and 5.9B, for every sample studied the initial intensity first increases with applied field, reaching a maximum between 75-150 mT, and then plateaus until approximately 500 mT, after which it decreases with applied field until the maximum field attainable in each experiment (the data from the dfb/5% MeOH sample was taken in a 1 cm cell as opposed to the 30 mm cell, so the maximum field attainable was around 1500 mT). The ΔI_0 is a calculated quantity which defines the apparent relative change in initial intensity between 0 mT and the field where the maximum value of initial intensity is obtained (between 50-100 mT). The values of ΔI_0 for each solvent composition were ca. 10%, 12%, and 5% for dfb only, dfb/2.3% MeOH, and dfb/5% MeOH, respectively. Further, repeated studies are necessary at each solvent concentration to determine if there is any real trend in the ΔI_0 value, however the values of ΔI_0 obtained in dfb/2.3% MeOH and dfb/5% MeOH are similar to those obtained on the C-AV diad in similar solvent compositions (See Chapter 3,

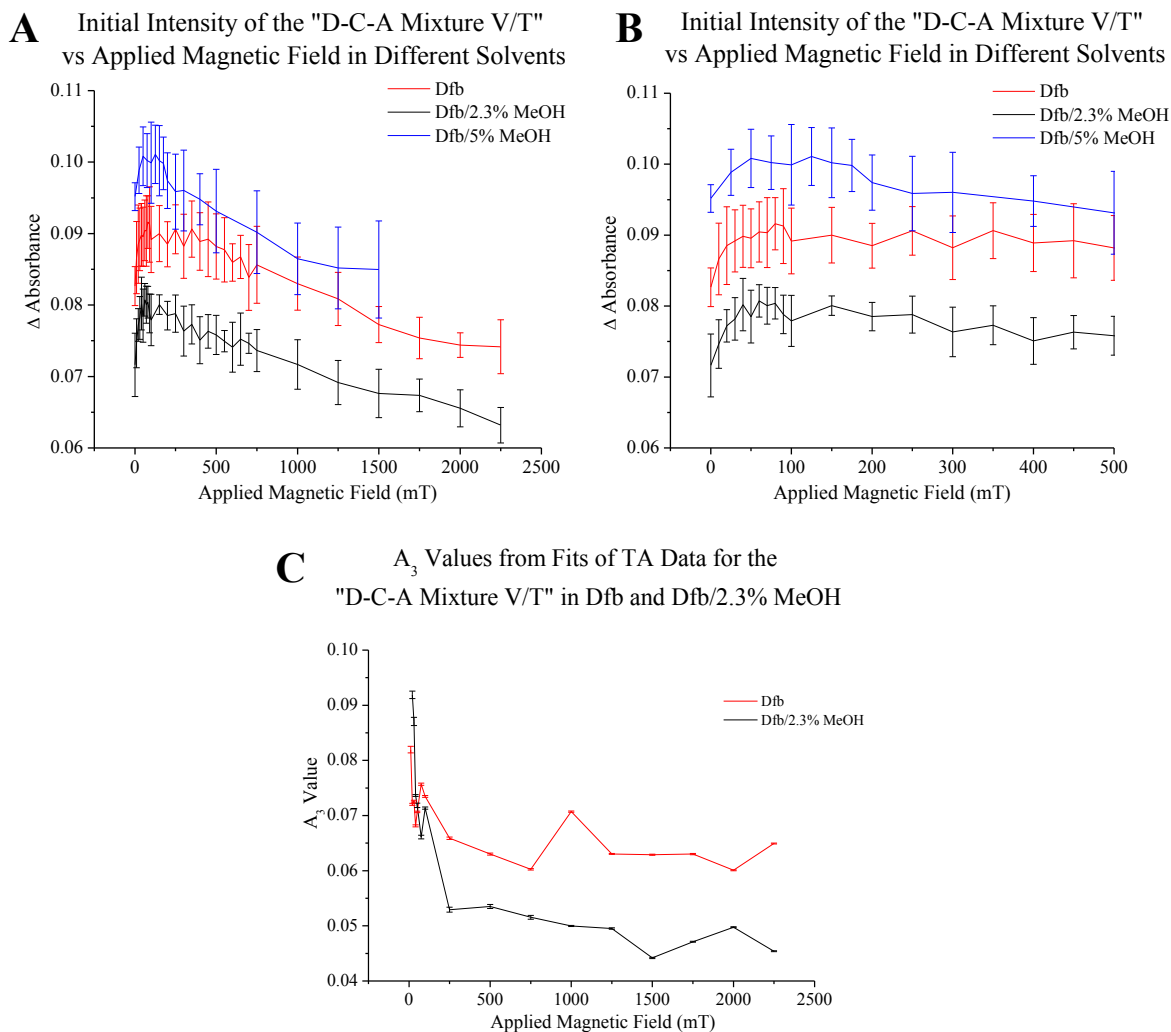


Figure 5.9. The initial intensity, I_0 , of the “D-C-A Mixture V/T” as a function of applied magnetic field in three different solvents (**A**) and the same data plotted from 0 to 500 mT (**B**). The data was obtained at 560 nm ($\lambda_{\text{ex}} = 450$ nm) for a sample in dfb (red trace), after which was added MeOH to make a new sample in dfb/2.3% MeOH. The same experiment was performed on the new sample in dfb/5% MeOH and the experiment was repeated on this sample at 396 nm ($\lambda_{\text{ex}} = 475$ nm, blue trace). To eliminate contributions from laser scatter and absorption due to the C-AV diad, the initial intensity values are actual the average data ca. 12-22 ns after $t = 0$ for each data set. The A_3 values obtained from fits of the TA data used to generate the ΔI_0 plots in (**A**) and (**B**) vs magnetic field (**C**), which should be free of any contributions from the CT absorption of the C-AV complex and only reflect changes in the CS absorbance from the D-C-A as a function of magnetic field.

Figure 3.11). Furthermore, the dfb data for the C-AV diad has the largest error due to a larger degree of uncorrected convolution between the C-AV lifetime in dfb ($\tau \approx 7$ ns) and the response function of the laser (pulse width ≈ 7 ns). Although no trend can be definitively outlined at this time, these data suggest that there are similarities between the ΔI_0 for the C-AV diad and the “D-C-A Mixture V/T” with solvent composition.

A possible complication with the previous interpretation results from the timescale on which the ΔI_0 data was obtained. As mentioned previously, the I_0 values were averaged values obtained ca. 12-22 ns after the laser pulse. In dfb, this timescale is not an issue because > 85% of the signal due to the C-AV diad has decayed away by 12-22 ns, so the ΔI_0 observed is primarily due to the D-C-A triad in solution. However, recall that as more MeOH is incorporated into the solvent composition the lifetime of the C-AV diad increases. Therefore, by 12-22 ns only ca. 40% and 25% of the signal due to C-AV diad has decayed away for the dfb/2.3% MeOH and dfb/5% MeOH samples, respectively. However, the I_0 value cannot be obtained on a timescale where ca. 85% of the C-AV diad has decayed away for every solvent because too much of the D-C-A would have decayed away for the value obtained to be considered an initial intensity, especially at zero field. Therefore, the presence of the C-AV diad in these samples complicates the interpretation of the ΔI_0 .

To address this issue, the A_3 values obtained from the fits of the dfb and dfb/2.3% MeOH data were plotted vs applied magnetic field in Figure 5.9C. In this Figure, the zero field data could not be considered because the long decay component is expected to be related to τ_2 and not τ_3 , if the Zeeman splitting mechanism is correct. Therefore, Figure 5.9C shows that the A_3 decreases from its value at low field (10 mT for dfb, and 20 mT for dfb/2.3% MeOH) until ca. 250 mT where the effect saturates and the A_3 value stays essentially constant with further applied field up to 2250 mT, the largest field applied in this study. Although this is not conclusive evidence that the observed ΔI_0 for the D-C-A is real, this value should theoretically represent the absorbance of the D-C-A without any contributions from the CT of the C-AV diad. Since the $A_2:A_3$ ratios are essentially constant (though there is a large degree of noise), these data add credence to the hypothesis that there could be an MFE on the I_0 of the D-C-A.

Studies on $[\text{Cu(I)(4OMQ)(TPZ)}]^{3+}(\text{TPFB})_3$: "D-C-A Mixture Q/T"

The CS recombination kinetics of the $[\text{Cu(I)(4OMQ}^{+})(\text{TPZ}^{+})]^{3+}(\text{TPFB}^{-})_3$ D-C-A complex in an applied magnetic field were studied by TA laser experiments with the altered laser setup described in the Experimental section. As was done for the TA studies at zero field, the ground state absorption spectrum (UV-vis) for each prepared sample was generally obtained before and after each set of experiments to determine the extent of sample degradation. Refer to Chapter 4, Figure 4.15 for a representation of the typical amount of change that occurs in the spectrum over the course of a normal experiment for this sample, which was prepared on the benchtop and degassed using the freeze-pump-thaw method.

The CS decay with respect to applied magnetic field was studied in dfb after excitation with 450 nm laser pulse. Figure 5.10 depicts a typical set of normalized single wavelength decay curves obtained at 560 nm in 1,2-difluorobenzene (dfb) on a 100 ns timescale. Again, these data were normalized, collected on both short (100 ns/division on the oscilloscope) and long time-

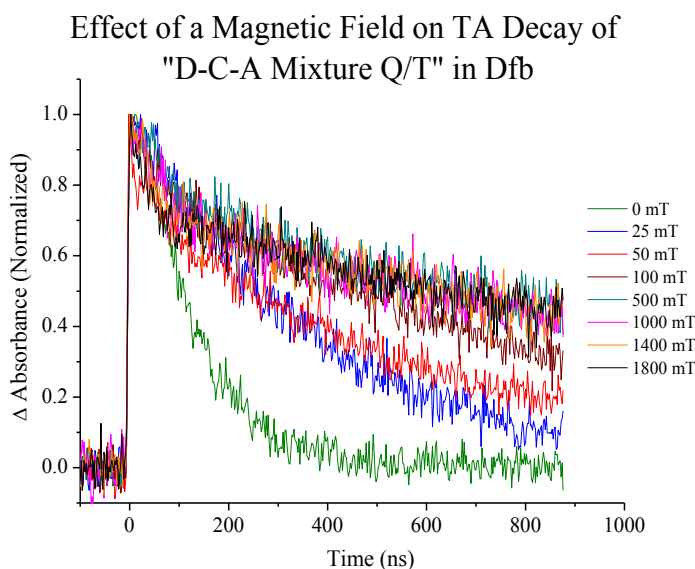


Figure 5.10. Normalized TA decay of the "D-C-A Mixture Q/T" at several applied magnetic fields (mT) at 530 nm in dfb ($\lambda_{\text{ex}} = 450 \text{ nm}$).

scales (200 ns–1 μs /division, depending on field strength), and fit in Origin in order to determine the lifetime of the slowest decay component. In these experiments, the long timescale data was obtained for a long enough duration that the absorbance had decayed to back to essentially zero. The value obtained from the fit for the lifetime

of the slow component was then plugged into the fit for the short timescale data and held constant, while the other fitting parameters were allowed to vary. As previously mentioned in Chapters 3 and 4, the fastest lifetime component should be the lifetime of the C-AQ diad present in the “D-C-A Mixture Q/T”. However, these data were taken using a 249 Ω measuring resistor due to poor signal-to-noise, which causes the initial lifetime to be unresolvable in the adjusted data. Therefore, instead of the CS decay kinetics changing from bi-exponential to tri-exponential as discussed for the “D-C-A Mixture V/T,” they change from mono-exponential to bi-exponential. This fitting procedure was used to obtain the lifetime (τ values) and intensity values (A values) given in Table 5.4. Again, the lifetime of the slowest decay component in these D-C-A’s is very sensitive to oxygen content and often varies on a sample-to-sample basis due to spin-catalysis. Therefore, since this sample was degassed using the freeze-pump-thaw method instead of preparing the sample in the glove box, the longest lifetime reported (τ_2) could be significantly shorter than the longest lifetime achievable for this complex when the oxygen content is minimized.

It is worthwhile to review, that the driving force for forward electron transfer to the CT state is ca. 540 mV smaller for this D-C-A (where $P_A = 40\text{MQ}$) than for the previously discussed D-C-A (where $P_A = 40\text{MV}$). According to Marcus theory, this change in driving force should significantly affect the rate of forward electron transfer to the CT state (k_{ct}), and therefore the Φ_{ct} (assuming that k_{bet} from the CT state is much slower than k_{ct}), but should not affect the rate of forward electron transfer from the CT state to the CS state. According to the results presented in Chapter 3, there was no discernable difference in the Φ_{ct} of the C-AV and C-AQ diads. Therefore, the absolute Φ_{ct} must be essentially unity for both the C-AV and C-AQ diads, although the apparent Φ_{ct} was measured to be $55 \pm 15\%$ for the C-AV diad in dfb/1.6% MeOH. Thus, any

changes in the Φ_{cs} must be due to the differences in driving force of the donor moieties for the different D-C-A's presented herein, unless k_{bet} from the CS state competes with k_{cs} . Since the D-C-A "Q/T" (where $P_A = 40MQ$ and $P_D = TPZ$) has the same donor as the previous D-C-A "V/T" (where $P_A = 40MV$ and $P_D = TPZ$), any real differences in the Φ_{cs} in these D-C-A's are not likely to be due to differences in driving force for CS formation, but could be due to the driving force for CS recombination. The driving force for back electron transfer from the CS (k_{bet}) is larger in this D-C-A than the previous D-C-A, as is evident from the estimated amount of energy stored in the CS shown in Figure 5.1. The increased driving force for CS recombination could either increase or decrease the rate of electron-hole recombination in this D-C-A "Q/T" relative to the previously discussed D-C-A "V/T," depending on if the recombination is the Marcus normal or Marcus inverted regime. Therefore, it is not unexpected to have different Φ_{CS} and τ_{cs} for this D-C-A "Q/T" relative to the D-C-A "V/T" discussed previously. Furthermore, changes in the spin-dynamics are also likely to occur. A similar argument can be made for all of the other D-C-A's presented herein.

As can be seen in Figure 5.10 and Table 5.4, the rate of CS decay is retarded in the presence of an applied magnetic field for the "D-C-A Mixture Q/T" as well. For this sample, the lifetime of the slowest decay component increases to a maximum value of ca. 1.6 μs at 1000 mT then decreases to ca. 1.5 μs by 1800 mT, which was the strongest field achievable for this sample. Although the initial change in lifetime from ca. 115 ns at zero field to ca. 1.6 μs at 1000 mT is large enough to be considered real without further studies (although they would still be recommended for more accurate lifetime determination) the decrease in lifetime from ca. 1.6 μs to 1.5 μs at high field is questionable due to the large amount of noise in these data. The CS decay changes from mono-exponential to bi-exponential in a field > 25 mT, which was expected. Once

Table 5.4. The values obtained by fitting the TA data at 530 nm for the “D-C-A Mixture Q/T” in dfb ($\lambda_{\text{ex}} = 450 \text{ nm}$) shown in Figure 5.10 with a bi-exponential decay. The error in τ_1 and τ_2 is quoted in the same way as all of the previous data.

Field Strength (mT)	Fit Values				
	R^2	A_1	τ_1	A_2	τ_2
0	0.982	0.0744	$115 \pm 1.6 \text{ ns}$	-	-
25	0.977	-	-	0.0683	$388 \pm 13 \text{ ns}$
50	0.969	0.0112	$65 \pm 12 \text{ ns}$	0.0587	$633 \pm 19 \text{ ns}$
100	0.953	0.0125	$103 \pm 12 \text{ ns}$	0.0538	$999 \pm 29 \text{ ns}$
250	0.927	0.0146	$106 \pm 10 \text{ ns}$	0.0511	$1399 \pm 30 \text{ ns}$
500	0.901	0.0143	$63 \pm 7.7 \text{ ns}$	0.0498	$1467 \pm 25 \text{ ns}$
1000	0.878	0.0191	$54 \pm 7.2 \text{ ns}$	0.0454	$1581 \pm 31 \text{ ns}$
1400	0.870	0.0199	$35 \pm 5.0 \text{ ns}$	0.0459	$1578 \pm 21 \text{ ns}$
1800	0.860	0.0183	$22 \pm 4.2 \text{ ns}$	0.0421	$1520 \pm 22 \text{ ns}$

a small magnetic field is applied the first decay component (τ_1) is not present until after 50 mT, where the TA decay becomes bi-exponential. The lifetime (τ_1) and the intensity (A_1) of the first decay component then increases with increasing field strength from ca. 65 ns at 50 mT to 106 ns at its maximum value in a 250 mT field. Again, the lifetime at its maximum value (ca. 106 ns) is almost identical to the lifetime of the D-C-A at zero applied field. As the field increases further, the lifetime of the first decay component decreases from 106 ns at 250 mT to 22 ns at 1800 mT, but the intensity of that decay component continues to increase with field ($A_1 = 0.0146$ at 250 mT and $A_1 = 0.0183$ at 1800 mT). The lifetime of the first and second decay components could decrease further at higher fields, which were not achievable during this experiment, and warrants further investigation. However, as with the “D-C-A Mixture V/T”, the ratios of A values are not considered to be exceedingly informative at this time and a more in-depth interpretation of the A values may be achieved by collaboration with Dr. Ulrich Steiner at the Universität Konstanz in Konstanz, Germany.

All of the CS decay data presented so far has been normalized so changes in lifetime were not complicated by changes in initial intensity (ΔI_0) that occur in an applied magnetic field.

However, the MFE on initial intensity was explored for the “D-C-A Mixture Q/T” in dfb. To evaluate the ΔI_0 , TA laser data was obtained at 530 nm on the short timescale (100 ns) for applied magnetic fields from 0-1800 mT. This study was much more preliminary than the ΔI_0 study on the “D-C-A Mixture V/T,” therefore, each TA decay curve was an averaged spectrum of 300 laser shots, but only one spectrum was obtained at each applied magnetic field strength for this sample. The error bars shown were calculated based on the average error calculated for the “D-C-A Mixture V/T” in dfb (ca. $\pm 4.6\%$) in the same manner as was done in Chapter 3. The absolute initial intensity, I_0 , values were obtained by averaging the data from 12-18 ns after $t = 0$ at all applied magnetic field strengths studied. By this time, nearly 87% of the signal due to C-AQ diad has decayed away.

However, the zero field data had to be omitted because it was performed on a different sample. Therefore, it is impossible to calculate the ΔI_0 for this sample, but these data can be used to observe other qualitative changes in I_0 with an applied magnetic field. As shown in Figure 5.11, the initial intensity first decreases from its maximum value as the field increases from 25-50 mT then increases with applied

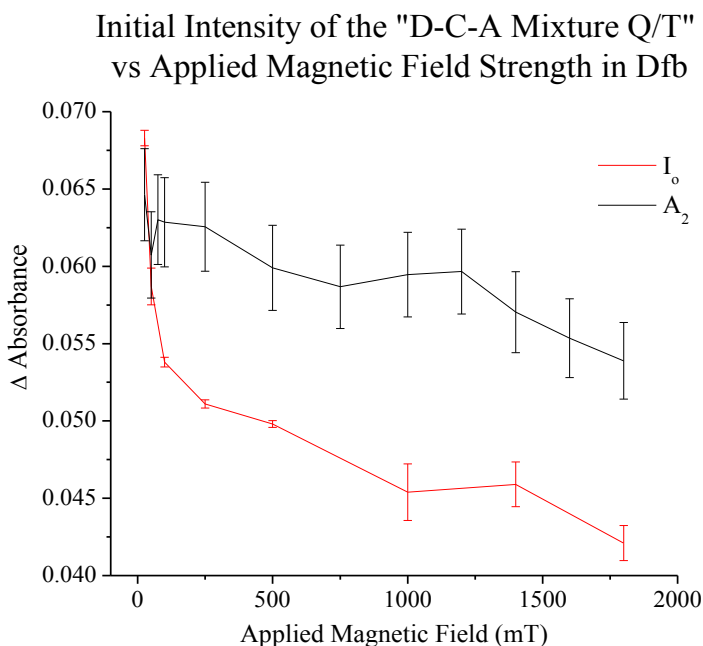


Figure 5.11. The initial intensity, I_0 , of the “D-C-A Mixture Q/T” as a function of applied magnetic field and the A_2 value obtained from fits in Table 5.4. The data was obtained at 530 nm ($\lambda_{\text{ex}} = 450$ nm) in dfb. To eliminate contributions from laser scatter, the I_0 values are averaged data from 12-18 ns after $t = 0$. The error bars on the I_0 data were calculated using the average error calculated from the “D-C-A Mixture V/T” in dfb from Figure 5.9. The error bars on the A_2 data is the error produce in the fit. The ΔI_0 for this sample cannot be determined because the 0 mT data was performed on a different sample of different concentration.

field reaching a local maximum at 75 mT. Between 75 and 250 mT, the I_0 stays essentially constant, and then decreases with applied field until 750 mT, increases slightly until 1200 mT and then decreases until the maximum field attainable for this experiment was reached (1800 mT). Also shown is the A_2 value obtained from fits in Table 5.4 from 25 mT-1800 mT, which should represent the initial intensity of the D-C-A without any influence from the CT absorption due to C-AQ diad. Again, although these data do not conclusively verify the existence of an MFE on the I_0 , the A_2 value clearly supports the hypothesis. Further, repeated studies are necessary to determine the ΔI_0 value, however the other trends in I_0 with magnetic field strength for this sample are similar to those obtained in dfb for the “D-C-A Mixture V/T”.

Studies on $[\text{Cu}(\text{I})(4\text{OMV})(\text{POZ})]^{5+}(\text{TPFB})_5$: “D-C-A Mixture V/P”

The effect of an applied magnetic field on the $[\text{Cu}(\text{I})(4\text{OMV}^{3+})(\text{TPZ}^{+o})]^{+5}(\text{TPFB})_5$ D-C-A CS recombination kinetics of the using the altered TA laser set-up with the electromagnet detailed in the Experimental section. As was done for the TA studies at zero field, the ground state absorption spectrum (UV-vis) for the prepared sample was generally obtained before and after each set of experiments to determine the extent of sample degradation. Refer to Chapter 4, Figure 4.18 for a representation of the typical amount of change that occurs in the spectrum over the course of a normal experiment for this sample, which was prepared on the benchtop and degassed using the freeze-pump-thaw method.

The CS decay with respect to applied magnetic field was studied in dfb after excitation with 450 nm laser pulse. Figure 5.12 depicts a typical set of normalized single wavelength decay curves obtained at 550 nm in 1,2-difluorobenzene (dfb) on a 100 ns timescale. Again, these data were normalized, but these data only needed to be collected on one timescale because the

Effect of a Magnetic Field on TA Decay of "D-C-A Mixture V/P" in Dfb

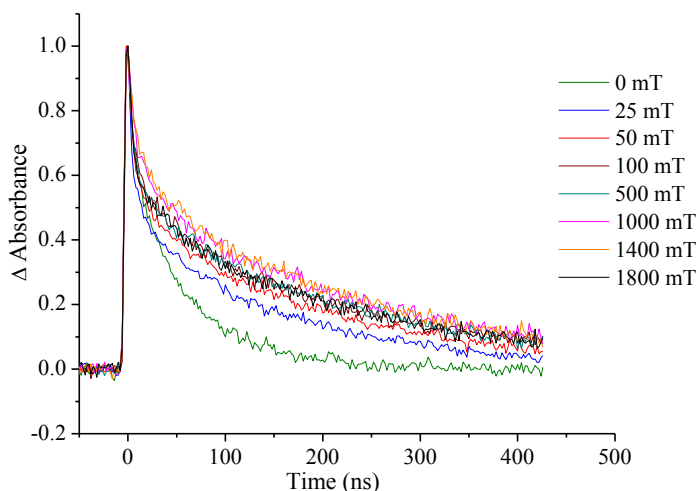


Figure 5.12. Normalized TA decay of the “D-C-A Mixture V/P” at several applied magnetic fields (mT) at 550 nm in dfb ($\lambda_{\text{ex}} = 450 \text{ nm}$).

lifetime of the slowest decay component was short enough at all magnetic field strengths to be fit well from the 100 ns timescale data. The zero applied magnetic field data that was included in Figure 5.12 and in Tables 5.5 and 5.6 were taken on a different day, so lifetimes can be compared, but initial intensities cannot. The fastest lifetime component is again assumed to be due to the presence of C-AV in the “D-C-A Mixture V/P” solution. Therefore, a value near 7 ns (the independently determined lifetime of the C-AV diad in dfb at zero field) that enabled a good fit for the curvature of the shortest decay component was plugged in for τ_1 and held constant while the other fitting parameters were allowed to vary. In this sample, the lifetimes used for τ_1 were somewhat shorter than expected based on the lifetime of the C-AV diad, but this is not completely unusual considering the previously discussed issues with the response function of the instrument. These data were obtained without using a 249 Ω measuring resistor, and therefore the decay should again change from bi-exponential to tri-exponential as mentioned above. Although oxygen content is considered an important variable in the observed lifetime of the previously discussed D-C-A complexes, it is not expected to have an appreciable effect in this D-C-A ($P_A = 40\text{MV}$ and $P_D = \text{POZ}$) since the lifetime is not long enough for spin-catalysis issues to arise at any applied field. Therefore, the freeze-pump-thaw technique should be an adequate method for degassing this sample.

lifetime of the slowest decay component was short enough at all magnetic field strengths to be fit well from the 100 ns timescale data. The zero applied magnetic field data that was included in Figure 5.12 and in Tables 5.5 and 5.6 were taken on a different day, so lifetimes can be compared, but initial intensities cannot. The fast-

Table 5.5. The values obtained by fitting the TA data at 550 nm for the “D-C-A Mixture V/P” in dfb ($\lambda_{\text{ex}} = 450$ nm) shown in Figure 5.12 with a tri-exponential decay. The error in τ_1 and τ_2 is quoted in the same way as all of the previous data.

Field Strength (mT)	Fit Values						
	R^2	A_1	τ_1	A_2	τ_2	A_3	τ_3
0	0.985	0.0730	6.0 ns	0.127	62 ± 1 ns	-	-
25	0.993	0.109	5.5 ns	0.0225	34 ± 11 ns	0.103	168 ± 5 ns
50	0.994	0.114	4.0 ns	0.0382	25 ± 4 ns	0.104	210 ± 4 ns
100	0.991	0.0778	5.5 ns	0.0326	44 ± 9 ns	0.0931	255 ± 12 ns
250	0.991	0.0850	5.0 ns	0.0279	27 ± 7 ns	0.0957	242 ± 6 ns
500	0.991	0.0635	4.0 ns	0.0291	26 ± 6 ns	0.0936	230 ± 6 ns
1000	0.991	0.0452	4.5 ns	0.0336	27 ± 4 ns	0.0950	245 ± 6 ns
1400	0.991	0.0402	6.0 ns	0.0269	26 ± 7 ns	0.0949	232 ± 6 ns
1800	0.989	0.0716	2.8 ns	0.0299	34 ± 6 ns	0.0893	236 ± 8 ns

As can be seen in Figure 5.12 and Table 5.5, the rate of CS decay is retarded in the presence of an applied magnetic field for the “D-C-A Mixture V/P,” but to a much lesser extent than the previous D-C-A complexes. For this sample, the lifetime of the slowest decay component increases to a maximum value of ca. 250 ns at 100 mT, and the lifetime stays essentially constant with increased magnetic field strength up to 1800 mT, which was the strongest field achievable for this sample (i.e. using a 1 cm sample cell). The CS decay kinetics seem to change from bi-exponential to tri-exponential in a field > 25 mT, which is expected. In contrast to the previous D-C-A complexes, the second decay component (τ_2) is present and the lifetime is relatively constant (ca. 25-35 ns) at all applied fields. However, since no data was taken for fields between 0 and 25 mT, it is possible that the second decay component does not appear until some field that is > 0 mT, but < 25 mT, which would be similar behavior to what was observed for the two D-C-A’s discussed previously. In this sample, the lifetime of the second decay component at its maximum value (ca. 44 ± 9 ns) is not identical to the zero field lifetime of the D-C-A. As stated above, it is questionable if the maximum value reflects a true change in the lifetime with magnetic field or a random fluctuation. However, it is still possible that the lifetime of the second decay

component could decrease at higher fields than 1800 mT, which was not achievable during this experiment, and warrants further investigation. Again, as with the other D-C-A complexes, the ratios of A values are not evaluated at this time.

It is worth mentioning that the TA decay profile for this D-C-A may not actually change from having two to three decay components in a magnetic field because the fits of the data using a bi-exponential fit are just as good as the fits of the data using a tri-exponential fit as shown in Table 5.6. There is very little difference in the fit quality, and upon visual inspection, both bi- and tri- exponential fits seem to provide equivalent matches of the decay curvature. However, based on the expected Zeeman splitting scheme presented in the Introduction section, it seems more plausible that a tri-exponential decay would result from the “D-C-A Mixture V/P” solution.

Studies were also performed to determine the changes in initial intensity (ΔI_0) that occur in an applied magnetic field for this complex at 550 nm in dfb, as shown in Figure 5.13. To evaluate the ΔI_0 , TA laser data was obtained at 550 nm on a short timescale (100 ns) for applied magnetic fields from 25-1800

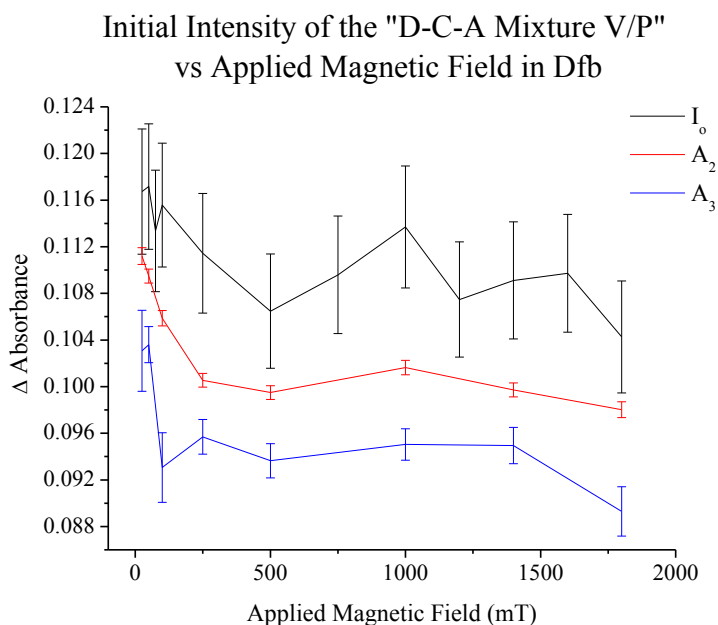


Figure 5.13. The initial intensity, I_0 , of the “D-C-A Mixture V/P” as a function of applied magnetic field and the A_2 and A_3 values generated from the fits shown in Tables 5.5 and 5.6. The data was obtained at 550 nm ($\lambda_{ex} = 450$ nm) in dfb. To eliminate contributions from laser scatter, the I_0 values are averaged data from 12-18 ns after $t = 0$. The error bars were calculated using the average error calculated from the “D-C-A Mixture V/T” in dfb from Figure 5.9. The error bars on the A_2 data is the error produce in the fit. The ΔI_0 for this sample cannot be determined because the 0 mT data was performed on a different sample of different concentration.

mT. Being a preliminary study, each TA decay curve obtained was an averaged spectrum of 300 laser shots, but only one spectrum was obtained at each field for this sample. The error bars shown were again calculated based on the average error calculated for the “D-C-A Mixture V/T” in dfb (ca. $\pm 4.6\%$) as was done for the “D-C-A Mixture Q/T”. The absolute initial intensity, I_0 , values were obtained by averaging the data from 12-18 ns after $t = 0$ at all applied magnetic field strengths studied. At this time, nearly 87% of the signal due to C-AQ diad had decayed away. However, the zero field data had to be omitted because it was performed on a different sample, which again, makes it impossible to calculate the ΔI_0 . As shown in Figure 5.13, the changes in initial intensity seem to be completely random for this sample which also contrasts the patterns obtained for the other two D-C-A complexes. However, the A_2 and A_3 values obtained from the bi- and tri-exponential fits in Tables 5.5 and 5.6 are also shown for 25 mT-1800 mT. Although no clear pattern was observed in the I_0 data, the A_2 and A_3 data clearly decreases with field until 250 mT, at which point the values remain essentially constant until 1400 mT, and then decrease further at 1800 mT. These changes are qualitatively very similar to the changes in I_0 observed for the previously discussed D-C-A complexes. However, repeated studies are necessary to determine if there is any ΔI_0 for this D-C-A.

Studies on $[\text{Cu}(\text{I})(4\text{OMQ})(\text{POZ})]^{3+}(\text{TPFB}^-)_3$: “D-C-A Mixture Q/P”

The effect of an applied magnetic field on the CS recombination kinetics of the $[\text{Cu}(\text{I})(4\text{OMQ}^{+})(\text{POZ}^{+})]^{3+}(\text{TPFB}^-)_3$ D-C-A was also studied using the altered TA laser set-up detailed in the Experimental section. As was done for the TA studies at zero field, the ground state absorption spectrum (UV-vis) for the prepared sample was generally obtained before and after each set of experiments to determine the extent of sample degradation. Refer to Chapter 4,

Figure 4.21 for a representation of the typical amount of change that occurs in the spectrum over the course of a normal experiment for this sample, which was prepared on the benchtop and degassed using the freeze-pump-thaw method.

The CS decay with respect to applied magnetic field was studied in dfb after excitation with 450 nm laser pulse. Figure 5.14 depicts a typical set of normalized single wavelength decay curves obtained at 540 nm in 1,2-difluorobenzene (dfb) on a 100 ns timescale. Again, these data are normalized, but only collected on one timescale because the lifetime of the slowest decay component is short enough at all fields to be fit well from the 100 ns timescale data. The zero field data was not taken during this data set and the data from another data set is very noisy, so it is not included in Figure 5.14, for clarity. However, the fit of the zero applied field data is shown in Table 5.7. It is important to note that the zero applied field data is mono-exponential because it was acquired using a 249 Ω measuring resistor and the rest of the data was not. Therefore, the fastest lifetime component in the data acquired in an applied magnetic field is

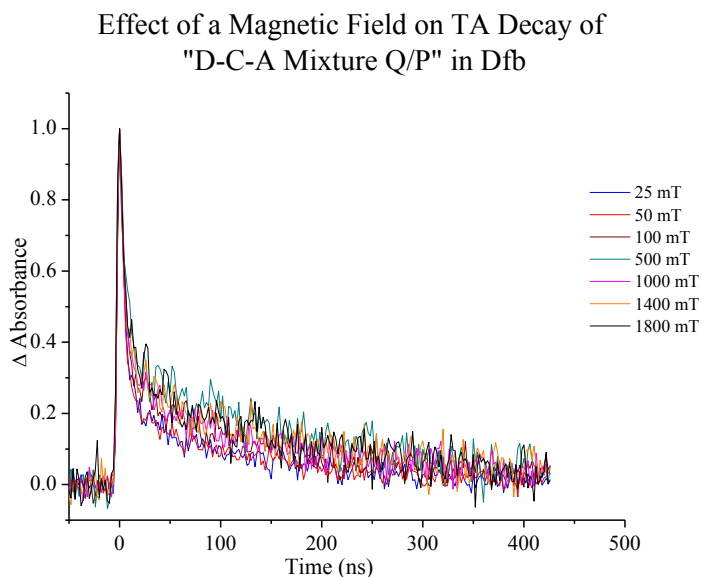


Figure 5.14. Normalized TA decay of the “D-C-A Mixture Q/P” at several applied magnetic fields (mT) at 540 nm in dfb ($\lambda_{\text{ex}} = 450 \text{ nm}$).

again assumed to be due to the C-AQ diad in the “D-C-A Mixture Q/P” solution. As done for the other D-C-A fits, a value near 7 ns (the independently determined lifetime of the C-AQ diad in dfb at zero applied field) that enabled a good fit for the curvature of the shortest decay component was plugged in for τ_1 and held

Table 5.7. The values obtained by fitting the 540 nm TA data for the “D-C-A Mixture Q/P” in dfb ($\lambda_{\text{ex}} = 450$ nm) shown in Figure 5.14 with a tri-exponential decay. The error shown for the lifetime data is the error in the fit as calculated by the “Advanced Fitting Tool” in Origin.

Field Strength (mT)	Fit Values						
	R ²	A ₁	τ_1	A ₂	τ_2	A ₃	τ_3
0	0.902	-	-	0.952	67 ± 2 ns		
25	0.862	0.0686	3.0 ns	0.0311	11 ± 3 ns	0.0237	135 ± 7 ns
50	0.894	0.0956	4.5 ns	0.0123	24 ± 15 ns	0.0228	161 ± 15 ns
100	0.843	0.0402	5.0 ns	0.00951	46 ± 26 ns	0.0170	200 ± 22 ns
250	0.862	0.0992	4.0 ns	0.0155	18 ± 10 ns	0.0189	187 ± 17 ns
500	0.849	0.0490	6.0 ns	0.00624	140 ± 536 ns	0.0140	215 ± 291 ns
1000	0.841	0.0528	3.0 ns	0.0143	23 ± 9 ns	0.0171	189 ± 12 ns
1400	0.821	0.0484	5.0 ns	0.00565	29 ± 30 ns	0.0170	193 ± 15 ns
1800	0.800	0.00515	3.0 ns	0.0155	17 ± 9 ns	0.0153	203 ± 23 ns

constant while the other fitting parameters were allowed to vary. Like the “D-C-A Mixture V/P,” the lifetimes used for τ_1 of this D-C-A were also consistently shorter than expected based on the CT lifetime of the C-AQ diad. Since these data were obtained without the measuring resistor, the decay should change from bi-exponential to tri-exponential as mentioned previously. As was the case for the “D-C-A Mixture V/P,” the observed lifetime of this D-C-A ($P_A = 40\text{M}\Omega$ and $P_D = \text{POZ}$) is not long enough for spin-catalysis issues to arise at any applied field. Therefore, minor changes in oxygen content are not likely to be a significant issue and the freeze-pump-thaw technique should be an adequate method for degassing this sample.

For the “D-C-A Mixture Q/P,” the rate of CS decay is again impeded in the presence of an applied magnetic field, but to the least extent of all of the D-C-A complexes studied in this thesis, as shown in Figure 5.14 and Table 5.7. For this D-C-A complex, the lifetime of the slowest decay component increases to a maximum value of ca. 200 ns at 100 mT, and the lifetime stays essentially constant with increased magnetic field strength up to 1800 mT. The CS decay changes from bi-exponential to tri-exponential in a field > 25 mT, which was expected. The second decay component (τ_2) is present at all applied magnetic fields studied, and remains essential-

ly constant around 10 - 30 ns, within experimental error. Since no data was taken in field between 0 and 25 mT it is possible that the second lifetime appears in a similar manner as the D-C-A complexes with the TPZ donor ligand. Furthermore, at all applied fields studied, the lifetime of the second decay component is not similar to the zero field lifetime, which also contrasts the results from the D-C-A's with the TPZ donor. However, similarly to the "D-C-A Mixture V/P" sample, these data may not actually change from having two to three decay components in a magnetic field. Comparing the fit data shown in Tables 5.7 and 5.8, the fits using a bi-exponential decay curve are just as good as the fits using a tri-exponential decay curve. Moreover, upon visual inspection, there is very little difference in the fit quality, and both fits appear to do a satisfactory job at modeling the decay curves. As mentioned previously, based on the expected Zeeman splitting scheme presented in the Introduction section, it seems more plausible that a tri-exponential decay would result from this "D-C-A Mixture Q/P" solution. However, the lifetime of the first decay component is closer to the independently determined value of ca. 7 ns for the C-AQ diad in the bi-exponential fits than the tri-exponential fits. This is also the

Table 5.8. The values obtained by fitting the 540 nm TA data for the "D-C-A Mixture Q/P" in dfb ($\lambda_{\text{ex}} = 450$ nm) shown in Figure 5.14 with a bi-exponential decay. The error shown for the lifetime data is the error in the fit as calculated by the "Advanced Fitting Tool" in Origin.

Field Strength (mT)	Fit Values				
	R^2	A_1	τ_1	A_2	τ_2
0	0.902	-	-	0.952	67 ± 2 ns
25	0.861	0.0970	5.5 ns	0.0257	127 ± 6 ns
50	0.892	0.102	5.5 ns	0.0260	141 ± 6 ns
100	0.839	0.0745	5.0 ns	0.0218	168 ± 9 ns
250	0.859	0.120	5.0 ns	0.0210	163 ± 9 ns
500	0.849	0.0380	7.0 ns	0.0199	194 ± 11 ns
1000	0.836	0.0546	6.0 ns	0.0200	167 ± 10 ns
1400	0.819	0.0514	6.0 ns	0.0185	180 ± 11 ns
1800	0.797	0.0373	7.0 ns	0.0169	178 ± 12 ns

case for the “D-C-A Mixture V/P” presented in Tables 5.5 and 5.6, above. Therefore, these data could suggest that using the POZ donor ligand instead of the TPZ donor ligand actually affects the spin-dynamics in a magnetic field. However, since these studies were very preliminary, further study on these complexes is necessary before any conclusion can be drawn. Again, as with the other D-C-A complexes, the ratios of A values are not evaluated at this time.

The changes in initial intensity (ΔI_0) that occur in an applied magnetic field were also briefly studied for this complex at 540 nm in dfb, as shown in Figure 5.15. The ΔI_0 was evaluated using TA laser data obtained on a short timescale (100 ns) for applied magnetic fields from 0 - 1800 mT. Being another preliminary study, each TA decay curve obtained was an averaged

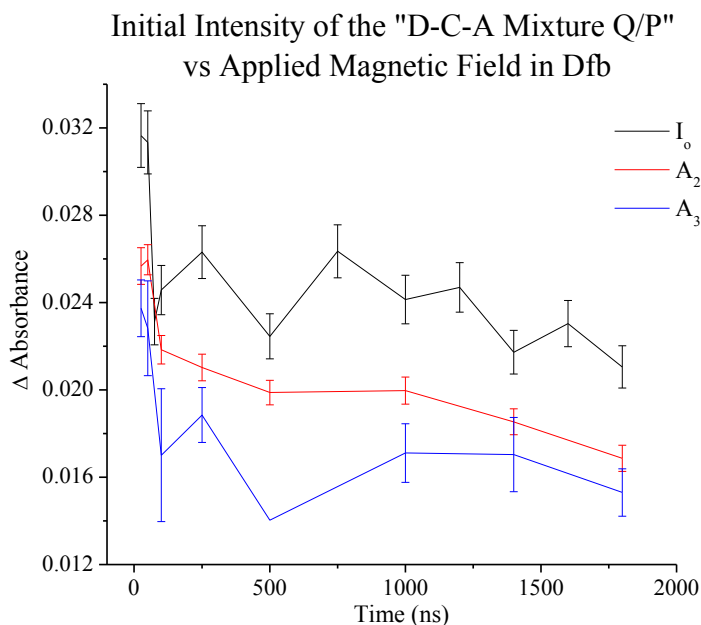


Figure 5.15. The initial intensity, I_0 , of the “D-C-A Mixture Q/P” as a function of applied magnetic field and the A_2 and A_3 values generated from the fits shown in Tables 5.7 and 5.8. The data was obtained at 540 nm ($\lambda_{\text{ex}} = 450$ nm) in dfb. To eliminate contributions from laser scatter, the I_0 values are averaged data from 12-18 ns after $t = 0$. The error bars were calculated using the average error calculated from the “D-C-A Mixture V/T” in dfb from Figure 5.9. The error bars on the A_2 and A_3 data is the error produce in the fit. The ΔI_0 for this sample cannot be determined because the 0 mT data was performed on a different sample of different concentration.

spectrum of 300 laser shots, and only one spectrum was obtained at each applied magnetic field strength. The error bars shown were again calculated based on the average error of the “D-C-A Mixture V/T” in dfb (ca. $\pm 4.6\%$). The absolute initial intensity, I_0 , values were obtained by averaging the data from 12-18 ns after $t = 0$ (ca. 87% of the signal due to C-AQ diad has decayed away) at all applied magnetic field strengths studied. Again, the zero

field data had to be omitted because it was performed on a different sample making it impossible to calculate the ΔI_0 . However, as shown in Figure 5.15, initial intensity seems to be at the maximum value in an applied magnetic field of 25-50 mT, quickly drops off at ca. 100 mT to $\Delta A \approx 0.024$, and then bounces between 0.026 and 0.022 until the field reaches its maximum value at 1800 mT. When comparing the changes in I_0 with magnetic field to the A_2 and A_3 values obtained from the bi- and tri-exponential fits in Tables 5.7 and 5.8, all of the data seem to follow the same trend. These changes are qualitatively very similar to the changes in I_0 observed for the previously discussed D-C-A complexes. Again, although these results seem to suggest a pattern in I_0 with magnetic field for all of the D-C-A complexes, the presence of the C-AX diads in the equilibrium mixtures precludes conclusive evidence of this effect. Therefore, it is clear that further studies are necessary to determine if this is a repeatable pattern in the ΔI_0 for this D-C-A and all of the D-C-A's presented in this thesis.

5.3 Discussion

When D-C-A's are incorporated into energy-harvesting devices as photosensitizers they must fulfill certain requirements in order for the device to function. As previously discussed, the D-C-A must be able to absorb a large portion of the incident radiation ($\epsilon \approx 10^3$ - 10^5 Lmol⁻¹cm⁻¹), the absorbed energy must be able to drive efficient CS formation with minimal energy loss ($\Phi \rightarrow 1$), and the CS must be able to store an adequate amount of energy for a long enough period of time (long τ_{cs}) to drive subsequent processes in the energy harvesting apparatus, again with minimal energy loss. Metal polypyridyl D-C-A's based on [Ru(II)L₃] fulfill all of the aforementioned requirements, but have marginal CS lifetimes ($\tau_{cs} \approx 100$ -300 ns) for some energy harvesting applications. Fortunately, application of moderate magnetic fields ($B_0 < 0.5$ T) enables facile

manipulation of CS lifetimes via changes in spin-dynamics. Since the data presented in Chapter 4 suggest that the mechanism of CS formation in $[\text{Cu(I)P}_2]$ D-C-A's is similar to CS formation in $[\text{Ru(II)L}_3]$ D-C-A's, it is possible that their spin-chemistry will be similar as well.

Since these are the first $[\text{Cu(I)P}_2]$ D-C-A's to be reported in which $[\text{Cu(I)P}_2]$ is the primary light harvesting moiety, very little is known about the energetics or spin-dynamics of the CS states formed in these complexes, or the mechanism and kinetics of CS recombination. To address these issues, the spin-chemistry of these $[\text{Cu(I)P}_2]$ D-C-A's was investigated via TA laser experiments in the presence of an applied magnetic field. It is clear from the TA data presented in Figures 5.3-5.5, 5.10, 5.12, and 5.14 that the rate of CS recombination is influenced by the presence of a magnetic field to differing degrees in each of the D-C-A complexes studied. This fact alone indicates that the di-radical CS state formed in each of the D-C-A complexes is, at least partially, triplet in nature, adding credence to the proposed CS mechanism in Chapter 4 (Chapter 4, Figure 4.25). Furthermore, in the "D-C-A Mixture V/T" the MFE on the CS lifetime is even more pronounced than in the $[\text{Ru(II)L}_3]$ complexes, achieving CS lifetimes up to 60 times longer (ca. 6 μs in fields of $B_0 \approx 1$ T) relative to zero field.

In the discussion below, the magnetic field effects are primarily rationalized based on the radical pair relaxation mechanism presented in Figure 5.2. However, the fact that the lifetime of the second CS decay component is not constant with magnetic field in the "D-C-A Mixtures V/T and Q/T" and may not exist for "D-C-A Mixtures V/P and Q/P" suggests a different mechanism. Elucidation of the spin-chemical behavior in these complexes requires a detailed kinetic analysis of these data and specific expertise. An in-depth examination of these results is underway with an expert collaborator, Dr. Ulrich Steiner at the Universität Konstanz in Konstanz, Germany. Therefore, the explanation of the results presented below should be considered speculative until

these collaborations are complete. It is worthwhile to note that even though the lifetime of the C-AX diads was found to depend on an applied magnetic field, the changes were very small (particularly in dfb). Consequently, the lifetime of the first decay component was assumed to be essentially constant in these studies.

Before delving into the effects of the magnetic field on the CS decay kinetics in detail, it is relevant to comment on the solvent effects that occur in the CS decay kinetics at zero field. As discussed in Chapter 3, τ_{ct} of the C-AV diad is highly solvent dependent, increasing with increased MeOH concentration until the effect saturates at $\tau_{ct} = 40\text{-}45$ ns in dfb/ > 4%MeOH. The increased lifetime of the CT state is rationalized on the basis of the MLCT and subsequent CT state stabilization due to solvent adduction in the J-T distorted $[\text{Cu(II)P}_2]$ MLCT state. Therefore, the reorganizational energy required for back electron transfer to the ground state is increased as the interaction between the flattened complex and the fifth ligand is strengthened, causing a longer CT lifetime. However, the CS state of the D-C-A triads is formed by the donor transferring an electron to the $[\text{Cu(II)P}_2]$ d_{yz} orbital in the J-T distorted D_2 geometry, formally changing the oxidation state of the copper back to +1 (See Introduction, Chapter 1, Figure 1.6). Therefore, the geometry should change back to pseudo-tetrahedral (D_{2d}) forcing dissociation of the adducted solvent molecule in the $[\text{P}_D^{+o}\text{-Cu(I)-P}_A^{n+}]$, CS state. Although this process must entail a large amount of reorganizational energy in itself, the resulting CS state should then have the same Cu(I) geometry as the ground state. Thus the rate of electron-hole recombination should not be affected by the changes in solvent composition *in the same way* as the C-AV diad. As expected, a much smaller effect on the lifetime of the CS decay was observed for the “D-C-A Mixture V/T” ($\tau_{cs} \approx 95$ ns in dfb and $\tau_{cs} \approx 140$ ns in dfb/5% MeOH, See Figure 5.6 and Table 5.2) than the C-AV diad complexes discussed in Ch. 3 ($\tau_{ct} \approx 7$ ns in dfb and $\tau_{ct} \approx 35\text{-}45$ ns in dfb/5% MeOH).

A different, unexpected solvent effect was observed for the “D-C-A Mixture V/T” in an applied magnetic field (see Figures 5.7 and 5.8). TA experiments performed in an applied field on a sample in dfb/5% MeOH solvent exhibited a decay component with an extremely long lifetime ($\gg 20 \mu\text{s}$) that is undetectable at zero applied field. This decay component became observable in very low fields ($< 50 \text{ mT}$). The relative contribution of the extremely long decay component to the overall CS decay decreases when: (A) the concentration of the “D-C-A Mixture V/T” solution is decreased, or (B) less MeOH is incorporated into the solvent. These data suggest that the extremely long decay component is a result of bi-molecular reactions in solution. Since the reaction is likely bi-molecular (Rate = $k[\text{D-C-A}^{4+}][\text{D}^{\circ}\text{-C-A}^{3+}]$), it is expected that a two-fold decrease in the concentration of the species would induce a four-fold decrease in the decay rate. However, this was not investigated completely since the contribution of the bi-molecular decay component was sufficiently depleted in the $1.75 \times 10^{-5} \text{ M}$ sample for the data to be fit and the CS lifetime to be evaluated. Furthermore, when TA studies were performed in dfb/2.3% MeOH, the contribution of the bi-molecular decay component was also sufficiently depleted even when the concentration of the “D-C-A Mixture V/T” solution was $4.1 \times 10^{-5} \text{ M}$. It is noteworthy, that the τ of the bi-molecular decay component does not seem to depend on the magnetic field, but must depend on the concentration of CS states in solution. At zero field, the rate of recombination must be faster than the rate of diffusion at the concentrations used for the laser studies; thus, the CS states produced will recombine to the ground state before they can encounter another D-C-A⁴⁺ complex. However, in a magnetic field, the lifetime of the CS state is increased dramatically. Therefore, an appreciable concentration of CS states can exist in solution for a long enough period of time to encounter other D-C-A⁴⁺ complexes and undergo bi-molecular reactions. Consequently, the bi-molecular reactions are not observable until a magnetic field is applied.

As stated in the Results section, it is likely that a large portion of the bi-molecular reactions occur via a mechanism such as shown in Eq. 5.1:



This reaction can occur via ligand scrambling or outer-sphere electron transfer. Therefore, it is not particularly surprising that the bi-molecular interactions are induced by incorporating a coordinating solvent, such as MeOH. Since the [Cu(I)P₂] ligands in the D-C-A complexes are labile, the introduction of MeOH increases the rate of ligand exchange, which facilitates the formation of a number of reactive species and could release oxidized/reduced P_D/P_A ligands into the bulk solvent all of which could lead to bi-molecular reactions. Furthermore, both the D^{+o}-C-A³⁺ and D-C-A⁴⁺ have an overall charge of 5+, which could create a considerable electrostatic barrier for the formation of encounter complexes that enable bi-molecular reactions in dfb, a solvent with a moderately low di-electric constant (13.8 at 28 °C)⁵⁹. However, the incorporation of a higher dielectric medium, such as MeOH (33.3 at 20 °C),⁶⁰ should reduce the electrostatic work term, facilitating encounter complex formation and subsequent bi-molecular reactions.

When comparing the rates of CS decay for the “D-C-A Mixture V/T” in dfb and dfb/2.3% MeOH and the “D-C-A Mixture Q/T” in dfb it seems that changes in τ₂ and τ₃ follow the same pattern for each sample. As shown in Table 5.9, the CS lifetime (τ₃) of the D-C-A’s increases with applied magnetic field up to 1000-1250 mT, then decreases again with further applied field. When considering these data with respect to the relaxation mechanism presented in Figure 5.2, the change in τ₃ could correlate to changes in energy of the T₊ and T₋ states up to the field at which the effect saturates for both samples (1000 mT in dfb and 1250 mT in dfb/2.3% MeOH). However, in this model it is assumed that the *k_{isc}* between the ¹CS and the T₀ state are equilibrated at all magnetic fields giving rise to a constant, field-independent τ₂ lifetime, that

Table 5.9. The τ_2 and τ_3 lifetimes of the “D-C-A Mixture V/T” in dfb and dfb/2.3% MeOH and the “D-C-A Mixture Q/T” in dfb with respect to applied magnetic field. The fit error is eliminated for clarity, except for pertinent values.

Fit Values							
Species	“D-C-A Mixture V/T”				“D-C-A Mixture Q/T”		
Solvent	Dfb Only		Dfb/2.3% MeOH		Dfb Only		
Field Strength (mT)	τ_2 (ns)	τ_3 (ns)	τ_2 (ns)	τ_3 (ns)	Field Strength (mT)	τ_2 (ns)	τ_3 (ns)
0	94	-	101	-	0	115	-
20	33	435 ± 11	-	463 ± 5	25	-	388 ± 13
50	50	1190 ± 26	111	1145 ± 19	50	65	633 ± 19
100	77	2297 ± 47	78	2182 ± 51	100	103	999 ± 29
250	95 ± 6	4049 ± 48	137 ± 17	3794 ± 75	250	106 ± 10	1399 ± 30
500	79	5052 ± 73	118	4637 ± 71	500	63	1467 ± 25
750	48	4879 ± 67	123	4666 ± 117	-	-	-
1000	36	5814 ± 86	39	4585 ± 71	1000	54	1581 ± 31
1250	23	5213 ± 68	55	4825 ± 77	-	-	-
1500	18	5127 ± 79	54	4170 ± 62	1400	35	1578 ± 21
2000	18	4815 ± 58	-	4413 ± 71	1800	22	1520 ± 22
2250	-	4916 ± 57	-	4335 ± 71	-	-	-

should be essentially identical to the lifetime of the CS decay at zero field. However, in each sample presented in Table 5.9, the τ_2 lifetime is initially non-existent at small fields (< 20-40 mT), at which point the decay seems to change from bi- to tri-exponential. The lifetime of the second decay component then increases with increasing field to a maximum value that is very near the zero field CS lifetime at 250 mT, then decreases with further applied field until 1500-2000 mT. At this field, the decay seems to change from tri-exponential back to bi-exponential. This behavior clearly does not agree with the relaxation mechanism. These data suggest that upon application of the magnetic field there is a change in $^1\text{CS}/^3\text{CS}$ state mixing that is restored to its zero field value as the field increases to 250 mT and diminishes with increasing field. However, the mechanism that would bring about this change is not clear at this time. As mentioned in the Introduction section, incoherent processes that occur in the presence of a magnetic field are also capable of affecting the CS decay kinetics and may be able to explain the changes in τ_2 life-

time in the presence of a magnetic field. Based on the previous work on [Ru(II)L₃] D-C-A's, anisotropic hyperfine interactions (AHFI), and electron spin-spin dipolar interaction (ESDI) were the most likely processes to occur at low fields, and the spin-rotational interaction (SRI) and local vibrational motions were used to explain differences from the proposed relaxation mechanism for D-C-A's containing PXZ type donors at high fields.^{48,50,53} Some comments on the possible mechanisms are afforded below after discussing the magnetic field data for each of the D-C-A complexes studied.

Another interesting result presented in Table 5.9, is the difference in the maximum “slow” lifetimes achieved at high field with respect to solvent composition for “D-C-A Mixture V/T” (e.g. $\tau_3 = 5814$ ns at 1000 mT in dfb only and $\tau_3 = 4825$ ns at 1250 mT in dfb/2.3% MeOH), which could again be an electrostatic effect. Although the two “D-C-A Mixture V/T” samples were both made in the glove box, when the CS lifetime gets this long it is not uncommon to have sample-to-sample variation of this magnitude due to the extreme sensitivity to oxygen spin catalysis. Assuming the differences in the TA decay characteristics are real, these data imply that the presence of a coordinating solvent influences the CS decay kinetics in a magnetic field. Since the lifetimes change in a similar way in both solvents it is likely that magnetic field affects the spin-dynamics via a similar mechanism. As mentioned in the Introduction section, at high field, incoherent processes (which can be magnetic field independent) can affect the rate of CS recombination. A more detailed kinetic analysis is required to determine the actual origin of the differences in lifetime due to solvent presented in Table 5.9. In order to verify that these differences are indeed real, repeated studies are necessary.

The difference in the “slow” lifetimes shown in Table 5.9 between the “D-C-A Mixture V/T” and “D-C-A Mixture Q/T” samples at their maximum value is also large enough to be con-

sidered significant. This change could again be due to the difference in oxygen content considering the “D-C-A Mixture Q/T” was degassed using the F-P-T method instead of preparing the sample in the glove box. However, the difference in lifetimes is larger than expected based on typical sample-to-sample fluctuations, even when degassed using the F-P-T method. Recall from the Marcus theory argument presented in the Results section, that changes in Φ_{CS} , and τ_{CS} in these D-C-A’s are not unexpected based on differences in the driving force for CS recombination. The driving force for CS recombination (k_{bet}) in this D-C-A “Q/T” is estimated to be ca. 540 mV larger than in the D-C-A “V/T” (c.f. Figure 5.1). With the exception of the lifetime in zero applied field, the lifetime of the “slow” decay component of the D-C-A “Q/T” is smaller than for the D-C-A “V/T” in all applied fields. Taken together, these data could indicate that the back electron transfer from D-C-A “Q/T” is in the Marcus normal regime at all applied fields. This is particularly interesting because at zero applied field, despite the large difference in ΔG , the lifetimes of D-C-A “Q/T” and D-C-A “V/T” are very similar, which may imply that k_{bet} is inverted for D-C-A “Q/T” but normal for D-C-A “V/T”. Alternatively, all of these data could imply that the rate of back electron transfer is primarily dictated by spin dynamics instead of thermodynamics at all applied fields. Or, if a change from Marcus inverted to Marcus normal behavior is actually occurring, it could have important implications about the mechanism of magnetic field dependent spin and electron transfer dynamics. These are fascinating results and warrant further studies on these complexes to verify and elucidate these effects.

The effect of a magnetic field on the CS decay kinetics of “D-C-A Mixture V/P” and “D-C-A Mixture Q/P” are also very interesting, as shown in Table 5.10. First, the bi- and tri-exponential fitting values were included in Table 5.10, because the fit quality (R^2) of both types of fit were nearly identical and, upon inspection, there were no obvious mismatches between the

Table 5.10. The R^2 , τ_1 , τ_2 and τ_3 lifetimes of the “D-C-A Mixture V/P” and “D-C-A Mixture Q/P” in dfb with respect to applied magnetic field when fit with bi- and tri-exponential fitting curves.

		Bi-Exponential Fit Values						
		“D-C-A Mixture V/P”			“D-C-A Mixture Q/P”			
Field Strength (mT)	R^2	τ_1	τ_2	R^2	τ_1	τ_2		
0	0.985	6.0 ns	62 ± 1 ns	0.902	-	67 ± 2 ns		
25	0.992	7.0 ns	156 ± 2 ns	0.861	5.5 ns	127 ± 6 ns		
50	0.993	7.0 ns	192 ± 2 ns	0.892	5.0 ns	141 ± 6 ns		
100	0.989	6.5 ns	211 ± 3 ns	0.839	5.0 ns	168 ± 9 ns		
250	0.991	7.5 ns	223 ± 3 ns	0.859	7.0 ns	163 ± 9 ns		
500	0.990	6.0 ns	210 ± 3 ns	0.849	6.0 ns	194 ± 11 ns		
1000	0.990	7.0 ns	219 ± 3 ns	0.836	6.0 ns	167 ± 10 ns		
1400	0.992	8.0 ns	215 ± 3 ns	0.819	7.0 ns	180 ± 11 ns		
1800	0.988	7.0 ns	206 ± 3 ns	0.797	5.5 ns	178 ± 12 ns		
		Tri-exponential Fit Values						
		“D-C-A Mixture V/P”			“D-C-A Mixture Q/P”			
Field Strength (mT)	R^2	τ_1	τ_2	τ_3	R^2	τ_1	τ_2	τ_3
0	0.985	6.0 ns	62 ± 1 ns	-	0.902	-	67 ± 2 ns	135 ± 7 ns
25	0.993	5.5 ns	34 ± 11 ns	168 ± 5 ns	0.862	3.0 ns	11 ± 3 ns	161 ± 15 ns
50	0.994	4.0 ns	25 ± 4 ns	210 ± 4 ns	0.894	4.5 ns	24 ± 15 ns	200 ± 22 ns
100	0.991	5.5 ns	44 ± 9 ns	255 ± 12 ns	0.843	5.0 ns	46 ± 26 ns	187 ± 17 ns
250	0.991	5.0 ns	27 ± 7 ns	242 ± 6 ns	0.862	4.0 ns	18 ± 10 ns	215 ± 291 ns
500	0.991	4.0 ns	26 ± 6 ns	230 ± 6 ns	0.849	6.0 ns	140 ± 536 ns	189 ± 12 ns
1000	0.991	4.5 ns	27 ± 4 ns	245 ± 6 ns	0.841	3.0 ns	23 ± 9 ns	193 ± 15 ns
1400	0.991	6.0 ns	26 ± 7 ns	232 ± 6 ns	0.821	5.0 ns	29 ± 30 ns	203 ± 23 ns
1800	0.989	2.8 ns	34 ± 6 ns	236 ± 8 ns	0.800	3.0 ns	17 ± 9 ns	135 ± 7 ns

data and fits in either case. However, for the tri-exponential fits the value that needed to be used to fit the curvature of the first decay component (τ_1) is consistently smaller than expected considering the lifetime of the C-AX diads in dfb (ca. 7 ns), the error for the second decay component (τ_2) is somewhat large compared to the bi-exponential fits, and the error in the third decay component (τ_3) is larger than for the bi-exponential fits. Furthermore, the values used to fit the curvature of the first decay component (τ_1) in the bi-exponential fits are much closer to the expected

value for the lifetime of the C-AX diads. These observations suggest that the TA decays are actually bi-exponential in character despite the slightly smaller R^2 values. The data obtained in a magnetic field were obtained without the use of a measuring resistor (as was done in Chapter 4) so the bi-exponential behavior is unexpected based on the relaxation mechanism presented in Figure 5.2 (accounting for the additional decay component due to the presence of C-AX diads). Therefore, the data will be considered to be bi-exponential for the analysis of the MFE on the spin-dynamics and lifetime of CS decay.

For both of the samples presented in Table 5.10, the lifetime of the τ_2 increases with applied magnetic field up to ca. 100 mT and stays essentially constant with further applied field up to 1800 mT, within experimental error (recall that the error quoted in Table 5.10 is the error of the fit, and does not necessarily represent the experimental error). As can be seen, the lifetime of “slow” decay components in the “D-C-A Mixtures V/P” and “D-C-A Mixture Q/P” are much smaller than for the “D-C-A Mixtures V/T” and even “D-C-A Mixture Q/T” at all applied fields. This is not completely unexpected since the same trend was also observed in these complexes at zero applied field. In these cases, it is highly improbable that oxygen spin catalysis is responsible for the short lifetimes observed for the “slow” component, as mentioned in the Results section. Therefore, it is likely that the differences in the lifetime of the “slow” decay component are at least partially due to the POZ donor. In the magnetic field effect studies on the $[\text{Ru(II)L}_3]$ D-C-A’s, the “slow” decay component was almost identical for D-C-A’s with POZ vs TPZ-type donors at all magnetic fields (in the $[\text{Ru(II)L}_3]$ studies phenothiazine, PTZ, was used instead of tetramethylphenothiazine, TPZ, although the authors suggest that the identity of the heteroatom is what determines the MFE).^{48,50,53} However, in $[\text{Ru(II)L}_3]$ D-C-A’s, once the acceptor has been reduced, $[\text{L}_D\text{-Ru(III)-L}_A^{n+}]$ has more than enough driving force to oxidize either donor moiety,

which is not the case for $[P_D\text{-Cu(II)-P}_A^{n+}]$. Recall from Chapter 4, that the spectroelectrochemistry of the $[\text{Cu(I)(POZ)(POZ}^{+\circ})]^{2+}(\text{TPFB}^-)_2$ indicated that there is a dynamic equilibrium between the oxidized donor moiety, $\text{POZ}^{+\circ}$, and the oxidized $[\text{Cu(II)(POZ)(POZ)}]^{2+}(\text{TPFB}^-)_2$. Since these data seem to suggest that there is change in the mechanism of CS formation in the D-C-A “V/P” and D-C-A “Q/P” relative to the D-C-A “V/T” and D-C-A “Q/T,” the observed differences in lifetime cannot be interpreted based on driving force alone, and it is unclear if these data suggest Marcus normal or inverted behavior for CS recombination. Furthermore, this dynamic equilibrium between $\text{POZ}^{+\circ}$ and Cu(II) could be contributing to the shorter lifetime of the “slow” decay component in the D-C-A’s incorporating POZ donor ligands in applied magnetic fields.

The fact that the data in Table 5.10 are bi-exponential again suggests that the applied magnetic field affects the CS recombination kinetics of $[\text{Cu(I)P}_2]$ D-C-A triads via a different mechanism than the one used to explain the behavior of the $[\text{Ru(II)L}_3]$ D-C-A’s. In the relaxation mechanism presented in Figure 5.2, the “fast” CS decay component, not present in these samples, is due to recombination via the following pathway: ISC from T_0 to ^1CS then IC to the ground state via electron-hole recombination. However, the fact that this decay component is not observed in the D-C-A “V/P” and D-C-A “Q/P” suggests that either the k_{isc} from T_0 to ^1CS has become so fast that it is not detectable with a nanosecond laser system, or this ISC channel has become inoperable altogether. With the current dataset, it is uncertain which of these scenarios is correct. However, the non-coherent processes mentioned previously could play a major role.

All of the data presented so far suggests that the spin-relaxation in $[\text{Cu(I)P}_2]$ D-C-A complexes follow different mechanisms than the $[\text{Ru(II)L}_3]$ analogs. Furthermore, it seems that those mechanisms are dependent on other factors than just the identity of the donor and acceptor

moieties, such as the mechanism of charge separation. Therefore, it does not seem exceedingly appropriate to try to interpret the influence of the incoherent mechanisms on the magnetic field effects in [Cu(I)P₂] D-C-A's based on the results of the [Ru(II)L₃] studies. However, one such incoherent process does seem to warrant mentioning: direct spin-forbidden recombination via spin-orbit coupling (SOC). The role of direct spin-forbidden recombination via spin-orbit coupling (SOC) was essentially ruled out for the [Ru(II)L₃] D-C-A's with PXZ type donors, because the SOC of the donor radical is dominated by the SOC of the heteroatom on the PXZ type donors, which have very small SOC values with the exception of phenoselenazine ($\zeta=154, 365$ and 1659 cm^{-1} for O, S, and Se, respectively).^{53,61} However, in [Cu(I)P₂] it seems likely that direct spin-forbidden recombination via SOC interactions could contribute to the anomalous magnetic field effects in [Cu(I)P₂] D-C-A's having POZ donors. First of all, recall from Chapter 3 that the geometric changes that occur in the MLCT state cause the energies of the ¹MLCT/³MLCT states to change which alters the energetically feasible ISC pathways.¹⁰ Therefore, the k_{isc} between the ¹MLCT/³MLCT states is small because the only energetically feasible ISC pathway occurs via weak, ligand centered SOC.¹⁰ Also recall, that there is likely a dynamic equilibrium between POZ^{+o} and Cu(II) which could cause the radical hole in the CS state to be distributed between the POZ donor and the copper, giving the copper some degree of Cu(II) character in the CS state: e.g. [POZ^{+o}-Cu(I)-4OMV^{3+•}]⁵⁺ and [POZ-Cu(II)-4OMV^{3+•}]⁵⁺. If the hole is distributed in such a way, and the copper has some Cu(II) character, there could be some important changes in the following parameters: (A) the geometry of the CS state, (B) the distance between the radical hole and radical electron, (C) the hole may be distributed onto a metal based orbital. Therefore, it is possible in these complexes that the distribution of the hole between POZ^{+o} and Cu(II) could cause changes in the ¹CS/³CS energetics similar to those observed in the ¹MLCT/³MLCT states.

If similar changes occur, then the SOC of the copper may become relevant when considering the k_{isc} between the $^1\text{CS}/^3\text{CS}$ states. Since the application of a magnetic field also changes the energetics of the $^1\text{CS}/^3\text{CS}$, which in turn affects k_{isc} , and ultimately the rate of CS recombination, it seems possible that the SOC of the copper may influence the spin-dynamics in a magnetic field when the donor is the POZ ligand. It is worthwhile to note that the copper SOC is twice as small as Se ($\zeta = 829$ vs 1659 cm^{-1} for Cu(I) and Se, respectively),^{10,61} and the SOC did not have an influence on the CS recombination for the $[\text{Ru}(\text{II})\text{L}_3]$ D-C-A's, as mentioned previously. However, in the $[\text{Ru}(\text{II})\text{L}_3]$ D-C-A triads the hole was located on a ligand based orbital (phenoselenazine) rather than a metal based orbital, which could have important implications due to the changes in spatial separation between the radicals and isotropic hyperfine coupling (IHC) interactions. However, the speculation detailed above should be considered just as it is, speculation, as no concrete evidence has been gained that would suggest that the CS recombination is at all influenced by SOC of any species involved in the D-C-A's. It is just as likely that the mechanism of CS decay is dominated by one or several of the incoherent processes mentioned above in addition to coherent effects due to IHC. At this point, further studies are required for any additional clarification about the spin-dynamics in these systems.

The changes in initial intensity with magnetic field were also studied for each of the D-C-A complexes. However, as mentioned in the Results section, the presence of the C-AX diads in the "D-C-A Mixtures" obscures the results. It is possible to estimate the time at which the majority of the C-AX diad has decayed away, but that time period is often too long to be considered representative of the initial intensity. Therefore, these studies are not extremely conclusive at this time. The changes in initial intensity presented for the "D-C-A Mixture V/T" were the most detailed and the only data sets in which the ΔI_0 was calculated. In all three solvents studied (dfb,

dfb/2.3% MeOH, and dfb/5% MeOH) the initial intensities increase with field to their maximum value around 50-100 mT, plateau until 200-500 mT and then decrease with field until the maximum field has been achieved. The ΔI_0 for each in each solvent was calculated to be 10%, 12% and 5% in dfb, dfb/2.3% MeOH, and dfb/5% MeOH, respectively. These values are in relatively good agreement with the values obtained in different solvents for the C-AV diads in Chapter 3, which could indicate that all of the changes in initial intensity are originating from the presence of C-AV diad in the “D-C-A Mixture V/T.” Of these data, the sample prepared in dfb solvent (0% MeOH) is likely to be the most representative of actual changes in the initial intensity of the D-C-A triad since the lifetime of the C-AV diad is shortest in dfb, and has decayed to ca. 90% of its initial value between 12-22 ns. Interestingly, in the dfb only sample the plateau region occurs from ca. 50 to 500 mT, whereas the plateau region occurs from ca. 50-200 mT in dfb/2.3% MeOH and dfb/5 % MeOH. The error bars are very large on these data, but the most obvious difference between the three samples seems to occur in the plateau region.

The ΔI_0 could not be calculated for the other three “D-C-A Mixtures” and the studies were more preliminary. With the exception of the “D-C-A Mixture V/P,” where the error bars are too large to infer a pattern, the data from each sample seems to suggest that the magnetic field could be influencing the I_0 . In each sample, the I_0 starts out at a high value in small magnetic fields and decreases with increased field strength. These data were obtained in dfb and could be representative of the D-C-A initial intensity, but again, the contribution of the C-AX diads cannot be completely discounted. In $[\text{Ru(II)L}_3]$ triads, a similar effect on I_0 was observed without the initial rise component from 0-50 mT. This behavior was attributed to increased singlet character of the radical pair in the CS state as the field increased from 500-1000 mT.^{48,50} It is possible that a similar change in CS spin multiplicity is occurring in the $[\text{Cu(I)P}_2]$ D-C-A's.

Moreover, when the A_2 (when A_2 represents the “slow” decay component) and A_3 values from the fits of each D-C-A are compared to the changes in I_0 for each respective sample, qualitatively very similar trends are observed with magnetic field. In all cases the A_2 and/or A_3 value starts out at a maximum value in low fields (ca. 10-25 mT) and decreases significantly by 150-500 mT, after which point it decreases slightly, or remains essentially constant with further applied field. This is relevant because the A_2 and A_3 values represent the initial intensity of the D-C-A component and should be relatively free of any contributions from absorption due to the CT state of the C-AX diads. This is far from conclusive evidence that there is an MFE on the I_0 for the $[\text{Cu(I)P}_2]$ D-C-A's, but it certainly suggests that the possibility exists.

5.4 Conclusion

The TA laser studies presented herein have unambiguously shown that the lifetime of the CS state in these $[\text{Cu(I)P}_2]$ D-C-A's is affected by the presence of a magnetic field. The fact that the lifetime of each complex is affected by a magnetic field indicates that the CS state formed is, at least partially, triplet in character. For the “D-C-A Mixture V/T” a ca. 60 fold increase in the CS lifetime was achieved in a 1 T magnetic field (5814 ns). The lifetimes of the other “D-C-A Mixtures” also increase in the presence of a magnetic field to lesser extents in the following order (maximum lifetime achieved): Q/T (1581 ns) \gg V/P (223 ns) $> \approx$ Q/P (194 ns). The differences in lifetime observed in this series of D-C-A complexes suggest that the redox potential of the POZ donor affects the mechanism of charge separation, and could also affect the spin-dynamics in the CS state of the $[\text{Cu(I)P}_2]$ D-C-A's studied. Although it was initially thought that the spin chemistry of these complexes would exhibit similar behavior to the $[\text{Ru(II)L}_3]$ analogs, such as described by the relaxation mechanism proposed by Hayashi and Nagakura, the data pre-

sented herein strongly suggests that this is not the case. At this time, the magnetic field effects are not well understood and require repeated studies and detailed kinetic analysis that is unable to be performed at this time. However, the differences between the [Cu(I)P₂] and [Ru(II)L₃] systems, pose a host of new, interesting questions about the mechanism of spin-dynamics occurring in these D-C-A's.

Finally, much of the difficulty in the interpretation of the data presented in this thesis (in the presence and absence of the magnetic field) arises from the fact that the "D-C-A Mixtures" are just that, mixtures of photo-active species. Very recently, much progress has been made within the Elliott group in the synthesis of new acceptor ligands, having the same viologen and monoquat acceptor moieties, but a greater degree of steric bulk. This has been achieved by replacing the methyl groups with phenyl groups in the 2,9-positions of the existing phenanthroline acceptor ligand architecture. Preliminary ¹H NMR studies have indicated that a solution containing equimolar amounts of the new acceptor ligand, Cu(I), and an existing donor ligand yields a new, heteroleptic [Cu(I)P₂] D-C-A, almost exclusively. Thus, this new ligand may enable more conclusive studies of the D-C-A complexes. If successful, many of the questions left unanswered in this thesis may be resolved.

References

- (1) Kalyanasundaram, K. *Photochemistry of polypyridine and porphyrin complexes*; Academic Press: London; San Diego, 1992.
- (2) Robertson, N. *Chem. Sus. Chem.* **2008**, *1*, 977–979.
- (3) Armaroli, N. *Chem. Soc. Rev.* **2001**, *30*, 113–124.
- (4) Lavie-Cambot, A.; Cantuel, M.; Leydet, Y.; Jonusauskas, G.; Bassani, D. M.; McClenaghan, N. D. *Coord. Chem. Rev.* **2008**, *252*, 2572–2584.
- (5) Scaltrito, D. V.; Thompson, D. W.; O’Callaghan, J. A.; Meyer, G. J. *Coord. Chem. Rev.* **2000**, *208*, 243–266.
- (6) Schmittel, M.; Michel, C.; Liu, S.-X.; Schildbach, D.; Fenske, D. *Eur. J. Inorg. Chem.* **2001**, 1155–1166.
- (7) Schmittel, M.; Ganz, A. *Chem. Commun.* **1997**, 999–1000.
- (8) Kalsani, V.; Schmittel, M.; Listorti, A.; Gianluca, A.; Armaroli, N. *Inorg. Chem.* **2006**, *45*, 2061–2067.
- (9) Pellegrin, Y.; Sandroni, M.; Blart, E.; Planchat, A.; Evain, M.; Bera, N. C.; Kayanuma, M.; Sliwa, M.; Rebarz, M.; Poizat, O.; Daniel, C.; Odobel, F. *Inorg. Chem.* **2011**, *50*, 11309–11322.
- (10) Siddique, Z. A.; Yamamoto, Y.; Ohno, T.; Nozaki, K. *Inorg. Chem.* **2003**, *42*, 6366–6378.
- (11) Iwamura, M.; Takeuchi, S.; Tahara, T. *J. Am. Chem. Soc.* **2007**, *129*, 5248–5256.
- (12) Iwamura, M.; Watanabe, H.; Ishii, K.; Takeuchi, S.; Tahara, T. *J. Am. Chem. Soc.* **2011**, *133*, 7728–7736.
- (13) Shaw, G. B.; Grant, C. D.; Shirota, H.; Castner, E. W.; Meyer, G. J.; Chen, L. X. *J. Am. Chem. Soc.* **2007**, *129*, 2147–2160.
- (14) Gothard, N. A.; Mara, M. W.; Huang, J.; Szarko, J. M.; Rolczynski, B.; Lockard, J. V.; Chen, L. X. *J. Phys. Chem. A.* **2012**, *116*, 1984–1992.
- (15) Asano, M. S.; Tomiduka, K.; Sekizawa, K.; Yamashita, K.; Sugiura, K. *Chem. Lett.* **2010**, *39*, 376–378.
- (16) McMillin, D. R.; Kirchoff, J. R.; Goodwin, K. V. *Coord. Chem. Rev.* **1985**, *64*, 83–92.
- (17) Everly, R. M.; Ziesel, R.; Suffert, J.; McMillin, D. R. *Inorg. Chem.* **1991**, *30*, 559–61.
- (18) Cuttell, D. G.; Kuang, S.-M.; Fanwick, P. E.; McMillin, D. R.; Walton, R. A. *J. Am. Chem. Soc.* **2002**, *124*, 6–7.
- (19) Palmer, C. E. A.; McMillin, D. R. *Inorg. Chem.* **1987**, *26*, 3837–3840.
- (20) Cunningham, C. T.; Cunningham, K. L. H.; Michalec, J. F.; McMillin, D. R. *Inorg. Chem.* **1999**, *38*, 4388–4392.
- (21) Everly, R. M.; McMillin, D. R. *J. Phys. Chem.* **1991**, *95*, 9071–9075.
- (22) Ahn, B.-T.; McMillin, D. R. *Inorg. Chem.* **1981**, *20*, 1427–32.
- (23) Ahn, B.-T.; McMillin, D. R. *Inorg. Chem.* **1978**, *17*, 2253–8.
- (24) Gunaratne, T.; Rodgers, M. A. J.; Felder, D.; Nierengarten, J.-F.; Accorsi, G.; Armaroli, N. *Chem. Commun.* **2003**, 3010–3011.
- (25) Castellano, F. N.; Ruthkosky, M.; Meyer, G. J. *Inorg. Chem.* **1995**, *34*, 3–4.
- (26) Ruthkosky, M.; Kelly, C. A.; Zaros, M. C.; Meyer, G. J. *J. Am. Chem. Soc.* **1997**, *119*, 12004–12005.
- (27) Scaltrito, D. V.; Kelly, C. A.; Ruthkosky, M.; Zaros, M. C.; Meyer, G. J. *Inorg. Chem.* **2000**, *39*, 3765–3770.
- (28) Ruthkosky, M.; Castellano, F. N.; Meyer, G. J. *Inorg. Chem.* **1996**, *35*, 6406–6412.

- (29) Leydet, Y.; Bassani, D. M.; Jonusauskas, G.; McClenaghan, N. D. *J. Am. Chem. Soc.* **2007**, *129*, 8688–8689.
- (30) Jakob, M.; Berg, A.; Rubin, R.; Levanon, H.; Li, K.; Schuster, D. I. *J. Phys. Chem. A.* **2009**, *113*, 5846–5854.
- (31) Jakob, M.; Berg, A.; Levanon, H.; Schuster, D. I.; Megiatto, J. D. *J. Phys. Chem. C.* **2011**, *115*, 24555–24563.
- (32) Megiatto, J. D.; Li, K.; Schuster, D. I.; Palkar, A.; Herranz, M. A.; Echegoyen, L.; Abwandner, S.; de Miguel, G.; Guldi, D. M. *J. Phys. Chem. B.* **2010**, *114*, 14408–14419.
- (33) Megiatto, J. D.; Schuster, D. I.; de Miguel, G.; Wolfrum, S.; Guldi, D. M. *Chem. Mater.* **2012**, *24*, 2472–2485.
- (34) Megiatto, J. D.; Schuster, D. I.; Abwandner, S.; de Miguel, G.; Guldi, D. M. *J. Am. Chem. Soc.* **2010**, *132*, 3847–3861.
- (35) Li, K.; Bracher, P. J.; Guldi, D. M.; Herranz, M. Á.; Echegoyen, L.; Schuster, D. I. *J. Am. Chem. Soc.* **2004**, *126*, 9156–9157.
- (36) Li, K.; Schuster, D. I.; Guldi, D. M.; Herranz, M. Á.; Echegoyen, L. *J. Am. Chem. Soc.* **2004**, *126*, 3388–3389.
- (37) Flamigni, L.; Talarico, A. M.; Chambron, J.-C.; Heitz, V.; Linke, M.; Fujita, N.; Sauvage, J.-P. *Chem.-Eur. J.* **2004**, *10*, 2689–2699.
- (38) Linke, M.; Chambron, J.-C.; Heitz, V.; Sauvage, J.-P.; Encinas, S.; Barigelletti, F.; Flamigni, L. *J. Am. Chem. Soc.* **2000**, *122*, 11834–11844.
- (39) Chambron, J. C.; Harriman, A.; Heitz, V.; Sauvage, J. P. *J. Am. Chem. Soc.* **1993**, *115*, 7419–7425.
- (40) Armaroli, N.; Diederich, F.; Dietrich-Buchecker, C. O.; Flamigni, L.; Marconi, G.; Nierengarten, J.-F.; Sauvage, J.-P. *Chem.-Eur. J.* **1998**, *4*, 406–416.
- (41) Armaroli, N. *Chem. Soc. Rev.* **2001**, *30*, 113–124.
- (42) Lazorski, M. S.; Gest, R. H.; Elliott, C. M. *J. Am. Chem. Soc.* **2012**, *134*, 17466–17469.
- (43) Weber, J. M.; Rawls, M. T.; MacKenzie, V. J.; Limoges, B. R.; Elliott, C. M. *J. Am. Chem. Soc.* **2007**, *129*, 313–320.
- (44) Cooley, L. F.; Larson, S. L.; Elliott, C. M.; Kelley, D. F. *J. Phys. Chem.* **1991**, *95*, 10694–10700.
- (45) Cooley, L. F.; Larson, S. L.; Elliott, C. M.; Kelley, D. F. *J. Phys. Chem.* **1991**, *95*, 10694–700.
- (46) Cooley, L. F.; Headford, C. E. L.; Elliott, C. M.; Kelley, D. F. *J. Am. Chem. Soc.* **1988**, *110*, 6673–6682.
- (47) Rawls, M. T.; Kollmannsberger, G.; Elliott, C. M.; Steiner, U. E. *J. Phys. Chem. A.* **2007**, *111*, 3485–3496.
- (48) Klumpp, T.; Linsenmann, M.; Larson, S. L.; Limoges, B. R.; Buerssner, D.; Krissinel, E. B.; Elliott, C. M.; Steiner, U. E. *J. Am. Chem. Soc.* **1999**, *121*, 4092.
- (49) Steiner, U. E.; Wolff, H. J.; Ulrich, T.; Ohno, T. *J. Phys. Chem.* **1989**, *93*, 5147–54.
- (50) Klumpp, T.; Linsenmann, M.; Larson, S. L.; Limoges, B. R.; Buerssner, D.; Krissinel, E. B.; Elliott, C. M.; Steiner, U. E. *J. Am. Chem. Soc.* **1999**, *121*, 1076–1087.
- (51) Hayashi, H.; Nagakura, S. *Bull. Chem. Soc. Jpn.* **1984**, *57*, 322–328.
- (52) Yamaguchi, M.; Tanimoto, Y. *Magneto-science magnetic field effects on materials : fundamentals and applications*; Kodansha ; Springer: Tokyo; Berlin; New York, 2006.
- (53) Rawls, M. T.; Kollmannsberger, G.; Elliott, C. M.; Steiner, U. E. *J. Phys. Chem. A.* **2007**, *111*, 3485–3496.

- (54) Shaw, G. B.; Grant, C. D.; Shirota, H.; Castner Jr., E. W.; Meyer, G. J.; Chen, L. X. *J. Am. Chem. Soc.* **2007**, *129*, 2147.
- (55) Ichinaga, A. K.; Kirchhoff, J. R.; McMillin, D. R.; Dietrich-Buchecker, C. O.; Marnot, P. A.; Sauvage, J. P. *Inorg. Chem.* **1987**, *26*, 4290–4292.
- (56) Kirchhoff, J. R.; Gamache, R. E.; Blaskie, M. W.; Paggio, A. A. D.; Lengel, R. K.; McMillin, D. R. *Inorg. Chem.* **1983**, *22*, 2380–2384.
- (57) Ruthkosky, M.; Kelly, C. A.; Castellano, F. N.; Meyer, G. J. *Coord. Chem. Rev.* **1998**, *171*, 309–322.
- (58) Scaltrito, D. V.; Thompson, D. W.; O’Callaghan, J. A.; Meyer, G. J. *Coord. Chem. Rev.* **2000**, *208*, 243–266.
- (59) Mansingh, A. *J. Chem. Phys.* **1971**, *54*, 3322.
- (60) Mohsen-Nia, M.; Amiri, H.; Jazi, B. *J. Solution Chem.* **2010**, *39*, 701–708.
- (61) Murov, S. L.; Hug, G. L.; Carmichael, I. *Handbook of Photochemistry*; M. Dekker: New York, 1993.

Chapter 6

Global Conclusions and Outlook

Plants and algae have the unique ability to harvest light from the sun, transform that energy into consumable carbohydrates and sugars, and thus, fuel all life on earth. Therefore, photosynthesis could be considered the most fundamentally important process to occur on this planet. However, what we have learned from the photosynthesis may prove to be just as important to the survival of life on this planet as the products it generates. The world today relies heavily on fossil fuels to produce energy that drives our modern society, and global energy consumption is increasing at an alarming rate (13.5 TW in 2001 and 27.6 TW projected for 2050; 1 TW = 1.0×10^{12} W).¹ Furthermore, the noxious by-products (e.g. CO₂) of fossil fuel combustion are accumulating in the atmosphere at unprecedented concentrations (> 380 ppm) which is likely to cause dramatic, unforeseeable consequences.^{1,2} Therefore, developing technologies that utilize abundant, renewable resources is essential to satisfy mounting global energy needs. Fortunately, the sun provides an enormous amount of energy to the earth (4.3×10^{20} J in one hour).¹ Furthermore, scientists have discovered that light is harvested and used during photosynthesis via a light-induced, multi-step, electron transfer mechanism resulting in a charge-separated state (CS).³⁻⁵ In photosynthesis, light energy is converted to chemical potential, stored in the CS state and subsequently used to drive chemical reactions that produce food. However, researchers realized that the energy stored in the CS state can also be used for solar energy harvesting apparatuses (e.g., solar cells and solar fuels as results from using light to split water into H₂ and O₂).

Therefore, the development of complexes that mimic the photosynthetic process is important to the progression of renewable energy technologies.

Metal polypyridyl donor-chromophore-acceptor (D-C-A) assemblies are one class of molecules that efficiently mimic the light-induced CS formation of photosynthesis. This type of D-C-A assembly is a supermolecular system with a metal-polypyridyl chromophore, an organic moiety that can accept an electron from the chromophore (acceptor), and an organic moiety that can donate an electron to the chromophore (donor) all within a single molecular unit. When incident light hits a D-C-A, the chromophore is excited to an energetic state from which an electron is transferred to the acceptor, after which an electron is transferred from the donor to the chromophore. This multi-step electron transfer results in an energetic configuration where the reduced acceptor is spatially separated from the oxidized donor, which stores the energy from the incident light: this is the CS state. In photosynthetic systems, the CS state is achieved analogously, but using different donor, chromophore, and acceptor moieties. The archetypal metal polypyridyl D-C-A's are based on ruthenium tris-bipyridine (e.g. $[\text{Ru(II)L}_3]$, where L=bipyridine) with electron donor and electron acceptor units appended to separate bipyridine ligands. The $[\text{Ru(II)L}_3]$ D-C-A's are prominent because they typically absorb and subsequently store a large portion of the incident light ($\epsilon \approx 10^3\text{-}10^5 \text{ L}\cdot\text{cm}^{-1}\cdot\text{mol}^{-1}$; up to 75% of incident light stored), nearly all of the absorbed light is used to produce a CS state (quantum efficiency, $\Phi_{\text{CS}\rightarrow 1}$), and the lifetime of the CS state is generally long enough to drive subsequent processes in light harvesting apparatuses (CS lifetime; $\tau_{\text{CS}} \approx 100 - 300 \text{ ns}$).⁶⁻⁸ Finally, the lifetime of the CS state can be dramatically lengthened in small to moderate magnetic fields (ca. 2 μs in $\beta_0 < 50 \text{ mT} \approx 1$ laboratory stir-bar).

Unfortunately, ruthenium is very expensive and not earth abundant, making [Ru(II)L₃] D-C-A's impractical for real-world solar energy harvesting applications.^{9,10} However, bis-phenanthrolinecopper(I) (i.e., [Cu(I)P₂]) complexes have similar light-induced properties to [Ru(II)L₃] complexes,¹⁰ which suggest that functional [Cu(I)P₂] D-C-A's could be attainable. Preparation of [Cu(I)P₂] D-C-A's has been a significant challenge in the metal polypyridyl D-C-A literature mainly due to the fluxional coordination environment of [Cu(I)P₂] complexes. Thus, the focus of this research was to synthesize a [Cu(I)P₂] D-C-A capable of photo-induced, multi-step electron transfer resulting in the formation of a CS state, as occurs in photosynthesis.

Towards this goal, the ligands shown in Figure 6.1 were successfully synthesized and used to assemble several [Cu(I)P₂] D-C-A's. Transient absorption (TA) laser spectroscopy was used to determine if these D-C-A's were capable of achieving CS states that I estimate to store between ca. 1.1-1.8 V of energy. The lifetime of the CS state was measured for each D-C-A and was found to be ca. 60-150 ns depending on the donor ligand used. The observed quantum efficiency of CS state formation was

estimated to be $55 \pm 15\%$ for the D-C-A having a TPZ donor and 4OMV acceptor. All of these values are comparable to what has been measured for [Ru(II)L₃] D-C-A systems, but using copper instead of non-earth abundant, expensive ruthenium. *Furthermore, the D-C-A's synthesized for this*

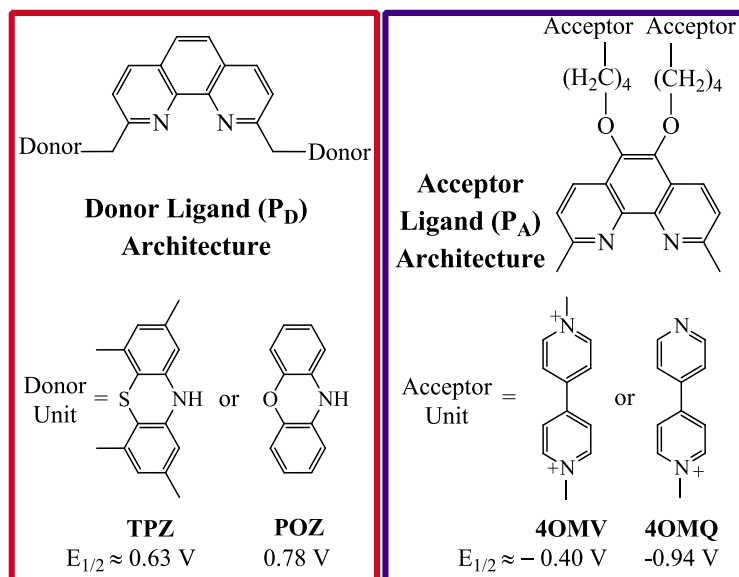


Figure 6.1. Donor and acceptor ligands based on 1,10-phenanthroline and their redox potentials (as free ligand).

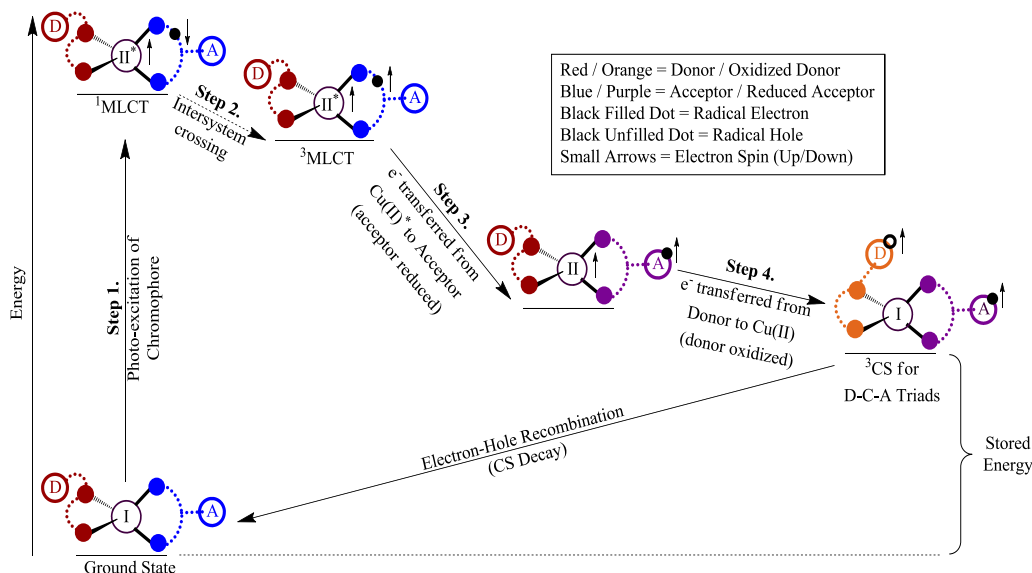


Figure 6.2. A schematic representation of CS formation in $[\text{Cu}(\text{I})\text{P}_2]$ D-C-A complexes. The center circle represents the copper ion and the roman numeral its oxidation state. The red/orange arcs represent the P_D ligands in different oxidation states and the blue/purple arcs represent the P_A in different oxidation states. This proposed mechanism of CS formation was supported experimentally using transient absorption laser studies.

project are the first bis-phenanthrolinecopper(I) D-C-A's to be reported that undergo multi-step electron transfer resulting in a CS state where $[\text{Cu}(\text{I})\text{P}_2]$ is the primary chromophore (Figure 6.2).^{11–15}

Although this project has enabled much progress to be made in this field, many questions remain to be answered. Fortunately, some very recent advances in ligand design should quickly clarify many of these questions. Recall that the most significant barrier to the synthesis of $[\text{Cu}(\text{I})\text{P}_2]$ D-C-A's is its coordination chemistry. In order to synthesize a $[\text{Cu}(\text{I})\text{P}_2]$ D-C-A, two different phenanthroline ligands (P) must be used: one appended with an acceptor unit (P_A), and one appended with a donor unit (P_D) (Figure 6.1). Since $[\text{Cu}(\text{I})\text{P}_2]$ complexes are inherently prone to ligand exchange in solution, a mixture of three products typically result: $[\text{Cu}(\text{I})\text{P}_\text{A}\text{P}_\text{D}]$ D-C-A, $[\text{Cu}(\text{I})(\text{P}_\text{A})_2]$, and $[\text{Cu}(\text{I})(\text{P}_\text{D})_2]$. While it is possible to design the ligands such that ca. 100% $[\text{Cu}(\text{I})\text{P}_\text{A}\text{P}_\text{D}]$ D-C-A complex self-assembles in solution, finding the optimal ligand architecture often requires extensive trial and error.^{16,17} The ligands synthesized for this project were designed to favor self-assembly of the D-C-A, but always resulted in a mixture of the three prod-

ucts mentioned above. Since the ligands exchange in solution, isolation of pure D-C-A is impossible. Although the presence of the two side products, $[\text{Cu(I)}(\text{P}_A)_2]$ and $[\text{Cu(I)}(\text{P}_D)_2]$, did not affect the CS formation mechanism it did complicate the interpretation of the results. Fortunately, as mentioned above, a new acceptor ligand (Figure 6.3) has been synthesized that is designed to impose greater steric restrictions in the Cu(I/II) coordination sphere. Preliminary ^1H nuclear magnetic resonance (NMR) spectra indicate that nearly 100% $[\text{Cu(I)}\text{P}_2]$ D-C-A is formed when complexed with Cu(I) and the existing TPZ donor ligand. Therefore, all TA data obtained for D-C-A systems with this new acceptor ligand should be much easier to analyze. Furthermore, comparison of the results from D-C-A's with the new acceptor ligand to those obtained for the $[\text{Cu(I)}\text{P}_2]$ D-C-A's outlined above will be possible. This type of comparison should enable the delineation of trends in the CS formation and decay in $[\text{Cu(I)}\text{P}_2]$ D-C-A complexes.

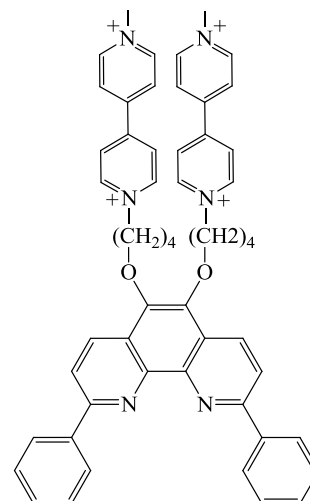


Figure 6.3. A new acceptor ligand that forms ca. 100% D-C-A when complexed with Cu(I) and the existing donor ligand shown in Figure 6.1.

The rate of CS decay in $[\text{Cu(I)}\text{P}_2]$ D-C-A's in the presence of a magnetic field ($\beta_0 = 0-2250$ T) and the CS lifetime was found to increase up to ca. 60x (maximum lifetime achieved = 5.8 μs in 1.0 T field) depending on the P_A and P_D ligands used. More importantly, for the D-C-A incorporating TPZ and 4OMV ligands, even in very low fields (50 mT) the CS lifetime increases to ca. 2 μs , which was the longest CS lifetime achievable in the $[\text{Ru(II)}\text{L}_3]$ triads.^{8,18} This demonstrates that the lifetime of the CS state is easily modulated by a magnetic field, which could be very important for real-world solar-energy harvesting applications. However, these studies also indicate that there is a change in the amount of CS formed (i.e. the quantum efficiency) with ap-

plied magnetic field. Since the D-C-A samples discussed herein always resulted in a mixture of products, the quantum efficiency of the D-C-A incorporating the TPZ donor and 4OMV acceptor had to be estimated based on a comparison to the measured quantum efficiency of the independently prepared $[\text{Cu(I)}(\text{P}_A)_2]$ complex. The problem with this approach is that the CS formed through single-step, electron transfer in the $[\text{Cu(I)}(\text{P}_A)_2]$ complex has a very short lifetime, and the time-resolution of the current laser set-up is too long (pulse width $\approx 6\text{-}7$ ns) to accurately measure very fast processes. Throughout these studies, a significant amount of evidence has suggested that very important photo-physical processes in the D-C-A samples occur on a shorter timescale than the resolution of the instrument. Therefore, a finite limit exists on what processes can be observed using our current system. Thus, it has not been possible to acquire data on the rates of CS formation. Determining the rate of each step leading to the CS state is crucial to understanding the factors that influence the efficiency of CS formation and finally optimizing $[\text{Cu(I)}\text{P}_2]$ D-C-A complexes for solar-energy harvesting applications. Consequently, in order to obtain more accurate information about the initial intensity of the CS in a magnetic field and the rates of each step in CS formation, more detailed studies on all of the photophysical processes leading to and from the CS state must be performed.

References

- (1) Lewis, N. S.; Nocera, D. G. *Proc. Natl. Acad. Sci. U.S.A.* **2006**, *103*, 15729–15735.
- (2) Ginley, D.; Green, M. A.; Collins, R. *MRS. Bull.* **2011**, *33*, 355–364.
- (3) Barber, J.; Andersson, B. *Nature* **1994**, *370*, 31–34.
- (4) Gust, D.; Moore, T. A.; Moore, A. L. *Acc. Chem. Res.* **2001**, *34*, 40–48.
- (5) Meyer, T. J. *Acc. Chem. Res.* **1989**, 163–170.
- (6) Weber, J. M.; Rawls, M. T.; MacKenzie, V. J.; Limoges, B. R.; Elliott, C. M. *J. Am. Chem. Soc.* **2007**, *129*, 313–320.
- (7) Larson, S. L.; Cooley, L. F.; Elliott, C. M.; Kelley, D. F. *J. Am. Chem. Soc.* **1992**, *114*, 9504–9509.
- (8) Klumpp, T.; Linsenmann, M.; Larson, S. L.; Limoges, B. R.; Bürssner, D.; Krissinel, E. B.; Elliott, C. M.; Steiner, U. E. *J. Am. Chem. Soc.* **1999**, *121*, 1076–1087.
- (9) Robertson, N. *Chem. Sus. Chem.* **2008**, *1*, 977–979.
- (10) Scaltrito, D. V.; Thompson, D. W.; O’Callaghan, J. A.; Meyer, G. J. *Coord. Chem. Rev.* **2000**, *208*, 243–266.
- (11) We are aware, through personal communication, that a related Cu(I)-based D-C-A triad having different donors and acceptor moieties is under study in the laboratory of Fabrice Odobel, Université de Nantes, CNRS. Results from these systems will be the subject of a future publication.
- (12) Lazorski, M. S.; Gest, R. H.; Elliott, C. M. *J. Am. Chem. Soc.* **2012**, *134*, 17466–17469.
- (13) Jakob, M.; Berg, A.; Rubin, R.; Levanon, H.; Li, K.; Schuster, D. I. *J. Phys. Chem. A.* **2009**, *113*, 5846–5854.
- (14) Megiatto, J. D.; Schuster, D. I.; Abwandner, S.; De Miguel, G.; Guldi, D. M. *J. Am. Chem. Soc.* **2010**, *132*, 3847–3861.
- (15) Megiatto, J. D.; Schuster, D. I.; De Miguel, G.; Wolfrum, S.; Guldi, D. M. *Chem. Mater.* **2012**, *24*, 2472–2485.
- (16) Kalsani, V.; Schmittel, M.; Listorti, A.; Gianluca, A.; Armaroli, N. *Inorg. Chem.* **2006**, *45*, 2061–2067.
- (17) Schmittel, M.; Michel, C.; Liu, S.-X.; Schildbach, D.; Fenske, D. *Eur. J. Inorg. Chem.* **2001**, 1155–1166.
- (18) Rawls, M. T.; Kollmannsberger, G.; Elliott, C. M.; Steiner, U. E. *J. Phys. Chem. A.* **2007**, *111*, 3485–3496.

LIST OF ABBREVIATIONS

4OMX	2,9-dimethyl-1,10-phenanthroline-5,6-bis(butoxy-MX) ligand <u>IF X=</u> <u>Q</u> <u>V</u>	<u>Acceptor Moiety (vide infra)</u> <u>MQ</u> <u>MV</u>
A	Acceptor	
C	Chromophore	
C-A	Chromophore-acceptor diad	
C-AX	Chromophore-acceptor diad <u>IF X=</u> <u>Q</u> <u>V</u>	<u>Acceptor Ligand (P_A)</u> <u>4OMQ</u> <u>4OMV</u>
C-DX	Chromophore-donor diad <u>IF X=</u> <u>P</u> <u>T</u>	<u>Donor Ligand (P_D)</u> <u>POZ</u> <u>TPZ</u>
CS	Charge separated state	
¹ CS/ ³ CS	Singlet CS/triplet CS state	
CT	Charge transfer state	
¹ CT/ ³ CT	Singlet CT/triplet CT state	
[Cu(I)L ₂]	Copper(I)bis-polypyridyl complex	
[Cu(I)P ₂]	Copper(I)bis-phenanthroline complex	
D	Donor	
D-C-A	Donor-chromophore-acceptor triad	
D-C-A “A/D”	<u>IF “A/D”=</u> <u>V/T</u> <u>Q/T</u> <u>V/P</u> <u>Q/T</u>	<u>D-C-A Complex=</u> <u>[Cu(I)(4OMV)(TPZ)]⁺⁵(TPFB)₅</u> <u>[Cu(I)(4OMQ)(TPZ)]⁺³(TPFB)₃</u> <u>[Cu(I)(4OMV)(POZ)]⁺⁵(TPFB)₅</u> <u>[Cu(I)(4OMQ)(POZ)]⁺³(TPFB)₃</u>

“D-C-A Mixture A/D”	1:1:1 solution of P _D : Cu(I): P _A
	<u>IF “A/D”=</u> <u>P_A=</u> <u>P_D=</u>
	<i>V/T</i> <i>4OMV</i> <i>TPZ</i>
	<i>Q/T</i> <i>4OMQ</i> <i>TPZ</i>
	<i>V/P</i> <i>4OMV</i> <i>POZ</i>
	<i>Q/T</i> <i>4OMQ</i> <i>POZ</i>
DPA	Donor-chromophore pre-association
DQ	Diquaternary amine type acceptor unit
ET	Electron transfer
FC- ¹ MLCT	Franck Condon singlet MLCT state
IHC	Isotropic hyperfine coupling
ISC	Intersystem crossing
J-T	Jahn-Teller
<i>k_x</i>	Rate of ET process
	<u>IF <i>x</i>=</u> <u>ET Process</u>
	<i>ar</i> <i>acceptor reduction</i>
	<i>bet</i> <i>back electron transfer from CT/CS</i>
	<i>cs</i> <i>charge separation</i>
	<i>ct</i> <i>charge transfer</i>
	<i>do</i> <i>donor oxidation</i>
	<i>et</i> <i>electron transfer</i>
	<i>fet</i> <i>forward electron transfer</i>
	<i>isc</i> <i>intersystem crossing</i>
	<i>nr</i> <i>non-radiative relaxation</i>
	<i>r</i> <i>radiative relaxation</i>
MFE	Magnetic field effect
MLCT	Metal-to-ligand charge transfer
¹ MLCT/ ³ MLCT	Singlet MLCT/ triplet MLCT state
MV	Methyl viologen acceptor unit (viologen)
MQ	Monoquaternary amine acceptor unit (mono-quat)
L	Polypyridyl ligand

$\Phi_{cs/ct}$	Quantum efficiency of CS or CT
P_A	Acceptor ligand based on 2,9-disubstituted-1,10-phenanthroline
P_D	Donor ligand based on 2,9-disubstituted-1,10-phenanthroline
P	2,9-disubstituted-1,10-phenanthroline
POZ	phenoxazine donor (unit or ligand) ligand=2,9-bis(methyl-POZ)-1,10-phenanthroline
PXZ	Azine type donor (also, see TPZ) $\frac{IF X=}{O}$ $\frac{Donor}{Phenoxazine (POZ)}$ S $Phenothiazine (PTZ)$
TA	Transient absorption
TPZ	tetramethylphenothiazine donor (unit or ligand) ligand= 2,9-bis(methyl-TPZ)-1,10-phenanthroline
$TPFB$	Tetrakis(pentafluorophenyl)borate
$[Ru(II)L_3]$	Ruthenium(II)tris-polypyridyl complex (although can be bis-polypyridyl if the L=terpyridine)
$\tau_{cs/ct}$	Lifetime of CS or CT